Technische Universität München
TUM School of Life Sciences

DEVELOPMENT OF NEW DOWNSTREAM PROCESSES FOR THE EXTRACTION OF ASTAXANTHIN FROM THE MICROALGAE *HAEMATOCOCCUS PLUVIALIS*

Andreas Bauer

Vollständiger Abdruck der von der TUM School of Life Sciences der Technischen Universität München zur Erlangung des akademischen Grades eines Doktors der Ingenieurswissenschaften (Dr.-Ing.) genehmigten Dissertation.

Vorsitz: Prof. Dr. Kang Yu

Prüfende/-r der Dissertation:

1. Prof. Dr. Mirjana Minceva
2. Prof. Dr. Thomas Brück

Die Dissertation wurde am 10.05.2022 bei der Technischen Universität München eingereicht und durch die TUM School of Life Sciences am 16.11.2022 angenommen.

Parts of this thesis have been published in the following journals:

1. A. Bauer, M. Minceva (2019). Direct extraction of astaxanthin from the microalgae *Haematococcus pluvialis* using liquid-liquid chromatography, *RSC Advances*, 40 (9) 22779-22789
2. A. Bauer, M. Minceva (2021). Examination of Photo-, Mixo-, and Heterotrophic Cultivation Conditions on *Haematococcus pluvialis* Cyst Cell Germination., *Appl. Sci.*, 11(16), 7201
3. A. Bauer, M. Minceva (2021). Techno-economic analysis of a new downstream process for the production of astaxanthin from the microalgae *Haematococcus pluvialis*, *Bioresources and Bioprocessing*, 8, 111

Parts of this thesis have been published in the following patent:

1. A. Bauer, M. Minceva, WO2020089173 - METHOD OF EXTRACTING A PIGMENT FROM MICROALGAE, 2020

Parts of this thesis have been presented at the following conferences:

1. Membrane-assisted extraction of astaxanthin from the microalgae *Haematococcus pluvialis*, *DECHEMA Jahrestreffen der ProcessNet-Fachgruppen Hochdruckverfahrenstechnik und Membrantechnik, Feb. 2020, Freising, Germany*
2. Extraction of astaxanthin from the microalgae *Haematococcus pluvialis* using a liquid-liquid chromatographic column, *DECHEMA Jahrestreffen der ProcessNet-Fachgruppen Fluidverfahrenstechnik, Adsorption und Extraktion, Feb. 2020, Berchtesgaden, Germany*
3. Extraction of astaxanthin from the microalgae *Haematococcus pluvialis* using liquid-liquid chromatography, *DECHEMA 12. Bundesalgenstammtisch, Sept. 2019, Kiel, Germany*
4. Extraction of astaxanthin from the microalgae *Haematococcus pluvialis* with liquid-liquid chromatography, *DECHEMA Jahrestreffen der ProcessNet-Fachgruppen Phytoextrakte und Extraktion, Feb. 2019, Muttenz, Switzerland*

Danksagung

Mein Dank gilt Frau Prof. Dr.-Ing. Mirjana Minceva für die Betreuung dieser Arbeit und die Unterstützung während der letzten Jahre. Des Weiteren möchte ich mich bei Prof. Dr. Thomas Brück bedanken, dass er als Zweitgutachter diese Dissertation bewertet.

Ein großer Dank geht an alle Studenten, die während der Zeit an der Professur für Biothermodynamik meine Arbeit unterstützt haben. In chronologischer Reihenfolge waren dies: Dominik Trinkl, Ference Raab, Michael Schobesberger, Leah Pitman, Amelie Kolb, Helen Chau, Fabian Börner, Tanja Wintzer und Said-Islombek Murodi. Es hat mir Spaß gemacht mit euch zusammenzuarbeiten.

Des Weiteren möchte ich mich bei Prof. Vogel (Technische Mikrobiologie) und Prof. Kulozik (Lehrstuhl für Lebensmittel- und Bio-Prozesstechnik) für die Nutzung der vorhandenen Laborgeräte bedanken.

An dieser Stelle möchte ich den Verlagen MDPI, Royal Society of Chemistry und Springer danken, meine bereits publizierten Daten in dieser Arbeit verwenden zu dürfen.

Ein weiterer Dank geht an die Stiftung der Deutschen Wirtschaft, die mein Promotionsvorhaben für drei Jahre finanziert hat.

Besonders möchte ich mich bei meinem Mentor Prof. Lindenberger für die Unterstützung bei meiner Arbeit bedanken.

Zudem möchte ich allen Kollegen, mit denen ich im Laufe meiner Zeit an der Professur für Biothermodynamik zusammengearbeitet danken.
Insbesondere bei meinen langjährigen Zimmerkollegen Vlad Simon Luca möchte ich mich für die ruhige und sachliche Unterstützung bedanken.
Des Weiteren möchte ich mich bei Rana Adeem Ghaffar für die mentale Unterstützung in stressigen Phasen der Dissertation bedanken.
Ein weiterer Dank geht an Raena Morley für ihr offenes Ohr in allen Lebenslagen.
Danke an Simon Röhrer, Martin Hübner und Ahmad Al-Hadid für eure kollegiale Unterstützung.

Der größte Dank geht zu guter Letzt an meine Familie und Freunde. Besonders meinen Eltern und meinen beiden Schwestern möchte ich für ihre Unterstützung während der sehr langen Zeit der Dissertation danken. Ohne euren Zuspruch hätte ich diese Arbeit nicht beenden können.

Table of Contents

Symbols and Abbreviation

Latin symbols

Letter	Description	Unit
a	Activity	-
a	Interfacial area	m^2
A	Cross sectional area	m^2
c	Concentration	g mol^{-1}
D	Diffusion coefficient	m^2 s^{-1}
d	Inner diameter	m
DW	Dry weight biomass	g L^{-1}
E	Extraction factor	-
E_{ff}	Extraction efficiency	-
f	Fugacity	N m^{-2}
F	Flow rate	m^3 s^{-1}
G	Molar Gibbs free energy	J mol^{-1}
K	Distribution coefficient	-
K	Overall mass transfer coefficient	m s^{-1}
k	Individual mass transfer coefficient	m s^{-1}
L	Characteristic length	m
M	Molecular weight	g mol^{-1}
m	Mass transfer	g s^{-1}
P	Partition coefficient	-
P	Pressure	bar
R	Gas constant	J $mol^{-1}K^{-1}$
R	Overall extraction factor	-
Re	Reynolds number	-
S_f	Stationary phase retention	%
Sh	Sherwood number	-
T	Temperature	°C
v	Molar volume	m^3 $kmol^{-1}$
v	Flow velocity	m s^{-1}
x	Molar fraction	-
Y	Yield	%

Greek symbols

Letter	Description	Unit
α	Association parameter	-
β	Membrane parameter	-
ε	Membrane porosity	%
μ	Chemical potential	kJ mol^{-1}
ρ	Density	kg m^{-3}
Φ	Fibre packing factor	%
γ	Activity coefficient	
η	Dynamic viscosity	mPas
τ	Residence time	s
τ	Tortuosity	%
ω	Angular velocity	rad s^{-1}

Superscripts

Letter	Description
‘	Phase ‘
‘‘	Phase ‘‘
0	Reference state

Subscripts

Letter	Description
c	column
DW	Dry weight biomass
E	Excess
f	Fibre
h	Hydraulic
i	Component i
i	Inner
inj	Injection
LP	Lower phase
MP	Mobile phase
m	Membrane
n	years
o	Outer
R	Retention

SP	Stationary phase
UP	Upper phase
w	Water

Abbreviations

Letter	Description
ATP	Adenosine triphosphate
ASC	Ascending
BBM	Bold Modified Basal Freshwater Nutrient Solution
BKT	ß-carotene ketolase
CCC	Countercurrent chromatography
CPC	Centrifugal partition chromatography
CPE	Centrifugal partition extractor
CrtR-b	ß-carotene hydroxylase
CS	Citrate synthase
DEG	Differentially expressed genes
DES	Descending
DMAPP	Dimethylallyl diphosphate
DOXP	1-deoxy-D-xylulose 5-phosphate pathway
DNA	Deoxyribonucleic acid
EAT	Earnings after Taxes
EBITDA	Earnings before Interest, Taxes, Depreciation, and Amortization
EBIT	Earnings before Interest and Taxes
EBT	Earnings before Taxes
EMP	Embden-Meyerhof Pathway
FA	Fatty acid
FCI	Fixed-capital investment
G3P	Glyceraldehyde 3-phosphate
GGPP	Geranylgeranyl pyrophosphate
GGPS	Geranylgeranyl pyrophosphate synthase
IPP	Isopentenyl pyrophosphate
IPI	Isopentyl pyrophosphate isomerase
IRR	Internal rate of return
LLC	Liquid-liquid chromatography
MEP	Non-mevalonate pathway
NADPH	Nicotinamide adenine dinucleotide phosphate
NB	Net cash flow
NPV	Net present value
PDS	Phytoene desaturases

PK	Pyruvate kinase
PPP	Pentose phosphate pathway
psy	Phytoene synthase
ROS	Reactive oxygen species
ROI	Return on investement
TAG	Triglyceride
TCA	Citric acid cycle
TCI	Total capital investment
TDIPC	Total direct and indirect plant costs
TEC	Total equipment costs
TKL	Transketolase
ZDS	ζ-carotene desaturase

Abstract

Biotechnologically, the red carotenoid astaxanthin is produced using the microalgae *Haematococcus pluvialis* (*H. pluvialis*). The synthesis of astaxanthin is accompanied by the formation of a resistant cyst cell wall, which requires a complex downstream process for product recovery. The downstream process includes harvesting of the cyst cells, mechanical cell wall disruption, drying and extraction with supercritical CO_2. The present work shows the development of a novel downstream process for the extraction of astaxanthin from the microalgae *H. pluvialis* using liquid-liquid chromatography and membrane-assisted extraction.

In the first part of the work, the germination of *H. pluvialis* cyst cells is studied. When growth conditions are applied to cyst cells, sporangium forms and zoospores containing astaxanthin are released. The zoospores have only a thin cell membrane, allowing direct astaxanthin extraction from the algal broth into certain solvents. In previous studies, germination of the cysts was generally done under phototrophic conditions. In this work, phototrophic, mixotrophic and heterotrophic germination conditions were evaluated to increase the number of zoospores released.

In the second part of this work, liquid-liquid chromatographic extraction of astaxanthin from germinated zoospores and homogenised cyst cells was performed. First, an evaluation of the operating parameters was performed using a countercurrent chromatography (CCC) unit. In the next step, a scale-up to a semi-preparative centrifugal partition extractor (CPE) was carried out. Process parameters were selected to increase the yield and productivity of the extraction process.

In the third part of the work, membrane-assisted extraction was evaluated. First, the operating parameters were selected, based on extracting of model compound camphor. In the next step, astaxanthin containing oleoresin (obtained from supercritical CO_2 extraction) was successfully extracted from the aqueous phase into a solvent. Finally, astaxanthin was extracted from homogenised cyst cells into a solvent.

A techno-economic calculation was carried out in the last part of the work. The liquid-liquid chromatographic extraction of astaxanthin from germinated zoospores and homogenised cysts was compared with the industrial supercritical extraction with CO_2.

Kurzfassung

Astaxanthin ist ein roter Farbstoff, welcher biotechnologisch mit der Mikroalge *Haematococcus pluvialis* (*H. pluvialis*) hergestellt wird. Die Synthese des Farbstoffs geht mit der Bildung einer resistenten Zellwand einher, was ein aufwendiges Downstream Verfahren notwendig macht. Der Downstream Prozess beinhaltet das Ernten der Zysten, den mechanischen Zellwandaufschluss, eine Trocknung und eine Extraktion mit überkritischem CO_2. Die vorliegende Arbeit zeigt die Entwicklung eines neuartigen Downstreamverfahrens für Astaxanthin aus der Mikroalge *H. pluvialis* mittels flüssig-flüssig Chromatographie und membrangestützter Extraktion.

Im ersten Teil der Arbeit wird die Keimung der *H. pluvialis* Zystenzellen untersucht. Werden Zystenzellen Wachstumsbedingungen ausgesetzt, bilden diese ein Sporangium aus und astaxanthin-haltige Zoosporen werden freigesetzt. Die Zoosporen besitzen lediglich eine dünne Zellmembran, wodurch Astaxanthin direkt aus diesen in bestimmte Lösungsmittel extrahiert werden kann. In bisherigen Studien erfolgte die Keimung der Zysten in der Regel unter phototrophen Bedingungen. In dieser Arbeit wurde neben den phototrophen Bedingungen auch mixotrophe und heterotrophe Keimungsbedingungen evaluiert, um die Anzahl freigesetzter Zoosporen zu erhöhen.

Im zweiten Teil der Arbeit wurde die flüssig-flüssig chromatographische Extraktion von Astaxanthin aus gekeimten Zoosporen und homogenisierten Zysten durchgeführt. Zunächst erfolgte eine Evaluierung der Betriebsparameter an der Gegenstromverteilungschromatographie (engl. countercurrent chromatography, CCC). Anschließend erfolgte eine scale-up auf die zentrifugale Verteilungschromatographie Anlage (engl. Centrifugal partition extractor, CPE). Es erfolgte eine Prozessparameterauswahl, um die Ausbeute und Produktivität des Extraktionsverfahrens zu erhöhen.

Im dritten Teil der Arbeit wurde die membrangestützte Extraktion evaluiert. Zunächst wurden die Betriebsparameter mittels der Extraktion des Modellstoffs Campher ausgewählt. Im weiteren Verlauf wurde astaxanthin-haltiges Oleoresin (aus der Extraktion mit überkritschen CO_2) erfolgreich aus der wässrigen Phase in ein Lösungsmittel extrahiert. Final wurde eine Extraktion von Astaxanthin aus homogenisierten Zysten durchgeführt.

Im letzten Teil der Arbeit wurde eine Wirtschaftlichkeitsrechnung durchgeführt. Hierbei wurde die flüssig-flüssig chromatographische Extraktion von Astaxanthin aus gekeimten Zoosporen und homogenisierten Zysten mit dem industriellen Prozess der überkritischen Extraktion mit CO_2 verglichen.

1 Introduction

1.1 State of the art

The microalgae *H. pluvialis* was scientifically described for the first time in 1899 [1, 2]. Almost another 100 years would pass before the start of commercial cultivation of *H. pluvialis* for astaxanthin in the 1980s and 1990s [3, 4]. It represents a green alternative to chemically synthesized astaxanthin, where petrochemicals are used for synthesis. The original use of chemically synthesized astaxanthin was as a coloring agent in the salmon and animal feed industries. In contrast to chemically synthesized astaxanthin, astaxanthin from *H. pluvialis* shows stronger anti-oxidative and health-promoting properties. Because of this, there is a sharp increase in consumer demand for biotechnological produced astaxanthin products in the cosmetic, dietary supplement and pharmaceutical industries. At this point in time, the biotechnologically produced astaxanthin from *H. pluvialis* cannot compete with synthetically produced astaxanthin in terms of production costs, which is why new process concepts are of great importance for industry [5].

Under favourable growth conditions, the microalgae live mainly as green, flagellated vegetative cells [6]. Under stress conditions such as nitrate, phosphate depletion, and high light intensity, the vegetative cells round off, start accumulating astaxanthin in the cell's cytoplasm and develop a rigid and resistant cyst cell wall [7, 8]. When growth conditions are applied to cyst cells these germinate, form a sporangium and release astaxanthin containing zoospores, which only have a thin cell matrix [9]. From zoospores, astaxanthin can directly be extracted into certain solvents [1].

The industrial cultivation process is usually performed phototrophically in two steps [10]. In the first stage of the process, high cell concentrations are reached under ideal growth conditions, with a sufficient supply of nutrients such as nitrates and phosphates, CO_2 [11] and an adequate light supply [12]. The astaxanthin synthesis is initiated under nitrate deficiency and light stress in the second step [13]. The accumulation of astaxanthin is accompanied by the creation of a resistant cyst cell wall, which hinders efficient and direct astaxanthin extraction. Therefore, a complex downstream process is needed, including biomass harvesting via centrifugation, mechanical cell-wall disruption, spray-drying, and the extraction of astaxanthin using supercritical CO_2 [14]. Microalgae harvesting can already account for up to 20-30% of the total production costs [14]. Due to the highly rigid cell wall of the *H. pluvialis* cyst cells, the mechanical cell-wall disruption also represents a process engineering challenge. Energy-intensive mechanical processes such as bead milling, or high-pressure homogenisation are used for industrial cell-wall disruption. Up to three-cycle repetitions are required to achieve adequate cell-wall disruption efficiency using high-pressure homogenisation [15]. Because of the high evaporation enthalpy of water, drying is an energy-intensive process step [16]. Commonly spray-drying is used in industry for drying *H. pluvialis* biomass. A decline in the

astaxanthin content might occur due to high temperatures and oxidation in this process step [13]. In addition, the dried biomass has to show defined bulk densities to be further processed via supercritical CO_2 extraction. For efficient supercritical CO_2 extraction, up to 1000 bars are required for astaxanthin extraction from *H. pluvialis*. Supercritical CO_2 extraction is usually not performed on site, but via specialized facilities. [17].

H. pluvialis cyst cell germination represents an interesting alternative to mechanical cell disruption. Applying growth conditions to cyst cells, these convert into a sporangium and release zoospores containing astaxanthin. Nevertheless, the cultivation conditions to convert cyst cells into zoospores, keeping the astaxanthin content high within the zoospores after release, are not yet thoroughly investigated [9, 18]. Previous studies have shown that the nitrate concentration [19], the light intensity [20] and composition [12] and the age of the cyst cells [21] influence the germination, i.e., the ratio of released zoospores compared to non-germinated cysts and the astaxanthin content in the zoospores. In these studies, germination was performed under phototrophic conditions. It has been shown that more zoospores were released from the cyst cells at higher light intensities than lower ones [19, 20]. However, this was also accompanied by a decline of the intracellular astaxanthin content at higher compared to lower light intensities. In addition, a stronger decrease of astaxanthin in the zoospores released occurred at higher than lower nitrate concentrations in the medium at the same light intensity [19]. It has also been shown, that germination with blue light benefits the number of released zoospores and their astaxanthin content compared to red or white light [12]. In conclusion in the literature, zoospores have been successfully released in large quantities under phototrophic conditions. This was usually accompanied by a decrease of the intracellular astaxanthin content. This was the motivation to investigate mixotrophic and heterotrophic germination conditions in addition to the well-known phototrophic conditions and to determine the influence on the number of released zoospores and the intracellular astaxanthin content.

Astaxanthin can be extracted directly from the germinated zoospores into green solvents, which form a second phase with the aqueous fermentation broth. In this work, two alternative technologies were investigated using two liquid phases, the liquid-liquid chromatography (LLC) and membrane contactors. In LLC two liquid phases are employed as stationary and mobile phases [22]. The separation of solutes is a result of the different partitioning of the components between these two phases. The phases are created by mixing two or more solvents [23]. One of the liquid phases is kept stationary through centrifugal forces in a specially designed column. LLC units have already been applied to extract torularhodin from the yeast *Rhodotorula rubra* [24] and ß-carotene from the microalgae *Dunaliella salina* [25].

Membrane contactors represent an interesting alternative to conventional extractors used in the chemical industry. Using a suitable membrane configuration such as a hollow fibre or a

flat sheet, fluids are contacted on opposite sides of the membrane and the fluid/fluid interface forms at the mouth of each membrane pore [26]. Mass transfer occurs by diffusion across the interface, just as in traditional contacting equipment. However, unlike most membrane operations, the membrane imparts no selectivity to the separation [27]. Membrane contactors allow non-dispersive contact via a microporous membrane. Furthermore, as opposed to more conventional membrane applications such as microfiltration, ultrafiltration and reverse osmosis, the driving force for separation is a concentration rather than a pressure gradient. Membrane contactors overcome the interdependence of the two fluid phases to be contacted, which sometimes leads to difficulties such as emulsions, foaming, unloading and flooding [28]. In addition, in contrast to classic extraction units, no phase separation is required. Most recently, membrane contactors were used for the in-situ extraction of carboxylic acids from fermentation broth [29]. In this work, LLC and membrane contactors were used for a direct extraction of astaxanthin from germinated zoospores and homogenised cyst cells into a green solvent.

1.2 Goal and structure of the thesis

As outlined in the previous Section 1.1, the downstream processing of astaxanthin from *H. pluvialis* includes several process steps, such as harvesting, mechanical cyst cell disruption, drying and extraction with supercritical CO_2. In this work, an alternative to the mechanical cell wall disruption, the cyst germination, was first examined. The aim of this work was to develop a new downstream process for the direct extraction of astaxanthin from homogenised cyst cell or zoospores into a solvent, using liquid-liquid chromatography and membrane-assisted extraction. Finally, a techno-economic analysis was done for the most promising process. The astaxanthin extraction from germinated zoospores and homogenised cyst cells using LLC was compared with the industrial process of supercritical CO_2 extraction.
The brief contents of the thesis are:
In Section 2, the theoretical background of the microalgae *H. pluvialis*, including the life cycle, germination and industrial production are described. In addition, the theoretical principles of the two extraction units examined, liquid-liquid chromatography and membrane extraction, are explained.
In Section 3, materials and methods are presented.
In Section 4, the results are presented and discussed. It starts with the presentation of the results of the cyst cell germination. There, the influence of photo-, mixo- and heterotrophic growth conditions on the germination of *H. pluvialis* cyst cells were examined. The influence of the germination conditions on the number of released zoospores, the extraction yield and the intracellular astaxanthin content was determined.

After successfully establishing the germination conditions, a solvent for the extraction of astaxanthin from germinated zoospores and mechanically disrupted cyst cells was selected. Subsequently, the results of the LLC extraction of astaxanthin from germinated zoospores and homogenised cyst cells are presented. First, a process scheme was developed using a laboratory scale CCC unit. It includes the selection of the process parameters rotational speed and flow rate, operating mode, as well as the volume and cell concentration of the injected biomass. For process evaluation, the stationary phase retention, extraction yield and productivity of the process was determined. Based on the obtained results, a scale-up to a CPE unit was carried out. Subsequently, the results of the membrane-assisted extraction are presented. First, a selection of the operating parameters aqueous feed and organic extract flow rate was done using the model compound camphor. The mass transfer coefficients of the extraction process were determined to select the ideal process conditions. Based on these results, an extraction of astaxanthin oleoresin into a solvent was performed. Finally, a membrane-assisted extraction of astaxanthin from homogenised cysts was done.

At the end of this section, a techno-economic analysis of the most promising downstream processes developed is presented. There, the extraction of astaxanthin from germinated zoospores and homogenised cyst cells using CPE was compared to the conventional industrial process of supercritical CO_2 extraction

Section 5 contains a conclusion and outlook.

2 Theory

This chapter comprises the concepts and fundamentals of the *H. pluvialis* cell metabolism and life cycle, liquid-liquid extraction, liquid-liquid chromatography, membrane-assisted extraction, and the techno-economic analysis.

2.1 Metabolism in microalgae

Microalgae are usually filamentous or single-cell microorganisms with a diameter of 3-10 µm [30]. The number of existing microalgae species is estimated to lie between 200000 and several million. Around 40000-60000 species are identified, but only several hundreds of them are investigated in more detail. Currently, fewer than 15 strains are used in industrial applications [31]. While most microalgae grow phototrophic, some can additionally grow mixotrophic and heterotrophic. The main metabolic pathways during phototrophic, mixotrophic, and heterotrophic cultivation of microalgae are shown, as shown in Figure 1. Phototrophic growth uses the inorganic carbon source CO_2 and light as an energy source [32]. In the thylakoid lumen of eukaryotic microalgae, ATP and NADPH are formed via the light-dependent reaction's electron transport chain (ETC). These are required for the reduction of CO_2 into glyceraldehyde 3-phosphate (G3P) in the Calvin cycle. G3P is used to synthesise carbohydrates such as pentoses and hexoses via the pentose phosphate pathway (PPP) and gluconeogenesis or converted into backbone structures of lipids [33]. In general, the lipid and amino acid anabolism depends on the pyruvate produced from G3P. In dark conditions, the Calvin cycle is inactive. In heterotrophic cultivation, growth is based on organic carbon sources, which replace the fixation of CO_2 from the atmosphere and takes place in the absence of light. During respiration, CO_2 is produced, and O_2 is consumed [34]. Sugars, sugar alcohols, phosphates, organic acids, and monohydric alcohols are used as an organic carbon source [34, 35]. In general, under heterotrophic cultivation conditions, an increase of the carbon flow into the citric acid cycle (TCA) is found compared to phototrophic cultivation. The oxidative assimilation of glucose starts with the phosphorylation of hexose and the formation of glucose-6-phosphate. In microalgae, aerobic glycolysis takes place either via the Embden-Meyerhof Pathway (EMP) or the PPP. Under heterotrophic conditions, glucose is mainly metabolized via PPP, whereas EMP predominates at light conditions [34, 36, 37]. Glucose uptake occurs via the hexose/H+ symport system protein, a transcript from the gene *hup1.* The mRNA of *hup1* is absent in photographically grown cells and is expressed within 5 minutes after adding glucose [34]. Glycerol as a carbon source for heterotrophic growth was used for several microalgae, but the knowledge about the metabolism at heterotrophic conditions is limited [38].

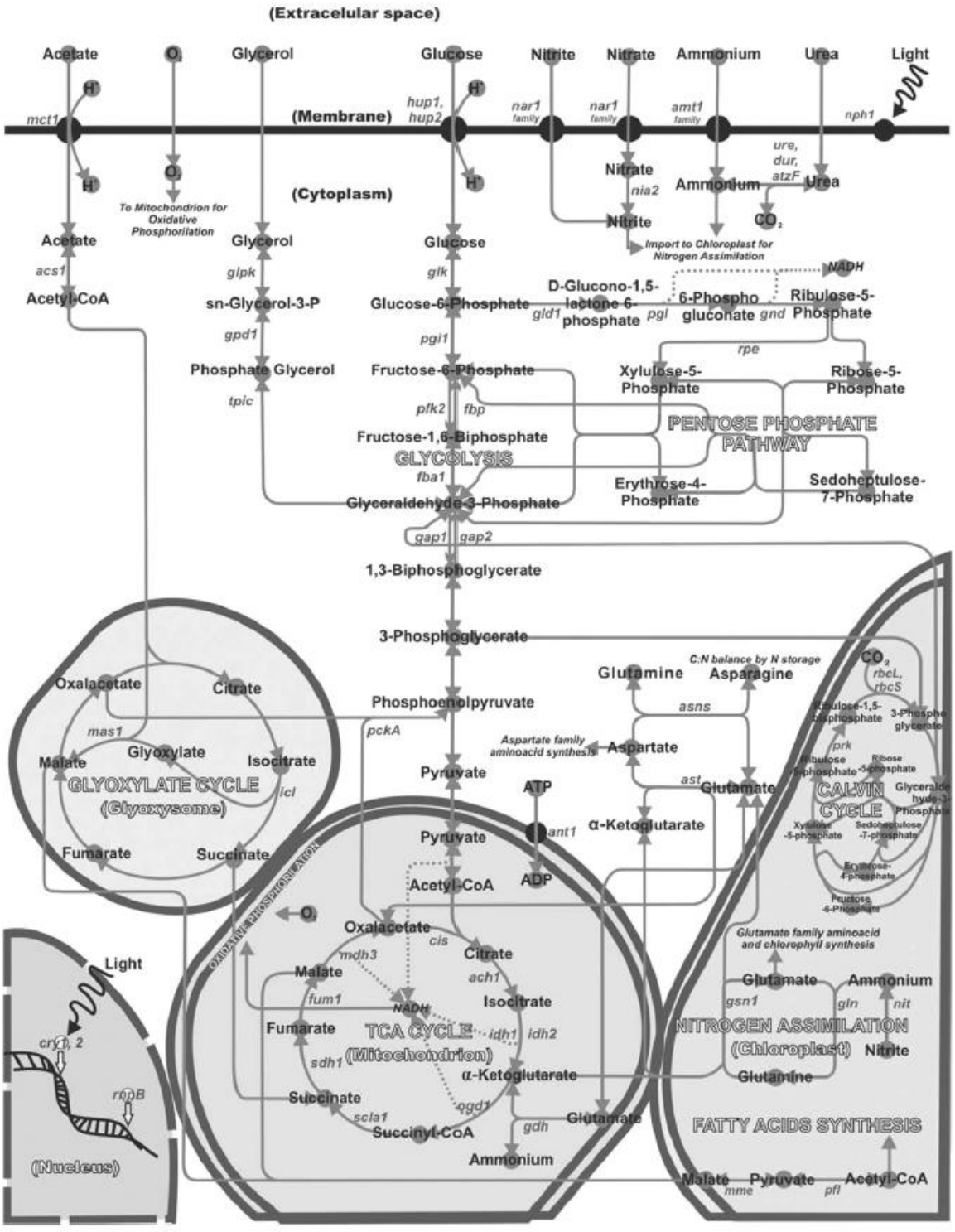

Figure 1: Basic metabolic pathways for phototrophic, mixotrophic and heterotroph growth of microalgae [34].

Glycerol usually enters the cells via diffusion, and several microalgae species have been reported to take up glycerol in the presence of light and without external CO_2 supply only [30, 34]. Acetate is a commonly used carbon source, which is oxidized metabolically either via the glyoxylate cycle where malate is formed in the glyoxysomes or the TCA in the mitochondria, where carbon skeletons, ATP, and reduction equivalents are synthesized [39]. If sodium or

potassium acetate is used, the pH rises as the remaining Na^+ and K^+ ions couple with hydroxyl ions (OH^-) to form alkalis. Significant sources of inorganic nitrogen in microalgae cultivation are nitrate, ammonium, and urea. Nitrate enters the cell via a transporting system, and it is reduced to nitrite within the cytosol by nitrate reductase. Nitrite is transported to the chloroplast and reduced to ammonium by nitrite reductase. Ammonium is incorporated into L-glutamate by the glutamine/glutamate synthase (GS/GOGAT) cycle [40]. Glutamate presents a key molecule as it couples the metabolic pathways of amino acids with those of lipids and carbohydrates. Ammonium is the preferred nitrogen source compared to the oxidized nitrogen forms NO_2^- and NO_3^-, as the assimilation requires less energetic costs [39]. Generally, the assimilation of the nitrogen source is faster with lighting compared to dark cultivation conditions. When microalgae are subjected to nitrogen depletion, the carbon flux shifts from biomass production to storage compounds, reducing growth rates and accumulation of lipids and starch [41]. These basic metabolic pathways can be found in microalgae species and can be further specified for the microalgae *H. pluvialis*.

2.2 The microalgae *H. pluvialis*

The essential metabolic pathways presented in Section 2.1 are also valid for the microalgae *H. pluvialis* and serve as the basis for understanding the complex life cycle and mechanism of astaxanthin biosynthesis in *H. pluvialis*.

2.2.1 The life cycle of *H. pluvialis* and astaxanthin biosynthesis

H. pluvialis belongs to the *Volvocales*, which is an order of flagellated green microalgae [30]. In nature, *H. pluvialis* mainly lives in temporary water and natural or artificial freshwater ponds in temperate regions of the world [42]. The complex life cycle of *H. pluvialis* is divided into a mobile and a non-mobile phase, in which the cells exist as mobile vegetative cells and immobile aplanospores [6]. At favourable growth conditions, the microalgae are mainly green, flagellated vegetative cells (Figure 2 a). The vegetative cells show the characteristic cell membrane of volvocalean motile cells, consisting of an extracellular gelatinous matrix [7]. Under stress conditions, the zoospores lose their flagella, expand cell size, and form immobile aplanospores (Figure 2 b) [43]. Under persistent stress conditions, the aplanospores accumulate astaxanthin in the cytoplasm (Figure 2 c). In the last stage of cyst formation, *H. pluvialis* builds a resistant cell wall made up of a trilaminar sheath, a secondary wall, and the tertiary wall (Figure 2 d). Nitrate and phosphate deficiency and light stress are the most commonly used stress conditions for cyst formation [8, 44-46]. Applying growth conditions, the cyst cells form a sporangium (Figure 2 e) and release zoospores into the medium (Figure 2 f). The zoospores round off after a certain time and form aplanospores (Figure 2 f). The described morphological changes from green zoospores to immobile cyst cells and the accumulation of astaxanthin in lipid droplets is accompanied by the formation of starch granules in the

cytoplasm and partial degradation of chlorophyll in the chloroplast. In the early stress phase, when the cells are still photosynthetic active, starch granules accumulate in the chloroplast (up to 63 wt%), and the first lipid droplets are formed in the cytoplasm [47].

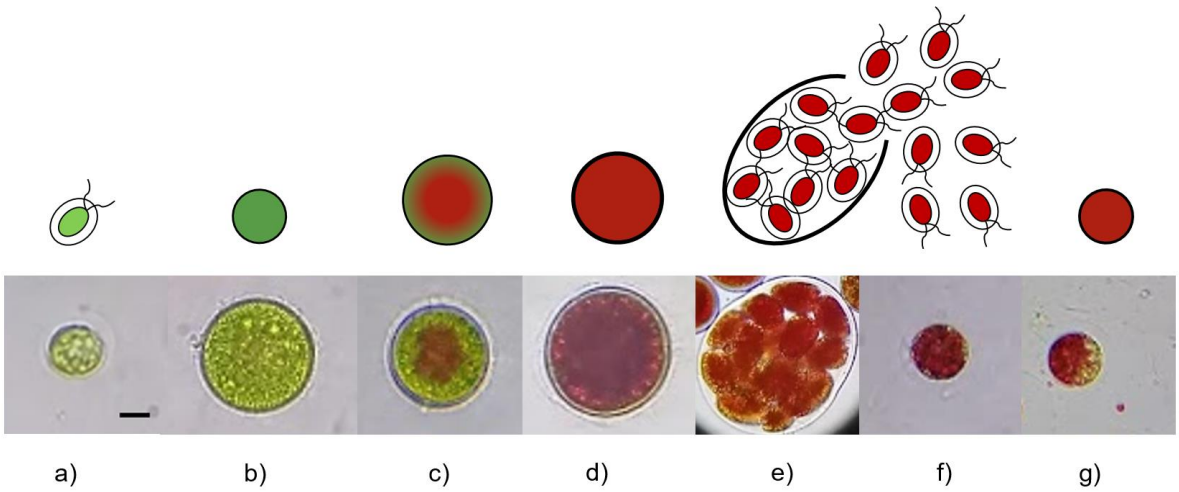

Figure 2: Cell cycle of *H. pluvialis*: a) motile, flagellated cell, b) aplanospore, c) astaxanthin-accumulating aplanospore, d) red cyst cell, e) dividing cells (sporangium), f) astaxanthin rich zoospores released from the sporangium, g) aplanospore derived from astaxanthin containing zoospore. Scale bar: 10 µm [9].

Under persistent stress conditions, the photosynthetic activity and chlorophyll content decrease further. Metabolic analysis revealed that the accumulated starch is converted into fatty acids and TAGs [46, 48, 49]. The TAG synthesis in *H. pluvialis* is coupled with the biosynthesis of astaxanthin. Inhibition of the TAG synthesis also inhibits astaxanthin accumulation, but not vice versa [50]. The central carbon flux during astaxanthin synthesis in *H. pluvialis* is presented in Figure 3. Up to the synthesis of ß-carotene, it takes place in the chloroplast of the cells. Isopentenyl pyrophosphate (IPP) is a key intermediate in carotenoid synthesis. It originates from two different pathways, the mevalonate pathway (MVA) in the cytosol and the non-mevalonate (MEP) or DOXY pathway located in the chloroplast. In *H. pluvialis*, IPP most likely originates from synthesis via the DOXP pathway since *H. pluvialis* lacks three enzymes to convert acetoacetyl-CoA into IPP via the MVA pathway [51]. The enzymatic conversion of pyruvate and G3P into IPP via the DOXP pathway is the predominant path in *H. pluvialis*. In the following step, isomerization into dimethylallyl diphosphate (DMAPP) takes place, which is catalyzed by isopentyl pyrophosphate isomerase (IPI), as it is unclear whether 4-hydroxy-3-methylbut-2-enyl diphosphate reductase (HDR) is involved as well [51]. The elongation of DMAPP takes place enzymatically with geranylgeranyl pyrophosphate synthase (GGPS), adding three molecules of IPP and forming the C_{20} component geranylgeranyl pyrophosphate (GGPP) [52, 53]. Condensation of two GGPP

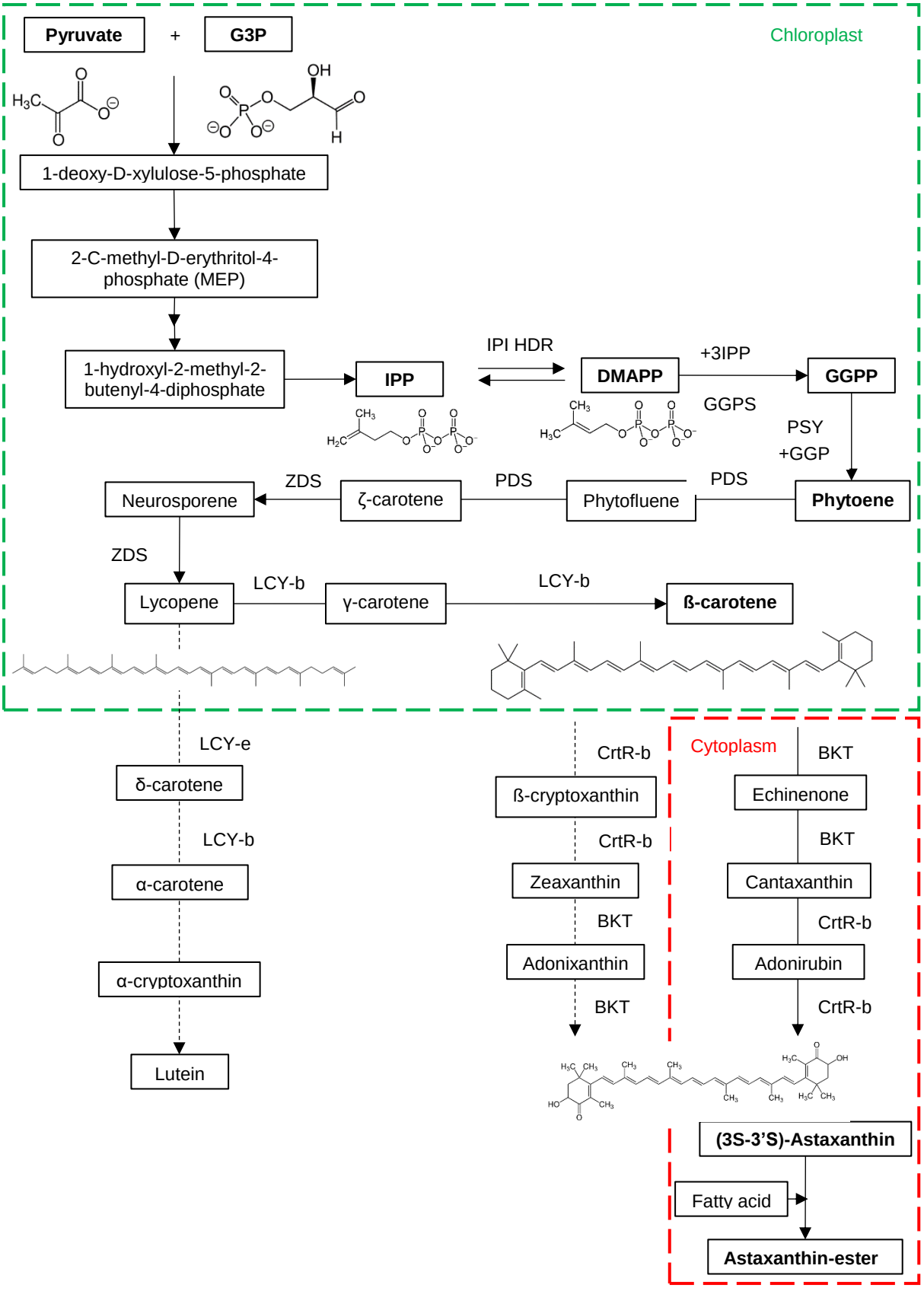

Figure 3: Biosynthesis and major carbon flux (solid line), during the (3S-3'S)-astaxanthin synthesis in *H. pluvialis* [13].

molecules by phytoene synthase (psy) yields to phytoene (C_{40} compound), which serves as a

precursor for carotenoids and astaxanthin. The subsequent lycopene synthesis is carried out by four desaturation steps catalyzed by two phytoene desaturases (PDS) and one ζ-carotene desaturase (ZDS). Using the lycopene cyclases (LCY-e and LCY-b), lycopene is cyclized into either α-carotene or ß-carotene [52]. In *H. pluvialis*, the major carbon flux is predominantly into ß-carotene, a precursor for astaxanthin. The two final oxidation steps are catalyzed by ß-carotene ketolase (BKT) and ß-carotene hydroxylase (CrtR-b) in the cytoplasm lipid bodies [54]. The transfer and control of ß-carotene from the chloroplast into the lipid bodies are not understood yet [47]. Since BKT has more significant substrate specificity for ß-carotene than zeaxanthin, the initial addition of the keto group occurs before the enantio-selective hydroxylation of canthaxanthin to astaxanthin via CrtR-b [51]. Since astaxanthin has two identical chiral centres at position 3 and 3', four configurations can exist, resulting in three different isomers (3R, 3'S), (3R, 3'R) and (3S, 3'S), depending on the position of the (OH) group around the chiral carbon. In chemical synthesis, the isomers (3R, 3'S), (3R, 3'R) and (3S, 3'S) are produced in a ratio of 2:1:1, whereas *H. pluvialis* synthesizes the (3S, 3'S) astaxanthin stereoisomer [13]. The transformation of *H. pluvialis* into a cyst cell and the accumulation of astaxanthin provide protection against various types of stress conditions, such as mechanical, irradiation and oxidative stress. Enhanced resistance is achieved by screening the photosynthetic pigments and channeling excess redox energy from the photosynthetic system, which can lead to photooxidative damage. This is done by reducing chlorophyll and cytochrome b_6f content, which results in a reduced electron flow. The astaxanthin accumulation itself protects the photosynthetic apparatus from photooxidative damage, acting as an internal sunscreen by removing excess light. This effect is further enhanced by the light-induced migration of astaxanthin-containing lipid droplets in the periphery of chloroplasts [55]. In addition, astaxanthin could protect nuclear DNA from photodamage. Since astaxanthin does not absorb light in the UV range, it cannot protect the cell against UV radiation. But it can shield the photosynthetic system against high light intensities and can directly quench photosynthetically generated ROS, thus protecting DNA [47].

2.2.2 Germination of *H. pluvialis* cyst cells

As shown in the previous Section 2.2.1, the transformation from motile zoospores into cyst cells and the accumulation of astaxanthin in *H. pluvialis* is a protective mechanism against nitrate deficiency and light stress. However, when growth conditions are applied to *H. pluvialis* cyst cells, these form a sporangium and release up to 64 zoospores [6]. As presented in Figure 4, cyst cell germination can be subdivided into three phases, in which physiological and morphological changes occur. The duration of the phases depends mainly on the germination conditions and cell status of the cyst cells. Germination of the cyst cells starts with water

uptake (phase 1), characterized by repetitive mitotic events and cell expansion [56]. Phase 2 is characterised by the formation of a sporangium, and zoospores formation is initiated via cytokinesis. In phase 3, the zoospores are released from the sporangium (Figure 4). *H. pluvialis* cyst germination is a complex process in which a total of 2202 differentially expressed genes (DEG) were identified.

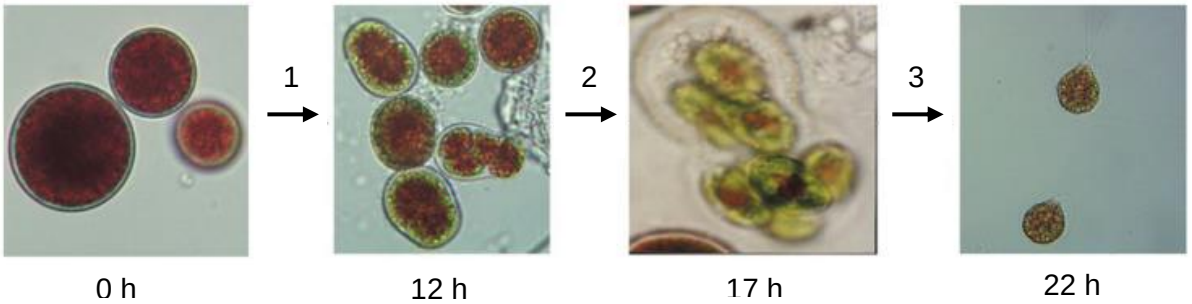

Figure 4: Phototrophic germination of *H. pluvialis* cyst cells duing a 14 h:10 h light/dark cycle with a fluorescent lamp at 20 µmol $m^{-2}s^{-1}$. 0 h: cyst cell, 12 h: mitotic events within the mother cyst cell, 17 h: Formation of a sporangium, 22 h: released zoospores [56].

DEGs are involved in carbohydrate metabolism during germination, particularly glycolysis, TCA cycle, PPP, pyruvate, fructose, mannose, amino sugar and nucleotide sugar, starch, and sucrose metabolism, are predominantly expressed. The DEGs participating in lipid metabolism are primarily involved in fatty and unsaturated fatty acid synthesis, sphingolipid, glycolipid, and glycerophospholipid metabolism [56]. The most common storage polysaccharide found in algae is starch, which also serves as the primary source of carbohydrates during germination [57]. Starch degradation starts with the upregulation of α-amylase throughout the germination process, which is introduced into glycolysis via dextrin and maltose [58]. As shown in Figure 5, most DEGs involved in the carbohydrate metabolism are up-regulated in phase 2, whereas they are down-regulated in phases 1 and 3. In phase 2, except for *np*-GADPH, all DEGs relevant for glycolysis are up-regulated [59]. The rate-limiting step of the TCA cycle, the citrate synthase (CS) is up-regulated in phase 2 [60]. The transketolase (TKL) represents the rate-limiting enzyme in the non-oxidative branch of the PPP. Thus, up-regulation of TKL in phase 2 is accompanied by increased production of G3P and sedoheptulose 7-phosphate [61]. The DEG expressions of the carbohydrate metabolism in phase 2 indicate that metabolic activity is increased at this stage of germination. Downregulation of *np*-GAPDH and *p*-GAPDH might be an efficient way to ensure sufficient NADPH provision [56]. Triacylglycerides (TAGs) serve as a source of metabolic intermediate, which can be used for germination. Lipid metabolism during seed germination usually occurs via ß-oxidation of fatty acids in the glyoxysome [62]. The acetyl-CoA acyltransferase (ACAA), which catalyses the last step of ß-oxidation, is the key enzyme of oil droplet degradation [63]. ACAA1 is consistently upregulated during germination, indicating degradation of fatty acids and accumulation of acetyl-CoA in the glyoxysome, which is converted into succinate and fed

into the TCA cycle [64]. The pyruvate formed during glycolysis can also be transported into the chloroplast, where it is converted into fatty acids via acetyl-CoA and other intermediates [56].

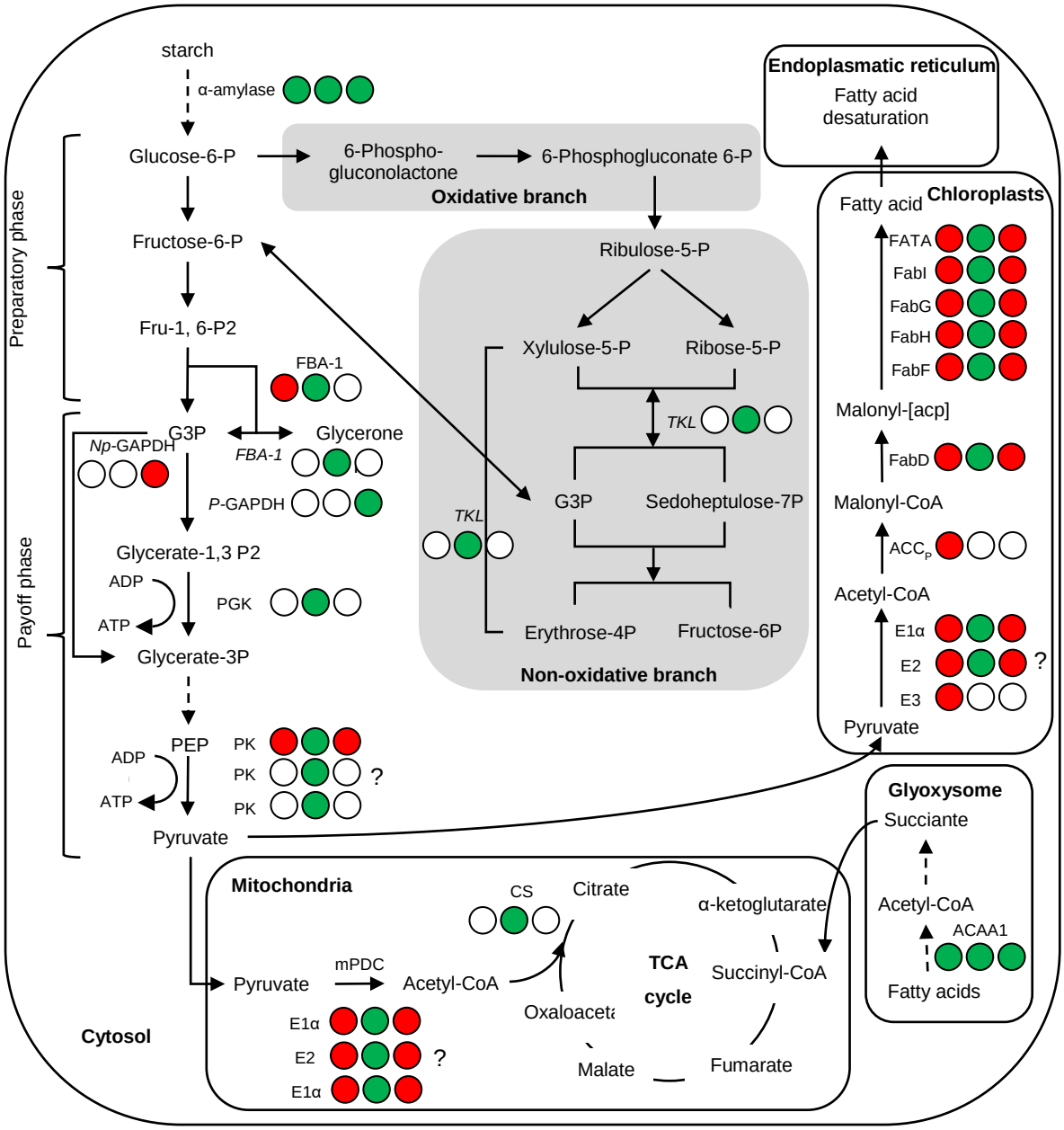

Figure 5: Schematic presentation of the major pathways of the carbohydrate and lipid metabolism during H. pluvialis cyst germination. Expression profiles of DEGs in the three phases of germination are shown with 1, 2, and 3 in a circle. A white background represents no significant difference; green presents up-, and red downregulation. [56].

Summarized for phase 1, the downregulation of fructose bisphosphate aldolase (FBA) and pyruvate kinase (PK) limit the provision of acetyl-CoA for the TCA cycle, which is compensated by fatty acid degradation in the glyoxysome. In addition to the low utilization of pyruvate in the chloroplast, the accumulation of acetyl-CoA in the glyoxysome indicate that these metabolites

are directed into the TCA cycle for the production of ATP, reduction equivalents and carboxylic skeletons.

In phase 2, there is probably an equilibrium between fatty acid synthesis and degradation since fatty acid synthesis in the chloroplast and fatty acid degradation in the glyoxysome are upregulated. In phase 3, most of the DEGs affecting the lipid metabolism are downregulated compared to those influencing the carbohydrate metabolism. This suggests a lower utilization of carbon intermediates and a diversion of carbon flux to carbohydrate metabolism to generate ATP and NADPH for zoospore release [56]. As shown in Figure 5, the *H. pluvialis* cyst germination represents a complex process [56]. To make cyst cell germination an interesting alternative to mechanical cell disruption, as many cyst cells as possible need to be transferred into a sporangium for zoospore formation in a minimum process time, and the internal astaxanthin content in the released zoospores should be kept constant. In previous studies, it was found that the nitrate content [19], the light intensity [20] and composition [12], the age of the cyst cells [21], as well as the type of mRNA stored during germination [56], influence the germination. Under phototrophic germination conditions, it was shown that a sharper decline of the intracellular astaxanthin content in the released zoospores was observed at higher compared to lower nitrate concentrations in the medium at identical light intensity [19]. Also, at higher compared to lower light intensities, usually more zoospores were released from the cyst cells [19, 20]. However, this is concomitant with a decrease in astaxanthin at higher compared to lower light intensities. In contrast to these results, an 20% increase in the intracellular astaxanthin content 12 hours and a decrease of 30%, 24 hours after the start of germination, was reported [18]. In addition, germination with blue light positively affects the number of zoospores released and their astaxanthin content compared to red or white light [12].

2.2.3 Biotechnological production of astaxanthin using *H. pluvialis*

Several commercial plants have been built for astaxanthin production from *H. pluvialis* since the past decades. Among those, Cyanotech Inc., USA, Mera Pharmaceuticals Inc., USA, Alga Technologies Inc., Israel, Fuji Chemical Industries Co. Ltd., Japan, and Parry Pharmaceuticals Inc., India, have established production facilities in the late 1990s and early 2000s [10]. As presented in Figure 6, the biotechnological astaxanthin production can be divided into the upstream and downstream process [1]. In the upstream process most companies usually use a two-step process for the cultivation of *H. pluvialis.* First, the biomass is cultivated phototrophically in photobioreactors in sunlight or using artificial light to reach high cell densities. After depletion of the nutrients, astaxanthin biosynthesis is further increased by photostress, which occurs either from artificial light or exposure to sunlight. This step takes place either in closed photobioreactors or open ponds [10].

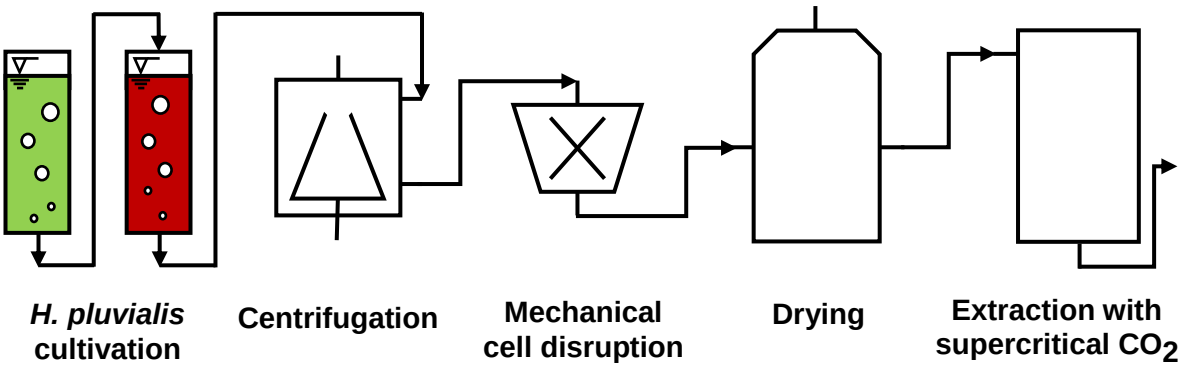

Figure 6: Schematically presentation of the biotechnological production of astaxanthin using the microalgae *H. pluvialis* [1].

In the first step of the downstream process the biomass is harvested by centrifugation to dewater the fermentation broth to 15-25% totals suspended solids (TSS) [14]. Afterwards, the cells are mechanically disrupted using high pressure homogenizers or bead mills. To achieve sufficient cell-wall disruption efficiency using high-pressure homogenization, up to three-cycle repetitions are required [15]. Spray-drying is commonly used in industry for drying of the disrupted *H. pluvialis* biomass. Due to the high evaporation enthalpy of water $h_{vap.}$ = 2442 kJ kg^{-1} at 25°C, it represents an energy-intensive process step. In spray drying, the risk of astaxanthin degradation due to oxidation or high temperatures exposure needs to be considered. Additionally, the biomass obtained after drying needs to show defined bulk densities for processing in the following supercritical CO_2 extraction. Astaxanthin extraction from the dried cyst cells is done by supercritical CO_2 extraction. Pressures up to 1000 bar are required to extract astaxanthin from *H. pluvialis*, via supercritical CO_2 extraction [17]. Due to high investment costs, this process step is usually performed off-site by an external contracted manufacturer [14, 17].

2.3 Liquid-liquid extraction

2.3.1 Liquid-liquid equilibrium

The thermodynamic equilibrium conditions for a closed system consisting of n phases and k components are defined as presented in the following Equations 2.1 to 2.3, where T is the temperature, p the pressure and μ_i the chemical potential of compound i [65].

Thermal equilibrium: $$T' = T'' = \ldots = T^n \quad (2.1)$$

Mechanical equilibrium: $$P' = P'' = \ldots = P^n \quad (2.2)$$

Chemical equilibrium: $$\mu_i' = \mu_i'' = \ldots = \mu_i^n \text{ ,(i=1…k)} \quad (2.3)$$

The chemical potential μ_i is the partial molar Gibbs energy G, as shown in Equation 2.4, where n_i are the moles of compound i at constant T and p and $n_i \neq n_j$.

$$\mu_i = \left(\frac{\partial G}{\partial n_i}\right)_{T,P,n_{j\neq i}}, (i=1\ldots k) \qquad 2.4$$

The relationship between the chemical potential and fugacity f_i for a compound i in any phase (solid, liquid, or gas) can be described as shown in Equation 2.5. There, f_i is the fugacity, f_i^0 is the standard fugacity at an arbitrary reference state and μ_i^0 the chemical potential at that reference state.

$$\mu_i = \mu_i^0 + RT \cdot \ln\left(\frac{f_i}{f_i^0}\right) \qquad 2.5$$

Under the assumption of identical reference states of two phases $f_i^{0,'}=f_i^{0,''}$ and $\mu_i^{0,'}=\mu_i^{0,''}$, the fugacity of compound i in both phases is identical (Equation 2.6).

$$f_i^{'} = f_i^{''}, (i=1\ldots k) \qquad 2.6$$

Instead of the concentration, the activity a_i of compound i is often used in liquid phase thermodynamic and is defined as presented in Equation 2.7. There, f_i^0 is the standard fugacity of the pure substance at a pressure P^0 at a temperature of T.

$$a_i(T, P, x_i) \equiv \frac{f_i(T, P, x_i)}{f_i^0(T, P^0)} \qquad 2.7$$

The activity coefficient γ_i can be calculated as presented in Equation 2.8, where a_i is the activity and x_i the molar fraction of component i.

$$\gamma_i = \frac{a_i}{x_i} \qquad 2.8$$

For the identical standard fugacity of a compound f_i^0 in both phases, the iso-fugacity criterion is simplified, as shown in Equation 2.9. Thus, the fugacity can be described via the mole fraction x_i and activity coefficients γ_i of the phases.

$$x_i^{'}\gamma_i^{'} = x_i^{''}\gamma_i^{''} \qquad 2.9$$

The distribution of component i between two phases is defined via the distribution coefficient K_i (Equation 2.10). At infinitive dilution of a compound i ($x_i^{'}$, $x_i^{''} \rightarrow 0$) between two phases, the distribution coefficient is constant. Consequently, the distribution coefficient can be described solely by the activity coefficent at infinitive dilution

$$K_i = \frac{x_i^{'}}{x_i^{''}} = \frac{\gamma_i^{''}}{\gamma_i^{'}} \qquad 2.10$$

The partition coefficient can also be defined using concentrations c_i of compund i, rather than mole fractions. Dividing the mole fractions by the molar volumes of the phases, the distribution coefficient K_i can be expressed as the partition coefficient P_i (Equation 2.11)

$$P_i = \frac{c_i^{'}}{c_i^{''}} = \frac{x_i^{'}v^{'}}{x_i^{''}v^{''}} = K_i\frac{v^{'}}{v^{''}} \qquad 2.11$$

The molar volume of the phases can be calculated as the weighted sum of the molar volume and the excess volume of mixing v^E (Equation 2.12). The partition coefficient depends on the pressure, the temperature, and the concentration of component i in the two-phase system [65].

$$v_{real} = v_{ideal} + v^E = \sum x_i v_{0i} + v^E \qquad 2.12$$

2.3.2 Liquid-liquid extraction

Liquid-liquid extraction is a process for separating a component i of a liquid feed mixture, (e.g. aqueous phase) by contact with a second liquid phase (e.g. organic solvent). It is used for a wide variety of applications in the chemical and pharmaceutical industry (e.g. in oil refineries to separate aromatics from aliphatic Hydrocarbons, in the food industry for the production of vitamins, and in biotechnology for the extraction of penicillin) [66, 67]. The process takes advantage of differences in the chemical properties of the feed components to separate them. This includes differences in polarity and hydrophobic/hydrophilic character, resulting in their different solubility in the two phases [66]. Transferring from one phase to the other, a solute i must overcome certain resistances, which includes the following steps: (1) movement from the bulk of the raffinate phase (e.g. aqueous phase) to the interface; (2) movement across the interface; and (3) movement from the interface to the bulk of the extract phase, as illustrated in Figure 7 [66]. The two-film theory, which was first used to model this process, assumes that motion in the two phases is negligible near the interface such that the entire resistance to mass transfer is contained within two laminar films on each side of the interface, and mass transfer occurs by molecular diffusion through these films. The thickness of the boundary layer is related to the hydrodynamics and the physical properties of the phase. Further, it is assumed that in the bulk phase the concertation is constant. The theory further assumes the following simplifications: First, the rate of mass transfer within each phase is proportional to the difference in concentration in the bulk liquid and the interface. Second, mass-transfer resistance across the interface itself is negligible, and the phases are in equilibrium at the interface. Third, steady-state diffusion occurs with negligible holdup of diffusing solute i at the interface. Within a liquid-liquid extractor, the rate of steady-state mass transfer between two phases, e.g. from an aqueous feed into a solvent, can be described as shown in Equation

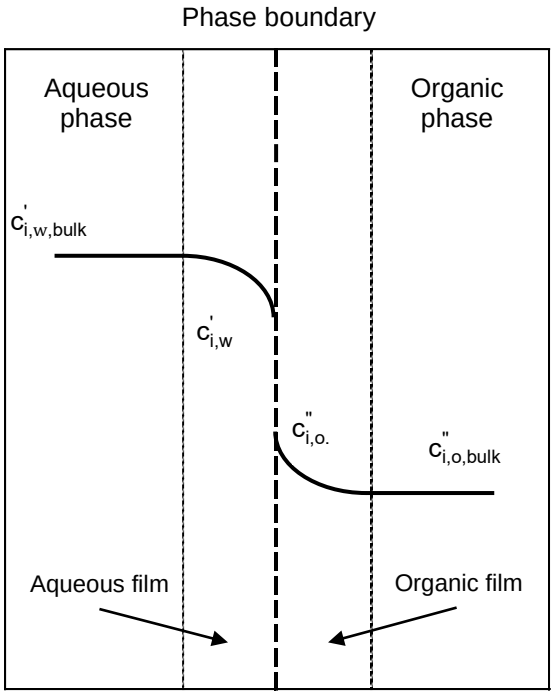

Figure 7: Film resistance and mass transfer between two immiscible liquids [69].

2.13 [66]. There, the aqueous bulk concentration of the solute is defined as $c'_{i,w,bulk}$ and $c'_{i,w}$ at the interface, and $c''_{i,o}$ is the interfacial concentration in the organic phase and $c''_{i,o\ bulk}$ in the organic bulk phase. There, $k_{i,w}$ and $k_{i,o}$ represent the individual mass transfer coefficients in the aqueous and organic boundary layer, and a is the interfacial area for mass transfer [66].

$$\dot{m}_i = a \cdot k_{i,w} \cdot \left(c'_{i,w,bulk} - c'_{i,w}\right) = a \cdot k_{i,o} \cdot \left(c''_{i,o} - c''_{i,o,bulk}\right) \qquad 2.13$$

At the interface the two phases are in equilibrium and the concentration of the solute $c'_{i,w}$ and $c''_{i,o}$ are correlated via the partition coefficient P_i (Equation 2.14) [68].

$$P_i = \frac{c''_{i,o}}{c'_{i,w}} \qquad 2.14$$

Rearranging and eliminating the interfacial concentrations $c'_{i,w}$ and $c''_{i,o}$ in Equation 2.13, the overall aqueous-phase mass transfer coefficient K_W can be defined as shown in Equation 2.15 [68, 69].

$$\frac{1}{a \cdot K_W} = \frac{1}{a \cdot k_{i,w}} + \frac{1}{a \cdot P_i \cdot k_{i,o}} \qquad 2.15$$

For $P_i >> 1$, the mass transfer of the solute is limited by the aqueous phase boundary layer, and the organic phase resistance can be neglected. Thus, the mass transfer coefficient K_W can be defined as presented in Equation 2.16 [68].

$$\frac{1}{a \cdot K_W} = \frac{1}{a \cdot k_{i,w}} \qquad 2.16$$

The mass transfer of solute i in the boundary layers of the organic and aqueous phase is a diffusive process. Laminar boundary layer and turbulent phase interior cannot be strictly separated from each other. They constantly merge into one another. The boundary layer thickness is therefore only a formal reference value. The mass transfer coefficient K_W depends on the flow condition (free flow vs. forced flow), from the geometry of the extraction unit and the material properties of the fluid phase. The calculation of K_W is possible with the help of dimensionless numbers such as the Sherwood number Sh, the Schmidt number Sc, Reynolds number Re [28]. As shown in Equation 2.17, the Sherwood number (Sh) is the ratio of the mass transfer via convection to diffusion, where k and D presents the individual mass transfer and diffusion coefficient within the boundary layer. L is the characteristic length.

$$Sh = \frac{kL}{D} = \frac{\text{convective mass transfer}}{\text{diffusive mass transfer}} \qquad 2.17$$

The Reynolds number (Re) presents the ratio of inertial forces to viscous forces. It is defined as shown in Equation 2.18, where v is the fluid velocity, L is the characteristic length, ρ the density, and η the fluid dynamic viscosity.

$$Re = \frac{vL\rho}{\eta} = \frac{\text{inertia forces}}{\text{viscous forces}} \qquad 2.18$$

The Schmidt number (Sc) is the ratio of the viscous to the molecular diffusion rate (Equation 2.19). It purely depends on material properties, the dynamic viscosity η, the diffusion coefficient D, and the density of the fluid ρ.

$$Sc = \frac{\eta}{D\rho} = \frac{\text{viscous diffusion rate}}{\text{molecular diffusion rate}} \qquad 2.19$$

According to Wilke and Chang, the diffusion coefficient D of diluted solution is defined and presented in Equation 2.20 [70]. There, T describes the absolute temperature, α is the association parameter, M the molecular weight of the solvent, η the dynamic viscosity of the solvent, and v_n the molar volume of the solute. For non-associated solvents such as *n*-heptane or ethyl acetate, α=1, while α=2.6 for water [71].

$$D = \frac{7.4 \cdot 10^{-8} T \sqrt{\alpha M}}{\eta v_n^{0.6}} \qquad 2.20$$

The mass transfer $\dot{m}_i$ can be expressed as presented in Equation 2.21. There, K_W is the overall mass transfer coefficient, and a is the specific area for mass transfer. The driving force of the extraction correlates with the concentration difference of the solute i in the two phases and the partition coefficient P_i [69].

$$\dot{m}_i = K_w \cdot a \cdot \left(c'_{i,w,bulk} - \frac{c''_{i,o,bulk}}{P_i} \right) \qquad 2.21$$

The selection of the extraction unit depends on many factors, including the required number of theoretical stages, residence time (depending on the extraction kinetics or limited stability of the solute), production rate, contamination tolerance, ease of cleaning, the availability of necessary building materials as well as the ability to cope with high or low interfacial tension, density differences and viscosities. Another important criteria is the ability to process feed mixtures containing particles (e.g. cells). Other factors affecting the choice of the extractor include familiarity and tradition (the preferences often different between designers and operators), trust in the scale-up, height restrictions, and of course, the relative capital and operating costs. Additionally, the flexibility of the extractor to adapt to changes in the feed properties can also play an important role [66]. The most commonly used extractors are static extractors (spray column, baffle column, packed column, and sieve tray column), mixer settler, rotary-agitated column (rotary disc contactor, asymmetric disc contactor, Oldshue-Rushton column, Scheibel, and Kühni column), reciprocating-plate column (Karr column), pulsed columns (packed or sieve tray column) and centrifugal extractors [66]. Figure 8 provides a decision guide for the selection of the extraction unit. Centrifugal extractors can facilitate a liquid-liquid extraction process by reducing diffusion path lengths (boundary layers). They enable the processing at very low liquid residence time and high specific throughput. Many extractor types are available, ranging from relatively simple devices used primarily for phase separation or for single-stage liquid-liquid contacting with separation to more complex

machines designed to provide the equivalent of multistage liquid-liquid contacting within a single unit. Some machines are designed to handle feeds containing solids such as whole fermentation broth [67] [72].

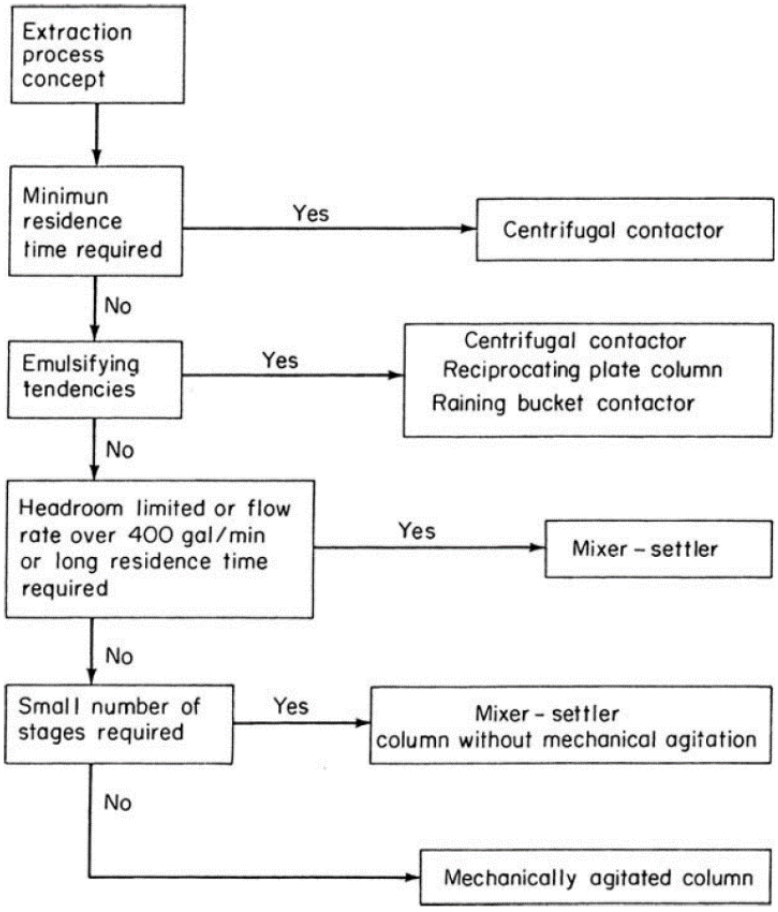

Figure 8: Decision guide for the selection of liquid-liquid extraction separators [66].

The original Sichelmair plot in Figure 9 compares conventional extractors, plotting the stage efficiency per meter vs the capacity (flow per cross-sectional area) [73]. This comparison was expanded by Visscher, including centrifugal extractors such as Rousselet-Robatel, Podbielniak, CINC, and a spinning disc extractor [72]. As can be seen, these tend to have lower efficiency stages per meter and capacities compared to conventional extractors. High-efficiency stages per meter reached with the spinning disc extractor go along with low capacities. In Figure 10, the extractors used in this work, membrane contactor and a CPE unit, are schematically presented. LLC units have already been used for the extraction of fermentation broth, such as ß-carotene from the microalgae *Dunaliella salina* [25]. Additionally, its application as an extraction unit was shown to directly extract torularhodin from the yeast *Rhodotorula rubra* [24]. LLC are characterized by a high number of theoretical separation stages, which can range from 50 to 800 depending on the column design [74]. For the CPE column used in this work (243 mL column volume), around 200 theoretical separation stages have been reported at a flow rate of 85 mL min^{-1} [74]. This results in efficiency stages per meter of around 2000 for the length of the CPE column used in this work of around 0.1 m. However, a significantly lower capacity of 33 m^3 $m^{-2}h^{-1}$ can be expected for the geomeomerty of the used CPE column (A=0.0154 m^2 for r=0.07 m) and a flow rate of 85 mL min^{-1}, compared to the extraction units presented in Figure 9.

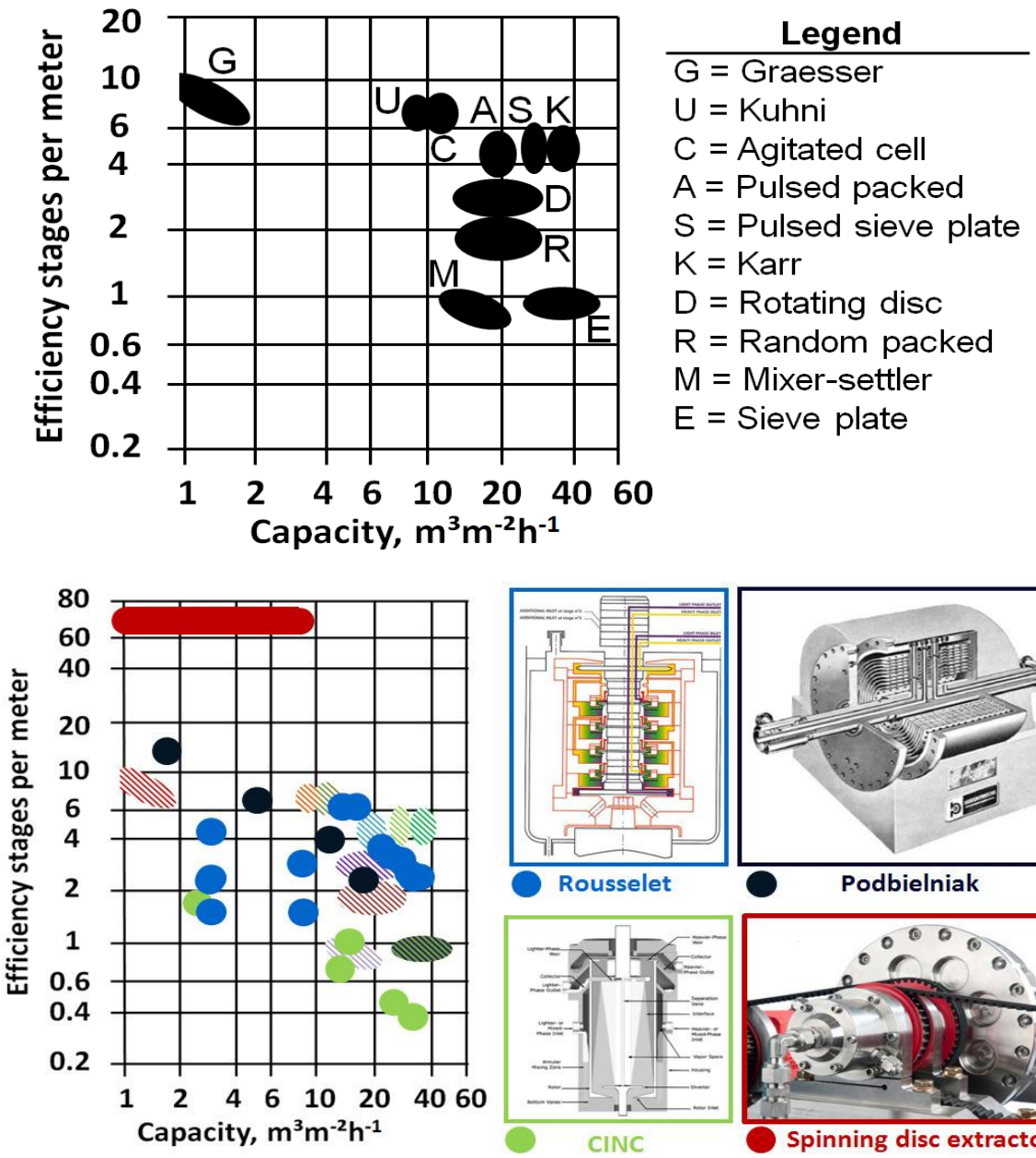

Figure 9: Left: Original Stichlmair plot, showing the number of efficiency stages per meter vs. the capacity [73].
Right: Stichlmair plot including centrifugal extractors Rousselet, Podbielniak, CINC, and a spinning disc extractor [72].

Membrane contactors have already been used for the extraction of fermentation broth, e.g. carboxylic acids from *Lactobacillus plantarum* [29]. HTU (height of transfer unit) values between 0.21 to 2.17 m have been reported for membrane-assisted extraction [27]. Considering the length of the used membrane contactors of around 16 cm, this would result in efficiency stages per meter of 8 to 88. For the geometry of the contactor used in that work

(r_{shell}= 0.0031 m and flow rates between 5 to11 mL min^{-1}), a capacities between 9 to 21 m^3 $m^{-2}h^{-1}$ were reached.

This shows that the CPE column used in this work operate at the extreme points of available extraction columns, extremely high efficiency per meter and very low capacity. These properties can be advantageous when a high number of theoretical stages are required. That

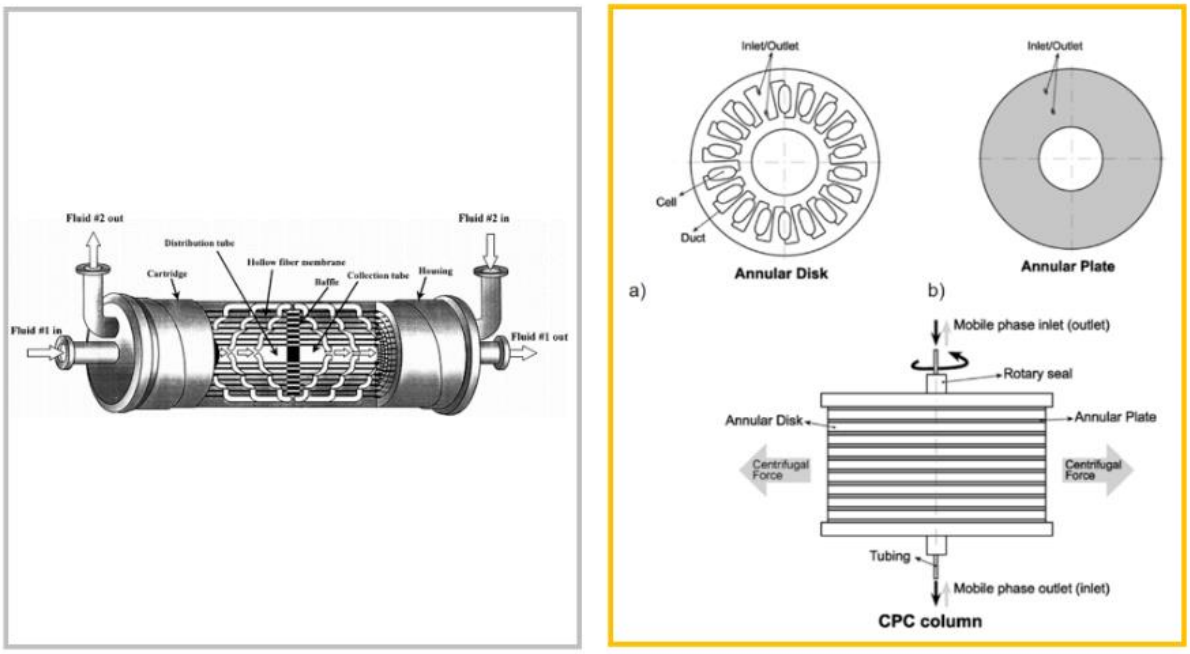

Figure 10: Schematic presentation of a membrane contactor [28] and a CPE column [78].

is the case when the kinetics of mass transfer limit the establishment of the partition equilibrium. This could be the case when extracting astaxanthin from *H. pluvialis* algal broth, since the presence of the cell matrix limits might limit the mass transfer. In contrast, membrane extractors operate at the lower range of the efficiency stages per meter, and an average capacity compared to the other extractors. A low number of efficiency stages is sufficient when there is a high partition coefficient of the component to be extracted. This could be the case for the partition coefficent of astaxanthin between an aquoeus feed and solvent.

In the following Sections 2.4 and 2.5 the theoretical background of membrane contactors and liquid-liquid chromatographic units will be presented in further detail.

2.4 Liquid-liquid chromatography

2.4.1 Principles of liquid-liquid chromatography

Liquid-liquid chromatography (LLC) is a solid support-free chromatographic method in which two liquid phases in thermodynamic equilibrium are used as mobile and stationary phases. The two liquid phases are obtained by mixing at least two solvents [75, 76]. One of the two phases is kept stationary in the column of the LLC through a centrifugal field. The second mobile phase is pumped through the column filled with the stationary phase. The solutes are

separated due to their different partition coefficient between the two phases. Those with lower values of P move faster through the column than those with higher values, therefore exit the column at different times and can be separated [77].

Unlike solid-liquid chromatography, LLC allows choosing not only the composition of the mobile but also that of the stationary phase. However, once selected, the composition of one phase cannot be changed independently of the composition of the other phase. In operation, usually, about 60-80% of the column volume is filled with the stationary phase. The entire column volume is available to the solute, allowing high sample loadings [22]. Due to the liquid nature of the stationary phase, it can be pumped out column and non-eluting components with a P value larger than 100 can be recovered, allowing high recovery. In addition, either phase of the two-phase system can be used as a mobile or stationary phase, and their role can be changed during operation.

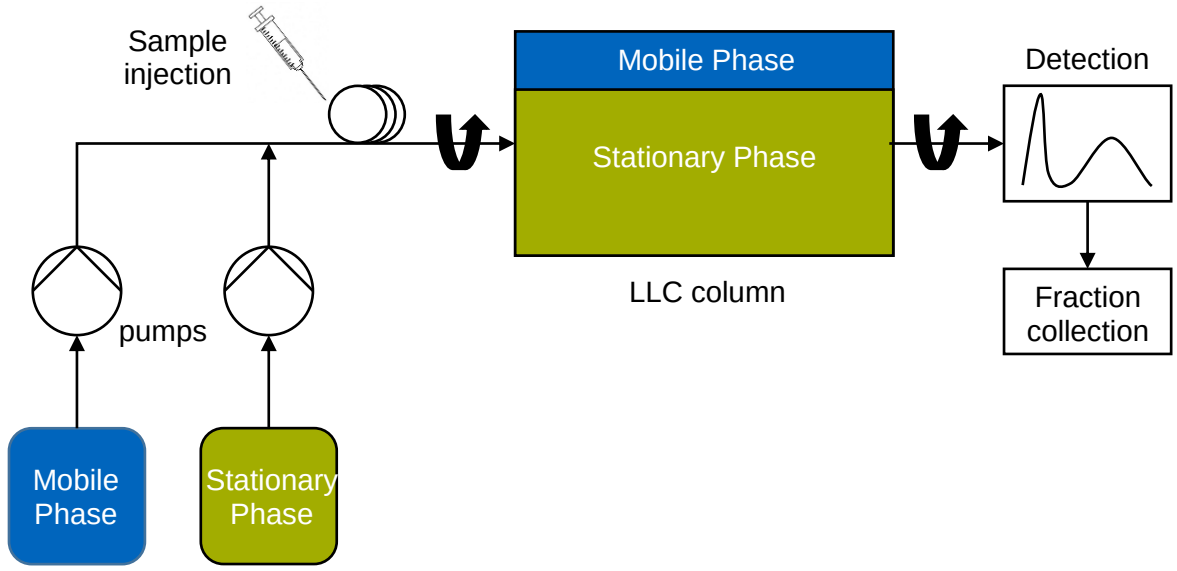

Figure 11: Schematic presentation of the liquid-liquid chromatographic set-up.

As presented in Figure 11, the set-up of an LLC system is similar to that of a solid-liquid system except that for classical cylindrical column packed with solid porous stationary phase, a hydrodynamic or hydrostatic column is installed (Section 2.4.2). All other pieces of equipment, including pumps, injection valve, detector, fraction collector, and software, are identical. For operation, the LLC unit is filled with one of the phases, which will act as the stationary phase. After that, the rotation is set, and the second phase, the mobile phase, is pumped. Depending on the set flow rate, a certain amount of the stationary phase will be displaced from the column until the hydrodynamic equilibrium is reached, and no more stationary phase elutes from the column. Subsequently, the solutes, dissolved in one of the phases, can be injected by means of a sample loop. In the classical elution mode, the solutes are pumped through the LLC column with the mobile phase and are separated according to their partition coefficient.

In this work, LLC was not used for chromatographic separation of solutes, but extraction of one target compound with a partition coefficient $P_i>>1$, which means that the target compound is not eluted from the column but retained in the stationary phase.

The volume fraction of the stationary phase V_{SP} in the column V_c is called stationary phase retention S_f and it is defined with Equation 2.22. S_f is a function of the flow rate of the mobile phase, the centrifugal field, the column geometry, and the physical properties of the two liquid phases [22].

$$S_f = \frac{V_{SP}}{V_c} \qquad 2.22$$

The retention volume $V_{R,i}$ of a component i can be calculated in the linear range of the partition equilibria as shown in Equation 2.23, where P_i is the partition coefficient, V_{SP} and V_{MP} are the stationary and mobile phase volumes, respectively.

$$V_{R,i} = V_{MP} + P_i V_{SP} = V_c[(1-S_f)+S_f P_i] \qquad 2.23$$

Dividing Equation 2.23 by the flow rate of the mobile phase F_{MP}, the retention time $t_{R,i}$ of the solute i can be determined. For chromatographic separations, biphasic solvent systems are chosen with partition coefficients of the target compounds in the range of the so-called sweet spot between 0.4 and 2.5, whereas for extraction partition coefficients $P_i>>1$ for the target compound is highly desirable [78].The mean residence time τ_x of the mobile phase, can be expressed as the quotient of the volume of the mobile phase V_{MP} to the mobile flow rate F_{MP} (Equation 2.24).

$$\tau_x = \frac{V_{MP}}{F_{MP}} \qquad 2.24$$

2.4.2 Hydrodynamic and hydrostatic column design

In addition to selecting the biphasic solvent system (i.e. the mobile and stationary phase) and the operating conditions such as flow rate and rotational speed, the column design in LLC is also crucial for separation success [79]. In LLC, a distinction is made between hydrostatic and hydrodynamic columns [22].

Hydrodynamic columns were invented in 1966 by Ito and are known as countercurrent chromatography (CCC) units [80]. In principle, these consist of a tube (coil) wound on a bobbin, which rotates around the axis of rotation with an angular velocity ω. In addition, the axis of rotation orbits the axis of revolution in planetary motion (Figure 12 a). One of the two phases is kept stationary in the CCC through a centrifugal field, while the second mobile phase is pumped through the unit. Regarding the rotation of the two axes, a distinction can be made between the I-type and J-type CCC, with the rotation of the axes in the former being in counter-rotation and the same rotation in the latter. The most widely used CCC units are of the J-Type (Figure 12 a). The planetary motion of the coil leads to a centrifugal force with variable

direction and magnitude along with the coil, resulting in mixing and settling zones. The phases mix in zones with low centrifugal force, whereas settling occurs in zones with high centrifugal force. The mixing and demixing zones in the column are shown in Figure 12 b and c [79].

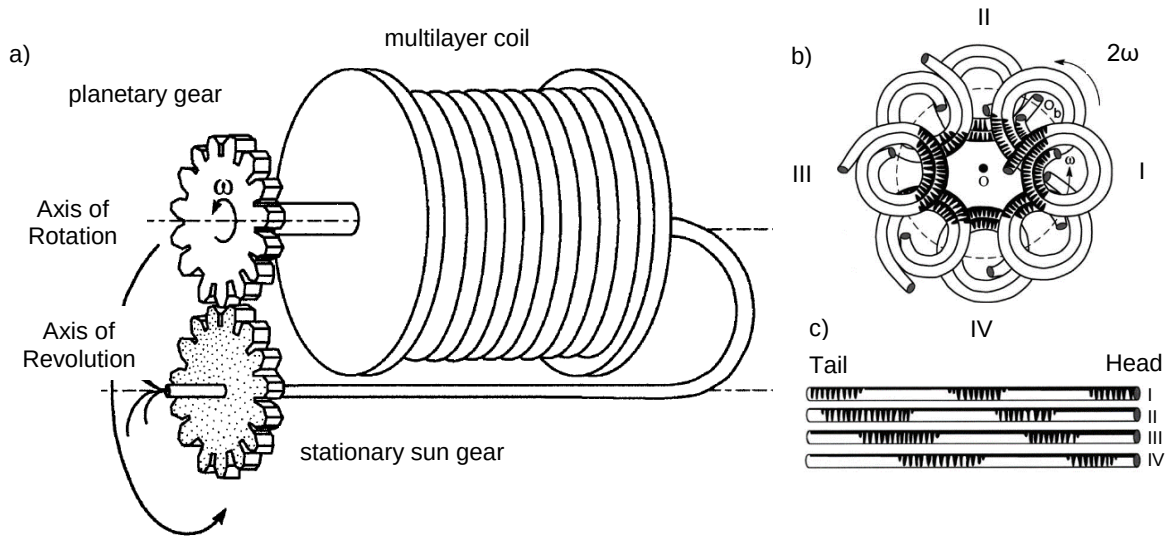

Figure 12: a) Type-J hydrodynamic column. b) Column position during one rotation around the axis of Revolution, including mixing (black) and settling zones (white). c) Illustration of the mixing and settling zones along the unwounded tube [79].

The schematic design of a hydrostatic column, which is also called centrifugal partition chromatography (CPC), is shown in Figure 13.

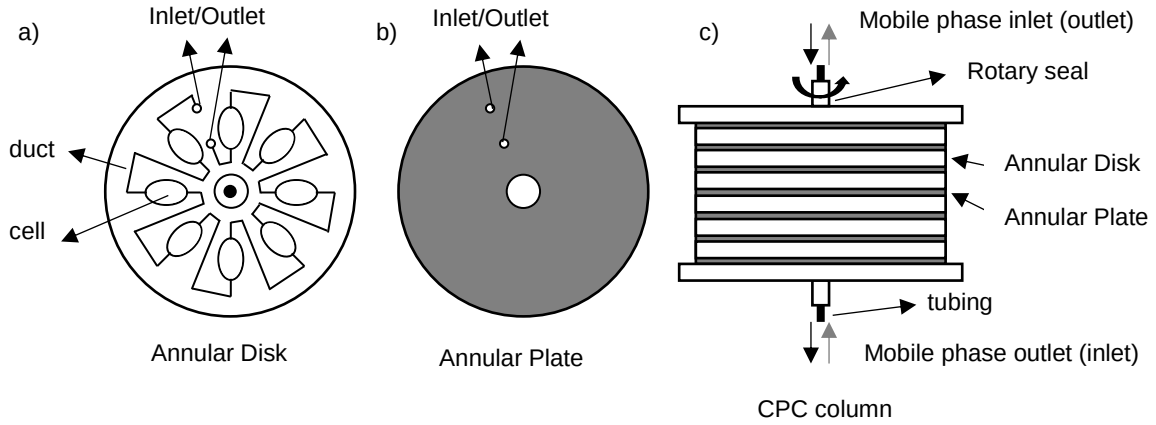

Figure 13: a) Annular disk with cells connected by ducts, b) Annular plates, c) CPC column constructed from stacked annular disk and plate.

In contrast to CCC columns, these have only one axis of rotation, which generates a centrifugal field and keeps one of the phases of a biphasic system stationary in the column. In CPC units, annular disks and plates are stacked on top of each other, allowing the total volume of the column to be adjusted by the number of disks. In each annular disk, the cells are connected by short channels (ducts). The mixing and settling of the two phases occur in the annular disk cells, whereby the ducts are only filled with mobile phase and hence do not contribute to mass transfer between the two liquid phases. The mixing and settling of the

phases in the cells occur due to the centrifugal force and the flow rate of the mobile phase. The mixing zones are at the entrance, the settling zones at the end of each cell [81, 82]. Different CPC column designs exist, which vary in the shape, size and number of chambers and enable application depend selection according to efficiency or high through put [25, 83].

2.4.3 Hydrodynamic properties of LLC columns

The hydrodynamics of LLC columns influence the mass transfer between the biphasic system and the stationary phase retention. Differences in flow regimes are a result of different geometries, which are fundamentally different between the hydrodynamic and the hydrostatic columns. As presented in Figure 12, the whole column volume participates in the separation in CCC columns, as no interconnecting ducts or channels reduce the effective column volume. The mixing and settling zones within the CCC coil, and the hydrodynamic motion are similar to the Archimedean screw effect [80]. This continuous contact between the mobile and stationary phase results in higher column efficiency of CCC compared to CPC columns. This continuous contact between the mobile and stationary phase results in a higher column efficiency of CCC compared to CPC [84].

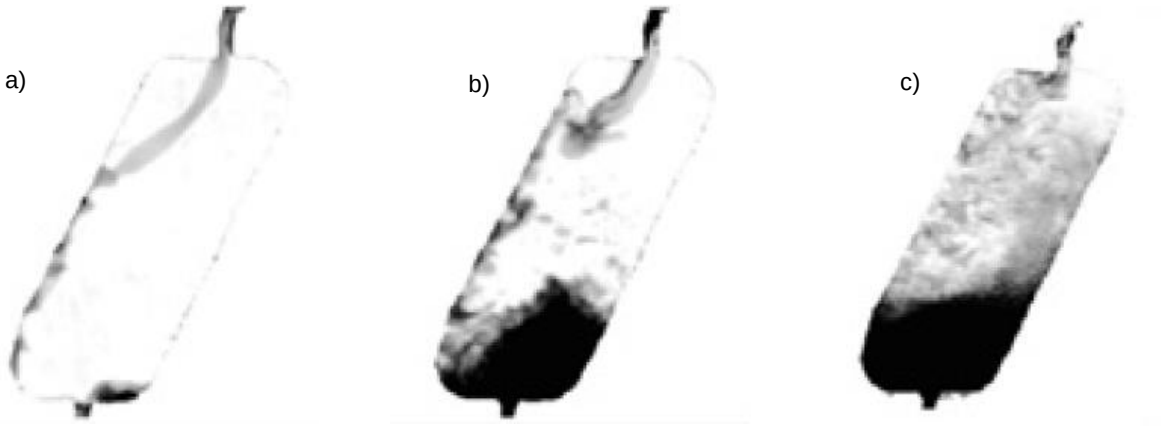

Figure 14: Flow regimes in CPC cells: a) stuck film, b) oscillating sheet and c) atomization. White represents the stationary phase, grey the two phases in contact and black the mobile phase in descending mode [81].

As shown in Figure 14, a subdivision into three flow regimes can be done in CPC: a) stuck film, b) oscillating sheet, and c) atomization [81, 82]. The flow regime properties change from stuck flow to atomization dispersion with an increase of the mobile phase flow rate and the rotational speed. Higher dispersion of the mobile in the stationary phase results in higher separation efficiencies [85]. The increase of the contact area, which also depends on the interfacial tension between the mobile and stationary phase, will increase the settling time of the two phases. This can result in “column bleeding” and loss of stationary phase. In hydrodynamic equilibrium, the residence time of the mobile phase within one cell and the settling time of the mobile and stationary phase are identical [78]. In the case of the extraction from a fermentation broth, the hydrodynamics within the LLC will additionally be effected by

the injected cell matrix, resulting in emulsification and stationary phase loss. Additionally, possible cell deposit in the chambers of the CPC column need to be considered. Thus, for an optimal mass transfer for the extraction of a target compound using LLC, the mobile phase flow and rotational speed should be optimized for the chosen biphasic system [24].

2.4.4 Operating modes

In addition to changing the pumping direction of the mobile phase, in LLC it is also possible to change the role of the two liquid phases in the course of the process.

Since two phases of the biphasic system can be used as stationary or mobile phases, two elution modes exist. In the ascending mode (ASC), also called "tail-to-head", the upper phase (UP) of the biphasic solvent system is used as a mobile phase, and the lower phase (LP) is the stationary phase. In descending mode (DES), also called "head-to-tail", the lower phase is the mobile phase, and the upper phase is the stationary phase. The lower phase is usually the more hydrophilic phase in the organic-aqueous systems used. Accordingly, the partition coefficient P_i in the ASC and DES elution mode can be defined as shown in Equations 2.25 and 2.26, respectively [86].

$$P_{i,ASC} = \frac{c_{LP,i}}{c_{UP,i}} \qquad 2.25$$

$$P_{i,DES} = \frac{1}{P_{i,ASC}} \qquad 2.26$$

In the LLC, changing the elution mode without changing the flow direction of the mobile phase and vice versa results in the displacement of the stationary phase from the column. Moreover, changing the elution mode also changes the elution order of the components, which can be explained via the inverse correlation between $P_{i,ASC}$ and $P_{i,DES}$ (Equation 2.26) [22], [87].

In LLC separation, these two modes can be used to reduce the processing time for the separation of two components with a very high and low P_i value.

In the back extrusion mode, shown in Figure 15 a, the classical elution mode is first performed, followed by an extrusion step. For displacement of the stationary phase, the pumping direction of the mobile phase is changed. The change in the flow direction of the mobile phase results in a disturbance of the hydrodynamic balance, which prevents the stationary phase from remaining inside the column. After the displacement of the stationary phase, only the mobile phase elutes [86]. The solutes with higher partition coefficients thus elute first. Thus, if the solute with the higher partition coefficient is of interest, back-extrusion is the preferred mode of operation. The described phenomena of back-extrusion were described for CCC units [87]. A different behaviour might occur in the cells of the CPC compared to CCC columns due to other hydrodynamic properties. Thus, it might be that the two phases do not entirely separate before extrusion and the stationary phase in the cells is only partially discharged. That could

lead to the co-elution of the components in a mixture of the two phases. [88].

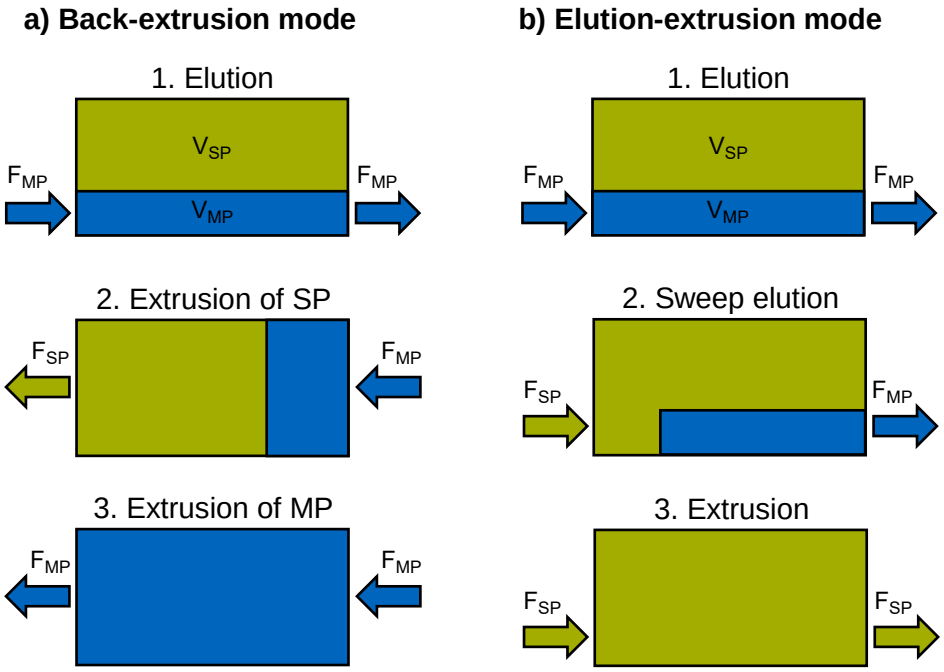

Figure 15: Schematic presentation of (a) the back-extrusion and (b) the elution-extrusion mode in LLC.

In elution-extrusion mode, after the performance of the classical elution mode, the stationary phase is pumped in the same direction instead of the mobile phase. After the collapse of the hydrodynamic equilibrium, the mobile phase elutes first (sweep elution), followed by the stationary phase in the extrusion step [89]. During the displacement of the mobile phase volume, some compounds might still undergo separation in the part of the column where both phases are present, while others are already overtaken by the stationary phase front. Theoretically, the compounds elute with the resolutions reached inside the column. If the whole spectrum of solutes with a broad range of partition coefficients is of interest, elusion-extrusion is the preferred operating mode [86]. In addition, elusion-extrusion extends the recommended value of the partition coefficient for the separation from $0.25<P_i<16$ [23]. Another advantage of elution-extrusion over back-extrusion is that the column will be filled with the stationary phase at the end of the extrusion.

Extractive back extrusion mode of operation has already been used in the literature to recover nonpolar components from algae and yeast cells [24, 25]. In this work (Section 4.2.2.4), back-extrusion and elusion-extrusion were examined for fractioning the stationary phase after extraction of astaxanthin from the *H. pluvialis* broth. [23]. The aim was to gain the astaxanthin-containing stationary phase fractions free of aqueous mobile phase. This is essential to avoid further phase separation of the fractioned stationary phase from the aqueous phase before evaporation of the solvent.

2.5 Membrane-assisted extraction

In addition to LLC, membrane-assisted extraction was also examined as an extraction technology. In the following, the principle of membrane-assisted extraction is described in more detail.

2.5.1 Principles of membrane-assisted extraction

Membrane-assisted extractor are usually implemented as a hollow fibre membrane (Figure 16) or flat sheets. Hollow fibre modules usually have a shell housing in which the membrane fibres are incorporated. The two phases flow on the opposite sides the membrane, and a liquid-liquid interface is formed at the mouth of the membrane pores [28].

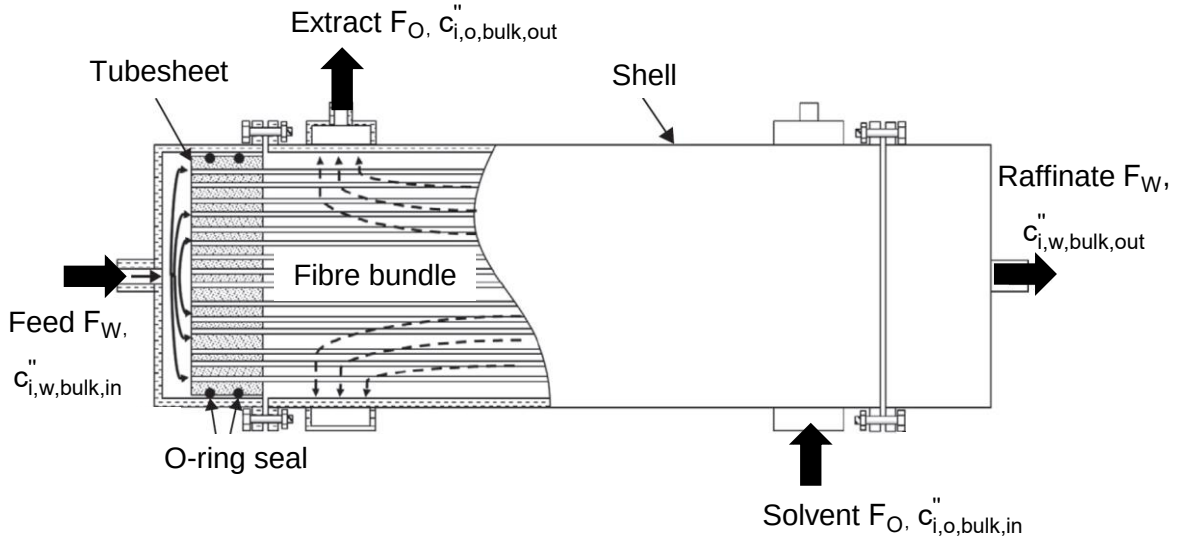

Figure 16: Schematic presentation of hollow fibre membrane module operated in counter-current mode [28].

A slight overpressure on the side of the non-wetting phase is required to stabilize the liquid-liquid interface in the mouth of the pore (Figure 17). When a hydrophobic PTFE membrane is used as in the case of extraction of astaxanthin from *H. pluvialis* algal broth into a solvent, the aqueous phase is the non-wetting phase, and the organic solvent is the wetting phase. Membrane contactors show a variety of advantages over classical extractors, allowing independent selection of the solvent to feed ratio, enabling high feed to solvent ratios during operation. In membrane-assisted extraction, the interfacial area of the two phases is constant and only depending on the available membrane area and pore size. Therefore, in contrast to conventional extractors, the mass transfer coefficient can be expressed separately from the interfacial area [69]. Since there is no dispersion of the two liquid phases, no formation of emulsions occurs. Additionally, only low-density differences between the phases are required for membrane extraction. In contrast, emulsification of the phases can occur using conventional extractors when liquids with a low-density difference are used. Membrane contactors can easily be scaled up linearly by increasing the number of membrane modules.

They can be used for aseptic applications, which is particularly advantageous for biotechnological processes. The fermentation broth can be guided on one side of the membrane and recirculated into the fermenter. Compared to dispersive contractors, significantly higher efficiency (height of transfer unit, HTU) can be achieved [28]. However, membrane contactors also have disadvantages compared to conventional extractors. The diffusion of the target components through the membrane pore represents an additional diffusive transport resistance, which is however not necessarily the transport-limiting step [27]. Shell-side bypass effects often occur in membrane contactors, which result in a loss of efficiency and usually appear at the scale-up from the laboratory to the industrial units. Membrane fouling mainly occurs during extraction from fermentation broths and reduce the mass transfer [28].

In principle, the mass transfer from the aqueous to the organic phase is identical to the film theory presented in Section 2.3.2, but extended by the additional resistance of the membrane [90]. The concentration profile for the extraction of a solute i from an aqueous feed bulk into an organic solvent bulk using a hydrophobic membrane is shown in Figure 17 b [28].

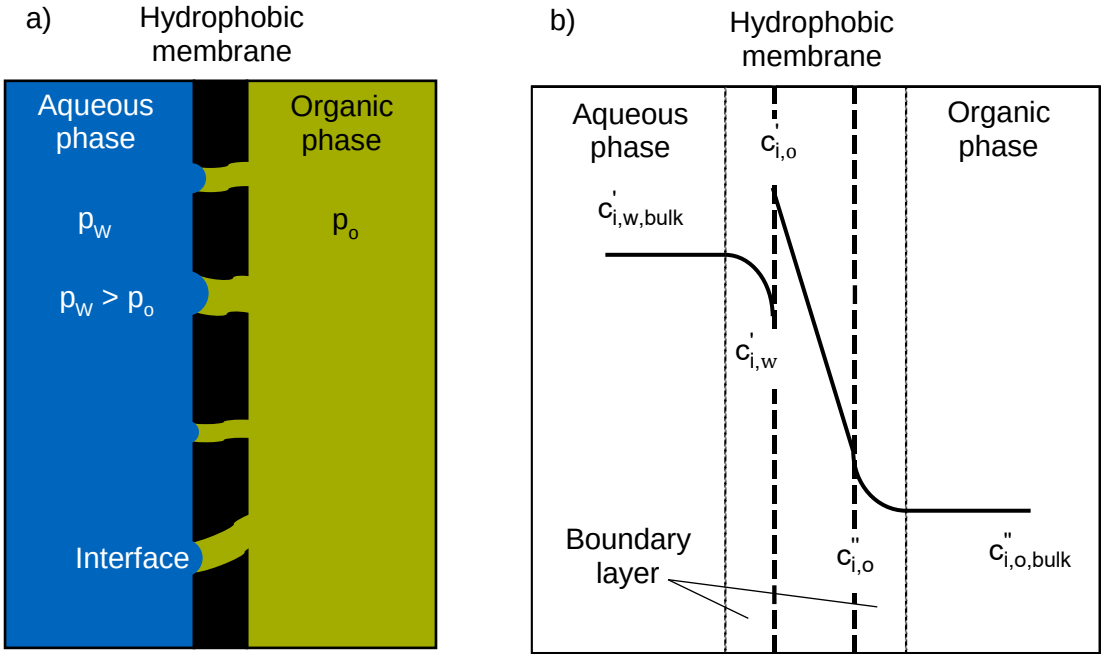

Figure 17: Schematic concentration of the wetting of a hydrophobic membrane (a) and the concentration profile for the extraction of a target compound i from an aqueous phase into an organic phase using membrane-assisted extraction (b) [28].

The overall aqueous mass transfer coefficient K_W for the extraction of a solute from the aqueous to the organic phase, using a hydrophobic membrane, pumping the organic phase on the shell side and the aqueous inside the fibres can be calculated as shown in Equation 2.27. In the resistance-in-series model $k_{w,f}$, $k_{o,m}$ and $k_{o,s}$ represent the individual mass transfer coefficients for the aqueous boundary layer in the fibre, the membrane wetted

with the organic phase, and the boundary layer of the organic phase of the shell side. The abbreviation of the inner, mean, and outer diameter of the fibre are d_i, d_{lm} and d_o.

$$\frac{1}{K_W d_i} = \frac{1}{d_i k_{w,f}} + \frac{1}{d_{lm} P_i k_{o,m}} + \frac{1}{d_o P_i k_{o,s}} \qquad 2.27$$

When the aqueous phase is pumped on the shell side and the organic phase inside the fibres, K_W value can be calculated as presented in Equation 2.28.

$$\frac{1}{K_W d_o} = \frac{1}{d_o k_{w,s}} + \frac{1}{d_{lm} P_i k_{o,m}} + \frac{1}{d_i P_i k_{o,f}} \qquad 2.28$$

For P_i>>1 and a hydrophobic membrane, the resistance of the boundary layer of the organic phase and the membrane can be neglected (Figure 17) and is only depending on the mass transfer resistance of the aqueous phase boundary layer as presented in Equation 2.29.

$$\frac{1}{K_W d_o} = \frac{1}{d_o k_{w,s}} \qquad 2.29$$

The individual mass transfer coefficient of component i in the boundary layer of the fibre can be calculated using the Lévèque equation. The mass transfer coefficient in the boundary layer of the fibre can be calculated according to Equation 2.30 [28, 69], where D is the diffusion coefficient of the compound i in the boundary layer, d_i the inner fibre diameter, v the flow velocity inside the fibre, and L the fibre length.

$$k_f = 1.62 \cdot \frac{D}{d_i} \left(\frac{d_i^2 v}{LD} \right)^{\frac{1}{3}} \qquad 2.30$$

Equation 2.30 describes the mass transfer for a flow range with the Graetz (Gz) number>4 with sufficient accuracy but is imprecise for Gz<4 and overestimates the mass transfer. The Graetz number is calculated according to Equation 2.31, where v is the flow velocity, d_i the inner diameter of the fibre, D the diffusion coefficient in the boundary layer and L the fibre length [91].

$$Gz = \frac{v \cdot d_i^2}{D \cdot L} \qquad 2.31$$

While the fibre flow is well understood, the shell-side stream mass transfer description represents a procedural challenge due to many possible module constructions (packing density, module length, design, etc.). A possible expression, for the description of the shell-sided mass transfer coefficient, valid for 0<Re>500 and a packing factor 0.04<ϕ<0.4, is shown in Equation 2.32. The parameter β is 5.8 for hydrophobic and 6.1 for hydrophilic membranes [91].

$$k_s = \beta \frac{D}{L} (1-\phi) Re^{0.6} Sc^{0.33} \qquad 2.32$$

The mass transfer through the membrane pores can be calculated as presented in Equation 2.33, where d_i and d_o are the inner and outer diameter of the fibre, D the diffusion

coefficient of compound i through the pore membrane, and ε and τ are the membrane porosity and tortuosity, respectively [69].

$$k_m = \frac{2\varepsilon D}{\tau(d_o - d_i)} \qquad 2.33$$

For the extraction of a solute from an aqueous feed into a solvent, the characteristic length L corresponds to d_i in case the aqueous phase is pumped in the fibres and to the hydrodynamic diameter d_h in case it is pumped on the shell side (Equation 2.34). There, d_o is the outer diameter of one fibre, A_{shell} and A_{fibres} the cross-sectional areas of the shell and all fibres, respectively [26].

$$d_h = d_h \frac{A_{shell} - A_{fibres}}{A_{fibres}} \qquad 2.34$$

2.5.2 Experimental determination of the mass transfer coefficient

The overall solute balance for a membrane extractor operated in counter-current mode can be expressed as presented in Equation 2.35. There, $c'_{i,w,bulk,0}$ and $c'_{i,o,bulk,0}$ are the initial solute concentrations of compound i in the aqueous and organic phase, $c''_{i,w,bulk}$ and $c''_{i,o,bulk}$ the solute concentrations in the aqueous and organic phase during extraction, and V_W and V_O represent the volume of the aqueous and organic phases, respectively.

$$V_O \cdot \left(c''_{i,o,bulk,0} - c''_{i,o,bulk}\right) = V_W \cdot \left(c'_{i,w,bulk,0} - c'_{i,w,bulk}\right) \qquad 2.35$$

Additionally, the time course of the extraction of component i from one phase into another phase can be calculated using Equation 2.36. Here, V_W and F_W are the volume and the flow rate of the aqueous phase. The module efficiency E_{ff} represents the ratio between mass of solute exchanged through the module and the assumed exchanged solute when the incoming solvent stream is in equilibrium with the outgoing aqueous feed [90].

$$V_W \cdot \frac{c'_{i,w,bulk}}{dt} = -F_W E_{ff} \left(c'_{i,w,bulk} - \frac{c''_{i,o,bulk}}{P_i}\right) \qquad 2.36$$

After integration of Equation 2.36 and inserting of Equation 2.35, Equation 2.37 is derived.

$$\underbrace{\ln\left[\left(1+\frac{1}{R}\right)\frac{c'_{i,w,bulk}}{c'_{i,w,bulk,0}} - \frac{1}{R}\right]}_{y} = \underbrace{-\left[\frac{F_W E_{ff}}{V_W}\left(1+\frac{1}{R}\right)\right]}_{m} \cdot t \qquad 2.37$$

There, R represents an overall extraction factor, defined according to Equation 2.38, where P is the partition coefficient of compound i between the two phases, and V_W and V_o are the volumes of the aqueous and organic phase.

$$R = \frac{V_O P_i}{V_W} \qquad 2.38$$

The extraction factor E is defined as shown in Equation 2.39, where P is the partition coefficient of compound i between the two phases, and F_W and F_o are the flow rates of the aqueous and organic phase.

$$E = \frac{F_O P_i}{F_W} \qquad 2.39$$

The efficiency E_{ff} is defined according to Equation 2.40, where E is the extraction factor, A the membrane surface and K_W the mass transfer coefficient.

$$E_{ff} = \frac{1-\exp\left[\frac{K_W A}{K_W A}\cdot\left(1-\frac{1}{E}\right)\right]}{1-\frac{1}{E}\exp\left[\frac{K_W A}{K_W A}\cdot\left(1-\frac{1}{E}\right)\right]} \qquad 2.40$$

Plotting Equation 2.37, as presented in Figure 18, the slope of the linear equation can be derived.

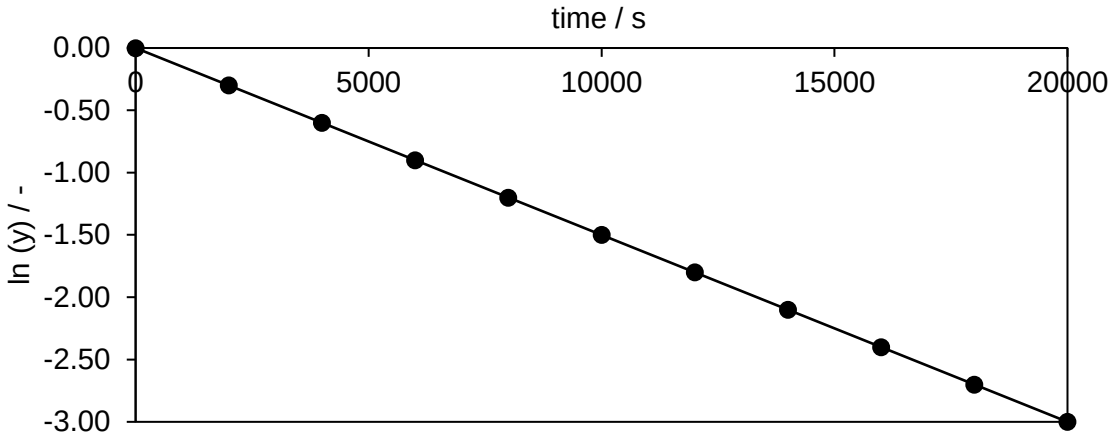

Figure 18: Plotting of Equation 2.37 to determine the slope of the linear equation for the calculation of the K_W value

By rearranging Equation 2.39, the experimental K_W value can be calculated according to Equation 2.41 [92].

$$K_W = -\frac{F_W}{A}\cdot\frac{E}{E-1}\cdot\ln\left[\frac{E\cdot(E_{ff}-1)}{E_{ff}-E}\right] \qquad 2.41$$

2.6 Techno-economic analysis

The techno-economic analysis was done according to the method described by Peters and Timmerhaus [93]. A graphical presentation of the cumulative cash flow vs. the operation time of an industrial plant is shown in Figure 19.

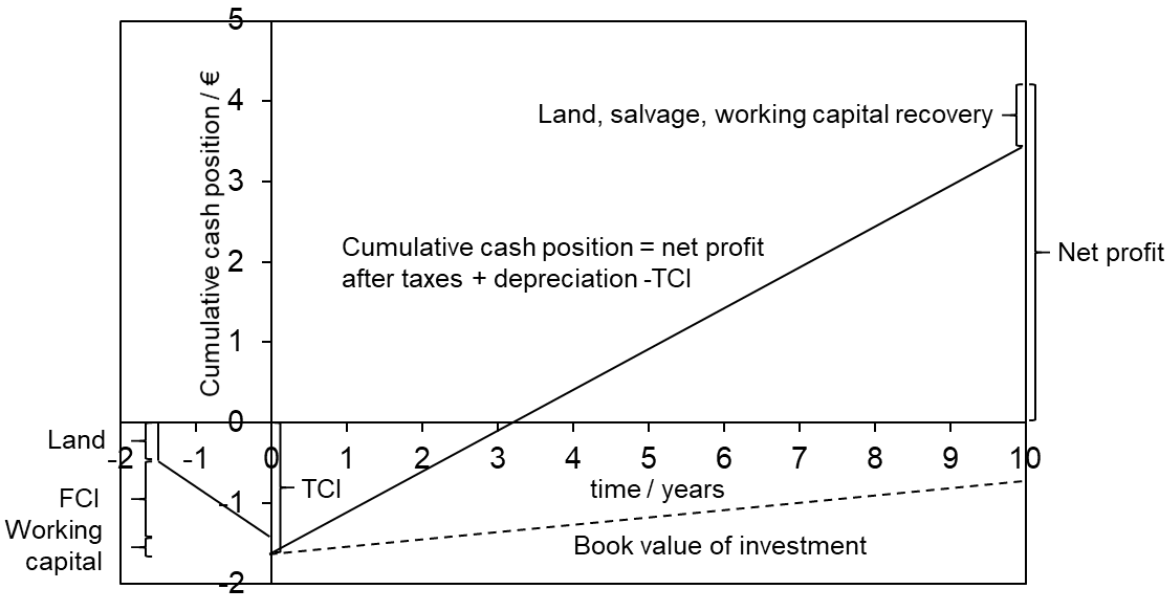

Figure 19: Graph of the cumulative cash position over time for an industrial operation [93].

A list of the upstream and downstream process's total equipment costs (TEC) was made. The fixed capital investments (FCI) and total capital investments (TCI) were determined based on these costs [94]. The total product costs were calculated as the sum of manufacturing costs and general expenses. The return on investment (ROI) and the net present value (NPV) were economic figures to determine the financial profitability of the new downstream process [95].

3 Material and methods

In this chapter, the materials, analytical and experimental methods are presented.

3.1 Materials

The solvents and chemicals used as received in this work are presented in Table 3.1.

Table 3.1: List of solvents and chemicals used in this work.

Solvents	Purity / %	Company
Acetone	≥99.0	VWR Chemicals (France)
Butan-1-ol	≥99.8	VWR Chemicals (France)
Dichloromethane	≥99.8	VWR Chemicals (France)
Ethyl acetate	≥99.5	Merck KGaA (Germany)
n-heptane	n.a.	VWR Chemicals (France)
n-hexane	≥98.0	Merck KGaA (Germany)
Methanol	≥99.8	VWR Chemicals (France)
Methyl t*ert*-butyl ether	≥99.6	VWR Chemicals (France)
Petroleum spirit 40-60°C	≥99.8	VWR Chemicals (France)
Potassium carbonate	≥99.0	VWR Chemicals (Germany)
Potassium bicarbonate	≥99.0	VWR Chemicals (Germany)
Water	-	Millipore 18-MOhm water
Chemicals		
Astaxanthin oleoresin	10	BDI-BioLife Science GmbH (Austria)
trans-astaxanthin standard	≥97.0	Dr. Ehrenstorfer GmbH
Bold Modified Basal Freshwater Nutrient Solution (50x concentrated)		Merck KGaA (Germany)
(1R)-(+)-camphor	≥98.0	ThermoFischer Kandel GmbH (Germany)
D-(+)-glucose	≥99.5	Merck KGaA (Germany)
F.A.M.E. Mix (C8-C24)	≥99.0	Merck KGaA (Germany)
Hydrochloric acid	≥35	VWR Chemicals (France)
Methyl heptadecanoate	≥99.0	Merck KGaA (Germany)
Peracetic acid	≥15	ITW Reagents (Spain)
Phenol	≥99.0	Merck KGaA (Germany)
Sodium acetate	≥99.5	VWR Chemicals (Germany)
Sodium chloride	≥99.5	VWR Chemicals (Germany)
Sodium hydroxide	≥99.5	VWR Chemicals (Germany)
Sodium nitrate	≥99.5	VWR Chemicals (Germany)
Sulphuric acid	≥96.0	VWR Chemicals (Germany)

3.2 Equipment

In Table 3.2, the major equipment used in this work is listed.

Table 3.2: List of major equipment used in this work.

***H. pluvialis* cultivation and germination**	Company
Orbital shaker SHO-2D	Witeg Labortechnik GmbH (Germany)
Photobioreactor HDC 1.100B	CellDEG GmbH (Germany)
Lamp with 90 LEDs	CellDEG GmbH (Germany)
LightScout Quantum Meter	Spectrum Technologies Inc. (USA)
HPLC unit	
LC-20AB	Shimadzu (Japan)
Diode array detector SPD-M20A	Shimadzu (Japan)
YMC carotenoid column (C30, 3 µm, 150×4.6 mm)	YMC Co.(Japan)
0.22 µm nylon syringe	VWR Chemicals (Germany)
GC unit	
6890N Network GC	Agilent Technologies (USA)
5973 Network Mass Selective Detector	Agilent Technologies (USA)
7683 Series Injector	Agilent Technologies (USA)
Restek Rtx-Wax column (30m, 0.25mm ID, 0.25 µm)	Restek GmbH (Germany)
LLC units	
HPCCC-Mini Centrifuge (V_{column}=18.2 mL, 0.8 mm ID, β=0.5 - 0.78)	Dynamic extractions (United Kingdom)
Two isocratic pumps model 306	Gilson (USA)
CPC 250 PRO SPECIAL BIO	Armen Instruments (France)
Membrane-assisted extraction	
Tubular Polytetrafluoroethylene (PTFE) unit (A=0.0587 m^2)	Memo3 GmbH (Schwitzerland)
Peristaltic pump Verderflex VANTAGE 3000 C	Verder International BV (Netherlands)
Centrifugal pump Iwaki MD-15FX-220N	Iwaki & Co., Ltd. (Japan)
Additional equipment	
High pressure homogeniser APV 1000	APV systems (Denmark)
Rotary evaporator Heidolph Hei-VAP	Heidolph Instruments (Germany)
UV/VIS spectrophotometer Specord 50plus	Analytic Jena (Germany)
Centrifuge Sigma 3-16KL	Sigma GmbH (Germany)
Centrifuge MicroStar12	VWR Chemicals (Germany)
Shaker Multi Bio RS-24	Biosan (Lativa)
Magnetic stirrer VELP SCIENTIFICA	VELP Scientifica Srl (Italy)
Vacuum concentrator RVC 2-18 CDplus SpeedDry	MartinChrist Gefriertrocknungsanlagen GmbH
Freeze dryer Alpha 3-4 LSCbasic	MartinChrist Gefriertrocknungsanlagen GmbH

3.3 Cultivation of *H. pluvialis* cyst cells

The *H. pluvialis* cyst cells for the germination and following extraction epxriments were cultivated in-house. The microalgae *H. pluvialis* (SAG number 192.80) was purchased immobilised on agar from “The Culture Collection of Algae” from the Goettingen University, Germany. Parts of the agar were transferred into a 250 mL Erlenmeyer flask, and 150 mL of Bold Modified Basal Freshwater Nutrient Solution (BBM) were added. The Erlenmeyer flask was placed on the orbital shaker SHO-2D from Witeg Labortechnik GmbH (Germany) at a rotation of 100 rpm. A lamp containing 90 light-emitting diodes (LEDs) was used for illumination. The light composition could be chosen to be “blue light” with a maximum of 451 nm or “red light”, with a maximum of the emitted light at 658 nm. For measuring the light intensity, the LightScout Quantum Meter from Spectrum Technologies, Inc. (USA) was used. For the growth of the microalgae, the Erlenmeyer flask was illuminated for two weeks at a light intensity (photon flux density) of 50 µmol $m^{-2}s^{-1}$ using “red light”. At this point, the microalgae are mainly present as green zoospores and aplanospores. These microalgae were used to inoculate four photobioreactors, model HDC 1.100B from the CellDEG GmbH (Germany) (Figure 20).

Figure 20: Photobioreactor HDC 1.100B for the cultivation of *H. pluvialis* at different cell stages [9].

The cultivation to high cell concentrations and stressing for cyst formation and astaxanthin accumulation was carried out using “blue light” at a light intensity of 200 µmol $m^{-2}s^{-1}$. The photobioreactors consist of a CO_2 buffer reservoir and a cultivation reactor, which is separated by a hydrophobic membrane. Bubble-free gassing of the microalgae culture through a hydrophobic membrane is done through an aqueous bicarbonate buffer solution placed in the buffer reservoir. Seven holes on the vessel upper side, covered with a hydrophobic membrane guarantee that released CO_2 can diffuse into the photobioreactor. The spherical photobioreactor made of transparent polystyrene is placed above the buffer reservoir and has a total volume of 250 mL. To inoculate the photobioreactors, aliquots of the microalgae from the Erlenmeyer flask were centrifuged at 5500 rpm with a centrifuge Sigma 3-16KL centrifuge from Sigma GmbH (Germany) for 5 min. The supernatant was discarded, and the microalgae

were suspended using distilled water, centrifuged, and the supernatant was removed. 200 mL of fresh BBM was added to each sample, and an OD of 0.2 at 750 nm was adjusted. The algal broth was transferred into the photobioreactors. For gassing of the microalgae culture with 3% v/v CO_2, 150 mL of aqueous bicarbonate buffer (12.55 g K_2CO_3 and 36.04 g $KHCO_3$) were added into each buffer reservoir. The photobioreactors were placed on the shaking plate at a rotation of 110 rpm. The light intensity was set to 100 µmol $m^{-2}s^{-1}$, using “red light”. When all *H. pluvialis* cells were present as aplanospores, “blue light” at a light intensity of 200 µmol $m^{-2}s^{-1}$ was used for seven days to enhance the astaxanthin synthesis within the cyst cell. The astaxanthin content and the biomass concentration was determined as presented in Section 3.8.2 and Section 3.8.3.

3.4 Germination of *H. pluvialis* cyst cells

For the germination experiments, aliquots of the *H. pluvialis* cyst cells from Section 3.3 were centrifuged at 5500 rpm, using the Sigma 3-16KL centrifuge from Sigma GmbH (Germany) for 5 min. The supernatant was discarded, removed, and distilled water was added to wash the biomass, centrifuged again, and the supernatant was removed. The cyst cells were suspended in 200 mL BBM and either germinated under phototrophic, mixotrophic or heterotrophic conditions. At defined time intervals after the start of germination biomass concentration was determined in triplicates (Section 3.8.3). The nitrate and glucose concentration in the supernatant were determined as shown in Section 3.8.4. The measurement of the glucose content was done in triplicate at each measured time point, and the nitrate content in the supernatant was measured by a single determination. The astaxanthin content of the biomass before extraction with ethyl acetate was determined in triplicate (n = 3) at the beginning of germination (t = 0 h), at the time where most zoospores were released (t = 49 h), and at the end (t = 141 h) for each biological sample. Astaxanthin can be directly extracted from released zoospores into ethyl acetate without prior mechanical cyst cell disruption and drying [1]. Consequently, the algal broth's extractability correlates with the number of released zoospores and cyst cell germination. Thus, solvent extraction was performed at different time points after germination to determine the extractable amount of astaxanthin into ethyl acetate. Therefore, 2 mL algal broth was pipetted into a 15 mL falcon tube and 2 mL ethyl acetate was added. The tubes were mixed for 60 minutes, using the Multi Bio RS-24 shaker from Biosan (Latvia), followed by centrifugation at 5500 rpm with a Sigma 3-16KL centrifuge from Sigma GmbH (Germany) for 15 min. The extracted carotenoids absorbance at 478 nm was measured once using the SPECORD 50 Plus spectrophotometer from Analytik Jena (Germany). In addition to the extraction experiments, the cell stage of the microalgae cultures was calssified using a light microscope, equipped with a Thoma hemocytometer from the BRAND GMBH + CO KG (Wertheim, Germany). As shown in Figure 2, a distinction between five different cell stages of

H. pluvialis, cyst cells, dividing cells, zoospores, aplanospores, and empty cysts was done. Cell counting was done as single determination for each measuring point.

3.5 Liquid-liquid chromatographic extraction of astaxanthin from *H. pluvialis*

The methodology of the extraction experiments of astaxanthin from *H. pluvialis* algae broth using LLC is presented in the following Section. The experiments for the extraction of astaxanthin from either homogenised cyst cells (Section 3.7) or flagellated cells were performed using a CCC or CPE unit.

In this work, a CCC unit (Dynamic Extractions Ltd., UK) with a column volume of 18.2 mL was used for preliminary experiments, extraction of astaxanthin from germinated zoospores and homogenised cyst cells. The scale-up was done using the centrifugal partition extractor CPC 250 PRO SPECIAL BIO Version (acronym, centrifugal partition extractor, CPE) from Armen Instrument (France) with an experimentally determined column volume of 244 mL. The CCC column consists of a PTFE tube with a total volume of 18.2 mL and a diameter of 0.8 mm. In the center of the bobbin, 240 g are reached at the maximum rotational speed of 2000 rpm. The ß value, the ratio of the coil to rotor radius is between 0.5 and 0.78. The maximum allowed flow rate is 2 mL min^{-1} and the maximum pressure loss is 17 bar. The column was tempered using a water bath Haake F3 FISONS. The upper and lower phases were pumped using two isocratic HPLC pumps Gilson 306 (USA). In addition, a diode array detector Gilson 171 (Gilson, USA) was installed.

The CPE column consists of 12 stacked disks, and in every disk, 20 twin-cells are engraved, resulting in 240 cells total. The disks are made of stainless steel and are coated with PTFE. The maximum rotational speed of the CPE unit is 3000 rpm with a permitted pressure drop of 100 bar. The same pumps as for the CCC extraction were used.

3.6 Membrane-assisted extraction

As presented in Figure 21, a hollow fibre membrane module from Memo3 GmbH (Switzerland) with the main characteristics presented in Table 3.3 was used for the membrane-assisted extraction. The fibre bundle was sealed to the shell on each side through three O-ring seals (Figure 21). When ethyl acetate was used as a solvent, seals made of ethylene propylene diene monomer (EPDM) were used, while seals of fluoro rubber (FKM) were utilised for *n*-heptane. The shell consisted of a glass tube with an inner diameter D_{shell} of 25.8 mm. The set-up for the membrane extraction is presented schematically in Figure 22 and Figure 23. The two-headed peristaltic pump Verderflex VANTAGE 3000 C from Verder International BV (Netherlands) was used for low-pulsation pumping of the aqueous phase. The flow rate was adjusted via the pump's rotational speed, and the pressure was regulated using a valve. The pipes used in the pump had an inner diameter of 4.8 mm and an outer diameter of 8 mm. The organic phase was pumped using the centrifugal pump Iwaki MD-15FX-220N from Iwaki &

Co., Ltd. (Japan). The flow rate and pressure could be adjusted via a regulation valve installed after the pump outlet. A flow meter was installed before the inlet to the solvent tank. The pressure in the periphery was measured with a pressure sensor BAROLI 02 from BD sensors GmbH (Germany).

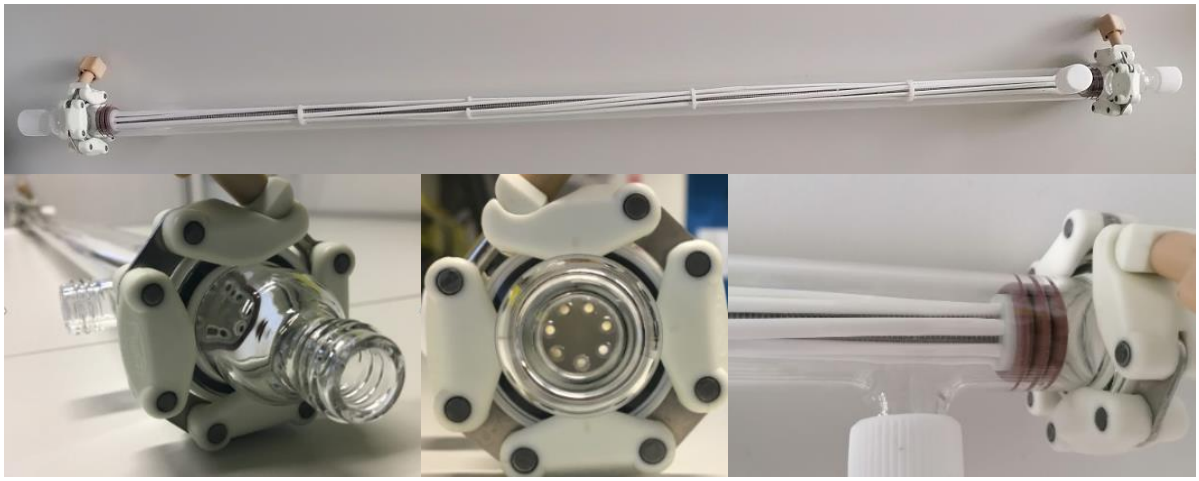

Figure 21: Membrane extractor used for liquid-liquid extraction.

Before each experiment, the partition coefficient of the substance to be extracted (camphor or astaxanthin oleoresin) was measured. For this purpose, feed and solvent with the identical phase ratio used for the membrane extraction was transferred into a falcon tube. The falcon tube was then mixed with the Multi Bio RS-24 shaker from Biosan (Riga, Latvia) for 30 minutes, centrifuged for 10 minutes using a Sigma 3-16KL centrifuge from Sigma GmbH (Germany) and equilibrated for 60 minutes. The astaxanthin content in the organic phase was measured using the HPLC method in Section 3.8.2, the astaxanthin content in the aqueous phase was calculated using the mass balance.

Table 3.3: Main characteristics of the membrane contactor.

Main characteristics of the memo3 hollow fibre module	
Membrane characteristics	
Material of fibres	PTFE
Porosity ε / -	0.55
Tortuosity τ / -	2
Nominal pore size / µm	1
Length of fibre / cm	87.5
Inner fiber diameter d_i / mm	3
Outer fiber diameter d_O / mm	3.5
Area-based on the fibre inside diameter / m^2	0.0577
Area-based on the fibre outside diameter / m^2	0.0597
Module characeteristics	
Number of fibres	7
Inner shell diameter / mm	25.8
Fiber packing factor / -	0.101

The concentration of camphor in water was determined using the photo spectrometric described in Section 3.8.5, while the concentration of camphor in the solvent was determined using the mass balance. The partition coefficient was calculated as shown in Equation 2.11.

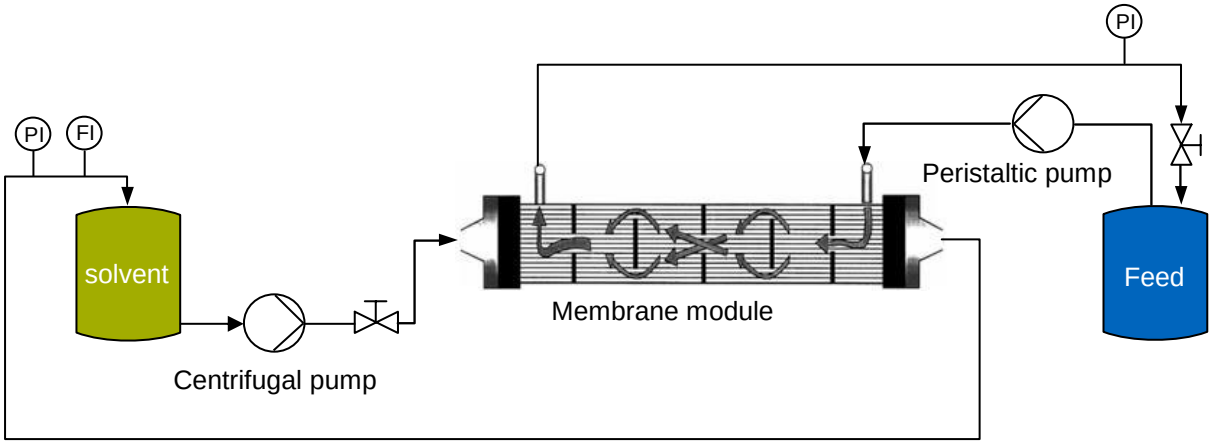

Figure 22: Schematic presentation of the membrane-assisted liquid-liquid extraction set up.

The aqueous phase can be pumped in the fibers of the membrane and the organic phase in the shell, or vice versa. In both cases the aqueous phase was first pumped and an overpressure of 0.1-0.15 bar was set.

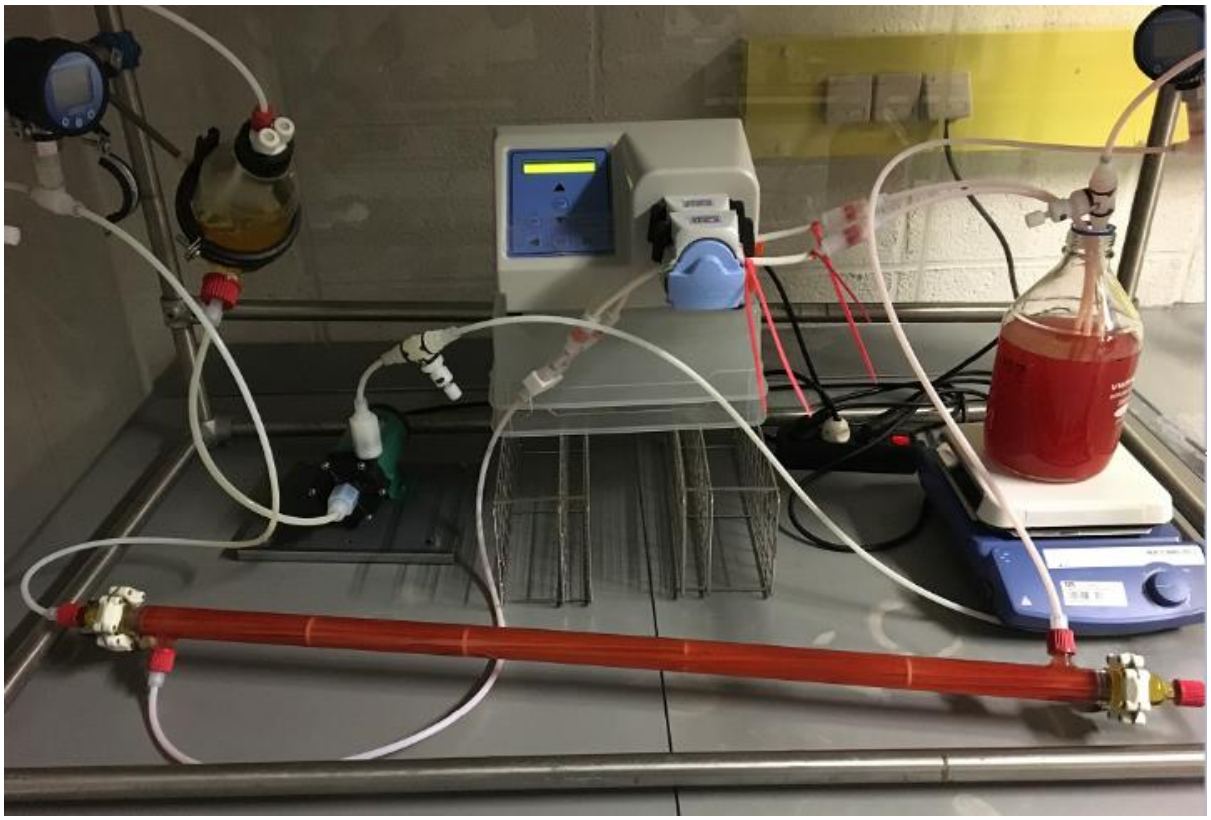

Figure 23: Used membrane contactor during operation.

After the periphery, e.g. tubes were filled with the aqueous feed, the organic phase was then switched on. The excess pressure of the aqueous feed phase was in the range of

0.05 - 0.15 bar during the extraction experiments. Extraction experiments with camphor, astaxanthin containing oleoresin (obtained from supercritical CO_2 extraction), and homogenised biomass were performed. In these experiments, samples were taken from the reservoir at defined time intervals. In the case of the extraction experiments with camphor, the samples were taken from the storage container of the aqueous phase, in the case of the extraction of astaxanthin from the organic phase. The camphor concentration was determined photo spectrometric as described in Section 3.8.5, and the astaxanthin concentration was measured using the HPLC method presented in Section 3.8.2. At the end of each experiment, the flow rate was determined in triplicate from each phase, measuring the time to fill a 100 mL measuring cylinder. After each experiment, the membrane and the periphery were cleaned with acetone and distilled water. The experiments usually lasted from a few hours to several days.

3.7 High pressure homogenisation

The mechanical cell disruption was carried out using a high-pressure homogeniser (APV 1000, APV Systems, Denmark), in which the algal broth is pressed through a gap at a pressure difference of 500 bar. This pressure difference causes the cell wall to burst and the cytoplasm and astaxanthin to be released into the medium.

3.8 Analytical methods

In the following Sections, the analytical methods used in this work are described.

3.8.1 Sample preparation

To determine the astaxanthin content of the *H. pluvialis* biomass, 5 mg of freeze-dried biomass were mechanically disrupted with mortar and pestle. Astaxanthin was extracted, adding 10 mL of dichloromethane, and the extraction was repeated until colourless debris was left. Subsequently, dichloromethane was evaporated, using the Heidolph Hei-VAP rotary evaporator from Heidolph Instruments (Germany). For astaxanthin quantification in the collected fractions of the stationary phase after liquid-liquid extraction using CCC and CPE, aliquots of the fractions were transferred into 4 mL vials and evaporated using the RVC 2-18 CDplus SpeedDry vacuum concentrator from MartinChrist Gefriertrocknungsanlagen GmbH (Germany). The extracts obtained after solvent evaporation were saponified for 3 hours in the dark, adding 2.25 mL acetone, 0.25 mL methanol, and 0.5 mL 0.05 M NaOH in methanol. The samples were transferred into three 15 mL falcon tubes filled with 3 mL of petroleum spirit and 5 mL of aqueous NaCl solution (10 wt%). The flacon tubes were mixed with the Shaker Multi Bio RS-24 from Biosan (Lativa) for 30 minutes and centrifuged at 5500 rpm with the centrifuge Sigma 3-16KL from Sigma GmbH (Germany) for 5 minutes. After centrifugation, the petroleum-rich phase was transferred into 5 mL of new NaCl solution. In total, the step with

NaCl solution was repeated two more times. The petroleum rich upper phase was evaporated using the Heidolph Hei-VAP rotary evaporator from Heidolph Instruments (Germany).

3.8.2 Astaxanthin quantification using high-performance liquid chromatography

A HPLC unit (LC-20AB, Shimadzu, Japan), equipped with a YMC carotenoid column (C30, 3 µm, 150×4.6 mm, YMC Co., Japan) and a diode array detector (SPD-M20A, Shimadzu, Japan) was used for astaxanthin quantification [1, 96]. The astaxanthin extract was solved in solvent B (methanol, MTBE, water, 8:89:3, v/v) used for HPLC analysis. The extract was filtered using a 0.22 µm disposable nylon syringe filter before HPLC analysis. Solvent A (methanol, MTBE, water, 81:15:4, v/v) and solvent B (methanol, MTBE, water, 8:89:3, v/v) were used as the mobile phases. The gradient of solvent A and B was as follows: 2% solvent B for 11 min, a linear gradient from 2% solvent B to 40% solvent B for 7 min, 40% solvent B for 6.5 min, followed by a linear gradient to 100% solvent B for 2.5 min, 100% solvent B for 3 min, a linear gradient to 2% solvent B for 3 min, held for 3 min. The injection volume was 10 µL, and the mobile phase flow rate was set to 1 mL min^{-1}. The signal of the diode-array detector at 478 nm was recorded [1]. For the astaxanthin quantification, a calibration curve with an astaxanthin standard from Dr. Ehrenstorfer GmbH (Germany) was established and is presented in the appendix (Figure A 1). The limit of quantification (LOQ) limit of detection (LOD) and were calculated using the calibration curve according to DIN 32645 [97]. The calculated values of the LOD and LOQ were 1.85 mg L^{-1} and 5.51 mg L^{-1}. To remain above the values of the LOD and LOQ, low concentrated fractions were concentrated before HPLC analysis.

3.8.3 Biomass concentration

To determine the DW concentration, 2 mL algal broth was transferred into microtubes from the Eppendorf AG (Germany) and centrifuged at 5500 rpm for 15 minutes, using the MicroStar12 from VWR Chemicals (France). The supernatant was discarded or used to determine the nitrate and sugar content, as described in Section 3.3.2. The microtubes with dewatered biomass were frozen at -80°C and afterwards lyophilised with an Alpha 3-4 LSC basic freeze dryer from Martin Christ Gefriertrocknungsanlagen GmbH (Germany). The weight difference between the microtube after freeze-drying and the empty microtube. The DW concentration was calculated as the weight of the dried biomass divided by the sample volume (2 mL). The dry weight biomass concentration was measured in triplicate for each experiment.

3.8.4 Nitrate and glucose quantification

In the germination experiments, the nitrate and glucose content in the medium was determined at defined time intervals. Therefore, 2 mL algal broth was transferred into microtubes from the Eppendorf AG (Germany) and centrifuged at 5500 rpm for 15 minutes, using the MicroStar12

from VWR Chemicals (France). The supernatant was used to determine the nitrate and sugar content. The nitrate concentration was measured spectroscopically using the UV/VIS spectrophotometer Specord 50plus from Analytik Jena (Germany), subtracting twice the absorbance at 275 nm from 220 nm [98]. The calibration curve was made with $NaNO_3$ dissolved in Milli-Q water and is presented in Figure A 2 in the appendix. The glucose, simple sugars, oligo- and polysaccharides content in the supernatant was determined calorimetrically [99]. Therefore, 400 µL supernatant, 40 µL 80% phenol solution, and 1 mL sulphuric acid (96%) were mixed in a 2 mL microtube. After the mixture had cooled to room temperature, the absorbance was measured spectroscopic at a wavelength of 488 nm. The calibration curve was created with glucose in BBM and is shown in Figure A 3. The glucose concertation of the supernatant was determined in triplicate, while a single determination measured the nitrate concentration.

3.8.5 Camphor quantification

The camphor concentration in the aqueous phase of the membrane extraction experiments was determined using the UV/VIS spectrophotometer Specord 50plus from Analytic Jena (Germany). Camphor was quantified at a wavelength of 285 nm in water. The calibration curve can be found in Figure A 4.

3.9 Single-stage extraction

The extractable amount of astaxanthin from the feed (mechanically disrupted cyst cells or zoospores) was measured for each extraction experiment. Therefore 5 mL algal broth with 5mL ethyl acetate were mixed using a Multi Bio RS-24 shaker from Biosan (Riga, Latvia) for 60 min. Using a Sigma 3-16KL centrifuge from Sigma GmbH (Germany), the samples were centrifuged at 5500 rpm for 15 min. The quotient of the mass of astaxanthin extracted into the solvent $m_{ATX,solvent}$ and the mass of astaxanthin in the feed before extraction $m_{ATX,F}$, gives the yield Y.

$$Y = \frac{m_{ATX,solvent}}{m_{ATX,F}} \qquad 3.1$$

From *H. pluvialis* cyst, astaxanthin cannot be extracted cells into ethyl acetate. Hence, Y depends on the amount of mechanically disrupted cysts or released zoospores. That's why a yield $Y_{extractable}$ which correlates the actual extractable quantity of astaxanthin from the algal broth was introduced. The extractable amount of astaxanthin from the algal feed (mechanically disrupted cyst cells or germinated zoospores) was measured for each extraction experiment. Therefore 5 mL algal broth with 5mL ethyl acetate were mixed using a Multi Bio RS-24 shaker from Biosan (Riga, Latvia) for 60 min. Afterwards the samples were centrifuged at 5500 rpm for 15 min using a Sigma 3-16KL centrifuge from Sigma GmbH (Germany). The extracted

amount of astaxanthin $m_{ATX,\ single\text{-}stage\ extraction}$ into the solvent was determined using the HPLC method described in Section 3.8.2.

$$Y_{extractable} = \frac{m_{ATX,solvent}}{m_{ATX,\ single\text{-}stage\ extraction}} \qquad 3.2$$

4 Results and discussion

In Figure 24, the structure of the results and discussion section of this work is presented schematically.

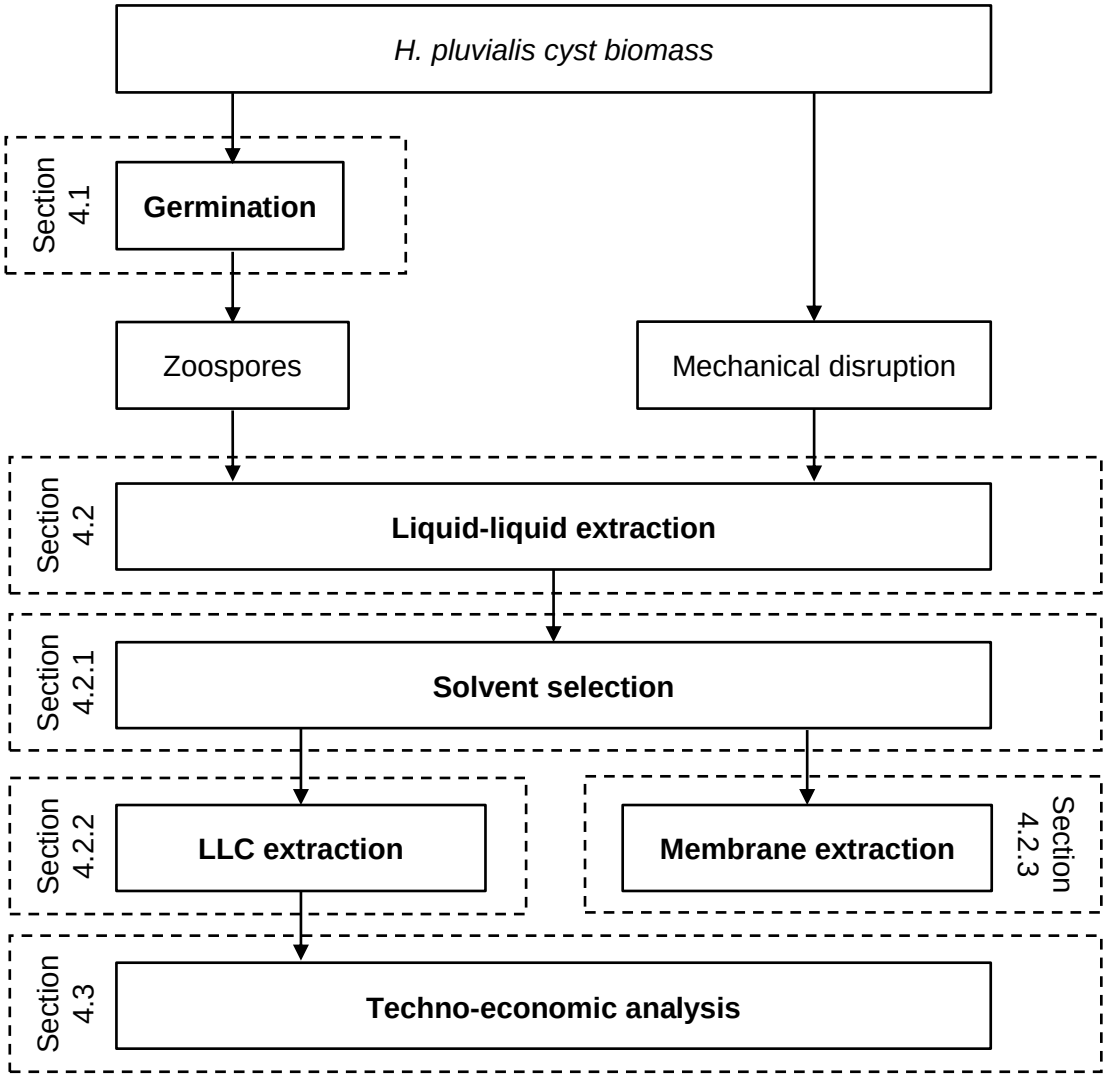

Figure 24: Schematic presentation of the structure of the results and discussion of this work.

In Section 4.1, the results of the *H. pluvialis* cyst germination are presented, which represent an alternative to the conventional mechanical cyst cell wall disruption. Photo-, mixo- and heterotrophic germination conditions were examined, with the aim of transforming as many cysts as possible into zoospores and preventing astaxanthin degradation in the released zoospores. After the germination conditions have been successfully selected, the liquid-liquid extraction experiments are presented in Section 4.2. These start in Section 4.2.1 with a solvent selection to find a suitable green solvent that allows astaxanthin extraction from mechanically disrupted cyst cells or zoospores containing algal broth. After the solvent selection, extraction of astaxanthin from homogenised cyst cells and germinated zoospores using an LLC column is presented in Section 4.2.2. First, a proof of concept was carried out using a CCC column on a laboratory scale. Based on these results, a scale-up to a semi-

preparative CPE column was carried out. In Section 4.2.3, the results of the membrane-assisted extraction are presented, starting with the extraction of the model compound camphor into *n*-heptane. Based on these findings, an extraction of suspended astaxanthin containing oleoresin (obtained from supercritical CO_2 extraction) and homogenised cyst cells into *n*-heptane was performed. In Section 4.3, a techno-economic study was carried out to evaluate the new downstream process comparing the extraction of astaxanthin from homogenised cyst cells and germinated zoospores using a CPE column to the industrial supercritical CO_2 extraction performed via an external service provider or in-house.

4.1 Germination of *H. pluvialis* cyst cells

The germination of *H. pluvialis* cyst cells represents an interesting alternative to mechanical cyst cell wall disruption [18]. In literature, germination was usually carried out under phototrophic conditions, with a high release of germinated zoospores usually being associated with a degradation of intracellular astaxanthin [20]. The aim of this work was to establish a germination method that enables rapid cyst germination and a conversion of as many cysts as possible into zoospores, without simultaneous intracellular astaxanthin degradation. The following section presents and discusses the conducted experiments and results of *H. pluvialis* cyst cell germination. In this work, germination experiments were carried out under photo-, mixo- and heterotrophic cultivation conditions, whereby the influence of CO_2, light intensity, glucose and nitrate concentration were considered.

4.1.1 Preliminary study to evaluate the influence of carbon source, CO_2 and light

In the first preliminary study, the germination of phototrophic and mixotrophic (organic carbon sources sodium acetate, glucose and ribose at a concentration of 8 mM), with 3% v/v CO_2 and a light intensity of 100 µmol $m^{-2}s^{-1}$ were applied. There, germination efficiency was evaluated by solvent extraction using ethyl acetate at defined time intervals and the absorbance of the extract was measured photo spectrometric at a wavelength of 478 nm. This presents a rapid method for evaluating germination, as astaxanthin can be extracted from the germinated zoospores but not from cyst cells. In Figure 25, the absorbance of the extract at 478 nm are plotted against time after the start of germination for the first preliminary study. At otherwise identical conditions, under phototrophic and mixotrophic conditions, more astaxanthin could be extracted into ethyl acetate from microalgae germinated at ambient air compared to gassing with CO_2. The maximum extracted astaxanthin concentration into ethyl acetate was reached 27.5 hours after the start of germination in all cultures. The maximum astaxanthin concentration in ethyl acetate was reached in the mixotrophic culture, germinated with glucose, at ambient air and a light intensity of 100 µmol $m^{-2}s^{-1}$. Phototrophic growth in the green stage of *H. pluvialis* is usually performed under phototrophic conditions, where CO_2 concentrations of up to 5 v/v% are most beneficial for growth compared to ambient air or CO_2

contents of 10% v/v or higher [11]. However, in the first preliminary study it could be shown that under phototrophic and mixotrophic conditions without additional CO_2, at ambient air, more astaxanthin can be extracted into ethyl acetate, which indicated enhanced *H. pluvialis* cyst cell germination at ambient air, compared to additional CO_2. Also, it could be shown that by adding an organic carbon source (mixotrophic growth), more astaxanthin was extracted into the solvent compared to phototrophic germination.

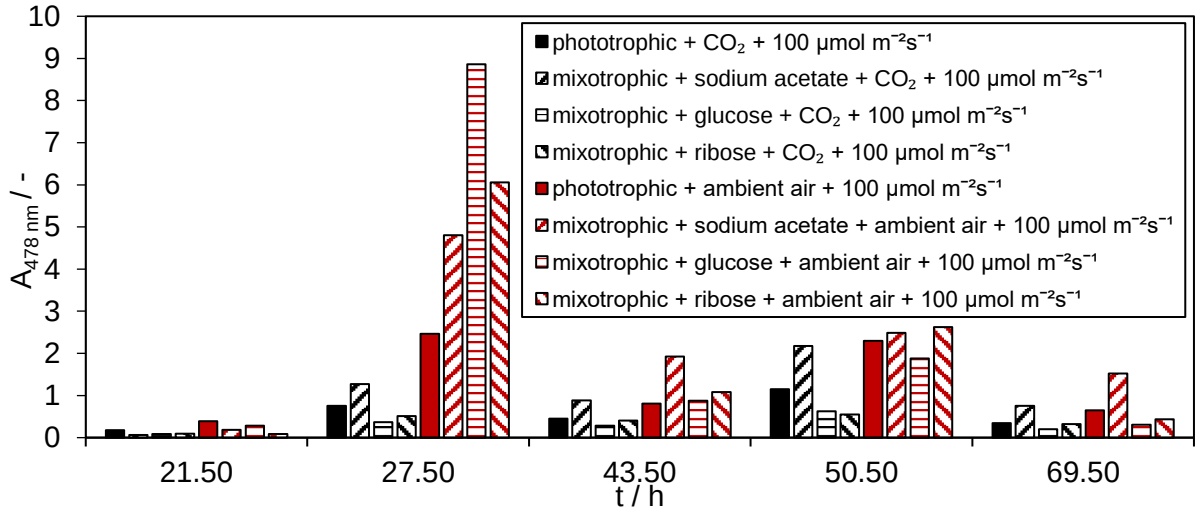

Figure 25: Absorbance of ethyl acetate after solvent extraction of phototrophic and mixotrophic germinated *H. pluvialis* cyst cells at defined time intervals. Influence of CO_2 on the phototrophic and mixotrophic (sodium acetate, glucose, and ribose) cyst cell germination at 100 µmol $m^{-2}s^{-1}$ [9].

As most astaxanthin could be extracted at mixotrophic conditions with glucose compared to ribose and sodium acetate in the first preliminary experiments, glucose was used in the second preliminary experiments. Additionally to the mixotrophic conditions, heterotrophic germination was conducted.

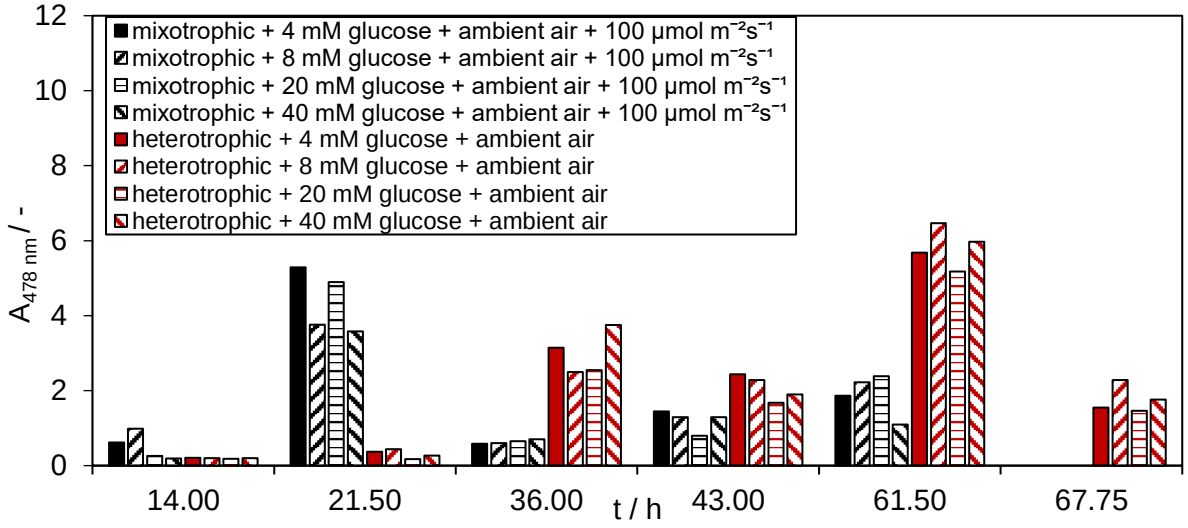

Figure 26: Absobance of ethyl acetate after solvent extraction of mixotrophic and heterotrophic germinated *H. pluvialis* cyst cells at 4, 8, 20 and 40 mM glucose at defined time intervals [9].

The influence of the glucose concentration of 4, 8, 20 and 40 mM was investigated under both, mixotrophic and heterotrophic germination conditions. As shown in Figure 26, the glucose concentration did not affect germination under mixotrophic or heterotrophic conditions. Under mixotrophic conditions, most astaxanthin was extracted 21.5 hours after the start of germination and under heterotrophic conditions after 61.5 hours. Thus, light accelerates the germination and the release of zoospores.

Additionally, more astaxanthin was extracted into ethyl acetate at heterotrophic compared to mixotrophic conditions, which indicates enhanced zoospores release. Based on the preliminary studies, it could be shown that both phototrophic and mixotrophic germination is enhanced at ambient air compared to additional CO_2. In addition, it was shown that germination is also enhanced under mixotrophic conditions compared to phototrophic conditions. With regard to the carbon source, increased germination was observed with glucose compared to sodium acetate and ribose. No influence of the glucose concentration on germination could be determined in the concentration range of 4 mM to 40 mM. Finally, enhanced germination could also be shown under heterotrophic compared to mixotrophic conditions.

4.1.2 Phototrophic, mixotrophic, and heterotrophic cyst cell germination

Four sets of experiments were carried out, as presented in Table 4.1.

Table 4.1: Applied germination conditions, each culture represents one biological sample [9].

Name	Germination conditions
culture 1	phototrophic+CO_2+100 µmol $m^{-2}s^{-1}$
culture 2	phototrophic+ambient air+100 µmol $m^{-2}s^{-1}$
culture 3	mixotrophic+4 mM glucose+CO_2+100 µmol $m^{-2}s^{-1}$
culture 4	mixotrophic+4 mM glucose+ambient air+100 µmol $m^{-2}s^{-1}$
culture 5	phototrophic+CO_2+75 µmol $m^{-2}s^{-1}$
culture 6	phototrophic+ambient air+75 µmol $m^{-2}s^{-1}$
culture 7	mixotrophic+4 mM glucose+CO_2+75 µmol $m^{-2}s^{-1}$
culture 8	mixotrophic+4 mM glucose+ambient air+75 µmol $m^{-2}s^{-1}$
culture 9	heterotrophic + “no external carbon source” + ambient air
culture 10	heterotrophic + 4 mM glucose + ambient air
culture 11	phototrophic + ambient air + 75 µmol $m^{-2}s^{-1}$
culture 12	mixotrophic + 4 mM glucose + ambient air + 75 µmol $m^{-2}s^{-1}$
culture 13	heterotrophic+4 mM glucose+ambient air
culture 14	heterotrophic+4 mM glucose+2xnitrate+ambient air
culture 15	mixo-/heterotrophic+4 mM glucose+ambient air+(75 µmol $m^{-2}s^{-1}$)
culture 16	mixo-/heterotrophic+4 mM glucose+2xnitrate+ambient air+(75 µmol $m^{-2}s^{-1}$)

Four germination experiments were done at different cultivation conditions in each set, using cyst cells from one batch. Based on the preliminary experiments, 4 mM glucose was used as organic carbon source for mixo-and heterotrophic germination. In the first set of experiments, the effect of 3% v/v CO_2 compared to a cultivation at ambient air was investigated using phototrophic culture 1 and culture 2 and mixotrophic culture 3 and culture 4 at a light intensity of 100 µmol $m^{-2}s^{-1}$. Germination conditions of cultures 1 to 4 were repeated at a lower light intensity of 75 µmol $m^{-2}s^{-1}$ and are presented in Table 4.1 as culture 5 to culture 8.
In the third set of experiments, cultures 9 to 12, the conditions of culture 6 and culture 8 at a light intensity of 75 µmol $m^{-2}s^{-1}$ were repeated (culture 11 and culture 12). These two cultures were germinated in the darkness by covering the reactors with aluminium foil for heterotrophic germination. 4 mM Glucose was added to culture 10, while no additional external carbon source was supplemented to culture 9. In the fourth and last series of experiments (cultures 13 to 16), all the cultures were germinated in the presence of 4 mM glucose. In culture 14 and culture 16, additional sodium nitrate was added, resulting in a two-times higher nitrate concentration in the BBM medium. Cultures 13 and 14 were germinated under dark conditions. Cultures 15 and 16 were first germinated with light, at a light intensity of 75 µmol $m^{-2}s^{-1}$. After nitrate was consumed 25 hours after the start of the germination, the germination was further done under dark conditions. The germination efficiency of culture 1 to culture 4 was determined by solvent extraction of astaxanthin into ethyl acetate. To evaluate the germination experiments of culture 5 to culture 16 (Table 4.1), the following analytical methods were used at the examined time intervals after the start of the germination:

- Solvent extraction of astaxanthin into ethyl acetate
- Cell counting (cyst cells, dividing cells, empty cyst cells, zoospores, and aplanospores)
- Determination of the biomass concentration
- Determination of the astaxanthin content in the biomass before solvent extraction
- Determination of the glucose and nitrate content in the supernatant

The two-tailed Student's t-test was used to compare changes of the astaxanthin biomass concentration to the initial value at the start of germination, and significant differences were registered at $p < 0.05$. Measurement replicates are presented as mean averages ± standard deviations [9]. As presented in Figure 27 in the first set of experiments, the influence of the CO_2 content on the phototrophic and mixotrophic cyst cell germination was examined. As can be seen, phototrophic and mixotrophic germination is enhanced at ambient air, compared to gassing with additional CO_2. 41 hours after the start of germination under phototrophic conditions and additional CO_2 (culture 1), 2.8 mg L^{-1} could be extracted, whereas 7.2 mg L^{-1} astaxanthin could be extracted into the solvent at ambient air (culture 2). A similar tendency

was measured for the mixotrophic conditions, where 8.9 mg L^{-1} and 4.5 mg L^{-1} astaxanthin were extracted into the solvent when germinated at ambient air (culture 4) and with additional CO_2 (culture 3). Additionally, glucose showed a positive effect on the germination, as with 8.9 mg L^{-1} more astaxanthin could be extracted at ambient air under mixotrophic (culture 4) compared to phototrophic (culture 2) conditions with 7.2 mg L^{-1}. The same tendency was measured for the germination with additional CO_2, where 41 hours after the start of germination, 4.5 mg L^{-1} astaxanthin could be extracted under mixotrophic (culture 3) and 2.8 mg L^{-1} under phototrophic (culture 1) conditions.

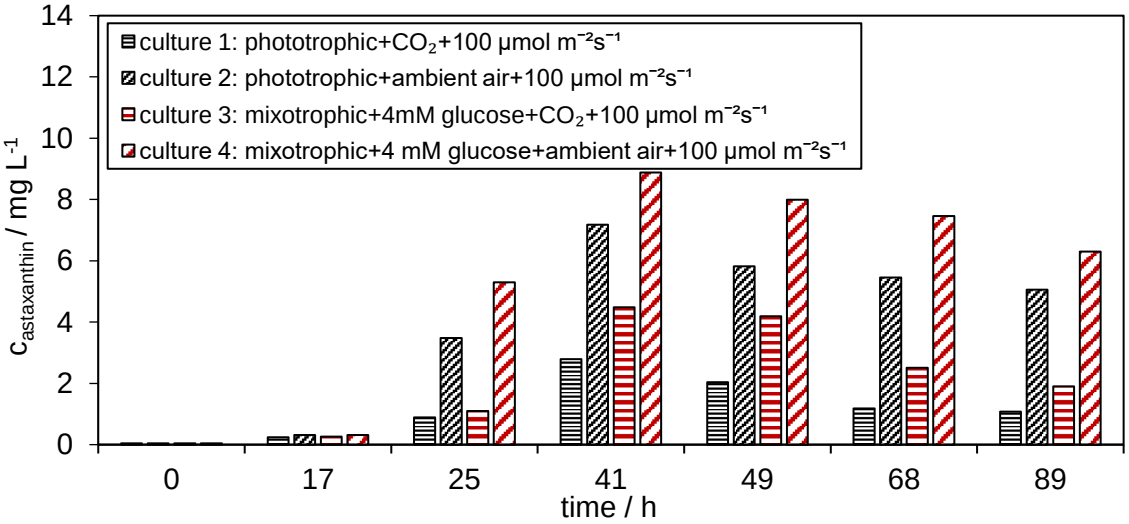

Figure 27: Astaxanthin concentration in the ethyl acetate extract of the phototrophic culture 1 (phototrophic + CO_2 + 100 µmol $m^{-2}s^{-1}$) and culture 2 (phototrophic + ambient air + 100 µmol $m^{-2}s^{-1}$), and the mixotrophic culture 3 (mixotrophic + 4 mM glucose + CO_2 + 100 µmol $m^{-2}s^{-1}$) and culture 4 (mixotrophic + 4 mM glucose + ambient air + 100 µmol $m^{-2}s^{-1}$) at different time points after the start of germination; data obtained by single determination [9].

Previous studies showed that zoospore release from the cysts is enhanced at higher light intensities compared to lower one. However, higher light intensities caused a stronger degradation of intracellular astaxanthin within the cells than lower light intensities [19, 20]. To reduce potential degradation of intracellular astaxanthin, the light intensity was adjusted to 75 µmol $m^{-2}s^{-1}$ in the next set of experiments. Ambient air and CO_2 had a similar effect on the phototrophic (culture 5) and mixotrophic (culture 6) germination as in the first set of experiments.

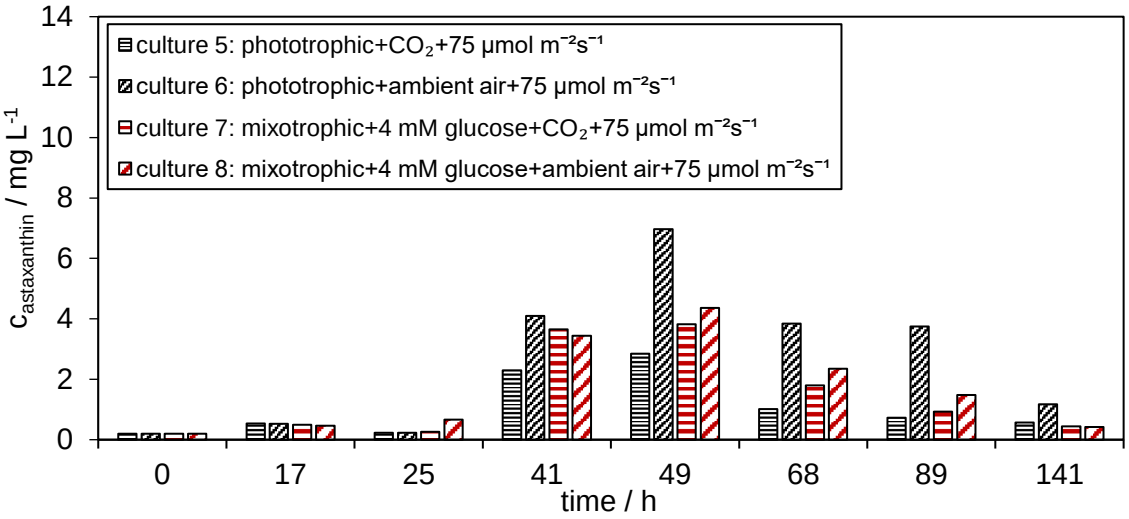

Figure 28: Astaxanthin concentration in the ethyl acetate extract of the phototrophic culture 5 (phototrophic + CO_2 + 75 µmol $m^{-2}s^{-1}$) and culture 6 (phototrophic + ambient air + 75 µmol $m^{-2}s^{-1}$), and mixotrophic culture 7 (mixotrophic + 4 mM glucose + CO_2 + 75 µmol $m^{-2}s^{-1}$) and culture 8 (mixotrophic + 4 mM glucose + ambient air + 75 µmol $m^{-2}s^{-1}$) at different time points after the start of germination; data obtained by single determination [9].

As shown in Figure 28, most astaxanthin could be extracted 49 hours after the start of germination under phototrophic and mixotrophic conditions. At this point in time, under phototrophic conditions at ambient air (culture 6), with 7.0 mg L^{-1} more astaxanthin could be extracted into ethyl acetate than with additional CO_2 (culture 5) with 2.8 mg L^{-1}. A similar influence of CO_2 on the germination could also be determined at mixotrophic conditions. Under Under mixotrophic germination conditions at ambient air (culture 8) with 4.4 mg L^{-1}, more astaxanthin could be extracted than with additional gassing with CO_2 (culture 7). As presented in Figure 29, at the beginning of the germination of culture 5 to culture 8, the astaxanthin content in the cyst cells was 1.4 wt%. A reduction ($p < 0.05$) of the astaxanthin content in biomass to 0.53 and 0.66 wt% compared to its starting value was measured for mixotrophic (culture 7) and phototrophic (culture 5) cultivation conditions with additional CO_2 141 hours after the start of the germination. Under phototrophic cultivation conditions at ambient air (culture 6), 49 hours after initializing germination, an increase of the astaxanthin concentration to 1.9 wt% was measured in the biomass, followed by a slight decline to 1.08 wt% at 141 hours after the start of germination (Figure 29). Additionally, as shown in Figure 29, 49 hours after the start of germination, the astaxanthin content in the biomass was 1.9 wt% in the phototrophic conditions at ambient air (culture 6) compared to 1.3 wt% with additional CO_2 (culture 5). As presented in Figure 28, under mixotrophic conditions, with 4.4 mg L^{-1}, only slightly more astaxanthin could be extracted at ambient air (culture 8) compared to 3.8 mg L^{-1} with additional CO_2 (culture 7), 49 hours after the start of germination. As shown in Figure 30,

around 38% of the cells of the mixotrophic culture 7 and culture 8 were in the zoospore stage, while 45% of the cells were in that stage in phototrophic conditions at ambient air (culture 6).

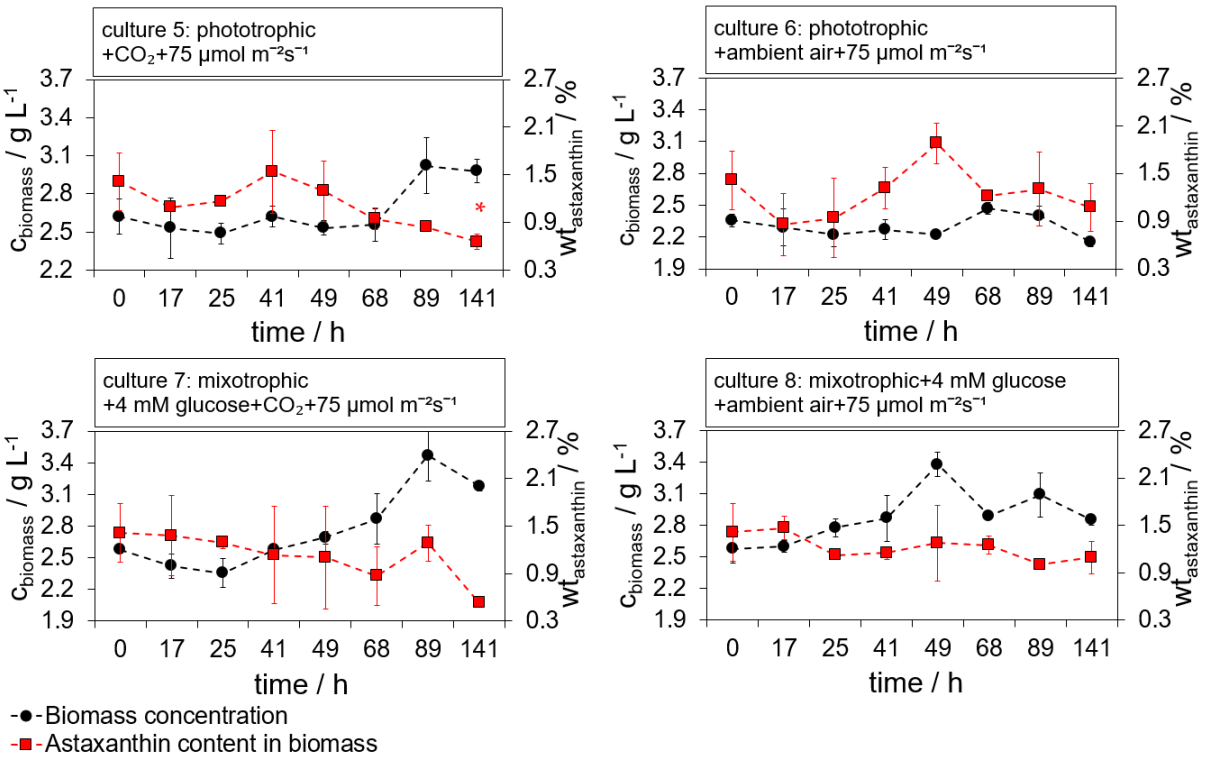

Figure 29: Time course of the biomass concentration and the astaxanthin content in the algal biomass of phototrophic culture 5 (phototrophic + CO_2 + 75 µmol $m^{-2}s^{-1}$) and culture 6 (phototrophic + ambient air + 75 µmol $m^{-2}s^{-1}$), and mixotrophic culture 7 (mixotrophic + 4 mM glucose + CO_2 + 75 µmol $m^{-2}s^{-1}$) and culture 8 (mixotrophic + 4 mM glucose + ambient air + 75 µmol $m^{-2}s^{-1}$). Biomass concentration: error bars show ±SD, n = 3. Astaxanthin content: error bars show ±SD, n = 3 at t = 0 h, t = 49 h, and t = 141 h and ±SD, n = 2 at t = 17 h, t = 25 h, t = 41 h, t = 68 h, and t = 89 h of one biological sample; asterisks indicate significant differences (t-test) of measured value vs. control (t = 0 h) at $p < 0.05$ [9].

Thus, as shown in Figure 28, the concentration of astaxanthin extracted into ethyl acetate was lower for the mixotrophic culture 7 and culture 8 than under phototrophic conditions at ambient air (culture 6). Besides the lower number of zoospores, this is also because of the lower astaxanthin concentration in the *H. pluvialis* biomass under mixotrophic conditions at ambient air (culture 8, 1.27 wt%) and additional CO_2 (culture 7, 1.1 wt%), compared to the phototrophic conditions at ambient air (culture 6, 1.88 wt%), 49 h after the start of germination. For all cultivation conditions, the highest astaxanthin extraction yield was achieved 49 hours after germination was initiated. Within the examined conditions, the highest extraction yield of 16% was reached under phototrophic conditions at ambient air (culture 6), compared to 9% with additional CO_2 (culture 5). Under mixotrophic cultivation conditions, an extraction yield of 11% at ambient air (culture 8), compared to 8% for germination, which additional CO_2 (culture 7) was obtained.

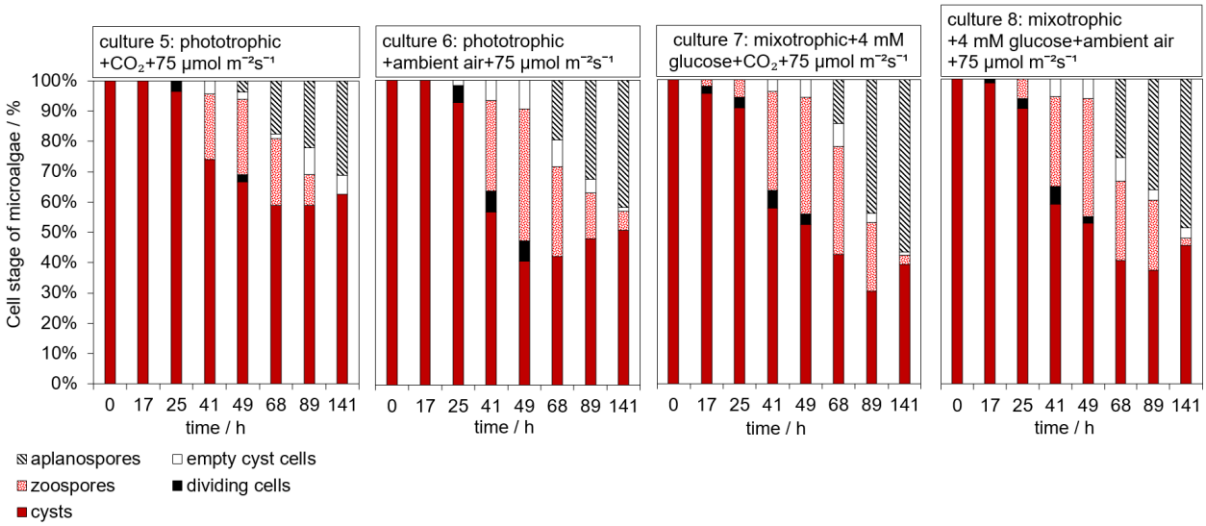

Figure 30: Relative distribution of the cell stages of *H. pluvialis* at different points in time after the start of germination for culture 5 (phototrophic + CO_2 + 75 µmol $m^{-2}s^{-1}$) and culture 6 (phototrophic + ambient air + 75 µmol $m^{-2}s^{-1}$), and culture 7 (mixotrophic + 4 mM glucose + CO_2 + 75 µmol $m^{-2}s^{-1}$) and culture 8 (mixotrophic + 4 mM glucose + ambient air + 75 µmol $m^{-2}s^{-1}$) [9].

The highest amount of astaxanthin could be extracted under mixotrophic conditions at ambient air (culture 4) in the first set of experiments (culture 1 to culture 4), while most astaxanthin was extracted under phototrophic conditions at ambient air (culture 6) in the second set of experiments (culture 4 to culture 8).

However, the course in the amount of astaxanthin extracted are similar within the first and second series of experiments for the cultivation conditions used, except the results of mixotrophic conditions at ambient air. Only the values of the extracted amount of astaxanthin into ethyl acetate under mixotrophic conditions at ambient air and a light intensity of 100 µmol $m^{-2}s^{-1}$ (culture 4) and mixotrophic conditions at ambient air at a light intensity of 75 µmol $m^{-2}s^{-1}$ (culture 8) show a deviation from the other three germination conditions. Therefore, it was assumed that the change in light intensity from 100 to 75 µmol $m^{-2}s^{-1}$ did not affect the trends obtained for the extraction of astaxanthin into ethyl acetate in the first and second series of experiments, but that the germination under mixotrophic conditions at ambient air and a light intensity of 100 µmol $m^{-2}s^{-1}$ (culture 8) compared to mixotrophic conditions at ambient air and a light intensity of 75 µmol $m^{-2}s^{-1}$ (culture 4) was worse due to a problem within the culture [9]. To assess whether cyst cell germination is increased under phototrophic or mixotrophic conditions at ambient air, the phototrophic (culture 11) and mixotrophic (culture 12) germination at ambient air and a light intensity of 75 µmol $m^{-2}s^{-1}$ was repeated in the third series of experiments. Since CO_2 showed a negative influence on phototrophic and mixotrophic germination, it was assumed that the overall photosynthetic activity of the cysts was reduced. Two heterotrophic conditions were applied to show that *H. pluvialis* cyst germination can be carried out independently of photosynthetic activity. Both

cultures were grown in dark conditions, without light and in ambient air. Once heterotrophic conditions without an external carbon source (culture 9) was applied and the energy consumption for germination was dependent on internal carbon reserves such as fatty acids, triacylglycerides (TAG) or starch. To the second heterotrophic approach (culture 10), additional 4 mM glucose was added into the BBM.

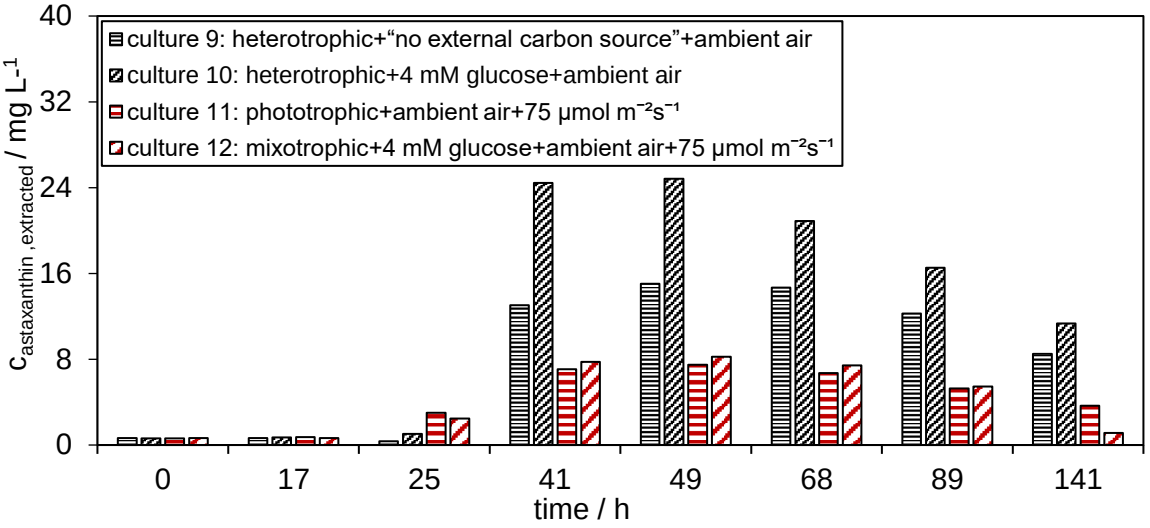

Figure 31: Astaxanthin concentration in the ethyl acetate extract of the heterotrophic culture 9 (heterotrophic + "no external carbon source" + ambient air) and culture 10 (heterotrophic + 4 mM glucose + ambient air), phototrophic culture 11 (phototrophic + ambient air + 75 µmol $m^{-2}s^{-1}$) and mixotrophic culture 12 (mixotrophic + 4 mM glucose + ambient air + 75 µmol $m^{-2}s^{-1}$) at different time points after the start of germination; data obtained by single determination [9].

As presented in Figure 31, 49 h after the start of germination, with 15.0 mg L^{-1} and 24.8 mg L^{-1}, more astaxanthin could be extracted under the heterotrophic conditions without additional carbon source (culture 9) and with extra glucose (culture 10) compared to the phototrophic (culture 11) and mixotrophic (culture 12) conditions with 7.5 mg L^{-1} and 8.3 mg L^{-1}, respectively. Slightly more astaxanthin could be extracted under mixotrophic compared to phototrophic conditions, similar to the first set of experiments (culture 1 to culture 4).

The percentage distribution of the cell stage of the microalgae over time is presented in Figure 32, showing that 49 hours after the start of germination under heterotrophic conditions with additional glucose (culture 10) most cells were in the zoospores stage, followed by heterotrophic conditions without additional glucose (culture 9), mixotrophic conditions (culture 12) and phototrophic conditions (culture 11). As presented Figure 33, the initial astaxanthin content in the cyst cells was 1.51 wt% for culture 9 to culture 12. Under heterotrophic conditions without an external carbon source (culture 9) and glucose (culture 10), no decline in the intracellular astaxanthin content was measured. 49 hours after the start of germination, an increase of the astaxanthin in the biomass to 2.28 wt%, with a relative standard deviation of 36%, was measured under heterotrophic conditions with an external

glucose source (culture 10). Similar to the previous set of experiments, a slight decline of the astaxanthin content in the biomass under mixotrophic conditions (culture 12) was measured in the course of germination to 1.11 wt% 149 h after the start of germination ($p > 0.05$). The astaxanthin concentration of the phototrophic culture 11 decreased to 1.42 wt% ($p > 0.05$). In the literature, an enhanced astaxanthin decrease in the biomass was measured at higher light intensities compared to without light. The astaxanthin content was reported to decrease to 116 pg cell^{-1} from initially 454 pg cell^{-1} under heterotrophic conditions (without external organic carbon source) and to 46 pg cell^{-1} under phototrophic conditions and a light intensity of 240 µmol m^{-2}s^{-1} [20].

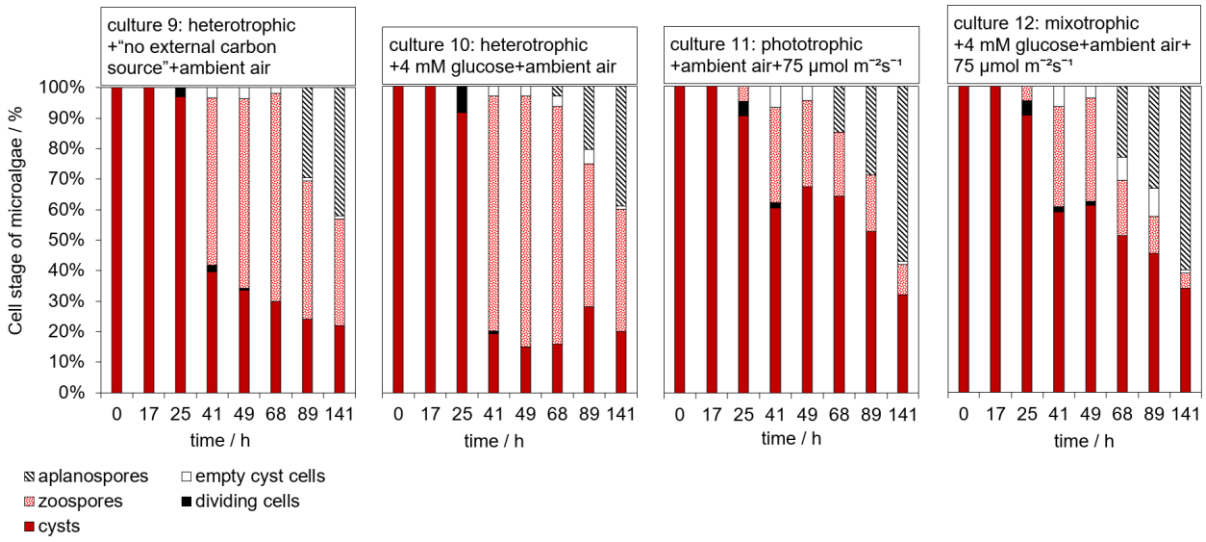

Figure 32: Relative distribution of the cell stages of *H. pluvialis* at different points in time after the start of germination for the heterotrophic culture 9 (heterotrophic + "no external carbon source" + ambient air) and culture 10 (heterotrophic + 4 mM glucose + ambient air), phototrophic culture 11 (phototrophic + ambient air + 75 µmol m^{-2}s^{-1}) and mixotrophic culture 12 (mixotrophic + 4 mM glucose + ambient air + 75 µmol m^{-2}s^{-1}) [9].

In this set of experiments (culture 9 to culture 12), the highest astaxanthin extraction yield of 50% was reached 49 hours after the start of germination under heterotrophic conditions and additional external glucose (culture 10). Under heterotrophic conditions without an external organic carbon source (culture 9), the second largest extraction yield of 45% was reached. From the concentrations of astaxanthin extracted into ethyl acetate of 24.8 mg L^{-1} and 15 mg L^{-1} (Figure 31), for heterotrophic culture with glucose compared to no additional organic carbon source, a larger difference of the extraction yields could have been expected. Due to the lower astaxanthin content in the biomass without additional close (culture 9), 49 hours after the start of germination, compared to with external glucose (culture 10), similar yields are reached. Under mixotrophic (culture 12) and phototrophic (culture 11) germination conditions, significantly lower extraction yields were reached with 22% and 16%, respectively.

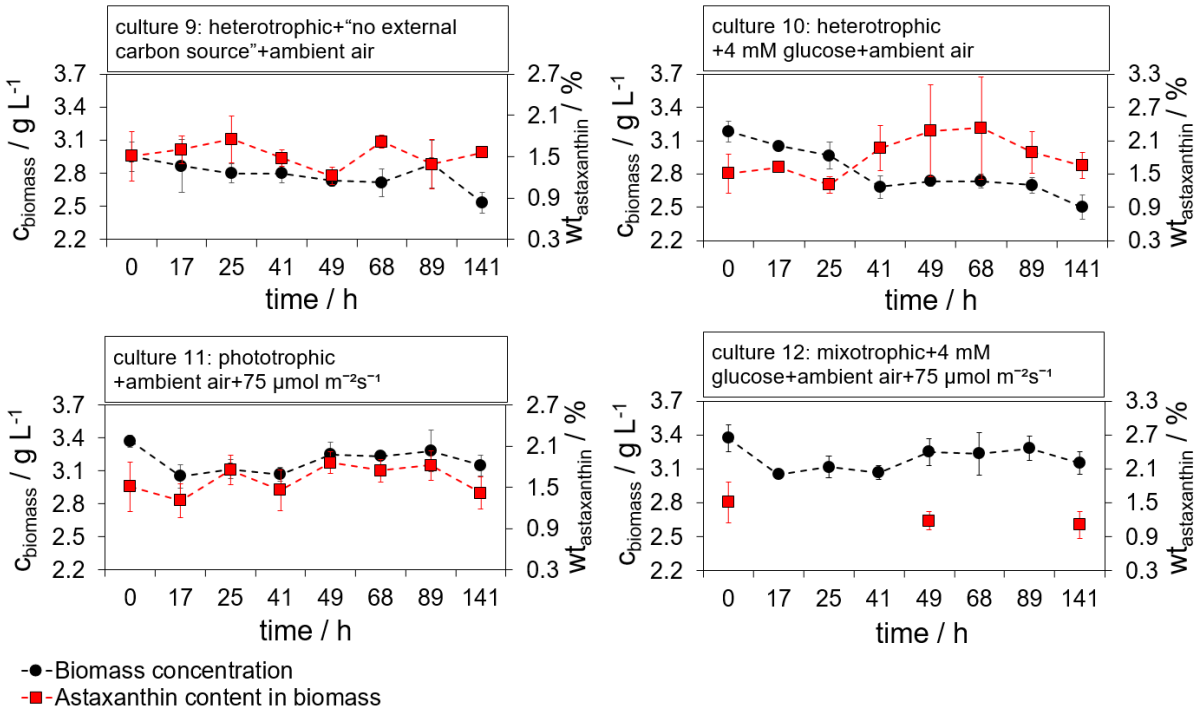

Figure 33: Time course of the biomass concentration and the astaxanthin content in the algal biomass of heterotrophic culture 9 (heterotrophic + "no external carbon source" + ambient air) and culture 10 (heterotrophic + 4 mM glucose + ambient air), phototrophic culture 11 (phototrophic + ambient air + 75 µmol $m^{-2}s^{-1}$) and mixotrophic culture 12 (mixotrophic + 4 mM glucose + ambient air + 75 µmol $m^{-2}s^{-1}$). Biomass concentration: error bars show ±SD, *n* = 3. Astaxanthin content: error bars show ±SD, *n* = 3 at t = 0 h, t = 49 h and t = 141 h and ±SD, *n* = 2 at t = 17 h, t = 25 h, t = 41 h, t = 68 h and t = 89 h of one biological sample; asterisks indicate significant differences (*t*-test) of measured value vs. control (t = 0 h) at $p < 0.05$ [9].

In the previous experiments (culture 9 to culture 12), the highest number of released zoospores, concentration of astaxanthin extracted into ethyl acetate, and yield were reached under heterotrophic conditions with additional glucose (culture 10). In the last set of experiments, these germination conditions were repeated as culture 13. To exclude a nitrate deficiency, heterotrophic cultivation conditions with glucose and double the nitrate content were applied (culture 14). In the previous set of experiments, it could be shown, that zoospore formation was slower under heterotrophy (culture 9 and 10) compared to phototrophic (culture 11) and mixotrophic germination conditions (culture 12). However, the maximum extracted amount of astaxanthin in ethyl acetate and the amount of zoospores was higher under heterotrophic compared to mixotrophic or phototrophic conditions. For that reason, mixotrophic and heterotrophic cultivation conditions were combined. Therefore, two cultures, culture 15 and culture 16 were illuminated with a light intensity of 75 µmol $m^{-2}s^{-1}$ until nitrate depletion, to speed up the formation zoospores and further grown under heterotrophic conditions to achieve a zoospore release in large quantities. One of these cultures was germinated without additional nitrate (culture 15), while in the other one the nitrate content in the medium was doubled (culture 16).

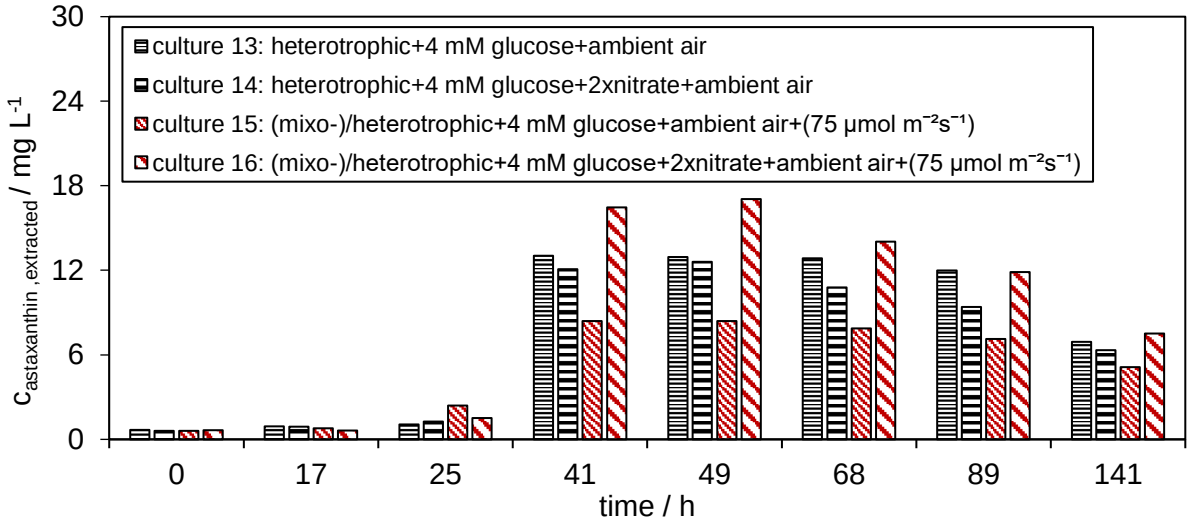

Figure 34: Astaxanthin concentration in the ethyl acetate extract of the heterotrophic culture 13 (heterotrophic + 4 mM glucose + ambient air) and culture 14 (heterotrophic + 4 mM glucose + 2xnitrate + ambient air), and culture 15 (mixo-/heterotrophic + 4 mM glucose + ambient air + (75 µmol $m^{-2}s^{-1}$) and culture 16 (mixo-/heterotrophic + 4 mM glucose + 2xnitrate + ambient air + (75 µmol $m^{-2}s^{-1}$); data obtained by single determination [9].

As shown in Figure 34, 49 hours after the start of germination, with 12.9 mg L^{-1} and 12.6 mg L^{-1} similar concentrations of astaxanthin extracted in ethyl acetate were measured under heterotrophic conditions with the standard nitrate (culture 13) and twice the nitrate concentration (culture 14). Thus, the nitrate concentration did not limit the germination under heterotrophic conditions. However, combining mixotrophic and heterotrophic germination conditions, 49 h after the start of germination, the astaxanthin concentration of extracted was 17.1 mg L^{-1} for twice the nitrate concentration (culture 16) and 8.4 mg L^{-1} at standard nitrate concentration (culture 15). With 8.4 mg L^{-1}, the lowest astaxanthin concentration was extracted 49 hours after the start of germination, at combinined mixotrophic and heterotrophic germination conditions at a nitrate concentration of the BBM (culture 15). This was poorer in comparison to the mixo-/heterotrophic germination with double nitrate concentration (culture 16) with 17.1 mg L^{-1} and the germination under heterotrophic conditions with 12.9 mg L^{-1} (culture 13) and 12.6 mg L^{-1} (culture 12). As presented in Section 2.2.2, the germination represents a complex procedure, including the up-and downregulation of hundreds of genes under phototrophic conditions. Thus, combining mixotrophic and heterotrophic germination conditions represents a complex process in which the interaction of the light intensity, nitrate and carbon source must be further investigated.

As shown in Figure 35, 49 h after the start of germination, under heterotrophic conditions with the nitrate concentration of the BBM (culture 13) and double nitrate (culture 14), approximately 70% of the cells were in the zoospore stage, showing that the depletion of nitrate did not limit the germination. Under mixo-/heterotrophic cultivation conditions at double nitrate

concentration (culture 16), 84% of cells were at the zoospore stage, while only 40% were in that cell stage with the nitrate concentration of the BBM (culture 15). The ratio of zoospores released at the different germination conditions correlates well with the concentration of astaxanthin extracted into ethyl acetate for all examined conditions.

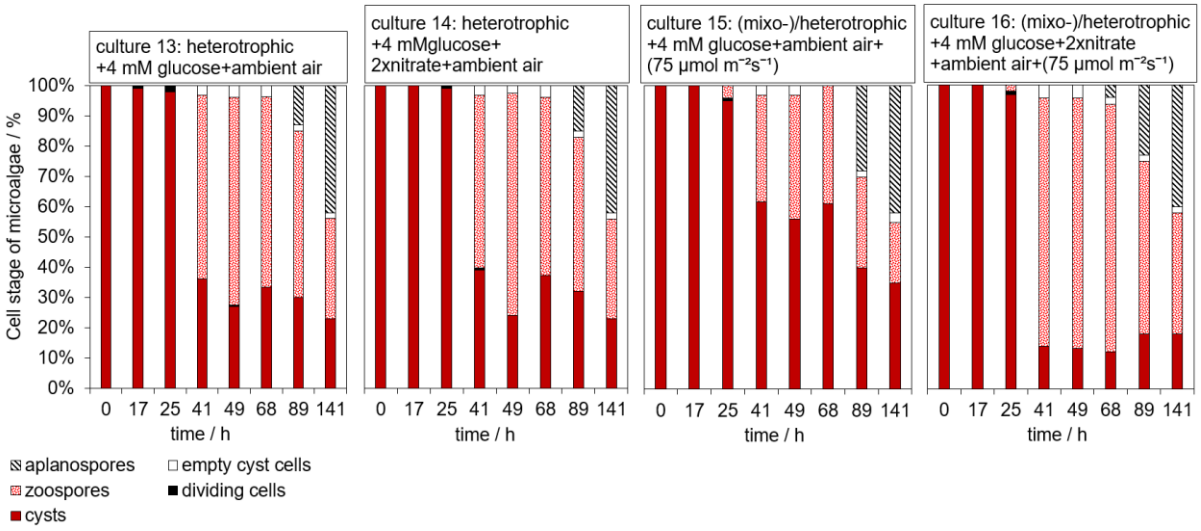

Figure 35: Relative distribution of the cell stages of *H. pluvialis* at different times after the start of germination for the heterotrophic culture 13 (heterotrophic + 4 mM glucose + ambient air) and culture 14 (heterotrophic + 4 mM glucose + 2xnitrate + ambient air), and culture 15 (mixo-/heterotrophic + 4 mM glucose + ambient air + (75 µmol $m^{-2}s^{-1}$) and culture 16 (mixo-/heterotrophic + 4 mM glucose + 2xnitrate + ambient air + (75 µmol $m^{-2}s^{-1}$); data obtained by single determination [9].

As presented in Figure 36, for the cultivation conditions examined, the astaxanthin concentration within the biomass was very stable over time ($p > 0.05$).

As presented in Figure 5, an increase of the glucose supply for the glycolysis might result in an increased carbon flux into the citric acid cycle. Consequently, this might prevent the degradation of intracellular stored astaxanthin fatty acid esters and astaxanthin for growth. With 64%, the largest yield of for the astaxanthin extraction was measured, combining the mixotrophic and heterotrophic cultivation conditions at double nitrate concentration (culture 16), followed by with 56% for the heterotrophic conditions and double nitrate concentration (culture 14), 45% for heterotrophic conditions at a nitrate concentration of the BBM (culture 13), and 26% combining mixotrophic and heterotrophic cultivation conditions at the standard nitrate concentration (culture 15) [9].

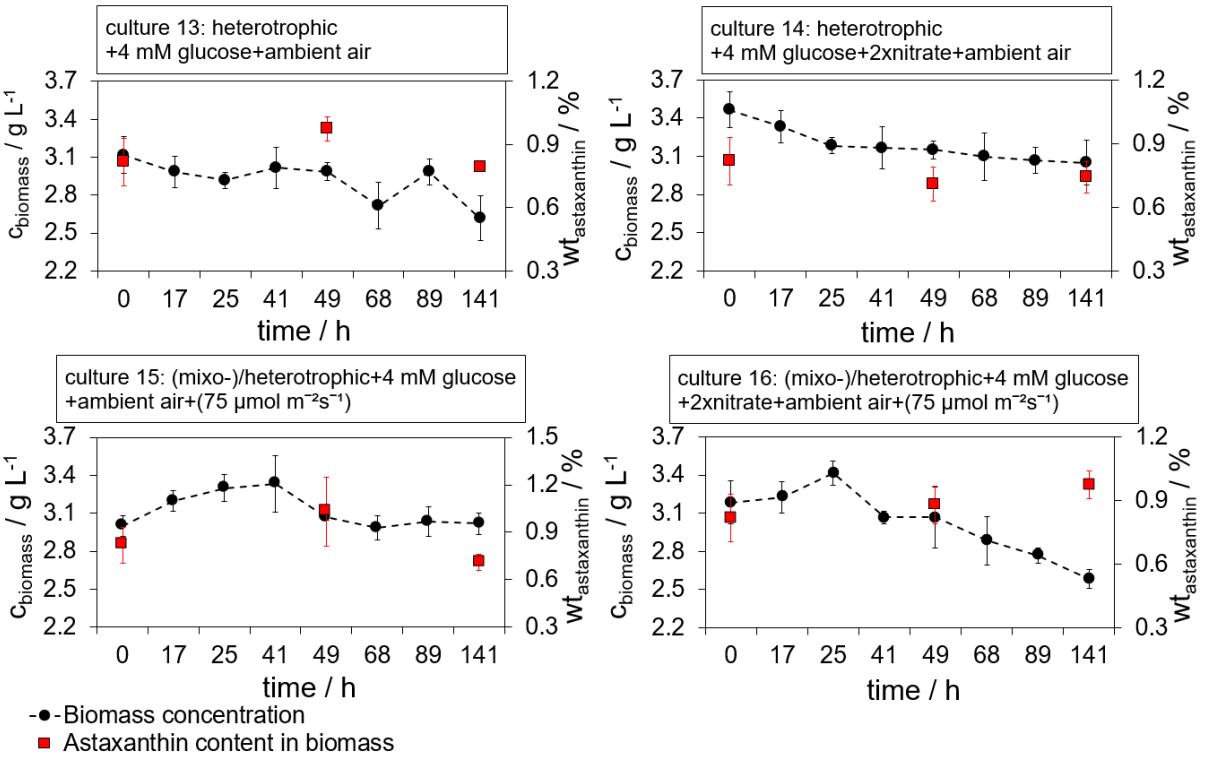

Figure 36: Time course of the biomass concentration and the astaxanthin content in the algal biomass of heterotrophic culture 13 (heterotrophic + 4 mM glucose + ambient air) and culture 14 (heterotrophic + 4 mM glucose + 2xnitrate + ambient air), and culture 15 (mixo-/heterotrophic + 4 mM glucose + ambient air + (75 µmol $m^{-2}s^{-1}$)) and culture 16 (mixo-/heterotrophic + 4 mM glucose + 2xnitrate + ambient air + (75 µmol $m^{-2}s^{-1}$)). Biomass concentration: error bars show ±SD, *n* = 3. Astaxanthin content: error bars show ±SD, *n* = 3 at t = 0 h, t = 49 h and t = 141 h and ±SD, *n* = 2 at t = 17 h, t = 25 h, t = 41 h, t = 68 h and t = 89 h of one biological sample; asterisks indicate significant differences (*t*-test) of measured value vs. control (t = 0 h) at $p < 0.05$ [9].

In summary it could be shown, that the phototrophic and mixotrophic germination is promoted under ambient air compared to 3% v/v CO_2. In addition, it was found that mixotrophic compared to phototrophic germination shows an enhanced zoospore release and extraction of astaxanthin into ethyl acetate at both ambient air and gassing with 3% v/v. Based on these results, heterotrophic germination (with and without addition of glucose) was performed, and a significantly higher release of zoospores and extraction of astaxanthin into ethyl acetate could be observed compared to mixo- and phototrophic conditions. The formation of zoospores in the cyst cells is accelerated with light (photo- and mixotrophic) compared to no light (heterotrophic), but higher extraction yields were measured under heterotrophic conditions. Finally, the highest extraction yield could be achieved by doubling the nitrate content and applying mixotrophic conditions until to nitrate depletion, followed by a heterotrophic cultivation. In addition, the astaxanthin content in the biomass could be kept constant under heterotrophic conditions and combining mixo-/heterotrophic germination conditions.

4.1.3 Influence of CO_2 on phototrophic and mixotrophic cyst cell germination

A systematic investigation of the influence of the CO_2 concentration of the supplied air on *H. pluvialis* cyst cell germination has not yet been reported. Germination of *H. pluvialis* was done phototrophically at different CO_2 levels, gassing of ambient air [12], in 10-second intervals every 10 minutes with CO_2 enriched air [20], and continuously with flue gas containing 3.5+/-0.5% v/v CO_2 [19]. That is what makes the comparison of the results obtained in this work for the influence of CO_2 on germination difficult to compare to literature data. The CO_2 fixation in *H pluvialis* takes place via the C_3 and C_4 photosynthetic pathways [100, 101]. It is catalyzed by the enzyme ribulose-1,5-bisphosphate carboxylase during the Calvin cycle, and G3P is formed (Figure 1). It is a central intermediate for synthesising carbohydrates and carbon skeletons, a preliminary stage of secondary metabolites such as astaxanthin [32] As presented in the first two sets of experiments (culture 1 to culture 8), the cyst cell germination under phototrophic and mixotrophic conditions was not enhanced by supplementing additional CO_2 compared to germination at ambient air. The constant influx of CO_2 and fixation via the Calvin Cycle could shift the equilibrium of internally stored carbon sources from degradation to formation (Figure 1). This might result in reduced available energy for germination, as storage compounds are formed and not used for germination (Figure 5Figure 2). Finally, this might result in a reduced release of zoospores. In contrast, through *H. pluvialis* cyst formation, reduced photosynthetic activity and degradation of the chloroplast has been shown and might be the explanation, that excess of CO_2 cannot be used efficiently for cell growth [101], [9].

4.1.4 Influence of glucose on the *H. pluvialis* cyst cell germination

Some microalgae can use glucose for cell growth via glycolysis [41]. As presented in Section 2.2.2, glycolysis and fatty acid oxidation provide the primary energy during *H. pluvialis* cyst cell germination (Figure 5). During germination and zoospore formation, starch is the most widely used storage polysaccharide in algae [56, 57]. Enzymes and genes that are involved into the glycolysis and ß-oxidation of fatty acids during the phototrophic cyst cell germination of *H. pluvialis* show up-and downregulation to different degrees. As presented in Figure 5, during germination, stored starch is degraded via the upregulated α-amylase and provides dextrin and maltose for glucose metabolism (Section 2.2.2). This study showed that the cyst germination was enhanced at mixotrophic compared to the phototrophic germination conditions, at otherwise identical parameters. The results were confirmed for CO_2 under phototrophic conditions (culture 1 and culture 5) compared to mixotrophic conditions (culture 3 and culture 7) and for ambient air under phototrophic conditions (culture 2 and culture 11) compared to mixotrophic conditions (culture 4 and 12). The phototrophic conditions at ambient air (culture 6) compared to mixotrophic conditions at ambient air (culture 8) might present an exception, which is most probably due to the status of the cysts at the start of the germination.

Also, the heterotrophic germination of *H. pluvialis* cysts is increasing by adding of an external glucose into the medium (culture 10), compared to heterotrophic germination without a carbon source (culture 9). Under heterotrophic cultivation conditions without external glucose (culture 9), a sugar concentration of approximately 150 mg L^{-1} was measured in the medium at the start of germination, probably caused by extra polymeric saccharides of the cyst cells (Figure 37). For both heterotrophic cultivation conditions, 25 hours after the start of germination, a decrease in the glucose concentration was measured, which might indicate glucose consumption. The increase of the sugar concentration 41 hours after the start of germination is most probably caused by extra polymeric saccharides, hexoses of the zoospores cell membrane and mannose of the cyst cell wall [7]. In the heterotrophic cultures, the astaxanthin concentration within the biomass remained relatively stable compared to its initial value ($p > 0.05$). A possible explanation for the constant astaxanthin content within biomass might be, that an increased supply of glucose for glycolysis results in an increased carbon flux into the citric acid cycle. Therefore, adding external glucose might reduce the need to consume astaxanthin fatty acid esters to produce energy (Figure 5).

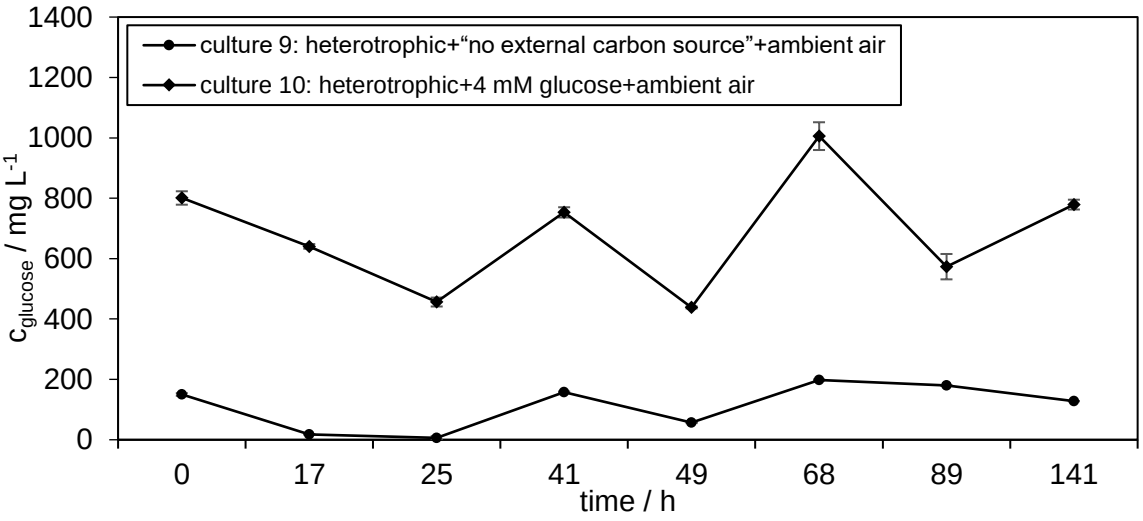

Figure 37: Time course of the glucose concentration in the medium of heterotrophic culture 9 (heterotrophic + "no external carbon source" + ambient air without external glucose) and culture 10 (heterotrophic + 4 mM glucose + ambient air with external glucose); error bars show ±SD, $n = 3$ [9].

4.1.5 Influence of light on the cyst cell germination

The formation and release of zoospores is enhanced at higher light intensity compared to a lower light intensity[19]. This tendency correlates with the velocity of taking up nitrate, while nitrate plays a crucial role in cell growth, and the synthesis of astaxanthin [101], and cyst germination in *H. pluvialis* [18-20]. The time course of the nitrate concentration of the illuminated phototrophic and mixotrophic germination conditions of culture 5 to culture 8 is

presented in Figure 38. 17 hours after the start of germination, all nitrate was nearly consumed under these conditions at a light intensity of 75 µmol $m^{-2}s^{-1}$.

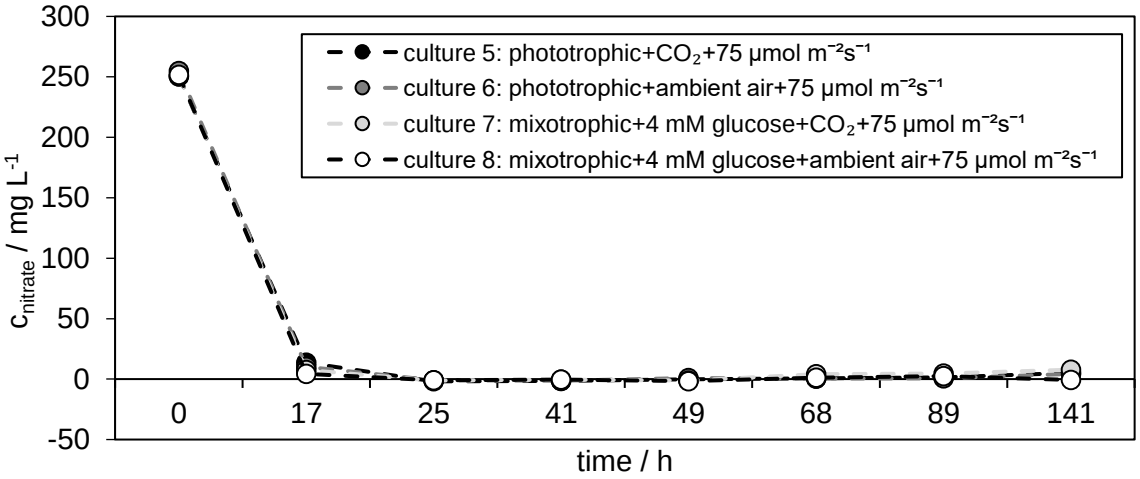

Figure 38: Time course of the nitrate concentration in the supernatant of the phototrophic culture 5 (phototrophic + CO_2 + 75 µmol $m^{-2}s^{-1}$) and culture 6 (phototrophic + ambient air + 75 µmol $m^{-2}s^{-1}$), and mixotrophic culture 7 (mixotrophic + 4 mM glucose + CO_2 + 75 µmol $m^{-2}s^{-1}$) and culture 8 (mixotrophic + 4 mM glucose + ambient air + 75 µmol $m^{-2}s^{-1}$) [9].

The time course of the nitrate concentration of illuminated phototrophic and mixotrophic conditions (culture 11 and culture 12) compared to heterotrophic conditions (culture 9 and culture 10) is shown in Figure 39. Nitrate is already consumed 17 hours after the start of germination under illuminated conditions, compared to 25 hours in heterotrophic conditions. Similar tendencies were observed in the literature for *H. pluvialis* cysts germinated at 300 µmol $m^{-2}s^{-1}$ compared to 150 µmol $m^{-2}s^{-1}$, where nitrate was consumed two days earlier under the higher light intensity [19].

As presented in Figure 40, a similar trend was also measured under heterotrophic conditions of (cultures 13 and 14), compared to the combination of mixotrophic and heterotrophic conditions (cultures 15 and 16). The mixo-/heterotrophic conditions were germinated at a light intensity of 75 µmol $m^{-2}s^{-1}$ until nitrate was depleted and further cultivated at heterotrophic conditions (without light).

As presented in Figure 32 and Figure 35, faster nitrate take up was accompanied by a faster formation and release of zoospores for the illuminated (photo-and mixotrophic) compared germination without light (heterotrophic).

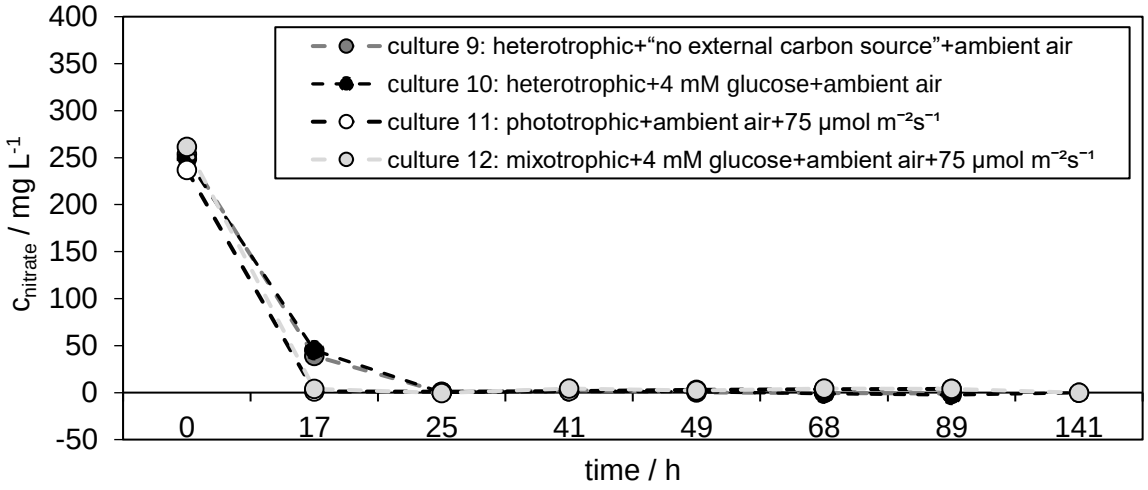

Figure 39: Time course of the nitrate concentration in the supernatant of the culture 9 (heterotrophic + “no external carbon source” + ambient air) and culture 10 (heterotrophic + 4 mM glucose + ambient air), phototrophic culture 11 (phototrophic + ambient air + 75 µmol $m^{-2}s^{-1}$) and mixotrophic culture 12 (mixotrophic + 4 mM glucose + ambient air + 75 µmol $m^{-2}s^{-1}$) [9].

The rate of nitrite and nitrate uptake in microalgae depends on the presence of other nitrogen components, the nitrogen status within the cells, and the light conditions [32, 47].

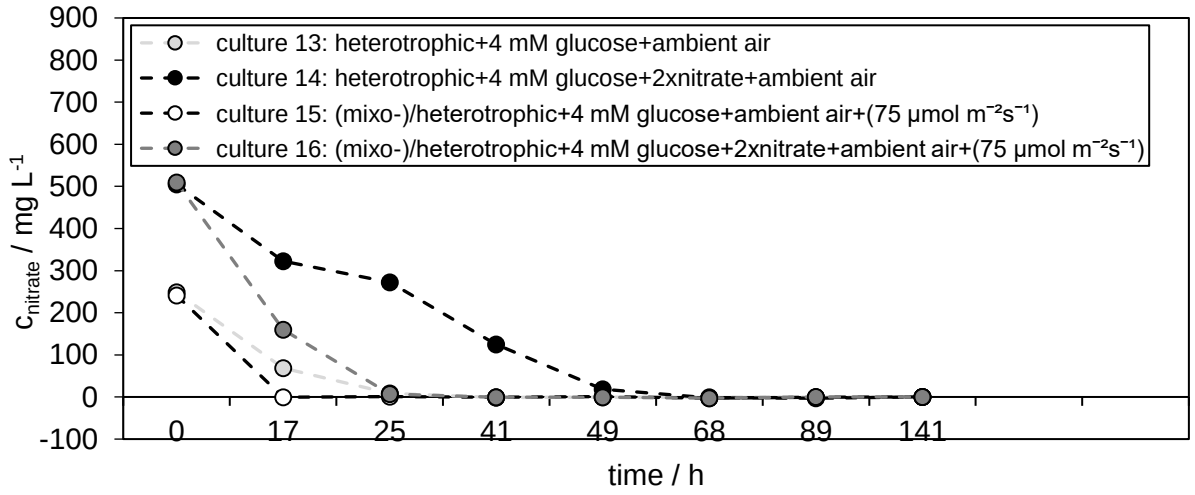

Figure 40: Time course of the nitrate concentration heterotrophic culture 13 (heterotrophic + 4 mM glucose + ambient air) and culture 14 (heterotrophic + 4 mM glucose + 2xnitrate + ambient air), and culture 15 (mixo-/heterotrophic + 4 mM glucose + ambient air + (75 µmol $m^{-2}s^{-1}$) and culture 16 (mixo-/heterotrophic + 4 mM glucose + 2xnitrate + ambient air + (75 µmol µmol $m^{-2}s^{-1}$); data obtained by single determination [9].

As shown in Figure 1, the nitrate uptake into the cell is done via a specific transport system, followed by a reduction to nitrite in the cytosol. Subsequently, nitrite is transported to the chloroplast and reduced to ammonium, which is incorporated into L-glutamate via the glutamine/glutamate cycle and enables cell growth and the formation of amino acids. After

nitrate depletion, supplemented carbon (CO_2 or glucose) is stored as fatty acids, starch or TAGs (Figure 1).

In conclusion, in the illuminated phototrophic and mixotrophic conditions, the nitrate uptake and formation of zoospores was accelerated compared to the heterotrophic conditions. However, fewer zoospores were released under illuminated phototrophic and mixotrophic conditions (culture 11 and culture 12) compared to heterotrophic conditions (culture 9 and culture 10).

4.2 Liquid-liquid extraction of astaxanthin from *H. pluvialis*

In this section an alternative extraction process for the extraction of astaxanthin from germinated zoospores and homogenised *H. pluvialis* cyst cells using LLC and membrane-assisted extraction was to established. Therefore, in the following section, first a green solvent was selected, which allows astaxanthin extraction with high yields from aqueous homogenised cyst cells and germinated zoospores. After selection of the solvent a feasibility study for the extraction of astaxanthin from germinated zoospores and homogenised cysts using a laboratory-scale CCC was first carried out. There, the process concept of the LLC extraction was successfully evaluated. After execution of the astaxanthin extraction from homogenised cyst cells and zoospores using a CCC column, the experiments were scaled up to a CPE column. Membrane extraction was used as an extraction unit, with the aim of achieving complete saturation of the solvent with astaxanthin. The selection of the operating parameters was carried out using the model substance camphor. Based on these results, an extraction of astaxanthin oleoresin into *n*-heptane was done. Finally, astaxanthin was extracted from homogenised cysts.

4.2.1 Solvent selection for astaxanthin extraction from *H. pluvialis*

After successfully establishing a method for *H. pluvialis* cyst cell germination in the previous Section 4.1, solvent selection is performed in this section. In this section a solvent that allows the extraction of astaxanthin from the algal broth containing *H. pluvialis* zoospores or homogenised cyst cells was selected. In the proposed extraction process using LLC, the solvent is used as a stationary phase and kept inside the column via a centrifugal field. The solvent should show high stationary phase retention in the column at high flow rates so that a large amount of astaxanthin can be extracted per extraction [1]. For a robust membrane-assisted extraction process, a stable interface between the solvent in the membrane's pores and the aqueous feed must be formed [28]. For both extraction technologies, the solvent should be almost immiscible with the algal broth, and extraction of astaxanthin from the cytoplasm of the released zoospores or homogenised cyst cells should be possible. Additionally, the solvent should have a low evaporation enthalpy to allow low-cost solvent recovery. As presented in Table 4.2, in this study, *n*-heptane, butan-1-ol, ethyl acetate, methyl-

tert-butyl ether and dichloromethane were tested to extract astaxanthin from the released zoospores and homogenised cyst cells. The solvents were selected using the “Pfizer Solvent Selection Guide”, in which "ethyl acetate" and "butan-1-ol" are the only "preferred” green solvents that are immiscible with water [102]. Additionally, two “usable” solvents that are non-miscible with water, *n*-heptane and methyl-*tert*-butyl ether, were tested. Also one frequently used solvent for extraction of carotenoids, dichloromethane was tested and is classified as an “undesirable” solvent [102-104].

Table 4.2: Physical properties of the tested solvents [1].

	Solubility in water / g L^{-1}	log $P_{octanol/water}$ / -	Enthalpy of vaporisation $\Delta_{vap}H$, (101.325 kPa, T_r= 25°C) / kJ mol^{-1}
n-heptane	0.0024 (25°C)	4.5	36.57
butan-1-ol	80 (25°C)	0.84	52.35
methyl-*tert*-butyl ether	44 (20°C)	0.84	29.82
ethyl acetate	87.9 (25°C)	0.73	35.60
dichloromethane	17.6 (25°C)	1.25	28.82

Astaxanthin was extracted from cyst cells and germinated zoospores, as shown in Figure 41. Therefore, as described in Section 3.9, algal broth containing cyst cells and zoospores were mixed with the solvents for 60 min, centrifuged and the astaxanthin content in the solvent was determined via HPLC analysis after the extraction. The biomass content before extraction was determined as described in Section 3.8.1. To evaluate the extraction, the yield was calculated as presented in Equation 3.8. When cyst cells were used, the extraction yields for all tested solvents was below 1%. An extraction yield of 85% was reached for the extraction of astaxanthin from germinated zoospores using ethyl acetate, followed by 76% for dichloromethane, 49% for methyl-*tert*-butyl ether, 44% for butan-1-ol and 2% for *n*-heptane [1]. Extraction yields of 65% were reported for the extraction of astaxanthin from wet germinated *H. pluvialis* zoospores using *n*-hexane as solvent [105]. Still, no astaxanthin extraction from released *H. pluvialis* zoospores was possible with *n*-heptane in this study, which is due to the poor solubility of *n*-heptane in water (0.0024 g L^{-1} at 25 °C) and the poor contact between the aqueous algal broth and the solvent. Conversely, when dewatered biomass is used, sufficient

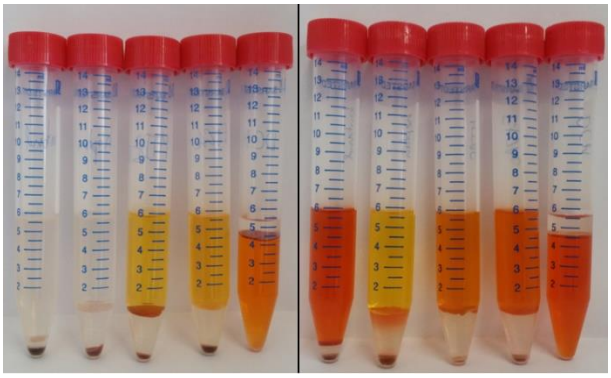

Figure 41: Extraction from cyst cells (left) and from germinated zoospores (right) using the solvents: butan-1-ol, *n*-heptane, methyl-*tert*-butyl ether, ethyl acetate and dichloromethane (from left to right) [1].

contact of the biomass with *n*-hexane might be possible. The relatively low yield with butan-1-ol could be due to the high solubility of water in this solvent (around 20 wt% at 20°C), which might limit the capacity of the solvent for non-polar astaxanthin. Also, the high viscosity (2.57 mPas at 25 °C) of butan-1-ol may reduce diffusion into the cell [1]. For the extraction from homogenised cyst cells, the following extraction yields were achieved: methyl-*tert*-butyl ether (98%), butan-1-ol (89%), ethyl acetate (86%), dichloromethane (84%), *n*-heptane (34%). Similar extraction yields are achieved for the solvents methyl-*tert*-butyl ether, butan-1-ol, ethyl acetate, and dichloromethane, that show a significant water solubility of 4 g L^{-1}, 80 g L^{-1}, 88 g L^{-1}, 18 g L^{-1}, respectively [16]. Considering the yields achieved, and the classification as a green solvent, ethyl acetate is the most promising solvent for LLC and membrane-assisted extraction. In the following sections, the development of the process concepts for the extraction of astaxanthin using LLC and membrane-assisted extraction will be presented.

4.2.2 Astaxanthin extraction from *H. pluvialis* biomass using LLC

In the previous section, the green solvent ethyl acetate was selected as the desired solvent for the extraction of astaxanthin from germinated zoospores and homogenised cyst cells. In this section a process concept for the extraction of astaxanthin from zoospores and homogenised cyst cells using an LLC column was implemented. First, the feasibility of the extraction process was evaluated using a laboratory CCC column. Based on these results, a scale-up to a CPE column was performed and the operating parameters were chosen to increase the yield and productivity of the process.

4.2.2.1 Process concept

In this section, the process concept for the extraction of astaxanthin from germinated zoospores or homogenised cyst cells into a solvent using CCC or CPE is presented. As shown schematically in Figure 42, the LLC unit (CCC or CPE column) was filled with solvent (saturated with water), which was used as a stationary phase (Figure 42 a). After the rotation was set, water (saturated with solvent) was pumped in the descending mode (Figure 42 b). Depending on the set flow rate, a certain amount of the stationary phase was pushes out from the column until the hydrodynamic equilibrium was reached at a time $t_{equilibration}$, where no more stationary phase was pushed out of the column. The displaced stationary phase volume was collected to determine the stationary phase retention S_f according to Equation 2.22. The algal broth (homogenised cyst cells or germinated zoospores) was injected via an injection loop (Figure 42 c). The mobile phase was continuously pumped in the descending mode, and astaxanthin was extracted from the algal feed (mechanically disrupted cyst cells or germinated zoospores) into an organic solvent (Figure 42 d).

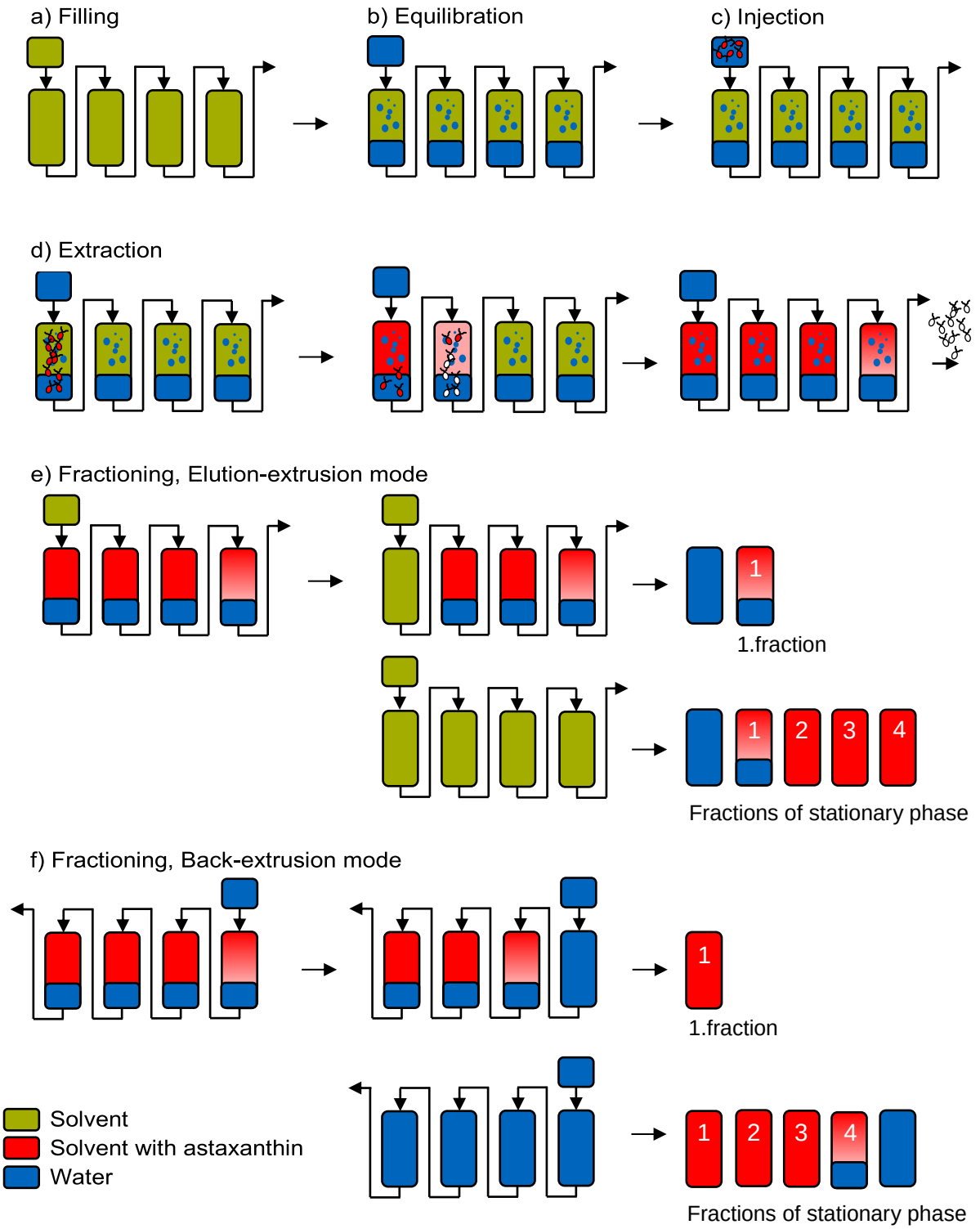

Figure 42: Schematic presentation of the extraction of astaxanthin into a solvent using a LLC column, including a) filling of the column with solvent, b) equilibration with water, c) Injection of the algal biomass (zoospores or mechanically disrupted cyst cells), d) Extraction of astaxanthin from the aqueous algal broth into the solvent, e) Fractioning of the stationary phase in the Elution - extrusion mode, f) Fractioning of the stationary phase in the Back - extrusion mode [95].

The algal biomass can be seen as a solute i with a partition coefficient $P_i \rightarrow 0$. Therefore, the time t_{switch}, where the extracted algal biomass left the LLC unit (Figure 42 d) can be calculated according to Equation 4.1.

$$t_{switch} = \frac{V_{MP} + V_{inj}}{F_{MP}} \quad 4.1$$

To recover the solvent containing astaxanthin, the stationary phase was discharged from the column and fractionated applying the elution-extrusion (Figure 42 e) or back-extrusion (Figure 42 f) mode (Section 2.4.4). In the elution-extrusion mode, to push the astaxanthin-containing stationary phase out of the column, the stationary phase (solvent) is pumped in the same flow direction as the mobile phase.

The first collected fraction is the least concentrated. In back-extrusion mode (Figure 42 f), the stationary phase is pushed out of the column by changing the flow direction of the aqueous mobile phase. The last collected fraction is the least concentrated. After discharging the stationary phase, astaxanthin adsorbed on the PTFE layer of the CPE column was recovered by injecting 80 mL acetone. The cleaning step was not required for the extraction using the CCC column, since no astaxanthin was adsorbed on the tube of the CCC unit. Aliquots of the collected fractions were pipetted into vials (4 mL), evaporated using an Alpha 3-4 LSC basic freeze dryer from Martin Christ Gefriertrocknungsanlagen GmbH (Germany). The astaxanthin content of the collected fractions was analyzed using the HPLC method described in Section 3.8.2.

The total process time $t_{Process}$ was defined as presented in Equation 4.2, where $t_{filling}$ is the time for filling the LLC unit with solvent (stationary phase), $t_{equilibration}$ the time for the hydrodynamic equilibration of the column, t_{switch} the time of extraction until discharging the stationary phase, $t_{fractioning}$ the time needed to fraction the stationary phase with extracted astaxanthin and $t_{cleaning}$ the time to clean the LLC unit.

$$t_{Process} = t_{filling} + t_{equilibration} + t_{switch} + t_{fractioning} + (t_{cleaning}) \quad 4.2$$

Based on the column volume, the productivity Pr can be calculated according to Equation 4.3. There $m_{astaxanthin/oleoresin}$ is the mass of astaxanthin or oleoresin extracted into the stationary phase and recovered after cleaning of the LLC unit, V_c the column volume and $t_{Process}$ the overall process time.

$$Pr = \frac{m_{astaxanthin/oleoresin}}{V_c \cdot t_{Process}} \quad 4.3$$

As presented in Equation 4.4, the astaxanthin extraction yield Y was defined as the sum of the extracted mass of astaxanthin into the solvent $m_{ATX,SP}$ and the quantity $m_{ATX,clean}$ recovered after CPE column cleaning, divided by $m_{ATX,F}$, which is the mass of astaxanthin in the injected algal feed. As astaxanthin cannot be directly extracted from cyst cells into ethyl acetate, Y depends on the number of mechanically disrupted cyst cells or released zoospores.

$$Y = \frac{m_{ATX,SP} + m_{ATX,clean}}{m_{ATX,F}} \quad 4.4$$

Therefore, the yield $Y_{extractable}$ which amounts the actual extractable mass of astaxanthin from the algal feed was defined as shown in Equation 4.5. For each extraction experiment the extractable amount of astaxanthin from the algal feed (mechanically disrupted cysts or zoospores) was determined. Therefore 5 mL algal broth with 5mL ethyl acetate were mixed using a Multi Bio RS-24 shaker from Biosan (Riga, Latvia) for 60 min. Afterwards the samples were centrifuged at 5500 rpm for 15 min using the Sigma 3-16KL centrifuge from Sigma GmbH (Germany) and the mass of astaxanthin extracted into the solvent $m_{ATX,\ single\text{-}stage\ extraction}$ was determined using the HPLC method described in Section 3.8.2.

$$Y_{extractable} = \frac{m_{ATX,SP} + m_{ATX,clean}}{m_{ATX,\ single\text{-}stage\ extraction}} \quad 4.5$$

The process scheme shown Figure 42 was evaluated in the following sections using a CCC column. First, the operating parameters flow rate and rotation speed of the CCC unit were selected. Subsequently an evaluation of the time t_{switch} was done and the operating mode, elution-extrusion, or back-extrusion mode, was selected.

4.2.2.2 CCC operating parameter selection

In this section the operating parameters of a laboratory CCC column for the extraction of astaxanthin from a zoospore-containing *H. pluvialis* algal broth were determined. Therefore, the operating parameters flow rate of the mobile phase and rotational speed of the CCC unit were varied and the influence on the stationary phase retention S_f (Equation 2.22), the concentration profile of astaxanthin in the stationary phase, and the yield (Equation 4.5) was determined.

The solvent methyl-*tert*-butyl ether was used for the extraction, as high extraction yields could be reached for the extraction from germinated zoospores with this solvent, as shown in Section 4.2.1. The preferred green solvent ethyl acetate could not be used, as it did not show stationary phase retention at 1900 rpm and 1.0 mL min^{-1}. In the literature, the ethyl acetate/water system is reported as a highly stable system, which is described through the ratio of the interfacial tension to density difference of the two phases. The ethyl acetate/water system also shows an extremely low Bond number of 0.03. This dimensionless value sets the gravitational force that acts on a liquid in relation to the surface tension force [1]. The dispersed droplets are stable for small Bond numbers, thus the droplets tend to be less dispersed in the stationary phase, resulting in the displacement of the stationary phase through the mobile phase from the column [1, 106]. As shown in Equation 2.22, S_f describes the ratio of stationary phase in the column to the total column volume.

A high stationary phase retention is wanted for the extraction process to enable high sample loading per extraction cycle. In general, high rotation speeds and low flow rates are beneficial

for a high stationary phase retention. However, above a certain flow rate, increasing the rotation speed does not further increase the retention of the stationary phase [107], [108]. In principle, in LLC units, the stationary phase retention decreases linearly with the square root of the flow rate of the mobile phase [22]. On the other hand, a high flow rate is desirable for good mixing of the mobile phase in the stationary phase for enhanced mass transfer [79].
As presented in Table 4.3, the stationary phase retention and the concentration profile of the collected stationary phase was determined for variations of the rotational speed (1500 and 1900 rpm) and flow rates (0.5 and 1.0 mL min^{-1}). These values represent the typical operation ranges of the used CCC column [74]. CCC extraction experiments were conducted as shown schematically in Figure 42. The CCC column was first filled with methyl-*tert*-butyl ether (saturated with water) and then the rotation of the CCC column was set. After pumping the mobile phase, the displaced stationary phase volume was collected and S_f was determined (Equation 2.22). Then 2 mL of germinated zoospores (saturated with methyl-*tert*-butyl ether) were injected and after the extracted biomass left the column at t_{switch}, the stationary phase was pumped out of the column with water (back-extrusion mode) and fractionated beginning with the most concentrated fraction. The astaxanthin content of the individual fractions was determined using the HPLC method presented in Section 3.8.2.

Table 4.3: Stationary phase retention of methyl-*tert*-butyl ether, $Y_{extractable}$ for injection volumes of 2 mL germinated zoospores, at rotational speeds of 1500 and 1900 rpm and mobile phase flow rates of 0.5 and 1.0 mL min^{-1} using a CCC column with 18.2 mL column volume [1].

ω / rpm	F_{MP} / mL min^{-1}	V_{SP} / mL	S_f / %	τ / min	$Y_{extractable}$ / %
1900	1.0	11.7	64.3	7.1	82.6
1900	0.5	13.2	72.5	10.0	43.0
1500	1.0	7.9	43.4	10.3	61.7
1500	0.5	13.0	71.4	10.4	69.6

As shown in Table 4.3, the highest stationary phase retention was measured at the lowest flow rate of 0.5 mL min^{-1} and the highest rotational speed of 1900 rpm and decreases with an increase of the flow rate to 1.0 mL min^{-1}. A similar tendency was measured for lower rotational speeds. The measured trends are in good agreement with literature [109]. For the extraction process, a high stationary phase retention and mobile phase flow rate and are favoured. A high stationary phase retention allows high sample loading per extraction process, while the dispersion of the mobile in the stationary phase and thus the mass transfer of astaxanthin into the solvent are enhanced at high flow rates of the mobile phase. The concentration profile of the fractionated stationary phase are presented in Figure 43 for the operating parameters examined, where 2 mL germinated zoospores (saturated with methyl-*tert*-butyl ether) were injected.

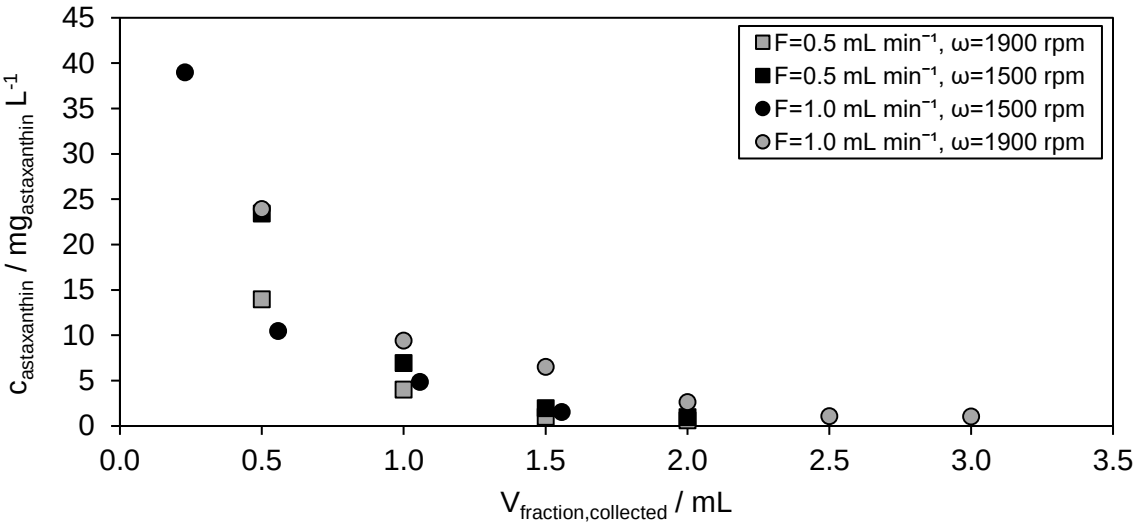

Figure 43: Concentration profile of the collected fractions after injection of 2 mL germinated zoospores extracted at a mobile phase flow rate of 0.5 and 1 mL min^{-1} and rotational speeds of 1500 and 1900 rpm [1].

As shown schematically in Figure 42, the fractions were pushed out of the column by means of the aqueous phase (back-extrusion), and the highest concentrated fractions collected first (Figure 44). The highest astaxanthin concentrations were measured in the fractions at a mobile phase flow rate of 1.0 mL min^{-1} and a rotational speed of 1900 rpm (Figure 43 and Figure 44 d). This is in good agreement with theory since for high flow rates better dispersion of the mobile in the stationary phase, and thus enhanced mass transfer can be expected [22] The higher astaxanthin concentration in the first collected fraction at 1.0 mL min^{-1} and 1500 rpm compared to 1.0 mL min^{-1} and 1900 rpm represents an outlier, due to the aqueous phase in that collected fraction (Figure 43 and Figure 44 c). As the highest yield, calculated as presented in Equation 4.5 (mass of astaxanthin in the fractions to extractable amount) of 82.6% was reached at the highest a flow rate and rotational speed (Table 4.3), the subsequent CCC experiments were conducted under these operating conditions.

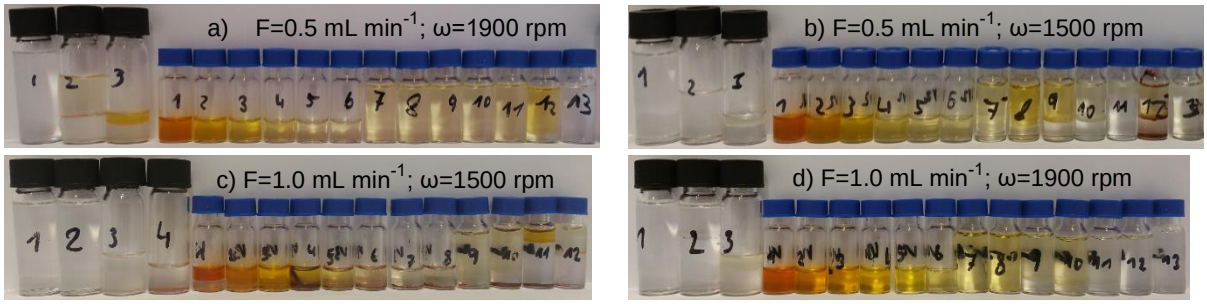

Figure 44: Collected fractions of the stationary phase for an injection volume of 2 mL germinated zoospores and operating conditions of 0.5 and 1.0 mL min^{-1} at 1500 and 1900 rpm.

4.2.2.3 Evaluation of the switching time

In the previous Section 4.2.2.2, the operating parameters flow rate and rotational speed of the CCC were successfully selected. In this section it was examined, whether the extracted biomass elutes from the CCC column at minimum defined time t_{switch} (Equation 4.1). Therefore, the CCC column was operated with methyl-*tert*-butyl ether at the rotational speed and mobile flow rate of 1900 rpm and 1 mL min^{-1}, selected in the previous Section 4.2.2.2. After hydrodynamic equilibrium was reached, 0.5 and 2.0 mL of flagellated zoospores (equilibrated with solvent) were injected. The minimum time t_{switch} to empty the column by pumping the aqueous phase (back-extrusion) was increased as shown in Figure 45. The concentration of the collected fractions was analysed using the HPLC method described in Section 3.8.2 and the yield was calculated according to Equation 4.4. As shown in Figure 45, the extracted biomass elutes at the minimum required time t_{switch}. In addition, as shown in Figure 45, yields of around 30% were achieved for the selected times of t_{switch}. The outlier with an injection volume of 2 mL and t_{switch} of 20.4 min could be due to inaccuracies in the HPLC method. The results show, that t_{switch} as defined in Equation 4.1 is sufficient for the extracted biomass to elute from the CCC column. Therefore, in all subsequent LLC experiments, after the injection of the biomass, fractionation was carried out after the time t_{switch}.

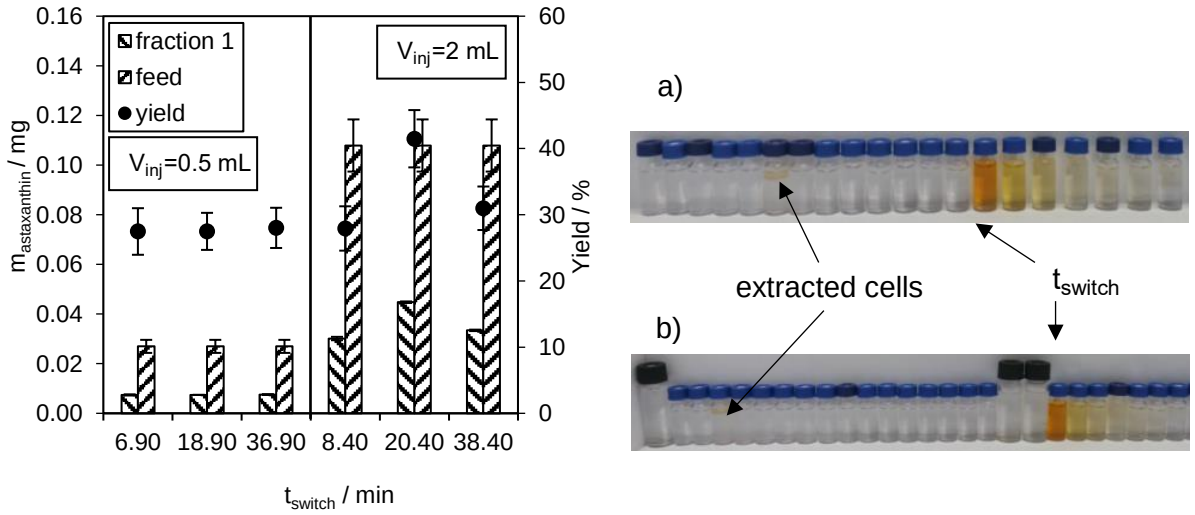

Figure 45: Left: Mass of astaxanthin in the first fraction the stationary phase, the injected mass of astaxanthin (feed) and the yield Y for injection volumes of 0.5 and 2.0 mL germinated zoospores and different times, t_{switch}
Right: Collected fractions of the CCC experiments with (a) an injection volume of 0.5 mL (t_{switch} = 18.9 min) and (b) an injection volume of 0.5 mL (t_{switch} = 36.9 min) [1].

4.2.2.4 CCC operating mode selection

In this section the operating mode for the extraction of astaxanthin from *H. pluvialis* using a CCC column were selected. Stationary phase collection without an additional aqueous phase is desired, so that no further gravimetric liquid-liquid separation is needed prior to solvent

evaporation. As presented in Figure 42, emptying of the column can be performed after the algal biomass ($P_i \rightarrow 0$) eluted from the column, either by pumping the aqueous phase in the descending mode (back-extrusion) or solvent in the ascending phase (elution-extrusion).

As presented in Figure 15, in the back-extrusion mode, when the aqueous phase is pumped in the "wrong" ascending direction, the upper phase (solvent) is pushed towards the column head [87]. In theory, the stationary phase can be collected continuously before the mobile phase is discharged from the column outlet [87]. In elution-extrusion mode, the stationary phase is pumped in the same direction instead of the mobile phase. After the collapse of the hydrodynamic equilibrium, the mobile phase elutes first (sweep elution), followed by the stationary phase in the extrusion step.

As presented schematically in Figure 42, methyl-*tert*-butyl ether (saturated with water) was pumped into the column and a rotational speed of 1900 rpm, and the CCC unit was equilibrated at a mobile flow rate of 1 mL min^{-1}. Subsequently, 2 mL of homogenised algal broth was injected, and after the time t_{switch}, the stationary phase was discharged and the fractions were collected. Four different modes for stationary phase fractioning were examined:

a) Back extrusion: ω=1900 rpm, F=1 mL min^{-1}

b) Back extrusion: ω=0 rpm, F=1 mL min^{-1}

c) Elution extrusion: ω=0 rpm, F=1 mL min^{-1}

c) Elution extrusion: ω=1900 rpm, F=1 mL min^{-1}

In Figure 46, the collected fractions of the stationary phase are presented. As can be seen, fractioning without an aqueous phase was only achieved in the elution-extrusion mode at a flow rate of 1.0 mL $min^{-1}$and a rotational speed of 1900 rpm (Figure 46 d).

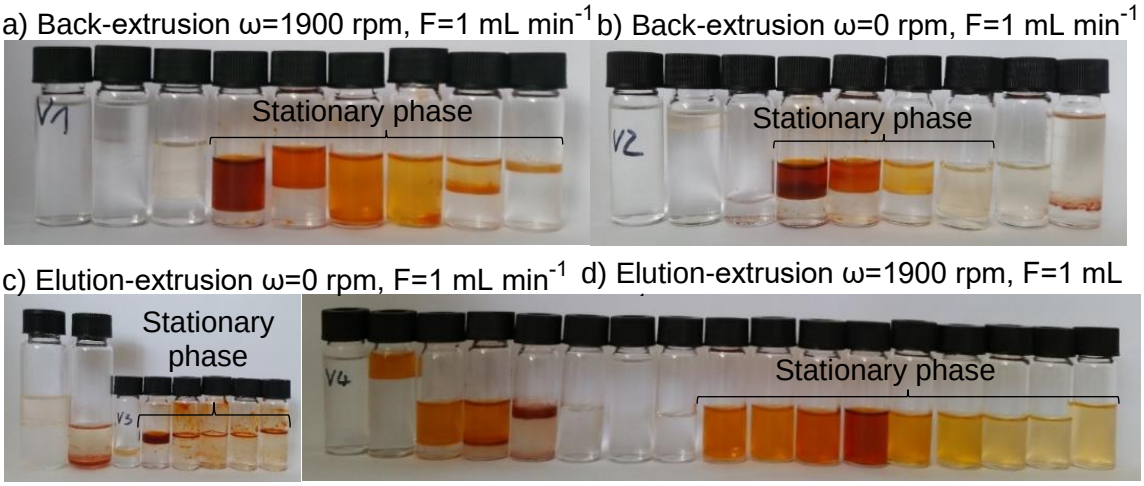

Figure 46: Fractioning of the stationary phase using the back-extrusion mode at a flow rate of the aqueous mobile phase of a) 1 mL min^{-1} and a rotational speed of 1900 rpm and b) 0 rpm, as well as using the elution-extrusion mode at a rotational speed of c) 0 rpm and d) 1900 rpm.

A possible explanation for this behaviour might be, that in the elution-extrusion (Figure 46 d) compared to the back-extrusion mode (Figure 46 a) the latter suddenly interrupts the solute partitioning. In elution-extrusion, there is still phase interaction until the aqueous phase leaves the column (Figure 15) [110]. In the elution-extrusion mode, the mobile phase (and any remaining emulsifying cell debris) is eluted from the column before the organic phase is discharged, which is the case when using the elution-extrusion mode. A possible explanation for the water in the collected stationary phase in the elution-extrusion mode without rotational speed (Figure 46 c) could be that the two phases do not separate gravimetrically, and thus an undefined discharging of the stationary phase takes place.

As a result, in the subsequent LLC experiments, the extraction of astaxanthin from zoospores or homogenised *H. pluvialis* cyst cells was done in the elution-extrusion mode and the fractioning was performed at the rotational speed of operation.

4.2.2.5 Influence of the injection volume and biomass concentration on productivity and yield using a CCC column

In the previous Sections, the operating parameters flow rate and rotational speed (Section 4.2.2.2), the minimum switching time t_{switch} (Section 4.2.2.3), and the operating mode elusion-extrusion (Section4.2.2.4) were successfully evaluated. In these experiments, only 2 mL of algal broth was injected, which corresponds to approximately 11% column volume.

In this section the productivity of the extraction process from homogenised cyst cells and flagellated zoospores was to increased. Therefore, the injected volume and biomass concentration were increased. The extraction was done at the operating parameters selected in Section 4.2.2.2: a rotational speed of 1900 rpm and a flow rate of 1.0 mL min^{-1}. After injection of the biomass the stationary phase was collected in the elution-extrusion mode, as described in the previous Section 4.2.2.4.

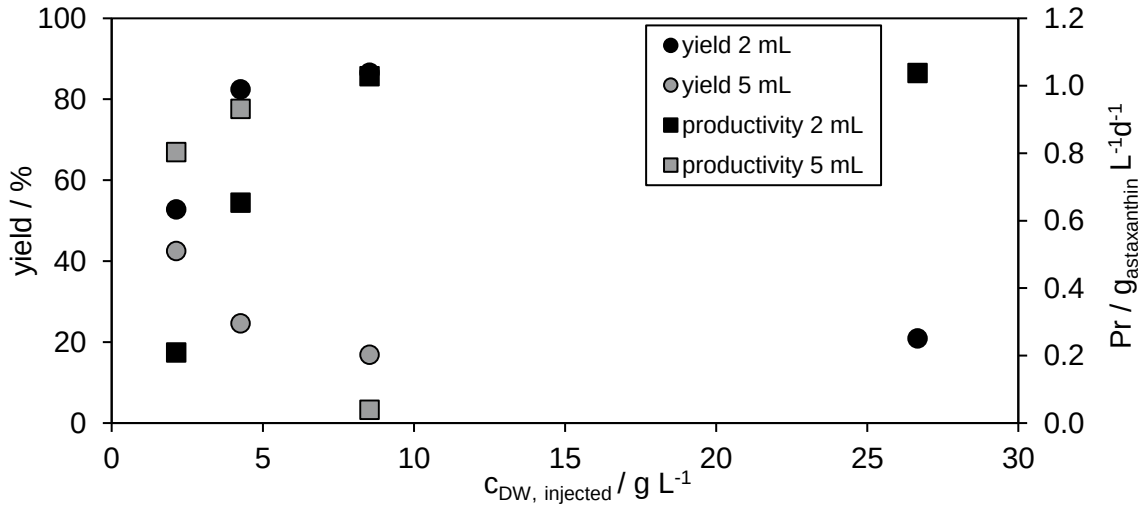

Figure 47: Productivity and yield at different biomass concentrations and 2 mL and 5 mL injection volumes for the extraction of astaxanthin from germinated zoospores using CCC.

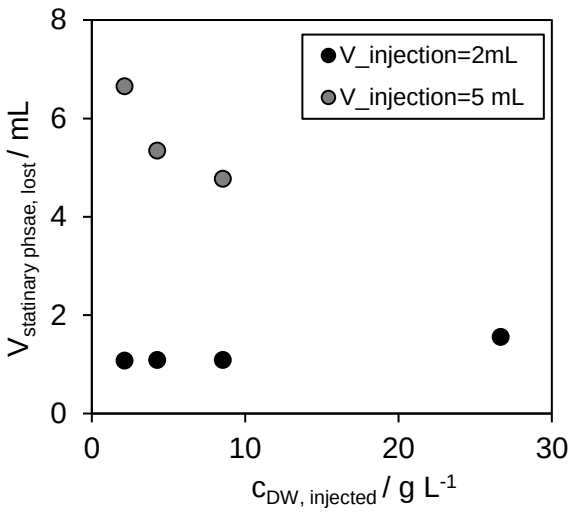

Figure 48: Loss of stationary phase at different biomass concentrations and 2 mL and 5 mL injection volumes for the extraction of astaxanthin from germinated zoospores using CCC.

The astaxanthin concentration in the collected fractions was determined via HPLC (Section 3.8.2). To evaluate the extraction process, the productivity (Equation 4.3), the yield (Equation 4.4) and the loss of stationary phase were measured. In Figure 47, the productivity and yield are presented for the extraction of astaxanthin from germinated zoospores at different biomass concentrations and volumes. The highest productivity of 1.04 $g_{astaxanthin}$ $L^{-1}_{column}d^{-1}$ was reached at the highest injected biomass concentration and a low injection volume of 2 mL. However, at these conditions a yield of only 21% was measured. A similar tendency was seen for injections volumes of 5 mL, where the yield declines with an increase of the injected biomass concentration. The reason for that is probably the increased viscosity of the feed, which increases with the biomass concentration and results in reduced astaxanthin mass transfer. The stationary phase retention before the injection was at around 64%, which corresponds to a volume of the stationary phase of 11.7 mL.

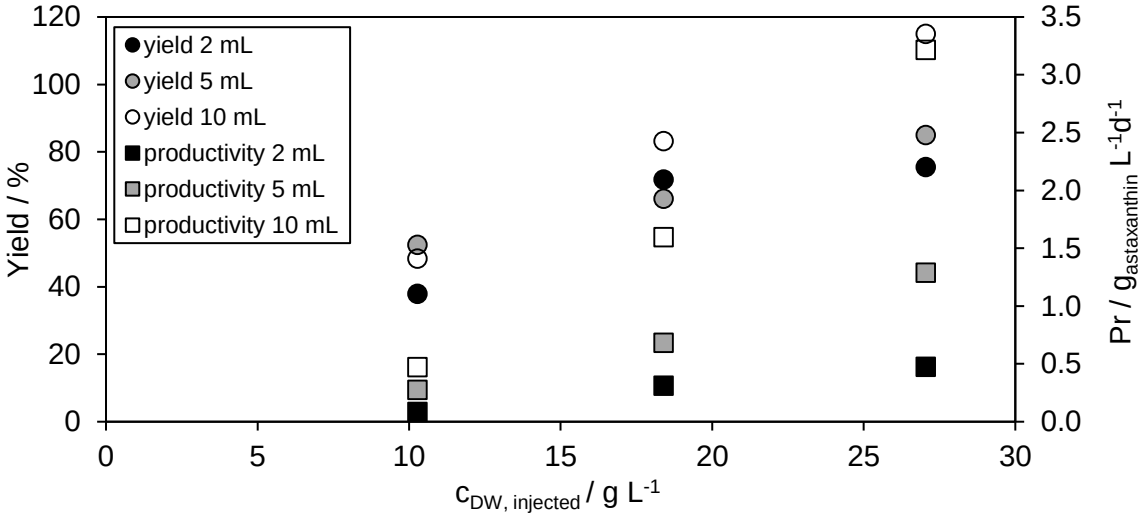

Figure 49: Productivity and yield at different biomass concentrations and 2 mL, 5 mL and 10 mL injection volumes for the extraction of astaxanthin homogenised cyst cells using CCC.

As shown in Figure 48, the injection of germinated zoospores is also accompanied by a strong discharge of the stationary phase through the biomass injection, where the loss of stationary phase is larger at the higher injection volume than at the lower one. The productivity and yield for the extraction of astaxanthin from homogenised cyst cells at different injection volumes

and biomass concentrations are presented in Figure 49. There, the maximum productivity of 3.22 $g_{astaxanthin}$ $L_{column}^{-1}d^{-1}$ was achieved at the maximum injected biomass concentration and injection volume examined. A yield of around 100% was reached.

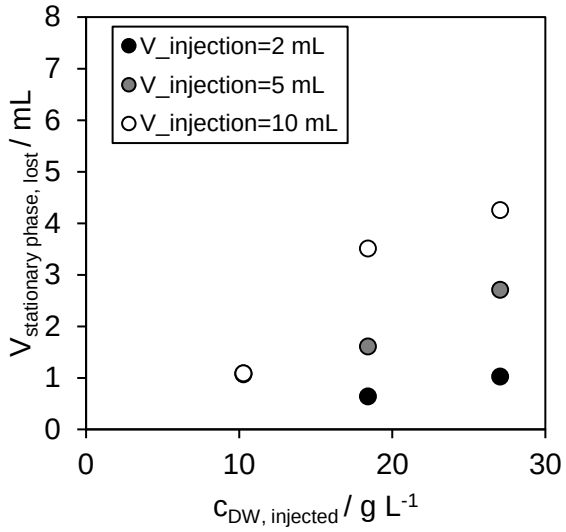

Figure 50: Loss of stationary phase at different biomass concentrations and 2 mL, 5 mL and 10 mL injection volumes for the extraction of astaxanthin homogenised cyst cells using CCC.

The loss of stationary phase for the injection of homogenised cyst cells at different biomass concentrations and volumes is presented in Figure 50. Here, an increase in the discharged stationary phase volume with increasing injection volume and biomass concentration can be observed. In general, loss of stationary phase occurs due to the disturbance of the hydrodynamic equilibrium, which is caused by the injected biomass (homogenised cyst cells or zoospores). The loss of stationary phase tended to be larger for the injection of germinated zoospores compared to homogenised cyst cells. The disturbance of the hydrodynamic equilibrium between the two phases might be larger for the extraction of zoospores with a cell size of around 20 µm diameter and a gel-like cell-matrix than for homogenised cyst cells [6]. Comparing the yields and productivities measured, tendentially lower yields and productivities were measured for the extraction from germinated zoospores compared to homogenised cyst cells at similar injection volumes and biomass concentrations. This is presumably because the zoospores still have an intact cell membrane, which provides an additional diffusion barrier [7]. A further increase in productivity by increasing the injection volume was not possible due to the stationary phase loss, which limits the process scale-up. Based on the results in this section, a scale-up of the extraction was performed using a CPE unit in the following Section 4.2.2.6. Due to their special column geometry, these columns enable high through puts at simultaneously low stationary phase loss [107].

4.2.2.6 CPE operating parameters selection

In the previous Sections 4.2.2.1-4.2.2.5, the process concept for the extraction of astaxanthin from germinated zoospores and homogenised cysts using a CCC column (Figure 42) was successfully evaluated. However, the use of the CCC column showed scale-up limitations. The preferred solvent for extraction, ethyl acetate (Section 4.2.1) did not show stationary phase retention in the CCC unit at the preferred operating conditions of 1900 rpm and 1 mL min^{-1} (Section.4.2.2.2). In addition, as presented in the previous Section 4.2.2.5, a

further increase of the productivity was limited through the high stationary phase loss caused by the sample injection. Due to their unique cell design, CPE columns overcome these limitations. The ethyl acetate/water system was reported to show high stationary phase retention in CPE columns [111].

In this section the operating parameters flow rate and concentration of the injected homogenised biomass for the CPE extraction were selected. The parameters examined are shown in Table 4.4.

Table 4.4: Stationary phase retention of ethyl acetate in the CPE column, at a rotational speed of 1800 rpm and mobile phase flow rates of 10, 20 and 40 mL min^{-1} and extraction yields for an injection volume of 20 mL homogenised biomass.

ω / rpm	F / mL min^{-1}	V_{SP} / mL	S_f / %	τ / min	c_{DW} / g L^{-1}	Yield / %
1800	40	188.1	77.1	1.4	72.5	46.0
1800	20	208.1	85.3	1.8	72.5	64.9
1800	10	224.0	91.8	2.0	72.5	58.2
1800	40	188.1	77.1	1.4	24.0	73.8

The experiments were performed at a rotation speed of 1800 rpm to ensure high stationary phase retention. As already mentioned in Section 4.2.2.1, this is desired to achieve high sample loading per extraction cycle. In addition, the flow rate was varied from 10 to 40 mL min^{-1}, which presents a typical operating range for the used CPE column [81]. As seen in Section 4.2.2.2 for the astaxanthin extraction using a CCC column, a high flow rate is desirable to allow good dispersion of the mobile phase in the stationary phase to reach high mass transfer and yields. Additionally, as shown in the previous Section 4.2.2.5, the injected biomass concentration has a significant impact on the yield and productivity of the extraction process. For this reason, the influence of the biomass on the extraction process was also examined in these experiments (Table 4.4).

The CPE column was first filled with ethyl acetate (saturated with H_2O) and the rotation was started. Then the mobile, aqueous phase (saturated with ethyl acetate) was pumped. After the hydrodynamic equilibrium was reached, 20 mL of homogenised cyst cells were injected. After injection of the biomass, the stationary phase was emptied in the elution-extrusion mode and the astaxanthin content in the collected fractions was determined using HPLC (Section 3.8.2). To evaluate the process performance, stationary phase retention (Equation 2.22) and the yield (Equation 4.4) were calculated. The highest yield was reached at the highest flow rate and lowest injected biomass concentration. This is in good accordance with theory, as for high flow rates best dispersion of the mobile in the stationary phase can be expected [22]. In comparison to that, the lowest yield was achieved at the highest flow rate and highest injected biomass concentration. This suggests that a high biomass concentrations compared to low ones leads to a reduced mass transfer of astaxanthin into the solvent, because of a higher viscosity at

larger biomass concentrations. The lower yield at 40 mL min^{-1}, compared to a flow rate of 20 or 10 mL min^{-1}, might be due to the shorter residence time (Equation 2.24), of the biomass in the CPE unit at a higher flow rate [95]. Consequently, all further CPE experiments were carried out at low biomass concentration and a high flow rate of 40 mL min^{-1}, to enable a high yield.

4.2.2.7 Influence of the injection volume and cell concentration on productivity and yield using a CPE column

In the previous Section 4.2.2.6, the operating parameters flow rate, rotational speed and injected biomass concentration of the CPE extraction were selected. There, 20 mL of homogenised cyst cells were injected, which corresponds to approx. 12% column volume. In this section the productivity of the CPE extraction from homogenised cyst cells and germinated zoospores was further increased. The yields and productivities measured in this section are used in the techno-economic study in Section 4.3 for the process scale-up to an industrial CPE column. The operating parameters were selected in the previous Section 4.2.2.6, and the extraction was performed at a rotational speed of 1800 rpm and a flow rate of 40 mL min^{-1}, using homogenised cyst cells with a biomass concentration of 33 g L^{-1}. The injection volume of the homogenised cyst cells was increased from 20 mL to 480 mL. The CPE extraction was performed according to the process scheme in Figure 42 in the elution-extrusion mode, and the astaxanthin content in the fractions was determined using the HPLC method described in Section 3.8.2. Additionally, the astaxanthin content of the astaxanthin oleoresin, which is obtained after the evaporation of ethyl acetate, was determined using the same HPLC method. 80 mL of acetone was injected after each experiment to recover residues adsorbed onto the CPE column. The extraction yield was calculated according to Equation 4.4.

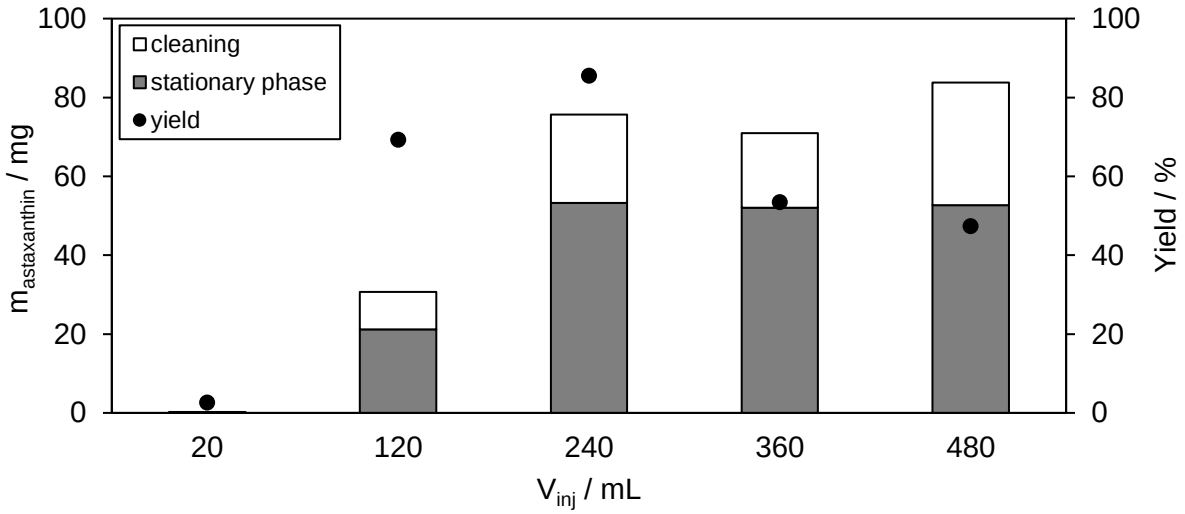

Figure 51: Extracted mass of astaxanthin in the stationary phase and after cleaning the CPE unit for an injected biomass concentration of 33 g L^{-1}, a flow rate of 40 mL min^{-1}, a rotational speed of 1800 rpm and injection volumes of 20, 120, 240, 360 and 480 mL [95].

In Figure 51 the mass of astaxanthin extracted into the stationary phase and in the cleaning

fraction with acetone are presented. For injection volumes of 240 mL to 480 mL the maximum amount of astaxanthin extracted into the solvent (stationary phase) was around 54 mg. The extraction yield declines from 85% at an injection volume of 240 mL to 48% at 480 mL [95]. That is because an increasing proportion of biomass, leaving the CPE unit non-extracted. In contrast to CCC extraction, no loss of stationary phase occurred through sample injection. Significant amounts of astaxanthin could be recovered from the column after fractioning by acetone injection. The relatively intense adsorption of astaxanthin oleoresin is probably due to the PTFE coating of the CPE. In Figure 52, the yield and productivity of the CPE extraction at different injection volumes are presented. The highest productivity and yield was reached at an injection volume of 240 mL. To avoid large product losses in this process step, the operating conditions at an injection volume of 240 mL using homogenised *H. pluvialis* biomass with a concentration of 33 g L^{-1} were selected for process scale-up in the techno-economic analysis presented in Section 4.3. The collected fractions and the astaxanthin concentration profile are presented in Figure 53 for these operating conditions. The highest astaxanthin concentration was measured in fraction 5, whereas significantly lower astaxanthin concentrations were measured in the other fractions of the stationary phase. The maximum solubility of astaxanthin in ethyl acetate was determined to be approx. 3 g L^{-1} and could not be reached in any of the fractions. According to the partition coefficient, the first chamber of the CPE unit should be completely loaded with astaxanthin before an algae cell with astaxanthin reaches the next chamber. Based on the concentration profile obtained, it is a non-ideal process. The extraction performance of homogenised cyst cells and germinated zoospores was compared in the last set of experiments. Therefore, cyst cells with a biomass concentration of 32 g L^{-1} were either mechanically disrupted or germinated and 240 mL of the homogenised cyst cells and germinated zoospores were injected into the column at a flow rate of 40 mL min^{-1} and a rotational speed of 1800 rpm. Similar yields of 70% and 80% were achieved, showing that the selected operating parameters can be used for CPE extraction from both, germinated zoospores, and homogenised cyst cells.

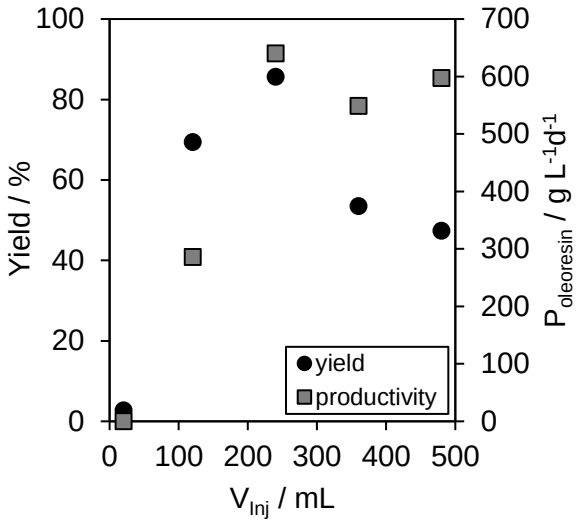

Figure 52: Yield and productivity of the CPE extraction of homogenised cyst cells and injection volumes of 20 to 480 mL.

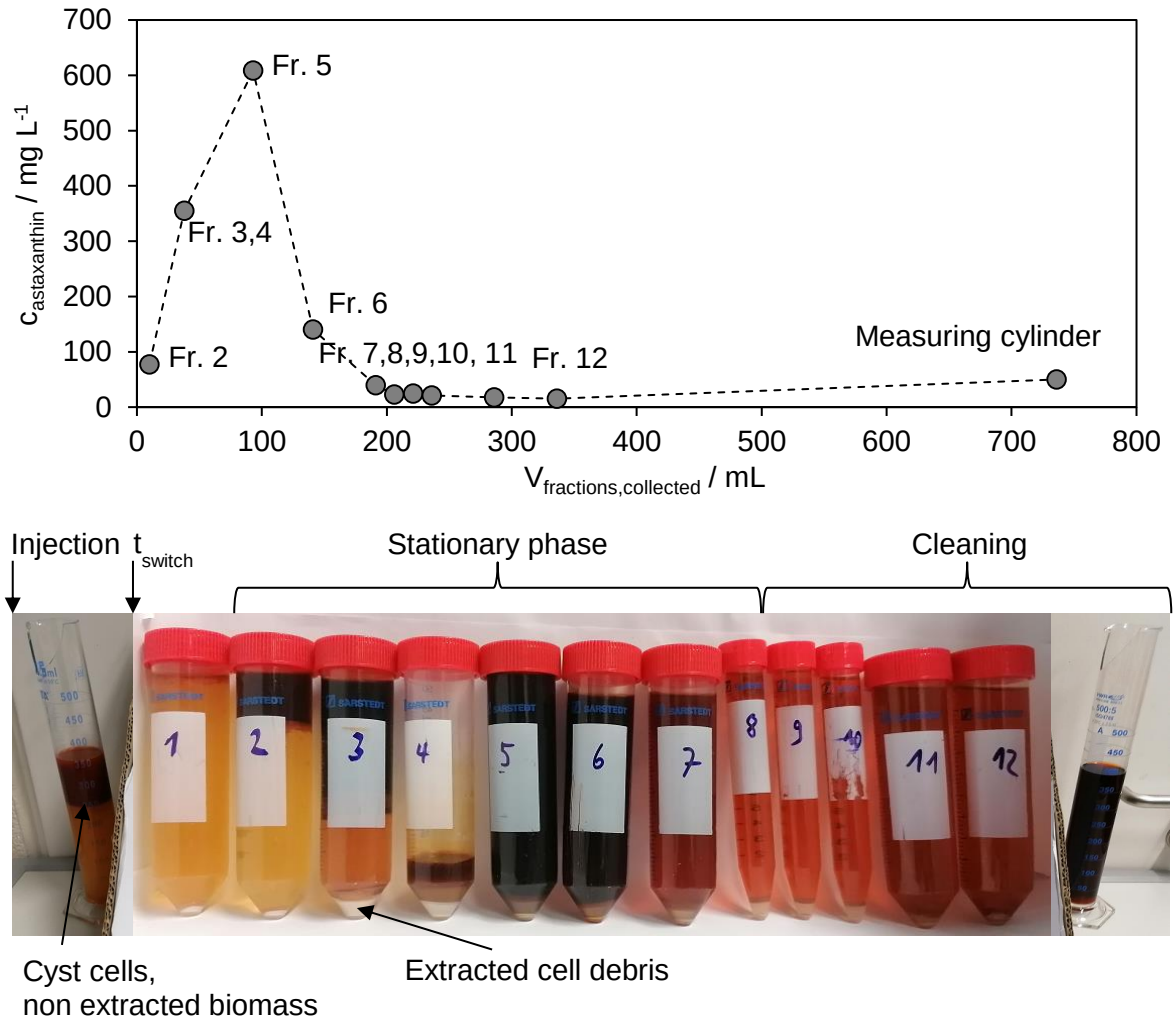

Figure 53: Collected fractions of the CPE extraction from 240 mL homogenised cyst cells with a biomass concentration of 33 g L^{-1} at a rotational speed of 1800 rpm and flow rate of 40 mL min^{-1}.

In summary, astaxanthin was successfully extracted from homogenised cyst cells and germinated zoospores using a CPE column. Limitations of stationary phase loss through sample injection in CCC can be overcome using CPE, allowing the use of the green solvent ethyl acetate. The operating conditions determined in this section were used in the techno-economic analysis (Section 4.3) to compare the economic performance of the newly developed CPE process of extraction of astaxanthin from homogenised cyst cells and germinated zoospores with the industrial process of astaxanthin production, including centrifugation, mechanical cell wall disruption, spray drying and supercritical extraction with CO_2.

In the following Section 4.2.3, membrane-assisted extraction was examined for the extraction of astaxanthin from *H. pluvialis*. This extraction unit was selected, as it is a dispersion-free extraction process and problems in the phase separation due to the emulsifying properties of the algal broth do not occur. In membrane-assisted extraction the two phases can be

continuously pumped and recirculated in countercurrent flow until the entire solvent is theoretically saturated with astaxanthin.

4.2.3 Membrane-assisted extraction of astaxanthin from *H. pluvialis*

In this section a membrane-assisted process for the extraction of astaxanthin from germinated zoospores or homogenised cyst cells into a solvent was developed. Therefore, first the extraction solvent and operating parameters were selected using the model compound camphor. The obtained results were used to successfully extract astaxanthin oleoresin, which was dissolved in water using an emulsifier, into a solvent. Finally, an astaxanthin extraction from homogenised cyst cells was performed.

4.2.3.1 Solvent selection

A solvent for the extraction of astaxanthin from *H. pluvialis*, using membrane-assisted extraction needed to be selected. As shown schematically in Figure 17, the solvent wets the pores of the hydrophobic PTFE membrane. At the mouth of the pores, the solvent is in contact with the algal broth. A slight overpressure on the side of the aqueous phase prevents the organic phase from bleeding into the aqueous phase [112].

Two solvents, ethyl acetate and *n*-heptane were selected to see which of the solvents enables stable operation of the used membrane contactor. Ethyl acetate is preferred solvent for the extraction of astaxanthin from homogenised *H. pluvialis* cyst cells and zoospores (Section 4.2). *n*-heptane, has been frequently used for the extraction of hydrophobic compounds from an aqueous feed [91].

To equilibrate the phases, the selected solvents were mixed with water, and separated using a separation funnel. For operation, the aqueous feed was first pumped inside the shell and after the aqueous circuit was closed, the solvent was pumped countercurrent inside the fibres. Flow rates of the aqueous and organic phases of about 220 mL min^{-1} were set, which represents flow rates in the operating range of the used set-up. An overpressure of 15 mbar was set on the aqueous side using valves to control the feed and solvent flow rate. The two phases were observed optically to detect breakthrough of one phase into the other phase.

The experiments were carried out for both solvents, pumping the aqueous feed on the shell side and the solvent inside the fibres countercurrent and vice versa. A stable operation was achieved for 48 hours using *n*-heptane. In the case of ethyl acetate, however, bleeding of the solvent into the aqueous phase and vice versa occurred latest after two hours of operation. With otherwise identical conditions and membrane material, the larger contact angle of the solvent (n-heptane >ethyl acetate) on the membrane allows the application of higher pressures. Due to the more non-polar nature of *n*-heptane compared to ethyl acetate [113], a larger breakthrough pressure (pressure untill wetting solvent bleeds out of the membrane pore) can be expected for *n*-heptane [114]. In addition, slight fluctuations in the flow rate of

the used two-channel peristaltic pump, can lead to a disturbance of the phase interface inside the pores of the membrane. Therefore, *n*-heptane was selected as solvent for the extraction for the used membrane contactor.

In the following section, the operating parameters of the membrane extraction for the extraction of camphor from an aqueous phase into *n*-heptane were determined. Camphor was selected, as similar to astaxanthin, it has a low water solubility and a high partition coefficient. The influence of the flow rate of the aqueous phase and the operating mode (feed in shell and extract in fibre, and vice versa) on the theoretical and experimental mass transfer coefficient was investigated.

4.2.3.2 Operating mode selection

In this section the operating parameters of the membrane-assisted extraction for the extraction of the hydrophobic compound camphor from the aqueous phase into *n*-heptane was determined using the set-up presented in Figure 23. Since the required quantities of algal broth for the membrane extraction could not be cultivated in-house and not be provided by the project partner Sea & Sun GmbH when the experiments were conducted, the preliminary experiments were carried out with the model compound camphor, which has a water solubility of 1.2-1.6 g L^{-1} and an octanol/water partition coefficient of $\log(P_{o/w})=2.38$ [115]. As presented schematically in Figure 54 a, either the aqueous phase can be pumped inside the fibres and the solvent inside the shell, or vice versa. The concentration profile for the extraction of a hydrophobic substance (camphor or astaxanthin) from the aqueous phase into the organic phase using a hydrophobic membrane is shown schematically in Figure 54 b.

The overall theoretical mass transfer $K_{W,theo}$ can be calculated according to the resistance-in-series model for pumping the feed on the shell side and the solvent in the fibres (Equation 2.27) and vis versa (Equation 2.28).The model consists of the individual mass transfer resistances in the aqueous and organic boundary layer and membrane pore. For high partition coefficients, only the mass transfer through the aqueous boundary layer is transport limiting (Equation 2.29). The individual mass transfer coefficient in the aqueous phase can be calculated as shown in Equation 2.30 in case the feed is pumped inside the fibres and as presented in Equation 2.32 for pumping in the shell. Increasing the flow rate of the aqueous feed phase increases the mass transfer through the aquoeus boundary layer (k_W) and ultimately the overall mass transfer coefficient K_W. Therefore, the flow rate of the aqueous phase was increased to examine the influence on the mass transfer coefficient of camphor. In addition, it was investigated which of the two operating modes (solvent in shell and aqueous feed in fibre and vice versa) results in a higher mass transfer coefficient.

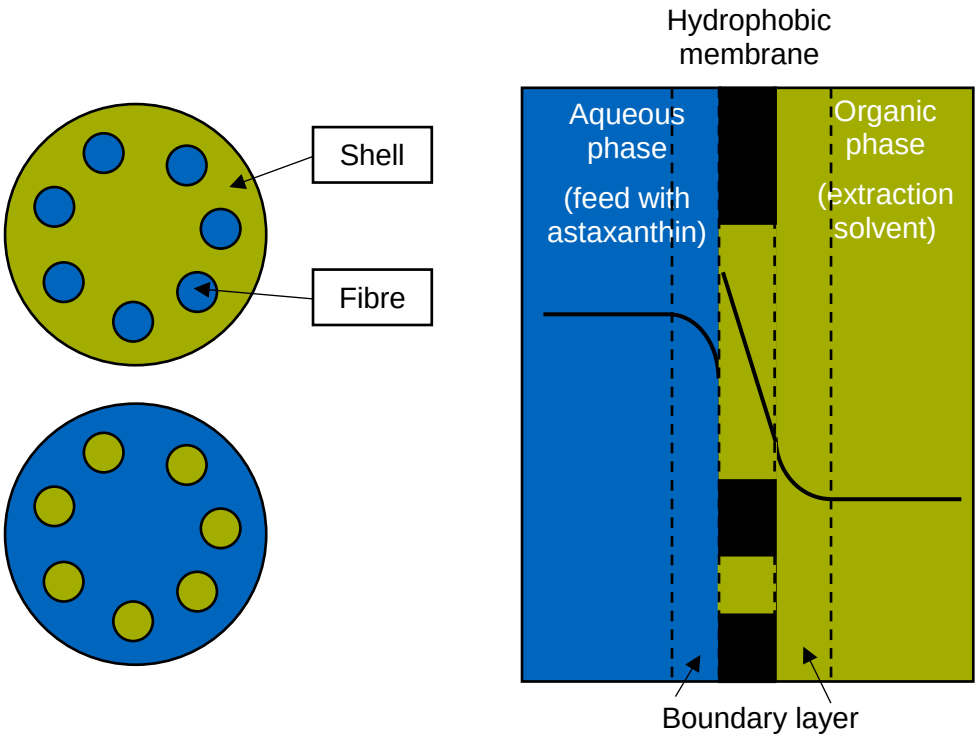

Figure 54: a) Schematic presentation of the two possible operating modes in the membrane-assisted extraction, pumping the aqueous phase inside the fibre and the solvent in the shell and vice versa. b) Concentration profile for the extraction of a hydrophobic component from the aqueous phase into a solvent using a hydrophobic membrane.

The experiments conducted are shown in Table 4.5. The range of aqueous flow rate was chosen such that a pressure difference to the organic phase of 15 mbar could still be set at the lowest and the highest aqueous flow rate. A volume ratio of V_W:V_O of 4 was selected to enable an increase of the original feed concentration by this factor. The camphor concentration in the organic phase was determined via the mass balance. In addition, the partition coefficient was determined as described in Section 3.6. Therefore, 5 mL of the feed was mixed with 1.25 mL *n*-heptane, and after equilibration of the two phases the concentration of camphor was measured in the aqueous phase and calculated for *n*-heptane via the mass balance.

Table 4.5: Selected parameters for evaluating the influence of the aqueous feed flow rate on the mass transfer coefficient.

Fibre	Shell	V_O / L	V_W / L	ω / rpm	F_W/ mL min^{-1}	F_O / mL min^{-1}
n-heptane	feed	0.55	2.2	35	151	259
n-heptane	feed	0.55	2.2	55	237	313
n-heptane	feed	0.55	2.2	100	382	272
feed	*n*-heptane	0.55	2.2	35	145	263
feed	*n*-heptane	0.55	2.2	55	243	269
feed	*n*-heptane	0.55	2.2	100	304	279

A partition coefficient, defined as in Equation 2.11 of 77.1 was calculated from measured concentrations. This value should be reached at the end of the membrane extraction process

[69]. In addition to the theoretical mass transfer coefficient $K_{W,theo}$ calculated from the resistance-in-series model, the experimental mass transfer coefficient K_W of the extraction was calculated as described in Section 2.5.2 in more detail. Therefore, the slope of Equation 2.37 was determined (Figure 18). The K_W value was calculated using the slope (Equation 2.41). For this purpose, samples were taken from the aqueous feed reservoir at certain time intervals after the start of the extraction. The concentration of camphor in the aqueous phase was determined photospectrometically as described in Section 3.8.5.

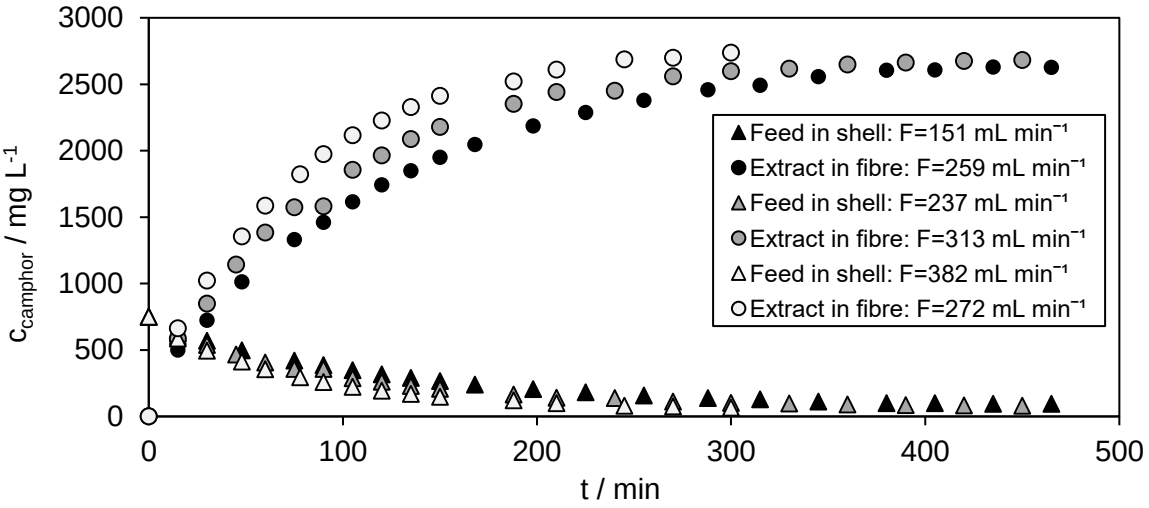

Figure 55: Concentration profile of the feed (shell) and extract (fibre) for the extraction of camphor from an aqueous feed into *n*-heptane at different flow rates of the feed phase.

The concentration profile of the membrane extraction of camphor from the aqueous feed pumped on the shell side into *n*-heptane inside the fibres is shown in Figure 55. As can be seen, the extraction of camphor from the aqueous feed into the solvent is faster with the increase of the feed flow rate, which is in good agreement with theory [90]. The ratio of the camphor concentration in extract to feed at the end of the extraction was 42, thus the equilibrium was not reached within the operating time. The experimental mass transfer coefficient was calculated according to Equation 2.41, using the slope of the linear equation shown in Figure 56. Using the slope, the efficiency and the K_W vlaue was calculated according to Equation 2.41. The experimentally derived K_W values are presented in Table 4.6 together with $K_{W,theo}$ calculated using the resistance-in-series model (Equation 2.28). The data for the calculations of K_W and $K_{W,theo}$ can be found in the Table A 1 to Table A 3 in the Appendix. Similar to the experimental K_W values, $K_{W,theo}$ increases with the flow rate of the aqueous feed. As can be seen, the experimental K_W values are about four times higher than the theoretically determined values. A possible reason is that Equation 2.32, which describes the shell-side mass transfer coefficient, was determined for a different membrane geometry than used in this work [27]. Further equations for calculating the shell side mass transfer are

described in the literature [28]. However, these were often used for even more special geometries (close-packed fibres) and assumptions (splitting and remixing of fluid elements, which constantly present the membrane surface with fresh fluid).

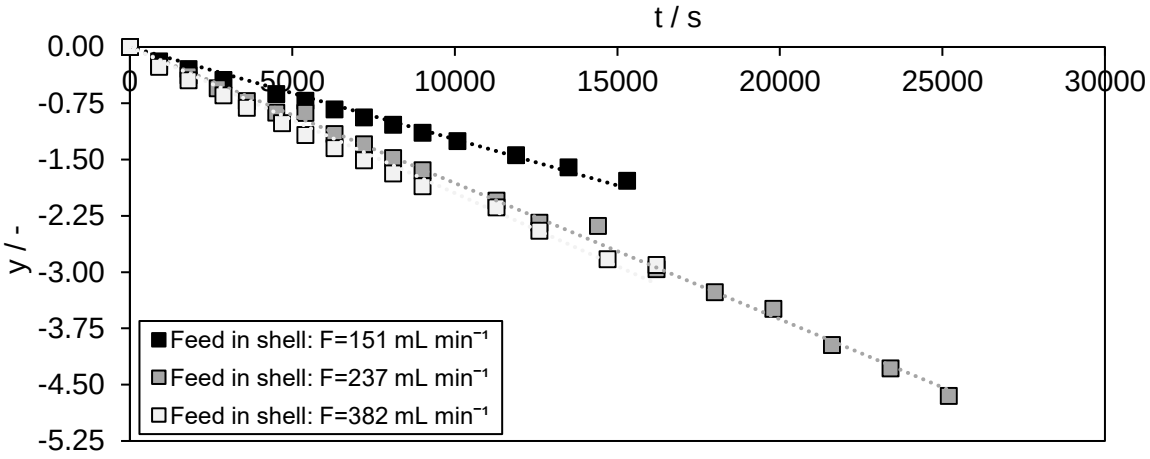

Figure 56: Determination of the experimental K_W for extraction of camphor from the aqueous feed (shell) into *n*-heptane (fibres), plotting ln(y) from Equation 2.37 vs. the extraction time.

Less strong deviations are reported for the extraction of (S)-(+)-carvone from aqueous feed into *n*-heptane, where the experimental K_W value was $5.9 \cdot 10^{-6}$ m s^{-1}, while the theoretical calculated mass transfer coefficient $K_{W,theo}$ was $4.5 \cdot 10^{-6}$ m s^{-1}. A similar membrane module was used there, but with a smaller module length of 20 cm and 3 PTFE fibres [91].

Table 4.6: Experimental K_W and theoretical $K_{W,theo}$ values for the extraction of camphor from the shell into *n*-heptane (fibre) at different feed flow rates.

	Feed in shell F=151 mL min^{-1}	Feed in shell F=237 mL min^{-1}	Feed in shell F=382 mL min^{-1}
K_W / 10^{-6} m s^{-1}	4.55	6.30	7.06
$K_{W,theo}$ / 10^{-6} m s^{-1}	1.14	1.44	1.98
K_W: $K_{W,theo}$ / -	3.99	4.38	3.57

Subsequently, the membrane extraction was performed, pumping the aqueous feed inside the fibres and *n*-heptane at the shell side. The concentration profile of the extraction process is presented in Figure 57. Like the previous experiments, the camphor concentration in the feed decreases faster with an increase in the aqueous phase flow rate. The experimental K_W values, calculated from the slope of the linear Equation 2.41, are shown in Table 4.7 together with the theoretical $K_{W,theo}$ values. The calculations to obtain $K_{W,theo}$ and K_W are listed in the appendix in Table A 4 to Table A 6. As can be seen in Table 4.7, the theoretical and experimental mass transfer coefficients match well for pumping the feed inside the fibres and the extract at the shell side, as the mass transfer coefficient within the fibre (Equation 2.30) can be calculated with high accuracy.

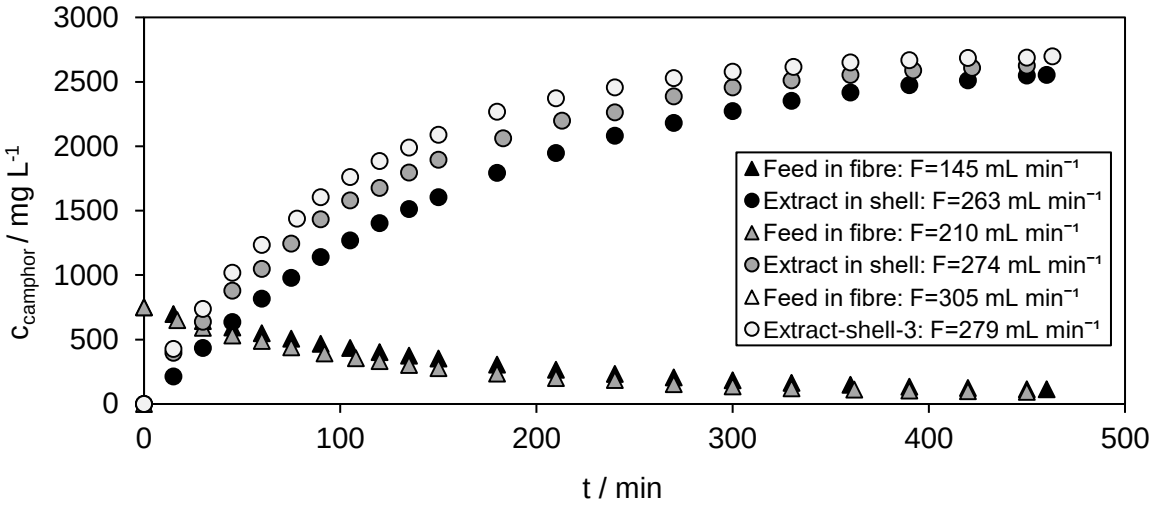

Figure 57: Concentration profile of the feed (fibre) and extract (shell) for the extraction of camphor from an aqueous feed into n-heptane at different flow rates of the feed phase.

Table 4.7: Experimental K_W and theoretical $K_{W,theo}$ values for the extraction of camphor from the fibre into *n*-heptane (shell) at different feed flow rates.

	Feed in fibre F=145 mL min^{-1}	Feed in fibre F=210 mL min^{-1}	Feed in fibre F=305 mL min^{-1}
K_W / 10^{-6} m s^{-1}	3.50	4.51	5.56
$K_{W,theo}$ / 10^{-6} m s^{-1}	4.05	4.79	5.16
K_W: $K_{W,theo}$ / -	0.86	0.94	1.08

In summary, it could be shown that, the mass transfer of a hydrophobic component from the aqueous phase into the solvent using a hydrophobic membrane can be increased by increasing the flow rate of the aqueous phase. This tendency was confirmed by the calculation of K_W and $K_{W,theo}$. The highest experimental K_W value was measured for pumping the aqueous feed stream on the shell side, which would therefore be the preferred operating mode for this used membrane contactor.

4.2.3.3 Influence of the organic phase flow rate on the mass transfer coefficient

In the previous Section 4.2.3.2 it could be shown that increasing the flow rate of the aqueous feed goes along with an increase of the mass transfer coefficient. In addition, it could be shown that the extraction is faster when the aqueous feed is pumped on the shell side and the solvent is pumped inside the fibres. In this section the influence of the flow rate of the organic phase on the mass transfer was investigated. Therefore, two experiments were conducted. In the first experiment, the organic phase was pumped and in the second experiment the organic phase was kept stationary. In both experiments identical flow rates of the aqueous phase were set. Keeping the organic phase stationary opens the possibility of saving one pump during operation in the industrial process, which reduces the operating costs. The operating parameters are shown in Table 4.8.

Table 4.8: Selected parameters for evaluating the influence of the organic feed flow rate on the mass transfer coefficient.

Fibre	Shell	V_O / L	V_W / L	ω / rpm	F_W/ mL min^{-1}	F_O / mL min^{-1}
n-heptane	feed	0.40	2.20	35	142	267
n-heptane	feed	0.10	0.55	35	143	-
feed	*n*-heptane	0.55	3.00	35	124	262
feed	*n*-heptane	0.40	2.20	35	148	-

The volume of the aqueous phase V_W and organic phase V_O was chosen that the phase ratios remained identical for all performed experiments. For all experiments conducted, the aqueous phase was first pumped into the module. The organic phase was then pumped at the selected flow rate and the transmembrane pressure was set to 15 mbar. When the organic phase was kept stationary, it was manually filled into the membrane using a funnel. This was done to save solvent, since when filling with a pump, solvent remains in the periphery. A low flow rate of the aqueous phase was selected, since the organic solvent, which is kept stationary, can only build up a low back pressure and the aqueous phase might break through into the organic phase. Samples were taken from the aqueous feed reservoir and the camphor concentration was determined photospectrometically as presented in Section 3.8.5. The camphor concentration in the organic phase was calculated via the mass balance.

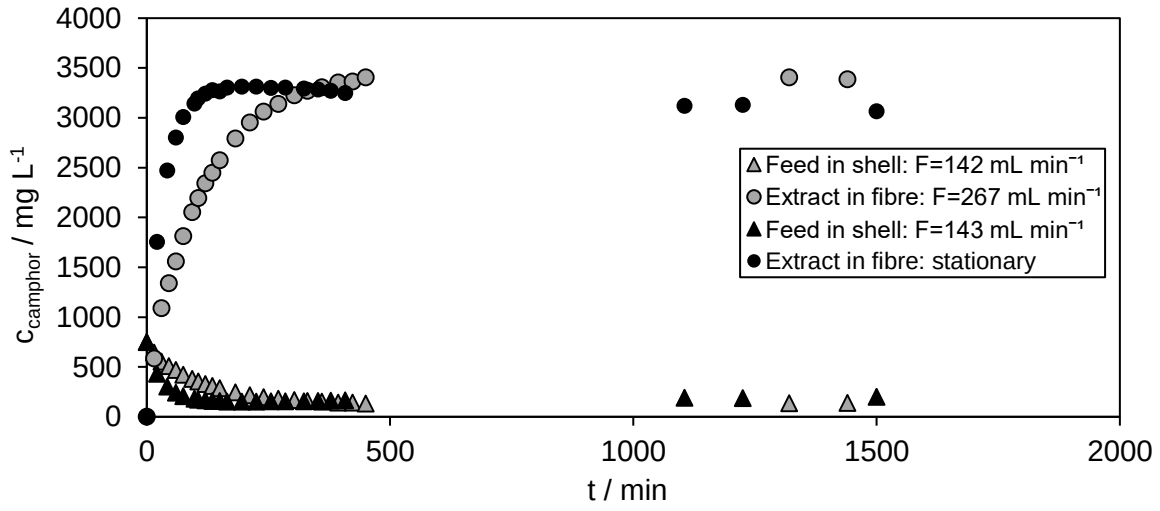

Figure 58: Concentration profile of the feed (shell) and extract (fibre) for the extraction of camphor from an aqueous feed into *n*-heptane at a flow rate of *n*-heptane of 267 mL min^{-1} and at stationary conditions.

The concentration profile of camphor for the feed pumped at the shell side, and the solvent pumped or kept stationary inside the fibres is shown in Figure 58. As can be seen, the extraction is even slightly faster with solvents kept stationary than with pumped solvents. A possible explanation for this might be, that the pressure in the extract phase is lower when the

solvent is held stationary compared to being pumped. Consequently, a larger interfacial area is formed in the pores when the organic phase is held stationary compared to pumping.

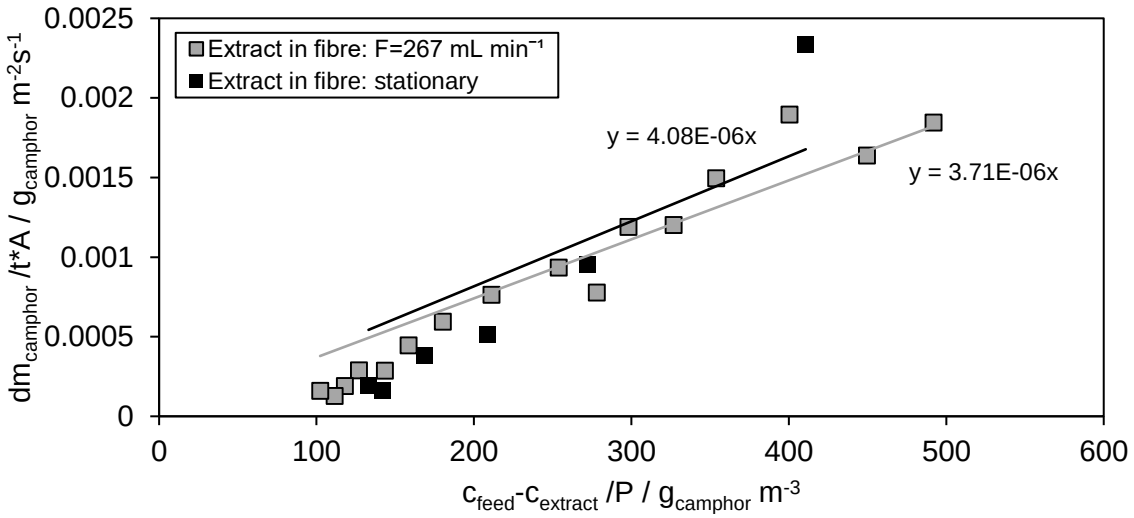

Figure 59: Specific mass flow of camphor vs. the driving force for the extraction of camphor from an aqueous feed solution into *n*-heptane at a flow rate of *n*-heptane of 267 mL $min^{-1}$and at stationary conditions.

To compare the two process options, the mass transfer coefficient was determined. However, the resistance in series model (Equation 2.27) is only valid for defined ranges of the Reynolds number, thus the theoretical mass transfer coefficient could not be calculated with this model when the organic phase is kept stationary. Also, the calculation of the experimental mass transfer coefficient presented in Section 2.5.2 is only possible with a flow rate of the organic phase above zero. Therefore, to determine the experimental K_W value, Equation 2.21 was plotted. There, the specific driving force is shown on the x-axis and the specific mass flow on the y-axis (Figure 59). K_W can be determined via the slope of the linear equation. A smaller K_W value of $3.71 \cdot 10^{-6}$ m s^{-1} was determined for pumping the solvent in comparison to $4.08 \cdot 10^{-6}$ m s^{-1} in case the solvent is kept stationary. In the next experiment the feed was pumped inside the fibres and the extract in the shell side. The concentration of camphor in the feed and extract is shown in Figure 60; the specific mass flow vs. the driving force is presented in Figure 61. The experimental K_W values for pumping the extract in the shell and keeping is stationary are approximately identical. The slightly higher K_W value in case of keeping the solvent stationary compared to pumping could be due to the higher flow rate of the aqueous phase F_W=147 mL min^{-1} compared to 123 mL min^{-1} at these conditions.

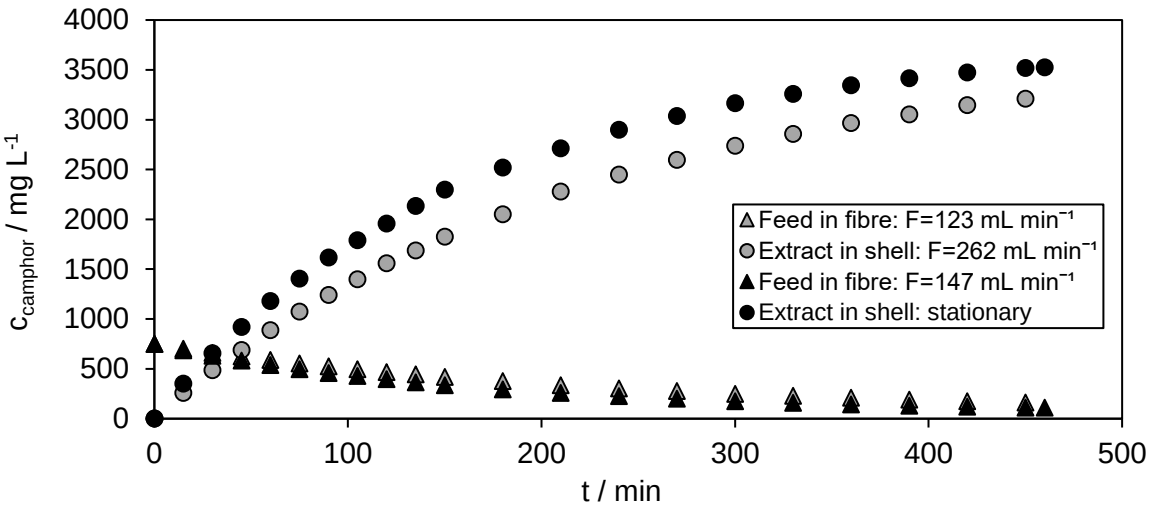

Figure 60: Concentration profile of the feed (fibre) and extract (shell) for the extraction of camphor from an aqueous feed into *n*-heptane at a flow rate of *n*-heptane of 262 mL min^{-1} and at stationary conditions.

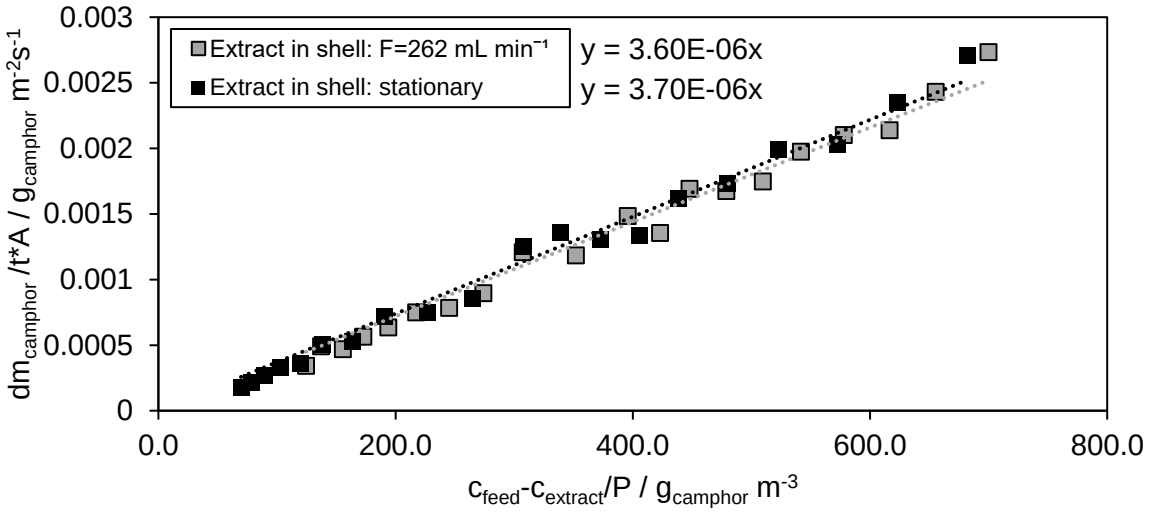

Figure 61: Specific mass flow of camphor vs. the driving force for the extraction of camphor from an aqueous feed solution into *n*-heptane at a flow rate of *n*-heptane of 262 mL min^{-1} and at stationary conditions.

In summary, for the extraction of camphor from aqueous feed using the PTFE membrane contactor, similar K_W values were reached in case the solvent was kept stationary or pumped. That opens the possibility to save one pump during the extraction process. However, it should be noted that the aqueous feed flow rate limits the mass transfer in this operation mode since no counter pressure can be built up in the solvent. At higher aqueous feed flow rates, bleeding of the aqueous phase into the organic solvent occurs. In the following section, the operating mode of pumping the extract on the shell side and keeping it stationary was transferred to the extraction of astaxanthin oleoresin from aqueous feed into *n*-heptane.

4.2.3.4 Extraction of astaxanthin from an aqueous feed

In the previous Section 4.2.3.2 it could be shown, that at a high flow rate of the aqueous feed on the shell side, leads to faster mass transfer of the solute from the aqueous feed into the solvent. In addition, it was shown in Section 4.2.3.3, that the mass transfer coefficient is similar when the solvent is pumped or kept stationary. In this section the operating parameters, pumping the solvent and keeping it stationary, to the extraction of astaxanthin from an aqueous feed into *n*-heptane were applied.

For this purpose, astaxanthin containing oleoresin was used, which is obtained from the conventional process after supercritical CO_2 extraction. It is an oily liquid containing between 5 to 10 wt% astaxanthin. These experiments already correspond to the final extraction process to be studied, except for the missing biomass. However, astaxanthin oleoresin is nearly insoluble in water, forming oil droplets on the water surface. [116]. Therefore, one of the most used surfactants, Tween 20 was uses to increase the solubility. The solubility is increased as result of the formation of micelles. Tween 20 has already been used in membrane-assisted extraction to increase the partition coefficients of lysozyme and bovine serum albumin in aqueous two-phase systems [112]. In addition several procedures for the preparation of stable astaxanthin water emulsions have been described in the literature [116, 117].The selected Tween 20 concentration corresponded to a critical micelle concentration (CMC) of 100 and $n_{Tween\ 20}$: $n_{astaxanthin}$ ratio of 104 [118]. The CMC describes the concentration of the pure emulsifier that is needed to form micelles. The operating parameter are presented in Table 4.9. The partition coefficient of astaxanthin oleoresin between the two phases, determined as described in Section 3.6, was 40.

Table 4.9: Parameters for the extraction of astaxanthin oleoresin from aqueous feed into *n*-heptane.

Fibre	Shell	V_O / L	V_W / L	ω / rpm	F_W/ mL min^{-1}	F_O / mL min^{-1}	$n_{Tween\ 20}$: $n_{astaxanthin}$ / -
n-heptane	feed	0.40	2.20	55	236	101	104
n-heptane	feed	0.10	0.55	55	239	-	104

The extraction process was started by pumping the feed on the shell side. Due to the better solubility of astaxanthin in *n*-heptane compared to water, samples for astaxanthin quantification (Section 3.8.2), were taken from the extract at defined time intervals. When the solvent was pumped, the sample was taken from the reservoir. With the solvent held stationary, the sealing caps were unscrewed, and samples were taken from the module. To prevent the aqueous phase from bleeding into the solvent when samples were taken from the module, the sample volumes taken were refilled with fresh *n*-heptane. The astaxanthin concentration in the fibres was assumed to be the mean value of its concentration at the

solvent inlet and outlet. The astaxanthin concentration of the feed was calculated via the mass balance and is shown in Figure 62.

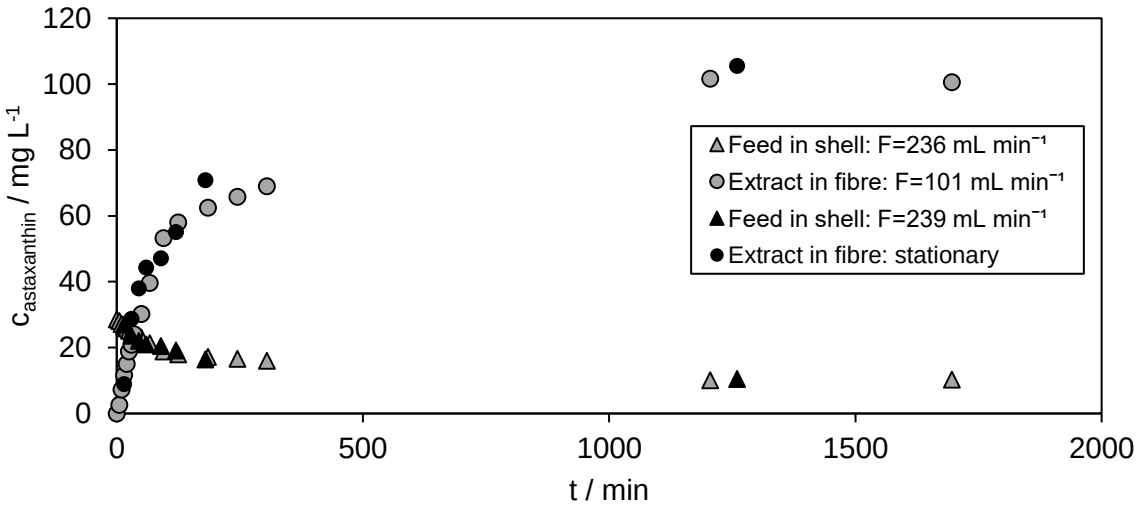

Figure 62: Concentration profile of the feed (shell) and extract (fibre) for the extraction of astaxanthin oleoresin from an aqueous feed into *n*-heptane at similar flow rates of the feed phase and an extract flow rate of 101 mL min^{-1}, and stationary conditions.

As can be seen, similar concentration profile has been measured for the two process options, which is in good agreement with the results from Section 4.2.3.4. The experimental K_W value was approx. $2.9 \cdot 10^{-6}$ m s^{-1} (Figure A 6 in Appendix). The ratio of the astaxanthin concentration in the solvent to feed at the end of the membrane extraction was 10, thus equilibrium was not reached when the extraction process was stopped. In this section it was shown, that astaxanthin containing oleoresin dissolved in water using Tween 20 can be extracted into *n*-heptane using membrane-assisted extraction. Similar mass transfer coefficients could be determined for pumping the solvent in the fibres and keeping the solvent stationary. Therefore, in the following section an extraction of astaxanthin from homogenised cyst cells using membrane-assisted extraction was carried out.

4.2.3.5 Extraction of astaxanthin from homogenised cyst cells

In the previous Section 4.2.3.4, it was shown, that the target compound astaxanthin can be extracted from the aqueous feed into *n*-heptane using membrane-assisted extraction. In this section astaxanthin was finally extracted from homogenised cyst cells. To achieve this, the following preliminary experiments were done. First, the amount of Tween 20, which was added to the homogenised biomass was increased to examine the influence on the partition coefficient and solubility in the feed. Mechanical cyst cell homogenisation was done as described in Section 3.6. The astaxanthin concentration in the aqueous phase was measured using the HPLC method described in Section 3.8.2. Subsequently the partition coefficient was measured for the Tween 20 concentrations examined. Therefore, *n*-heptane was added to the

homogenised feed at different Tween 20 concentrations and after mixing, and centrifugation at 5000 rpm, the astaxanthin content in *n*-heptane, and solved in water was measured using HPLC (Section 3.8.2). The partition coefficient was calculated using Equation 2.11, as the ratio of astaxanthin concentration in the solvent to water. The conducted experiments are presented in Table 4.10.

Table 4.10: Parameters for membrane-assisted extraction of astaxanthin from homogenised cyst cells into *n*-heptane.

Fibre	Shell	V_O / L	V_W / L	$n_{Tween\ 20}$: $n_{astaxanthin}$ / -	F_W / mL min^{-1}	F_O / mL min^{-1}
n-heptane	feed	0.55	2.2	-	374	266
n-heptane	feed	0.55	2.2	5	385	272
feed	*n*-heptane	0.55	2.2	-	245	263
feed	*n*-heptane	0.55	2.2	5	243	269

Figure 63 shows the concentrations of astaxanthin in the aqueous feed and the measured partition coefficients.

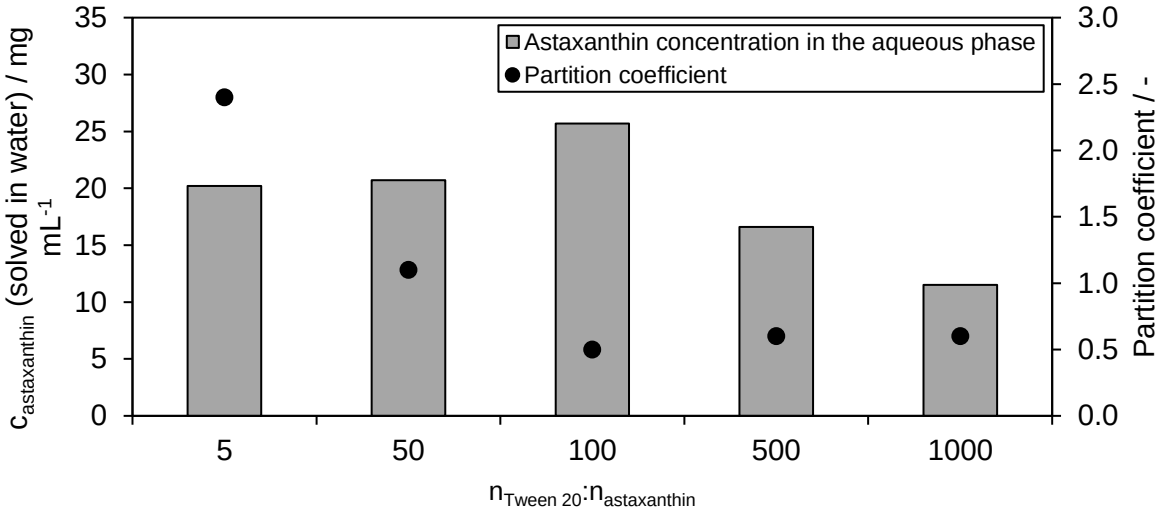

Figure 63: Astaxanthin concentration in the aqueous phase, and partition coefficient of astaxanthin between the aqueous phase and *n*-heptane five tifmes at different ratios of $n_{Tween\ 20}$:$n_{astaxanthin}$.

Due to the insoluble nature of astaxanthin oleoresin in water, the partition coefficient without the addition of Tween 20 is infinity. A $n_{Tween\ 20}$:$n_{astaxanthin}$ ratio of 5 was selected for the subsequent membrane extraction experiments, since the value of the partition coefficient with 2.4, is still above 1. The addition of Tween 20 did not allow a stable operation of the membrane extraction for the extraction of astaxanthin from homogenised cyst cells. The aqueous feed phase always bled into the solvent. This shows that the disrupted biomass disturbs the solvent feed interface inside the pores, as in the previous Section 4.2.3.4, a stable operation of the membrane for the extraction of oleoresin using Tween 20 was possible. For the extraction of astaxanthin from homogenised cyst cells into *n*-heptane without the addition of Tween 20, no

mass transfer of astaxanthin took place. This is due to the insolubility of astaxanthin in water. In addition, depending on the operating mode, depositing of the biomass in the shell or fibre took place (Figure 64).

Figure 64: Deposit of homogenised *H. pluvialis* cyst cells in the shell of the membrane.

This phenomenon has been described in the literature and limits the scale-up of membrane extractors for the extraction from fermentation broth [28].

In summary, the operating parameters for the extraction of astaxanthin into an aqueous phase, using membrane-assisted extraction were selected using the model compound camphor. A good agreement between the mass transfer coefficients calculated theoretically via the resistance-in-series model and determined experimentally could be shown, when the feed was pumped inside the fibres. The highest mass transfer coefficient was found for pumping the aqueous feed on the shell side, which is therefore the preferred mode of operation for this membrane module. In addition, it could be shown that pumping of the extraction solvent does not limit the mass transfer, which thus can be kept stationary. Based on the experiments with camphor, a successful extraction of astaxanthin containing oleoresin (obtained from supercritical CO_2 extraction) into *n*-heptane was carried out. Here, Tween 20 was used as an emulsifier to increase the solubility of astaxanthin in the aqueous phase. The transfer of these parameters for the extraction of astaxanthin from homogenised biomass was not successful. The addition of Tween 20 caused the aqueous phase to bleed into the solvent. Astaxanthin could not be extracted into *n*-heptane without the addition of the emulsifier since astaxanthin is insoluble in water. In addition, the biomass was deposited on the membrane and in dead volume. Therefore, the extraction of astaxanthin from homogenised cyst cells using membrane-assisted extraction was not considered in the following economic study.

4.3 Techno-economic analysis of the CPE extraction process

As shown in the previous Section 4.2.2 an extraction process for the extraction of astaxanthin from germinated zoospores and homogenised cyst cells using a CPE column was successfully established. However, as presented in Section 4.2.3, membrane-assisted extraction could not be applied for the extraction of astaxanthin from homogenised cyst cells.

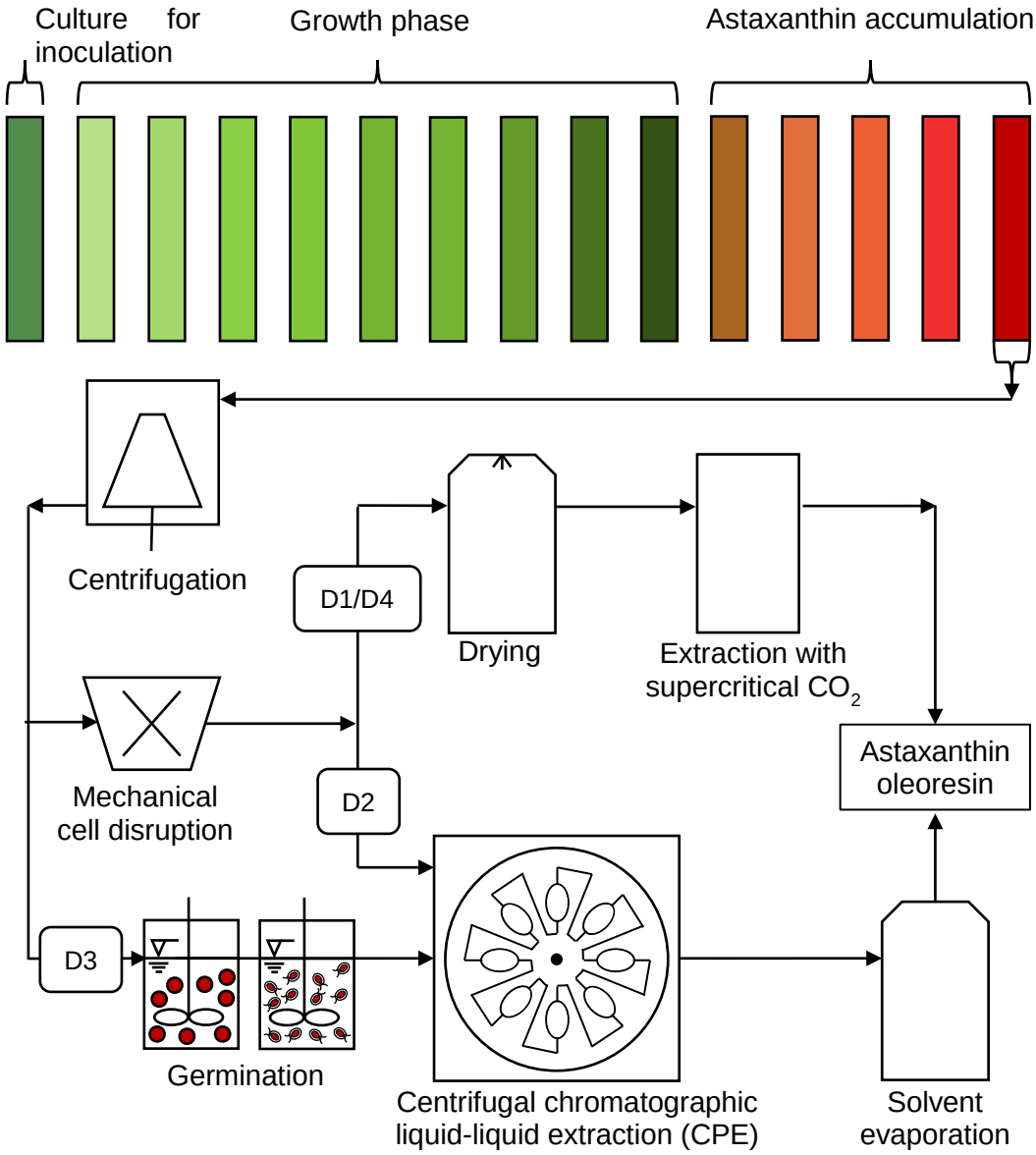

Figure 65: Schematic presentation of the biotechnological production of *H*. pluvialis, including centrifugation, mechanical cyst cell disruption, drying and a supercritical CO_2 extraction performed in-house (D1) and by an external service provider (D4), as well as liquid–liquid chromatographic extraction of astaxanthin from mechanical disrupted cyst cells (D2) and germinated zoospores (D3) into ethyl acetate, and a subsequent solvent evaporation step [95].

In this section a techno-economic analysis to compare the new developed process for the extraction of astaxanthin from homogenised cyst cells (D2) and zoospores (D3) using CPE, with the industrial process of supercritical CO_2 extraction performed in-house (D1) or via an

external service provider (D4) was performed. The different processes are shown schematically in Figure 65. The techno-economic analysis of the four different process schemes was done according to the method described by Peters and Timmerhaus [93]. First, the mass flows to be processed daily were determined, based on which the size of the required unit operations was selected. A list of the total equipment costs (TEC) was made. Based on these costs, the fixed capital investments (FCI) and total capital investments (TCI) were determined [94]. The total product costs are the sum of manufacturing costs and general expenses. Finally, the return on investment (ROI) and the net present value (NPV) were calculated and used to compare the probability of the four different processes.

4.3.1 Mass balances of the unit operations

In this section the capacity of the chosen algal production was selected. Based on this, the required sizes of the units were selected, and a mass balance for the four downstream processes was calculated. Based on the selected unit operations, the TEC, TCI, and the total production costs were calculated in the subsequent section. An overview of the selected units including installed capacity and operating time for upstream and downstream processing is shown in Table 4.11. Additional information for calculating the mass balances can be found in Table A 7 to Table A 10 in the appendix.

Table 4.11: Summary of the used equipment for downstream processing, including operating mode/capacity, operating hours per harvest, MWh a^{-1} and yield.

Unit operation	Commercial device	Operating mode/ Capacity	Operating time per harvest/ hours	Installed/required power / kW	MWh a^{-1}	Yield / %
Upstream processing						
Photobioreactor	Schott AG (Germany)	170 m^3	24			
Lighting	Osram AG (Germany)	2 W $L^{-1}_{algal\ broth}$	12	300	592	
Rotary vane pumps	Schott AG (Germany)	4x1200 L h^{-1}	24	75	1,188	
Temperature control	Literature [5]]		24	42	660	
Control sensors	Literature [119]]		24	4	66	
Downstream processing						
Centrifugation	Disc-stack centrifuge, (GEA, Germany)	2500 L h^{-1}	4	4	5	98
Cell disruption	GEA Ariete NS3006H, (GEA, Germany)	25 L h^{-1}, p=1500 bar	4	6	8	98
Germination	Photobioreactor (Schott AG Germany)	2x1000 L	41	0.2	2.3	98
Spray drying	GEA production minor (GEA, Germany)	16 L h^{-1}	4	23	48	98
Supercritical CO_2 extraction	NATEX Prozesstechnologie GesmbH (Austria)	2x40 L	24	29	230	87
Centrifugal Partition Extractor	CPE Gilson (USA)	3x5 L	23	8	57	85
Solvent evaporation	Ecodyst (USA)	100 L, 50 L h^{-1}	2	13	67	100

4.3.2 Upstream processing

The upstreaming of the algal production was done on a hypothetical algal production in Germany. A plant size with an annual production (330 operating days) of 8910 kg of biomass was selected, which represents a medium-sized plant [10]. Due to the low solar radiation in Germany, a cultivation on a day-night cycle (12 hours per day) was considered, which is often done for *H. pluvialis* algal farms in European latitudes. The installed power was selected to be 2 W $L^{-1}_{algal\ broth}$, as recommended from the Sea&Sun GmbH, Germany. Biomass concentrations of around 2.7 g L^{-1} with 5 wt astaxanthin can be expected under these conditions (personal talk with Schott AG, Germany). Therefore, the total tubular photobioreactor volume installed was planned to be 170 m^3 (17 photobioreactors with 10 m^3 each). Four rotary vane pumps with a flow rate of 1200 L h^{-1} each was considered for daily recirculation of 10m^3 of algal broth (personal talk with Schott AG, Germany). Data for temperature control and sensors were taken from literature data [5, 119]. A two-stage process was assumed for the upstreaming, divided into a ten-day growth phase and a five-day stress phase for the astaxanthin accumulation for each 10m^3 of algal broth, which corresponds to typical process times for *H. pluvialis[30]*. Based on the biomass composition of $C_{1.83}O_{0.48}N_{0.11}$ [14] and a CO_2 conversion rate of 0.75 [120], 2.66 kg of CO_2 was considered to produce 1 kg algal biomass [95]. CO_2 supply into the algal broth was assumed to be done using a CO_2 sprinkler. The nitrogen consumption was calculated based on the chemical composition of *H. pluvialis*, while the amount of other nutrients was determined on their proportion in the BBM. In summary, a volume of 10 m^3 with a biomass concentration of 2.7 g L^{-1} (with 5 wt% astaxanthin) must be harvested daily. This is done by centrifugation, the first step of downstream processing, which will discussed in the following Section 4.3.2.

4.3.3 Downstream processing

A daily harvesting of 10,000 L of algal broth (cyst cell concentration of 2.7 g L^{-1} and an astaxanthin content of 5 wt%) was considered. In this section the units for downstream processing for the investigated downstream scenarios, extraction of astaxanthin from germinated zoospores and homogenised cysts, as well as for the extraction using supercritical CO_2 (Figure 65) were selected. The selection was based on the process times, expected yields of commonly used industrial plants, as well as experimental derived data for CPE extraction (Section 4.2.2.7) and germination (Section 4.1.4). An overview of the selected units for downstream processing is presented in Table 4.11 .

A mass balance of the biomass flow was calculated according to these yields. An overview of the mass balance is presented in Figure 66 for the four downstream scenarios examined, extraction from homogenised cyst cells and germinated zoospores using CPE, and

supercritical CO_2 extraction from homogenised cyst cells. The calculations are presented in Table A 7 to Table A 10in the appendix. Subsequently, the capacities of the selected units for downstream processing are discussed in further detail.

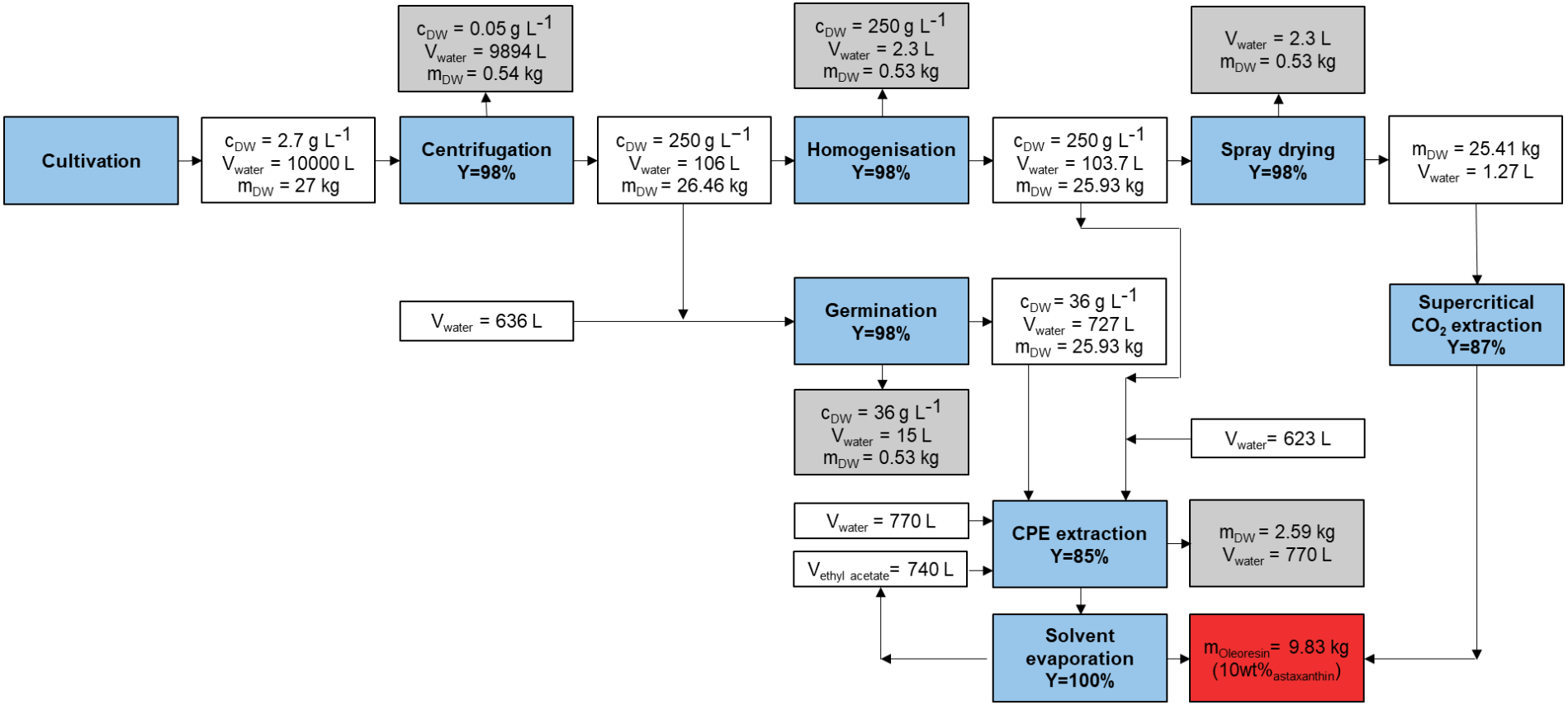

Figure 66: Process flow scheme including the unit operations and yields obtained in examined downstream processes of astaxanthin extraction from germinated zoospores and homogenised cyst cells using CPE, and supercritical CO_2 extraction, including the mass stream (white) and losses (grey) after each process step.

4.3.4 Centrifugation

The first step of the downstream processing is centrifugation of the *H. pluvialis* cyst cells to reduce the process volume for further process steps. As presented inFigure 66, after the upstream processing, the cyst cell concentration in the algal broth was 2.7 g L^{-1}. Process times of around 4 hours are commonly used for harvesting the algal broth (personal talk with GEA SEE). Therefore, a disc-stack centrifuge (GEA SEE) was planned as unit for harvesting algal broth harvesting. A final concentration of 250 g L^{-1} (25% TSS), can be reached using these centrifuges, which is in good accordance with literature [14]. As presented in Figure 66, 9894 L water can be separated from the fermentation broth. For this process step a yield of 98% was assumed [14], corresponding to 29.4 kg of cyst cells after centrifugation (Figure 66). After centrifugation a cyst cell disruption is either done by mechanical disruption or cyst cell germination.

4.3.5 Mechanical cyst cell disruption and germination

After the centrifugation and concentration of the biomass a disruption of the cyst cells needs to be done. As cyst cells have a very rigid cell wall pressures above 1000 bar should be applied for disruption of cells in high quantity [15]. Therefore, for mechanical cyst cell disruption, the high-pressure homogeniser GEA Ariete NS3006H was selected, which can operate at pressures up to 1500 bar. As presented in, 106 L of algal broth must be disrupted after centrifugation. Applying typical operating ranges of 25 L h^{-1}, operating times of 4.15 hours can be calculated (Table 4.11). According to the literature, yields of 98% can be expected for this process step [121].

For cyst cell germination, the photo/mixotrophic germination presented in Section 4.1.2 was scaled to a 1000 L reactor. Combining mixotrophic or heterotrophic cyst cell germination enabled astaxanthin extraction yields of up to 64%, 41 hours after the start of germination (section 4.1). Two photobioreactors with a total volume of 1000 L operating in parallel (727 L cultivation volume with a cell concentration of 36 g L^{-1}) were considered. BBM with additional 4 mM glucose was selected as medium for germination. A yield of 98% was considered for this process step. 25.9 kg of biomass are available after cell disruption (Figure 66). Before supercritical extraction with CO_2, the homogenised cyst cells need to be dried using spray drying, which will be discussed in the following section [95].

4.3.6 Spray drying

After cyst cell homogenisation, drying of the cells is done prior to supercritical CO_2 extraction. After cyst cell homogenisation, 104 L water from the fermentation broth need to be processed. This corresponds to a small amount of water for industrial spray dryer, which is why the GEA production minor was selected. This unit operates within an evaporation rate of 16 L_{water} h^{-1}.

According to the manufacturer, the aqueous mass can be reduced to 1.27 L (5 wt% water in the biomass) within 6.4 hours (Table 4.11). In literature yields of 98% can be expected dor this unit operation, which corresponds to 25.4 kg of dry biomass at the end of the process [14].

4.3.7 Extraction with supercritical CO_2

After spray drying, in-house supercritical CO_2 extraction was considered for the downstream process D1 (Figure 65). Therefore, a supercritical CO_2 extractor from NATEX Prozesstechnologie GesmbH 2x40L (40L net extractor volume) was selected, as this extractor allows applying operating pressures of up to 1000 bar, which is required for astaxanthin extraction with high yields. At these pressures, the supercritical CO_2 extraction can be done without a co-solvent [17]. According to the manufacturer this device allows the processing of 10 tonnes biomass within 330 days of annual operation. Annual losses of 12 tonnes CO_2 were considered according to the manufacturer [95]. For the supercritical CO_2 extraction via contracted manufacturer (D4), a storage of the daily produced biomass at -20°C in a cold storage until 1000 kg are collected for shipment, was assumed. This correponds to a 40-day accumulation time, as 25.4 kg biomass are dried daily. In the next section, the scale-up of the astaxanthin extraction from germinated zoospores and homogenised cyst cells using CPE is presented.

4.3.8 CPE extraction

After germination of the cysts or mechanical cell wall disruption, extraction of astaxanthin using CPE is performed in the downstream process D2 and D3 as presented in Figure 65.

A scale-up from the used CPE column with 240 mL to 5 L was done. 5 L CPE columns are currently the largest commercially available columns from Gilson (USA). For the scale-up, the CPE operating parameters with the highest yield, presented in Section 4.2.2.7 were taken (Figure 51). The operating conditions are given in Table 4.12 for the selected experiment, where 240 mL homogenised cyst cells with a concentration of 33 g L^{-1} and a flow rate of 40 mL min^{-1} were injected. The scale up from the 244 mL to 5 L CPE column was done, that the selected flow rate has similar contact time with the stationary phase. A linear scale up of the injection volume was done. As presented in Figure 42 the CPE column is first filled with ethyl acetate ($t_{filling}$). After the rotation is set, the mobile phase is pumped until no more stationary phase is discharged from the column ($t_{equilibrium}$). After injection of the biomass, the stationary phase concentrated with astaxanthin is pushed out of the column (t_{switch}) and fractionated ($t_{fractioning}$). After that, the column is cleaned with acetone ($t_{cleaning}$). The 5 L CPE unit is made of stainless steel, no daily cleaning of the column was considered.

Table 4.12: Process step times in CPE columns with a volume of 244 mL and 5 L [95].

	V_{column} / L	F / mL min^{-1}	V_{inj} / mL	$t_{filling}$ / min	$t_{equilibrium}$ / min	t_{switch} / min	$t_{fractioning}$ / min	$t_{cleaning}$ / min	$t_{extraction}$ / min
CPE, V_{inj} = 240 mL	0.244	40	240	6.1	6.1	7.27	6.1	6.1	31.67
Industrial scenario	5	820	4918	6.1	6.1	7.27	6.1	0	25.57

Table 4.13: The injected amount of biomass, extracted amount of oleoresin and astaxanthin in a 24 hour and 330 days operation schedule, and the required amount of CPE units for 330 days of operation [95].

	$t_{extraction}$ / min	Injections in 24 h	Biomass injected in		Oleoresin extracted in		Astaxanthin extracted		CPE unit
			24 h / kg	330 days / kg	24 h / kg	330 days / kg	24 h / g	330 days / kg	
CPE,V_{inj}= 240 mL	31.7	45	0.35	117	0.16	52	15.8	5.2	85.7
Industrial scenario	25.6	56	9.01	2974	4.02	1325	402	132.5	2.9

In the CPE experiment (Section 4.2.2.7) selected for the scale-up, an extraction yield of 85% was reached. From 7.85 g biomass with an astaxanthin content of 1.13 wt%, 5 g of oleoresin with an astaxanthin content of 2.16 wt% were extracted. For further calculations in the scale-up, an astaxanthin content in the biomass of 5 wt% and in the extracted oleoresin is around 10 wt%, was assumed.

The mass of algal biomass that can be extracted using a 5 L industrial CPE column in 24 hours and 330 days is present Table 4.13. In the examined downstream scenarios D2 and D3, presented in Figure 66, 25.9 kg of homogenised cyst cells or zoospores need to be processed daily using CPE. To be able to extract the annual 8910 kg (445.5 kg astaxanthin), 2.9 CPE units 5 L column volume would be needed. This results in a daily process time of 22.9 hours for each of the 3 CPE columns.

The solubilty of 7.47 v/v ethyl acetate in water and 2.96 v/v water in ethyl acetate was taken from literature data [122]. For CPE extraction the feed needs to be saturated with ethyl acetate in both scenarios (germinated D3 and homogenised D2), and solvent saturation with water was considered. For cost and environmental reasons, ethyl acetate should be reused after extraction. Therefore, selection of the evaporator is discussed in the next section.

4.3.9 Solvent recovery

After the CPE extraction presented in the previous Section 4.3.8, astaxanthin oleoresin is solved in ethyl acetate (saturated with water) (Figure 53). To obtain solvent-free astaxanthin oleoresin, ethyl acetate (saturated with water) needs to be evaporated. This corresponds to 638 L of solvent rich phase, consisting of 619 L ethyl acetate and 19 L water. A separation of ethyl acetate from the water-rich phase was planned, although according German law it was not required for the quantities. The ethyl acetate content in water can be reduced to around 0.01 v/v% in a single-stage evaporation at atmospheric pressure and a distillate with around 89 v/v% ethyl acetate and 11 v/v% water can be collected [95, 123]. A high-speed rotary evaporator from ecodyst (100L EcoChyll X7 Hi-Speed Evaporator) with a maximum evaporation rate of 55 L h^{-1} and a capacity of 100 L was selected for the solvent evaporation. An average evaporation rate of 50 L h^{-1} was assumed, resulting in a process time of 12.8 hours to evaporate 638 L solvent rich phase, and 2.4 hours for the evaporation of 119 L ethyl acetate from the water-rich phase. As hydrolysis of ethyl acetate to acetic acid and ethanol takes place with time [124], a total solvent replacement after 10 days was assumed.

In the Section 4.3.1 to 4.3.9 the units of the upstream and downstream process were successfully selected for the extraction of astaxanthin from homogenised cyst cells (D2) and germinated zoospores (D3) using CPE, and the supercritical CO_2 extraction performed in-house (D1) or via an external service provider (D4) (Figure 65). Using the equipment costs of

the selected units, the total capital investment (TCI) and total production costs can be determined, as presented in the next section.

4.4 Determination of the total capital investment and total product costs

In the previous section, the equipment for the biotechnological production of astaxanthin using *H. pluvialis* was selected for the scenarios presented in Figure 65. A techno-economic analysis was done to compare the four different downstream processes, supercritical CO_2 extraction performed in-house (D1), solvent extraction from mechanically homogenised cyst cells (D2) and germinated zoospores (D3), and supercritical CO_2 extraction performed by an external service provider (D4). The procedure described by Peters and Timmerhaus [93] was used, as presented schematically in Figure 19. The manufacturers of the units listed in Table 4.14 were contacted to receive the acquisition costs of the major equipment used in the four downstream scenarios.

The costs of the photobioreactors are about 50% of the upstreaming equipment costs, which are €965,600 in total. The highest costs for the equipment of the downstream process were determined for the in-house supercritical CO_2 extraction (D1) with €1.88 million, and the lowest were calculated for the external supercritical CO_2 extraction (D4) at €0.58 million (Table 4.14). The reason for this are the huge investment costs of €1.3 million for the supercritical CO_2 extractor in D1. High investment costs are required for the spray dryer (€450,000) in the conventional downstream processes D1 and D4. The listing price of one 1 L CPE column is around €92,000. A price of €241,900 per 5 L CPE column can be determined from the purchasing price of a 1 L CPE column, using the six-tenth-factor rule [93]. The total direct plant in Table 4.15. They include the piping, instrumentation and control, installation costs, buildings, yard improvements, service facilities, as well as land. These costs can be estimated by a share of the TEC [93, 94]. In addition, indirect costs, fixed-capital investment (FCI), and the working capital need to be estimated to calculate the total capital investment (TCI) [120]. The manufacturing costs (I) were calculated as the sum of the direct production costs (A), fixed charges (B), and the plant overhead costs (C). The sum of the manufacturing costs (I) and general expenses (II) gives the total product costs (III) and are presented in Table 4.16 [95].

Table 4.14: List of major equipment and total equipment costs (TEC) for the upstream and the four downstream scenarios, supercritical CO_2 extraction performed in-house (D1), solvent extraction from mechanically disrupted cyst cells (D2) and germinated zoospores (D3), and supercritical CO_2 extraction committed by an external service provider (D4) [95].

List of major equipment	Description	Price / €			
Photobioreactors	170 m^3				419,900
Light installation	2 W $L^{-1}_{algal\ broth}$				480,000
Pumps for cultivation	68, 1200 L h^{-1} each				27,200
CO_2 sparkler	17				8,500
Medium preparation tank	10 m^3				30,000
Upstreaming					**965,600**
		D1	**D2**	**D3**	**D4**
Cooling cell	A=60 m^3, k=0.25 W $m^{-2}K^{-1}$ [1]	-	-	-	7,230
Centrifuge	2.5 m^3 h^{-1}	50,000	50,000	50,000	50,000
Homogeniser	50 L h^{-1}, 1500 bar	75,000	75,000	-	75,000
Spray dryer	20 L h^{-1}	450,000	-	-	450,000
Supercritical CO_2 extractor	2x40 L, 1000 bar	1,300,000	-	-	-
Reactor and light for germination	2x1000 L	-	-	6176	-
CPE units	3x5 L columns	-	725,631	725,631	-
Pumps for CPC	1000 mL min^{-1}	-	105,000	105,000	-
Rotary evaporator	100 L	-	116,199	116,199	-
Downstream	**€**	**1,875,000**	**1,071,830**	**1,002,875**	**582,230**
Total equipment costs (TEC)	**€**	**2,840,600**	**2,037,430**	**1,968,475**	**1,540,600**

Table 4.15: List of the total direct plant costs, the indirect plant costs, the fixed-capital investment and the total capital investment of the four downstream processes examined, supercritical CO_2 extraction performed in-house (D1), solvent extraction from mechanically disrupted cyst cells (D2), and germinated zoospores (D3), as well as supercritical CO_2 extraction performed by an external service provider (D4) [95].

		D1	D2	D3	D4
Total equipment costs (TEC)	Share of TEC	**2,840,600**	**2,037,430**	**1,968,475**	**1,540,600**
Installation costs	0.20	568,120	407,486	393,695	308,120
Instrumentation and control	0.13	369,278	264,866	255,902	200,278
Piping	0.20	568,120	407,486	393,695	308,120
Electrical	0.10	284,060	203,743	196,848	154,060
Buildings	0.23	653,338	468,609	452,749	354,338
Yard improvements	0.12	340,872	244,492	236,217	184,872
Service facilities	0.20	568,120	407,486	393,695	308,120
Land	0.05	142,030	101,872	98,424	77,030
Total direct plant costs	Share of TEC	**6,334,538**	**4,543,469**	**4,389,700**	**3,435,538**
Engineering supervision	0.30	852,180	611,229	590,543	462,180
Construction expenses	0.10	633,454	454,347	438,970	343,554
Indirect costs		**1,485,634**	**1,065,576**	**1,029,513**	**805,734**
Total direct and indirect plant costs (TDIPC)	Share of TDIPC	**7,820,172**	**5,609,045**	**5,419,213**	**4,241,272**
Contractors fee	0.03	234,605	168,271	162,576	127,238
Contingency	0.07	547,412	392,633	379,345	296,889
Fixed-capital investment (FCI)	Share of TCI	**8,602,189**	**6,169,949**	**5,961,134**	**4,665,399**
Working capital	0.11	1,063,231	762,606	736,796	576,643
Total capital investment (TCI)		**9,665,420**	**6,932,555**	**6,697,930**	**5,242,042**

Table 4.16: Total production costs of the examined downstream scenarios D1, D2, D3 and D4 [95].

	Share of	D1	D2	D3	D4
1. Raw materials		39,347	51,987	58,799	29,096
2. Operating labour	approx. 0.15 of (III)	567,188	444,763	436,035	456,408
3. Supervisory/Clerical labour	0.12 of (2)	68,063	53,372	52,324	54,769
4. Electricity		503,452	475,599	474,664	462,965
5. Maintenance and Repairs	0.04 (of FCI)	344,088	246,798	238,445	186,616
6. Operating supplies	0.1 of (5)	34,409	24,680	23,845	18,662
7. Laboratory charges	0.1 of (2)	56,719	44,476	43,603	45,641
8. Patents and royalties	approx.0.015 of (III)	56,828	44,561	43,686	45,728
9. External CO_2 extraction	(50 € per kg biomass)				419,301
A. Direct production costs	Sum of (1 to 9)	**1,670,092**	**1,386,235**	**1,371,401**	**1,719,185**
Initial costs for equipment		6,897,829	4,947,491	4,780,049	3,741,039
Salvage value of equipment		689,783	494,749	478,005	374,104
Depreciation equipment per year	10%	620,805	445,274	430,204	336,694
Initial costs for buildings		1,562,330	1,120,587	1,082,661	847,330
Salvage value of buildings		156,233	112,059	108,266	84,733
Depreciation buildings per year	3%	42,183	30,256	29,232	22,878
10. Depreciation total per year		662,988	475,530	459,436	35,9571
11. Local taxes	0.01 of (FCI)	86,022	61,699	59,611	46,654
12. Insurance	0.04 of (FCI)	344,088	246,798	238,445	186,616
B. Fixed charges	Sum of (10 to 12)	**1,093,097**	**784,028**	**757,493**	**592,841**
C. Plant overhead costs	0.5 of (2., 3., 5.)	**489,669**	**372,466**	**363,402**	**348,897**
I. Manufacturing costs (A.+B.+C.)		**3,252,858**	**2,542,728**	**2,492,296**	**2,660,923**
14. Administrative costs	0.2 of (2)	113,438	88,953	87,207	91,282
15. Distribution and marketing	approx. 0.05 of (III)	189,067	148,204	145,287	152,276
16. Research and development	0.02 of (IV)	80,009	80,009	80,009	80,009
17. Interest	0.05 of (FCI)	172,044	123,399	119,223	93,308
II. General expenses	Sum of (14 to 17)	**554,558**	**440,565**	**431,726**	**416,875**
III. Total product cost (I.+II.)		**3,807,416**	**2,983,294**	**2,924,022**	**3,077,798**

The costs that contribute to the direct production costs (A) are explained below in more detail (Table 4.17). These include the raw material costs, which range from €30,873 (D4) to €65,253 (D3). The CO_2 price for the *H. pluvialis* cultivation was assumed to be €0.39 per kg [125]. In total, nutrient costs of €0.50 per kilogram biomass were determined which is in a similar range as reported in literature for $0.58 US per kilogram of biomass [125]. Daily harvesting of 10 m^3 algal broth represent the main water costs with €3.97 m^3 [126]. Ethyl acetate and acetone for cleaning were the main raw material costs for the CPE extraction. A loss of 12 tonnes of CO_2 per year for supercritical CO_2 extraction results in costs of €4,687, considering a price of €0.39 per kilogram CO_2 [127]. For germination the costs of water, glucose and nutrients were considered.

Table 4.17: Raw material costs of the biotechnological production of *H. pluvialis,* comparing four different downstream scenarios, supercritical CO_2 extraction performed in-house (D1), solvent extraction from mechanically disrupted cyst cells (D2) and germinated zoospores (D3), and supercritical CO_2 extraction performed by an external service provider (D4) [95].

1. Raw materials costs		**D1**	**D2**	**D3**	**D4**
Water cultivation		13,101	13,101	13,101	13,101
CO_2 cultivation		9,260	9,260	9,260	9,260
Nutrients cultivation		6,736	6,736	6,736	6,736
CO_2 for extraction		4,687	-	-	-
Ethyl acetate		-	17,327	17,327	-
Acetone cleaning		5,564	5,564	5,564	-
Water germination		-	-	6	-
Nutrients germination		-	-	6,736	-
Glucose		-	-	70	-
Total Raw material costs	**Euro**	**39,347**	**51,987**	**58,799**	**29,096**

In chemical production facilities, the operating labour costs are usually between 10-20% of the total product cost (III) [93]. In this work, 15% was assumed. Based on the costs for operating labour, the supervisory labour costs and laboratory charges can be roughly calculated (Table 4.16). The costs for patents and royalties, as well as maintenance and repairs were calculated as shown in Table 4.16. The annual electricity costs as presented in Table 4.18 were calculated using the daily operating time of the units and the installed capacity (Table 4.11). An electricity price of €0.18 kWh^{-1} was considered for Germany [128]. Regarding the electricity costs, reduced costs of astaxanthin extraction from *H. pluvialis* using CPE extraction (D2 and D3) compared to in-house extraction with supercritical CO_2 (D1) could be calculated. As presented in Table 4.15, a higher electricity consumption for the mechanical high-pressure homogenisation (7.53 MWh a^{-1}), compared to the cyst cell germination (2.34 MWh a^{-1}) can be expected.

Table 4.18: Annual electricity costs of the biotechnological production of H. pluvialis, comparing four different downstream scenarios, supercritical CO_2 extraction performed in-house (D1), solvent extraction from mechanically disrupted cyst cells (D2) and germinated zoospores (D3), as well as supercritical CO_2 extraction performed by an external service provider (D4) [95].

4. Electricity costs		**D1**	**D2**	**D3**	**D4**
Upstream	MWh a^{-1}	2,506	2,506	2,506	2,506
Downstream	MWh a^{-1}	291	136	131	66
Total Electricity	MWh a^{-1}	2,797	2,642	2,637	2,572
Total electricity costs	**Euro**	**503,452**	**475,599**	**474,664**	**462,965**

In total, as shown in Table 4.16, the highest direct production costs (A) were calculated for the external (D4) and in-house (D1) supercritical CO_2 extraction. For the supercritical CO_2 extraction via a contracted manufacturer (D4), lower electricity, raw materials, and repair costs are outweighed by the fees for paying the external service provider.

For the determination of the manufacturing costs (I), the direct production costs (A), the fixed charges (B) and plant overhead costs (C) were calculated (Table 4.16). The sum of depreciation for equipment and buildings, local taxes, and insurances represent the fixed charges [95]. A 10 year linear depreciation period with a residual value of 10% of the initial value were assumed for the equipment. The buildings were depreciated by 3% annually. The fixed charges were highest for the in-house supercritical CO_2 extraction (D4), due to the highest annual depreciation on equipment and buildings. Also, the overhead costs (C) were highest for internal CO_2 extraction (D1) due highest labour and maintenance costs. Consequently, also the manufacturing costs (I) were highest for the in-house CO_2 extraction (D1). The highest general expenses (II) were calculated for the internal CO_2 extraction (D1) as well, due to highest interest payments and administrative costs.

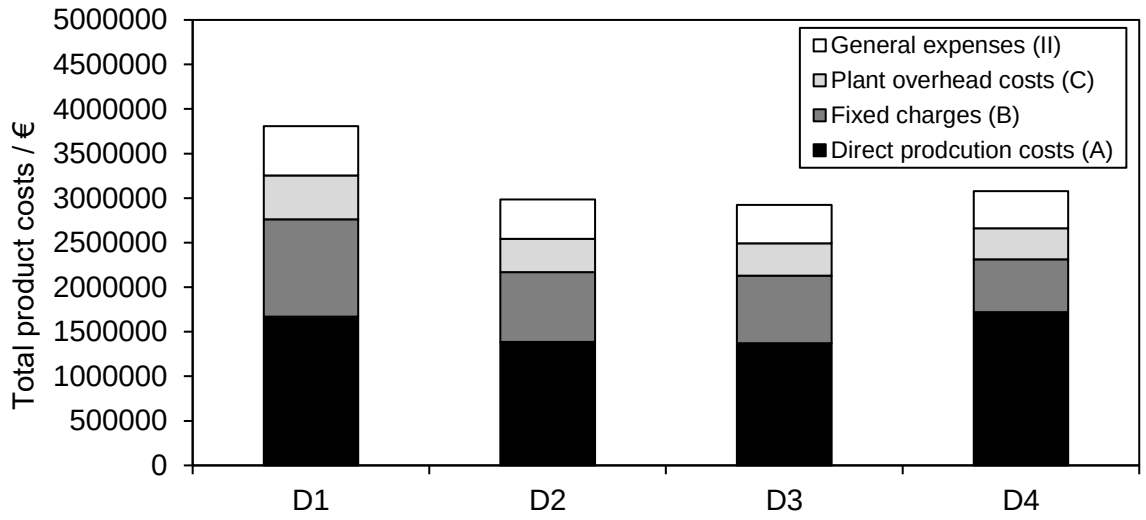

Figure 67: Composition of the total product costs (III), including the direct production costs (A), fixed charges (B), plant overhead costs (C) and general expenses (II) for the four downstream scenarios examined [95].

The total product costs (III) are the sum of the manufacturing costs (I) and general expenses (II) and are presented in Table 4.16 and Figure 67. With €3.81 million, the highest total product costs (III) were calculated for the conventional process, with an in-house supercritical CO_2 extraction (D1). Similar total product costs were determined for the alternative downstream processes using CPE extraction from homogenised cysts (D2) and germinated zoospores (D3), as well as for supercritical CO_2 extraction via a service provider (D4). Higher direct production costs for external CO_2 extraction (D4), caused by the payment for the external service provider are offset by lower costs of the fixed charges (mostly because of lower depreciation) [95].

In summary, it could be shown in this section that the highest total product costs can be expected for an internal supercritical CO_2 extraction (D1). Similar total product costs were calculated for the other three scenarios, extraction of astaxanthin from homogenised cysts cells (D2) and germinated zoospores (D3) using CPE, and external supercritical CO_2 extraction (D4). In the subsequent section, the economic performance of the four different downstream scenarios is presented.

4.5 Economic performance of the four examined downstream scenarios

In the previous section, the TCI and the total product costs (III) of the four examined downstream processes (Figure 65) was determined. These data are needed to determine the economic performance of the four downstream scenarios in the last section of this thesis. To describe the economic profitability, the return on investment (ROI) and the net present value (NPV) were calculated. As presented in Equation 4.6, the ROI is the quotient of the profit after depreciation, interest, and taxes (EAT) and the TCI [93].

$$ROI = \frac{EAT}{TCI} \qquad 4.6$$

The discount factor d_n (Equation 4.7) is the factor by which the future cash flow must be multiplied to obtain the present value of the cash flow after n years if invested at interest i [93]. The discount factor was defined for annual compounding.and yearly payments.

$$d_n = \frac{1}{(1+i)^n} \qquad 4.7$$

The NPV of the processes compares the difference between the present value of annual cash flows after defined time interval with the initial TCI. The NPV was calculated according to Equation 4.8, where net benefits NB corresponds to the discounted net cash flow at year n,

$$NPV = \sum_{n=1}^{t} \frac{NB_n}{(1+d)^n} - TCI \qquad 4.8$$

and TCI to the total capital investment.

The internal rate of return (IRR) was calculated and corresponded to a discount factor at NPV=0 and gave the interest rate i at which the initial investment breaks even with the generated discounted cash flows [95].

Table 4.19: Economic figures for the evaluation of the four downstream scenarios, supercritical CO_2 extraction performed in-house (D1), solvent extraction from mechanically disrupted cyst cells (D2), and germinated zoospores (D3), and supercritical CO_2 extraction committed by an external service provider (D4) [95].

Price of oleoresin (10 $wt_{astaxanthin}$) per kg	**€**	**1200**			
Oleoresin (10 $wt_{astaxanthin}$) produced per year	**kg**	**3241**			
		D1	**D2**	**D3**	**D4**
Gross revenue	**€**	**3,889,620**	**3,889,620**	**3,889,620**	**3,889,620**
Total product cost	€	3,805,199	2,981,077	2,921,805	3,075,581
Interest	€	172,044	123,399	119,223	93,308
Depreciation	€	662,988	475,530	459,436	359,571
EBITDA	**€**	**919,453**	**1,507,472**	**1,546,474**	**1,266,918**
EBIT	**€**	**256,465**	**1,031,942**	**1,087,038**	**907,347**
EBT	**€**	**84,421**	**908,543**	**967,815**	**814,039**
Profit tax (29%)	€	24,482	263,478	280,666	236,071
EAT	**€**	**59,939**	**645,066**	**687149**	**577,968**
ROI	**%**	**0.62**	**9.30**	**10.26**	**11.03**
Operating cash flow (NB)	**€**	**722,927**	**1,120,596**	**1,146,585**	**937,539**

In the scenario presented in this section, 3241 kg of oleoresin (10wt% astaxanthin) can be produced in the four downstream scenarios (Figure 66). A sales price of €1,200 per kilogram of oleoresin was considered (personal talk with Schott AG and Sea&Sun AG), resulting in gross revenues of around €3.89 million (Table 4.19). The earnings before interest, taxes, depreciation, and amortisation (EBITDA), are the difference between gross revenues and total product cost (III), excluding depreciation and interest payments. The highest EBITDA was reached for the two new downstream processes, using CPE extraction (D2 and D3), due to the lowest total production costs (Table 4.19). Due to higher interest payments, depreciation, and paid taxes, the profits after depreciation, interest payments, and taxes (EAT) converge for the processes D2 and D3 compared to D4. The lowest EAT was reached for D4, due to the highest depreciation and interest payments. For an adequate economic comparison of the processes, also the TCI needs to be considered. That is why the ROI was calculated according to Equation 4.6 [14, 127]. With 11%, the highest ROI was calculated for the downstream process, performing supercritical CO_2 extraction via a service provider (D4), followed by 10.3% by CPE extraction from zoospores (D3) and 9.3% from homogenised cyst cells (D2). The lowest ROI (0.6%) was reached for in-house supercritical CO_2 extraction (D4). For costs higher than 65 € per kilogram of biomass for supercritical CO_2 extraction via a contracted

manufacturer (D4), the alternative processes of solvent extraction (D2 and D3) would reach higher ROI. For long-term investments, the calculation of the NPV is needed, as it also consideres the time value of money. The NPV was calculated as presented in Equation 4.9. As presented in Table 4.20, the highest NPV was determined for scenario D3, while a negative NPV of €3.7 million is reached for the in-house supercritical CO_2 extraction (D1). The discount factor for which the NPV of the project is equal to zero is defined as IRR and represents the interest rate at which the investment breaks even [95]. Common rates for IRR are 10% for conventional technology improvements, 15% for the expansion of traditional technologies, 20 % for product development, and 30 % for speculative ventures [129]. As shown in Table 4.20, the highest IRR can be expected using external supercritical CO_2 extraction, followed by the novel downstream scenarios of solvent extraction from homogenised cyst cells and flagellated zoospores.

Table 4.20: Total present value of annual cash flows at an interest rate of 2%, NPV after ten years and IRR of the four downstream scenarios of supercritical CO_2 extraction performed in-house (D1), solvent extraction from mechanically disrupted cyst cells (D2), and germinated zoospores (D3), and supercritical CO_2 extraction performed by an external service provider (D4) [95].

		D1	**D2**	**D3**	**D4**
TCI		9,665,420	6,932,555	6,697,930	5,242,042
Total present value of discounted cash flows	€	5,900,698	9,146,567	9,358,698	7,652,416
NPV	**€**	**-3,764,721**	**2,214,012**	**2,660,767**	**2,410,374**
IRR	%	< 0	8.25	9.65	10.75

In this section, the economic performance of the four different downstream scenarios was examined. According to the ROI and NPV, in-house supercritical CO_2 extraction tends to be the least profitable. The highest ROI could be calculated for an external supercritical CO_2 extraction. On the other hand, the highest NPV is achieved for the new downstream scenarios, the extraction of astaxanthin from germinated zoospores. In principle, the two newly developed processes for the extraction from homogenised cyst cells and zoospores using CPE, are therefore on par with an external supercritical extraction with CO_2. Another advantage of CPE extraction compared to external CO_2 extraction is that it can be operated in-house. This can be beneficial in times of uncertain supply chains. The Technical University of Munich has registered a patent for the presented method of extracting astaxanthin from *H. pluvialis* zoospores and homogenised cyst cells using CPE, which underlines the potential of the work [130].

5 Conclusion

In this work, new downstream processes for the extraction of astaxanthin from the microalgae *H. pluvialis* were developed. The synthesis of astaxanthin in *H. pluvialis* is accompanied by the formation of a resistant cyst cell wall. The industrial downstream process includes harvesting of the cyst cells, mechanical cell wall disruption, drying and extraction with supercritical CO_2. The present work shows the development of a novel downstream process for the extraction of astaxanthin from the microalgae *H. pluvialis* using liquid-liquid chromatography and membrane-assisted extraction. This is of interest to improve the economics of biotechnological produced astaxanthin compared to chemically synthesized one.

An alternative method for mechanical cell wall disruption of the cyst cells, germination, was examined. It was shown that cyst germination works best under heterotrophic conditions. Extraction yields from the astaxanthin available in the biomass of 50% could be achieved under these conditions. In addition, the astaxanthin content in the biomass remained constant. With twice the nitrate content and short-term illumination of the culture until nitrate depletion, the extraction yield could further be increased up to 64%.

Subsequently, astaxanthin extraction from germinated zoospores and homogenised cysts was done using liquid-liquid chromatographic columns. A process concept was developed using a laboratory-scale CCC unit. To overcome the limitations of CCC units, such as loss of stationary phase due to sample injection, a CPE unit was considered for scale-up. The operating conditions of the CPE extraction of astaxanthin from homogenised cysts and zoospores were determined experimentally. The highest yield of 85% and productivity of 640 $g_{astaxanthin}\ L_{column}^{-1} d^{-1}$ of could be determined with an injection volume of about one column volume and a biomass concentration of 33 g L^{-1}.

In the further course, the membrane-assisted extraction for an extraction of astaxanthin from *H. pluvialis* algal broth was examined using a hollow fibre module. Selecting the operating parameters it could be shown, that the fastest mass transfer can be achieved with high flow rates of the aqueous phase and pumping it in the shell (solvent in fibre). In addition, it was shown that pumping the solvent has no influence on the mass transfer coefficient, i.e. it can be kept stationary. Based on the selected parameters, astaxanthin containing oleoresin (obtained from supercritical CO_2 extraction) could be successfully back-extracted from the aqueous phase into a solvent. However, the extraction of astaxanthin from homogenised cyst cells was not successful due to the insoluble nature of astaxanthin in water

In the last section of the work, a techno-economic analysis was made for the most promising newly developed process option, the extraction of astaxanthin from homogenised cysts and

germinated zoospores using CPE. These were compared to the conventional industrial process including centrifugation, mechanical cyst cell disruption, spray drying and supercritical CO_2 extraction. It could be shown that the total product costs for the CPE extraction compared to the CO_2 extraction via an external service provider are similar. Significantly higher total product costs need to be expected for an in-house CO_2 extraction. The highest net present value was determined for the newly developed process of extracting astaxanthin from germinated zoospores using CPE.

For a better process control (e.g. oxygen transfer), germination could be transferred to a fermenter in the future. In addition, other centrifugal extractors (Podbielniak, Rousselet, and CINC) could be investigated, which might enable a higher throughput. In addition, it would be interesting to compare the performance of supercritical CO_2 extraction from zoospores with that from homogenised cyst cells. Also the application of deep eutectic solvents for extraction would be interesting to avoid the use of organic solvents.

6 References

1. Bauer, A. and M. Minceva, *Direct extraction of astaxanthin from the microalgae Haematococcus pluvialis using liquid–liquid chromatography.* RSC Advances, 2019. **9**(40): p. 22779-22789.
2. Hazen, T.E., *The Life History of Sphaerella lacustris (Haematoccus pluvialis).* Memoirs of the Torrey Botanical Club, 1899. **6**(3): p. 211-246.
3. *Algatech*. 2021 20210809]; Available from: https://www.algatech.com/.
4. *Cyanotech*. 2021; Available from: https://www.cyanotech.com/.
5. Li, J., et al., *An economic assessment of astaxanthin production by large scale cultivation of Haematococcus pluvialis.* Biotechnol Adv, 2011. **29**(6): p. 568-74.
6. Zhang, C.H., J.G. Liu, and L.T. Zhang, *Cell cycles and proliferation patterns in Haematococcus pluvialis.* Chinese Journal of Oceanology and Limnology, 2017. **35**(5): p. 1205-1211.
7. Hagen, C., S. Siegmund, and W. Braune, *Ultrastructural and chemical changes in the cell wall of Haematococcus pluvialis (Volvocales, Chlorophyta) during aplanospore formation.* European Journal of Phycology, 2002. **37**(2): p. 217-226.
8. Boussiba, S., *Carotenogenesis in the green alga Haematococcus pluvialis: Cellular physiology and stress response.* Physiologia Plantarum, 2000. **108**(2): p. 111-117.
9. Bauer, A. and M. Minceva, *Examination of Photo-, Mixo-, and Heterotrophic Cultivation Conditions on Haematococcus pluvialis Cyst Cell Germination.* Applied Sciences, 2021. **11**(16).
10. Li, X., et al., *Biotechnological production of astaxanthin from the microalga Haematococcus pluvialis.* Biotechnol Adv, 2020. **43**: p. 107602.
11. Chekanov, K., et al., *Effects of CO2 enrichment on primary photochemistry, growth and astaxanthin accumulation in the chlorophyte Haematococcus pluvialis.* J Photochem Photobiol B, 2017. **171**: p. 58-66.
12. Ma, R., et al., *Blue light enhances astaxanthin biosynthesis metabolism and extraction efficiency in Haematococcus pluvialis by inducing haematocyst germination.* Algal Research, 2018. **35**: p. 215-222.
13. Shah, M.M., et al., *Astaxanthin-Producing Green Microalga Haematococcus pluvialis: From Single Cell to High Value Commercial Products.* Frontiers in Plant Science, 2016. **7**: p. 531.
14. Panis, G. and J.R. Carreon, *Commercial astaxanthin production derived by green alga Haematococcus pluvialis: A microalgae process model and a techno-economic assessment all through production line.* Algal Research, 2016. **18**: p. 175-190.
15. Praveenkumar, R., et al., *Morphological Change and Cell Disruption of Haematococcus pluvialis Cyst during High-Pressure Homogenization for Astaxanthin Recovery.* Applied Sciences, 2020. **10**(2).
16. Lide, D.R., *CRC Handbook of Chemistry and Physics, Internet Version 2005*, ed. C. press. 2005, Boca Raton, FL.
17. Tippelt, M. *From lab scale to pilot and production scale using scCO2 at 1000 bar with special focus on Haematococcus pluvialis*. in *17th European Meeting on Supercritical Fluids 2019*. 2019.
18. Praveenkumar, R., et al., *Breaking dormancy: an energy-efficient means of recovering astaxanthin from microalgae.* Green Chemistry, 2015. **17**(2): p. 1226-1234.
19. Choi, Y.Y., M.-E. Hong, and S.J. Sim, *Enhanced astaxanthin extraction efficiency from Haematococcus pluvialis via the cyst germination in outdoor culture systems.* Process Biochemistry, 2015. **50**(12): p. 2275-2280.
20. Fabregas, J., et al., *Interactions between irradiance and nutrient availability during astaxanthin accumulation and degradation in Haematococcus pluvialis.* Appl Microbiol Biotechnol, 2003. **61**(5-6): p. 545-51.
21. Vidhyavathi, R., et al., *Differential expression of carotenogenic genes and associated changes in pigment profile during regeneration of Haematococcus pluvialis cysts.* Appl Microbiol Biotechnol, 2007. **75**(4): p. 879-87.

22. Berthod, A., *Countercurrent chromatography*. Vol. 38. 2002.
23. Friesen, J.B. and G.F. Pauli, *Rational development of solvent system families in counter-current chromatography.* J Chromatogr A, 2007. **1151**(1-2): p. 51-9.
24. Ungureanu, C., et al., *Centrifugal partition extraction, a new method for direct metabolites recovery from culture broth: case study of torularhodin recovery from Rhodotorula rubra.* Bioresource Technology, 2013. **132**: p. 406-9.
25. Marchal, L., et al., *Centrifugal partition extraction of beta-carotene from Dunaliella salina for efficient and biocompatible recovery of metabolites.* Bioresource Technology, 2013. **134**: p. 396-400.
26. Tompkins, C.J., A.S. Michaels, and S.W. Peretti, *Removal of P-Nitrophenol from Aqueous-Solution by Membrane-Supported Solvent-Extraction.* Journal of Membrane Science, 1992. **75**(3): p. 277-292.
27. Prasad, R. and K.K. Sirkar, *Dispersion-free solvent extraction with microporous HFM.* AIChE Journal, 1988. **34**(2): p. 177-188.
28. Gabelman, A. and S.T. Hwang, *Hollow fiber membrane contactors.* Journal of Membrane Science, 1999. **159**(1-2): p. 61-106.
29. Gössi, A., et al., *In-situ recovery of carboxylic acids from fermentation broths through membrane supported reactive extraction using membrane modules with improved stability.* Separation and Purification Technology, 2020. **241**.
30. Amos, R., *Handbook of Microalgal Culture: Biotechnology and Applied Phycology*, ed. R. Amos. 2004.
31. Bux, F. and Y. Christi, *Algae Biotechnology*. 2016.
32. Tibocha-Bonilla, J.D., et al., *Advances in metabolic modeling of oleaginous microalgae.* Biotechnol Biofuels, 2018. **11**: p. 241.
33. Nelson, D.L., A.L. Lehninger, and M.M. Cox, *Lehninger principles of biochemistry*. 2008: W.H. Freeman.
34. Perez-Garcia, O., et al., *Heterotrophic cultures of microalgae: metabolism and potential products.* Water Res, 2011. **45**(1): p. 11-36.
35. Boyle, N.R. and J.A. Morgan, *Flux balance analysis of primary metabolism in Chlamydomonas reinhardtii.* BMC Syst Biol, 2009. **3**: p. 4.
36. Knoop, H., et al., *Flux balance analysis of cyanobacterial metabolism: the metabolic network of Synechocystis sp. PCC 6803.* PLoS Comput Biol, 2013. **9**(6): p. e1003081.
37. Tanner, W., *The Chlorella Hexose/H/(+) -Symporters.* International Review of Cytology, 2000. **200**: p. 101-141.
38. Neilson, A.H. and R.A. Lewin, *The uptake and utilization of organic carbon by algae- an essay In comparative biochemistry.* 1974. **13**(3): p. 227-264.
39. Ahmad, I. and J.A. Hellebust, *Regulation of Chloroplast Development by Nitrogen Source and Growth Conditions in a Chlorella protothecoides Strain.* Plant Physiol., 1990. **94**: p. 944-949.
40. Fernández, E., Á. Llamas, and A. Galván, *Nitrogen Assimilation and its Regulation*, in *The Molecular Biology of Chloroplasts and Mitochondria in Chlamydomonas. Advances in Photosynthesis and Respiration*, J.D. Rochaix, M. Goldschmidt-Clermont, and S. Merchant, Editors. 2009. p. 637-659.
41. Morales-Sanchez, D., et al., *Heterotrophic growth of microalgae: metabolic aspects.* World J Microbiol Biotechnol, 2015. **31**(1): p. 1-9.
42. Czygan, F.C., *Blood-rain and blood-snow: nitrogen-deficient cells of haematococcus pluvialis and chlamydomonas nivalis.* Arch Mikrobiol, 1970. **74**(1): p. 69-76.
43. Grünewald, K., C. Hagen, and W. Braune, *Secondary carotenoid accumulation in flagellates of the green algaHaematococcus lacustris.* European Journal of Phycology, 1997. **32**(4): p. 387-392.
44. Xi, T., et al., *Enhancement of astaxanthin production using Haematococcus pluvialis with novel LED wavelength shift strategy.* Appl Microbiol Biotechnol, 2016. **100**(14): p. 6231-6238.

45. Sun, H., et al., *Enhancement of cell biomass and cell activity of astaxanthin-rich Haematococcus pluvialis.* Bioresour Technol, 2015. **186**: p. 67-73.
46. Lemoine, Y. and B. Schoefs, *Secondary ketocarotenoid astaxanthin biosynthesis in algae: a multifunctional response to stress.* Photosynth Res, 2010. **106**(1-2): p. 155-77.
47. Pick, U., et al., *A hypothesis about the origin of carotenoid lipid droplets in the green algae Dunaliella and Haematococcus.* Planta, 2019. **249**(1): p. 31-47.
48. Recht, L., A. Zarka, and S. Boussiba, *Patterns of carbohydrate and fatty acid changes under nitrogen starvation in the microalgae Haematococcus pluvialis and Nannochloropsis sp.* Appl Microbiol Biotechnol, 2012. **94**(6): p. 1495-503.
49. Recht, L., et al., *Metabolite profiling and integrative modeling reveal metabolic constraints for carbon partitioning under nitrogen starvation in the green algae Haematococcus pluvialis.* J Biol Chem, 2014. **289**(44): p. 30387-30403.
50. Zhekisheva, M., et al., *INHIBITION OF ASTAXANTHIN SYNTHESIS UNDER HIGH IRRADIANCE DOES NOTABOLISH TRIACYLGLYCEROL.* Journal of Phycology, 2005. **41**(4).
51. Gwak, Y., et al., *Comparative analyses of lipidomes and transcriptomes reveal a concerted action of multiple defensive systems against photooxidative stress in Haematococcus pluvialis.* J Exp Bot, 2014. **65**(15): p. 4317-34.
52. Solovchenko, A.E., *Recent breakthroughs in the biology of astaxanthin accumulation by microalgal cell.* Photosynth Res, 2015. **125**(3): p. 437-49.
53. Cunningham, F.X. and E. Gantt, *GENES AND ENZYMESOF CAROTENOID BIOSYNTHESISIN PLANTS.* Annual Review of Plant Physiology and Plant Molecular Biology, 1998. **49**.
54. Vidhyavathi, R., et al., *Regulation of carotenoid biosynthetic genes expression and carotenoid accumulation in the green alga Haematococcus pluvialis under nutrient stress conditions.* J Exp Bot, 2008. **59**(6): p. 1409-18.
55. Peled, E., et al., *Light-Induced Oil Globule Migration in Haematococcus Pluvialis (Chlorophyceae).* J Phycol, 2012. **48**(5): p. 1209-19.
56. Li, Q., L. Zhang, and J. Liu, *Examination of carbohydrate and lipid metabolic changes during Haematococcus pluvialis non-motile cell germination using transcriptome analysis.* Journal of Applied Phycology, 2018. **31**(1): p. 145-156.
57. Tuncay, H., et al., *A forward genetic approach in Chlamydomonas reinhardtii as a strategy for exploring starch catabolism.* PLoS One, 2013. **8**(9): p. e74763.
58. Shaik, S.S., et al., *Starch bioengineering affects cereal grain germination and seedling establishment.* J Exp Bot, 2014. **65**(9): p. 2257-70.
59. Araujo, W.L., et al., *Metabolic control and regulation of the tricarboxylic acid cycle in photosynthetic and heterotrophic plant tissues.* Plant Cell Environ, 2012. **35**(1): p. 1-21.
60. Fatland, B.L., B.J. Nikolau, and E.S. Wurtele, *Reverse genetic characterization of cytosolic acetyl-CoA generation by ATP-citrate lyase in Arabidopsis.* Plant Cell, 2005. **17**(1): p. 182-203.
61. Kochetov, G.A. and O.N. Solovjeva, *Structure and functioning mechanism of transketolase.* Biochim Biophys Acta, 2014. **1844**(9): p. 1608-18.
62. Quan, S., et al., *Proteome analysis of peroxisomes from etiolated Arabidopsis seedlings identifies a peroxisomal protease involved in beta-oxidation and development.* Plant Physiol, 2013. **163**(4): p. 1518-38.
63. Miltiadou, D., et al., *Variants in the 3' untranslated region of the ovine acetyl-coenzyme A acyltransferase 2 gene are associated with dairy traits and exhibit differential allelic expression.* J Dairy Sci, 2017. **100**(8): p. 6285-6297.
64. Graham, I.A., *Seed Storage Oil Mobilization.* Annual Review of Plant Biology, 2008. **59**(1): p. 115-142.
65. Gmehling, J., et al., *Chemical Thermodynamics for Process Simulation*. 2019.
66. Green, D.W. and R.H. Perry, *Perry's Chemical Engineers' Handbook*. 8th Revised edition ed. 2007: McGraw-Hill Education Ltd.

67. Stanbury, P., A. Whitaker, and S. Hall, *Principles of Fermentation Technology*. 3 ed. 2016: Butterworth-Heinemann.
68. Doran, P.M., *Bioprocess Engineering Principles*. 2012.
69. Prasda, R. and K.K. Sirkar, *Membrane-Based Solvent Extraction*. Membrane Handbook. 1992, Boston, MA: Springer.
70. Wilke, C.R. and P. Chang, *Correlation of diffusion coefficients in dilute solutions.* American Institute of Chemical Engineers Journal, 1956. **1**(2): p. 264-270.
71. Miyabe, K. and R. Isogai, *Estimation of molecular diffusivity in liquid phase systems by the Wilke-Chang equation.* J Chromatogr A, 2011. **1218**(38): p. 6639-45.
72. Visscher, F., *Liquid-liquid processes in spinning disc equipment*. 2013, Technische Universiteit Eindhoven.
73. Stichlmair, J., *Leistungs- und Kostenvergleich verschiedener Apparatebauarten für die Flüssig-Flüssig-Extraktion.* Chemie Ingenieur Technik., 1980.
74. Roehrer, S. and M. Minceva, *Evaluation of Inter-Apparatus Separation Method Transferability in Countercurrent Chromatography and Centrifugal Partition Chromatography.* Separations, 2019. **6**(3).
75. Berthod, A., *Countercurrent chromatography and the journal of liquid chromatography: A love story.* Journal of Liquid Chromatography & Related Technologies, 2007. **30**(9-12): p. 1447-1463.
76. Minceva, M., *Model-based design of preparative liquid-chromatography processes*. 2013, University of Erlangen-Nuremberg.
77. Goll, J., A. Frey, and M. Minceva, *Study of the separation limits of continuous solid support free liquid-liquid chromatography: separation of capsaicin and dihydrocapsaicin by centrifugal partition chromatography.* J Chromatogr A, 2013. **1284**: p. 59-68.
78. Brent Friesen, J. and G.F. Pauli, *G.U.E.S.S.—A Generally Useful Estimate of Solvent Systems for CCC.* Journal of Liquid Chromatography & Related Technologies, 2007. **28**(17): p. 2777-2806.
79. Ito, Y., *Golden rules and pitfalls in selecting optimum conditions for high-speed counter-current chromatography.* Journal of Chromatography A, 2005. **1065**(2): p. 145-68.
80. Ito, Y., et al., *The coil planet centrifuge.* Nature, 1966. **212**.
81. Adelmann, S. and G. Schembecker, *Influence of physical properties and operating parameters on hydrodynamics in Centrifugal Partition Chromatography.* J Chromatogr A, 2011. **1218**(32): p. 5401-13.
82. van Buel, M.J., et al., *Flow regimes in centrifugal partition chromatography.* AIChE Journal, 1998. **44**.
83. Pruvost, J., J. Legrand, and A. Foucault, *METHOD FOR THE INTENSIVE EXTRACTION OF CELLULAR COMPOUNDS FROM MICRO-ORGANISMS BY CONTINUOUS CULTURE AND EXTRACTION, AND CORRESPONDING DEVICE*. 2008.
84. Berthod, A. and K. Faure, *Separations with a Liquid Stationary Phase Countercurrent Chromatography.* Analytical Separation Science, 2015.
85. Marchal, L. and J. Legrand, *Mass Transport and flow regimes in centrifugal partition chromatography.* AIChE Journal, 2002. **48**.
86. Morley, R. and M. Minceva, *Operating mode and parameter selection in liquid-liquid chromatography.* J Chromatogr A, 2020. **1617**: p. 460479.
87. Lu, Y., Y. Pan, and A. Berthod, *Using the liquid nature of the stationary phase in counter-current chromatography V. The back-extrusion method.* J Chromatogr A, 2008. **1189**(1-2): p. 10-8.
88. Morley, R. and M. Minceva, *Operating mode selection for the separation of intermediately-eluting components with countercurrent and centrifugal partition chromatography.* J Chromatogr A, 2019. **1594**: p. 140-148.
89. Berthod, A., M.J. Ruiz-Angel, and S. Carda-Broch, *Elution-Extrusion Countercurrent Chromatography. Use of the Liquid Nature of the Stationary Phase To Extend the Hydrophobicity Window.* Analytical Chemistry, 2003. **75**.

90. Sciubba, L., et al., *Membrane-based solvent extraction of vanillin in hollow fiber contactors.* Desalination, 2009. **241**(1-3): p. 357-364.
91. Janoschek, L., L. Grozdev, and S. Berensmeier, *Membrane-assisted extraction of monoterpenes: from in silico solvent screening towards biotechnological process application.* R Soc Open Sci, 2018. **5**(4): p. 172004.
92. Schlosser, Š., R. Kertész, and J. Marták, *Recovery and separation of organic acids by membrane-based solvent extraction and pertraction.* Separation and Purification Technology, 2005. **41**(3): p. 237-266.
93. Peters, M.S. and K.D. Timmerhaus, *Plantdesign and economics for chemical engineers*. 1991: McGraw-Hill, Inc.
94. Turton, R., et al., *Analysis, Synthesis and Design of Chemical Processes*. 2012.
95. Bauer, A. and M. Minceva, *Techno-economic analysis of a new downstream process for the production of astaxanthin from the microalgae Haematococcus pluvialis.* Bioresources and Bioprocessing, 2021. **8**(1).
96. Taucher, J., S. Baer, and P. Schwerna, *Cell Disruption and Pressurized Liquid Extraction of Carotenoids from Microalgae.* Journal of Thermodynamics & Catalysis, 2016. **7**(1): p. 7.
97. *DIN 32645:2008-11, Chemische Analytik - Nachweis-, Erfassungs- und Bestimmungsgrenze unter Wiederholbedingungen - Begriffe, Verfahren, Auswertung.* 2010.
98. Association, A.P.H., *APHA Metohd 4500-NO3: Standard Methods for the Examination of Water and Wastewater*. 1992.
99. Dubois, M., et al., *Colorimetric Method for Determination of Sugars and Related Substances.* 1956.
100. Li, K., et al., *Transcriptome-based analysis on carbon metabolism of Haematococcus pluvialis mutant under 15% CO2.* Bioresour Technol, 2017. **233**: p. 313-321.
101. Zhao, Y., et al., *Transcriptome analysis of Haematococcus pluvialis of multiple defensive systems against nitrogen starvation.* Enzyme Microb Technol, 2020. **134**: p. 109487.
102. *Green chemistry at Pfizer*.
103. *GreenChemWeb_A4Poster_Solvents*.
104. Alfonsi, K., et al., *Green chemistry tools to influence a medicinal chemistry and research chemistry based organisation.* Green Chemistry, 2008. **10**(1): p. 31-36.
105. Sun, H., et al., *Repeated cultivation: non-cell disruption extraction of astaxanthin for Haematococcus pluvialis.* Scientific reports, 2016. **6**.
106. Foucault, A.P., et al., *Centrifugal Partition Chromatography: Stability of Various Biphasic Systems and Pertinence of the "Stoke's Model" to Describe the Influence of the Centrifugal Field Upon the Efficiency.* Journal of Liquid Chromatography, 1994. **17**(1): p. 1-17.
107. Roehrer, S. and M. Minceva, *Characterization of a centrifugal partition chromatographic column with spherical cell design.* Chemical Engineering Research and Design, 2019. **143**: p. 180-189.
108. Schwienheer, C., J. Merz, and G. Schembecker, *Investigation, comparison and design of chambers used in centrifugal partition chromatography on the basis of flow pattern and separation experiments.* Journal of chromatography A, 2015. **1390**: p. 39-49.
109. Ito, Y. and W.D. Conway, *High-speed countercurrent chromatography.* Critical Reviews in Analytical Chemistry, 1986. **17**(1): p. 65-143.
110. Berthod, A., et al., *Elution-Extrusion Countercurrent Chromatography: Theory and Concepts in Metabolic Analysis.* Analytical Chemistry, 2007. **79**.
111. Adelmann, S., et al., *Selection of operating parameters on the basis of hydrodynamics in centrifugal partition chromatography for the purification of nybomycin derivatives.* J Chromatogr A, 2013. **1274**: p. 54-64.
112. Riedl, W. and T. Raiser, *Membrane-supported extraction of biomolecules with aqueous two-phase systems.* Desalination, 2008. **224**(1-3): p. 160-167.

113. Faure, K., et al., *Limonene in Arizona liquid systems used in countercurrent chromatography. II Polarity and stationary-phase retention.* Anal Bioanal Chem, 2014. **406**(24): p. 5919-26.
114. Riedl, W., *Membrangestützte Flüssig-Flüssig-Extraktion bei der Caprolactamherstellung*, in *Technische Fakultät*. 2002, Universität Erlangen-Nürnberg.
115. *Camphor*. 2021.
116. AFFANDI, M.M.M., T. JULIANTO, and A. MAJEED, *DEVELOPMENT AND STABILITY EVALUATION OF ASTAXANTHIN NANOEMULSION.* Asian Journal of Pharmaceutical and Clinical Research, 2011. **4**.
117. Li, M., et al., *Preparation and stability of astaxanthin solid lipid nanoparticles based on stearic acid.* European Journal of Lipid Science and Technology, 2016. **118**(4): p. 592-602.
118. Mahmood, M.E. and D.A.F. Al-Koofee, *Effect of temperature changes on critical micelle concentration for tween series surfactant.* Global Journal of Science Frontier Research Chemistry, 2013. **13**(4).
119. Derwenskus, F., et al., *Economic evaluation of up- and downstream scenarios for the co-production of fucoxanthin and eicosapentaenoic acid with P. tricornutum using flat-panel airlift photobioreactors with artificial light.* Algal Research, 2020. **51**.
120. Acien, F.G., et al., *Production cost of a real microalgae production plant and strategies to reduce it.* Biotechnol Adv, 2012. **30**(6): p. 1344-53.
121. Thomassen, G., et al., *A techno-economic assessment of an algal-based biorefinery.* Clean Technologies and Environmental Policy, 2016. **18**(6): p. 1849-1862.
122. Stephenson, R. and J. Stuart, *Mutual Binary Solubilities - Water Alcohols and Water Esters.* Journal of Chemical and Engineering Data, 1986. **31**(1): p. 56-70.
123. Toth, A.J., *Comprehensive evaluation and comparison of advanced separation methods on the separation of ethyl acetate-ethanol-water highly non-ideal mixture.* Separation and Purification Technology, 2019. **224**: p. 490-508.
124. Ghobashy, M., et al., *Kinetic study of hydrolysis of ethyl acetate using caustic soda.* International Journal of Engineering & Technology, 2018. **7**(4).
125. Molina Grima, E., et al., *Recovery of microalgal biomass and metabolites: process options and economics.* Biotechnol Adv, 2003. **20**(7-8): p. 491-515.
126. *VEA: Wasserpreise für Industriekunden bleiben 2016 stabil*. 2021 [cited 2021 14.04.2021]; Available from: https://www.euwid-wasser.de/news/wirtschaft/einzelansicht/Artikel/vea-wasserpreise-fuer-industriekunden-bleiben-2016-stabil.html.
127. Zgheib, N., et al., *Extraction of astaxanthin from microalgae: process design and economic feasibility study.* IOP Conference Series: Materials Science and Engineering, 2018. **323**: p. 012011.
128. *Industriestromrechner*. 2021 [cited 2021; Available from: https://www.eon.de/de/gk/strom/industriestromrechner.html?adobe_mc_sdid=SDID%3D6C0D58C71AB0F351-46A932B6BA0F57E1%7CMCORGID%3D17923CDE5783D4787F000101%40AdobeOrg%7CTS%3D1619600881&adobe_mc_ref=https%3A%2F%2Fwww.google.com%2F&utm_term=industriestrom&mc=0512222000&gclid=CjwKCAjwj6SEBhAOEiwAvFRuKD1BD_x7p8JWQK7FiwQujLgwOXLM_riCU2UVcACoaGrf9EesV1bA5hoCwlYQAvD_BwE&gclsrc=aw.ds.
129. Van Dael, M., et al., *Techno-economic Assessment Methodology for Ultrasonic Production of Biofuels*, in *Production of Biofuels and Chemicals with Ultrasound*. 2015. p. 317-345.
130. Minceva, M. and A. Bauer, *METHOD OF EXTRACTING A PIGMENT FROM MICROALGAE, WO2020089173*. 2019.

7 List of Figures

8 List of Tables

9 Appendix

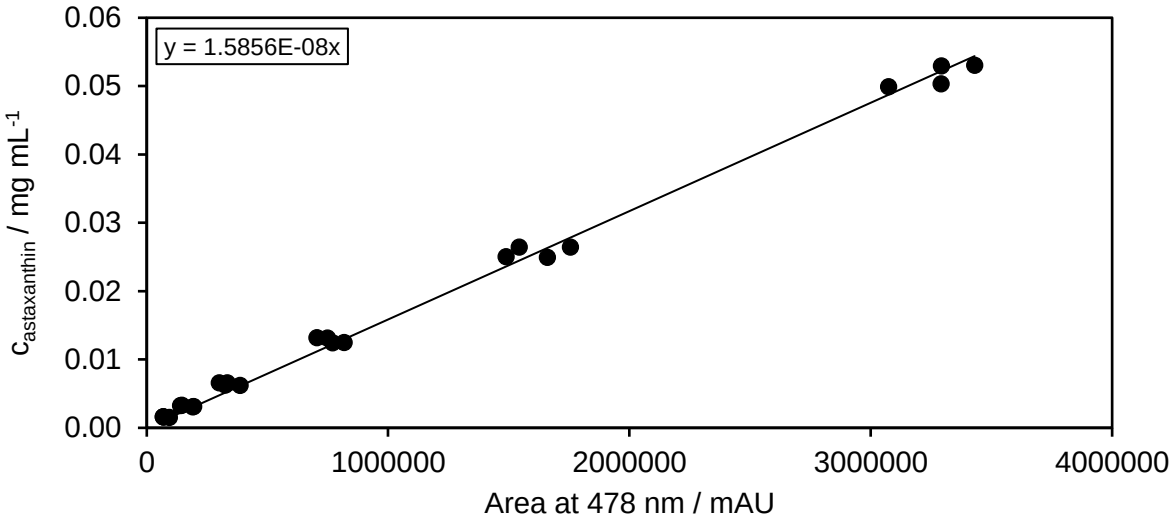

Figure A 1: Calibration curve of trans-astaxanthin for HPLC analysis.

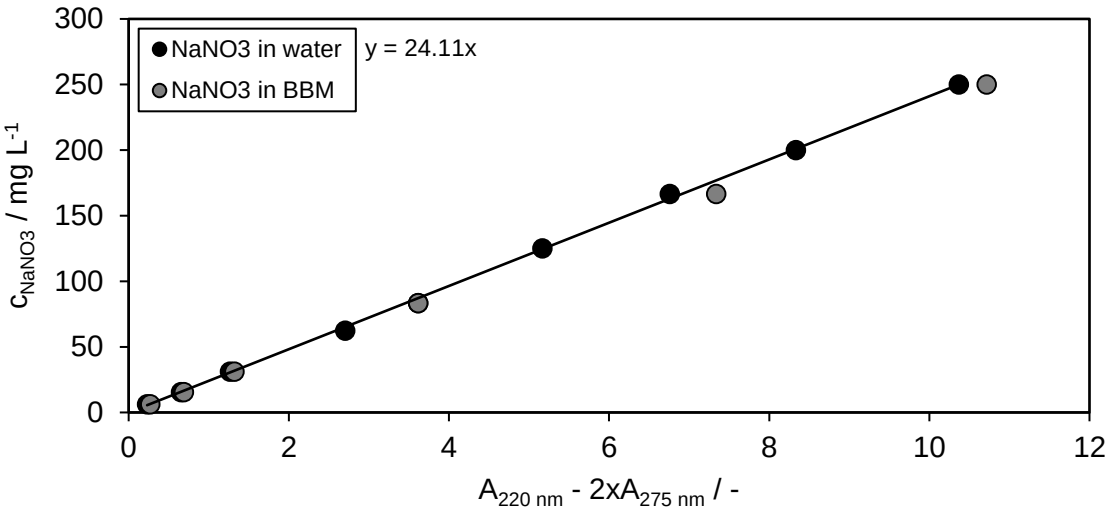

Figure A 2: Calibration curve of sodium nitrate in water and BBM.

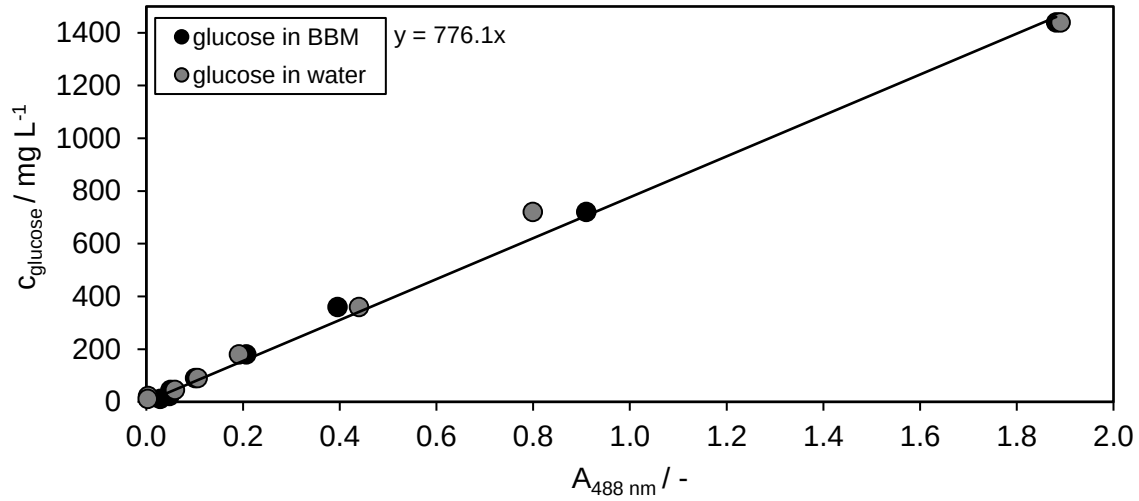

Figure A 3: Calibration curve of glucose in water and BBM.

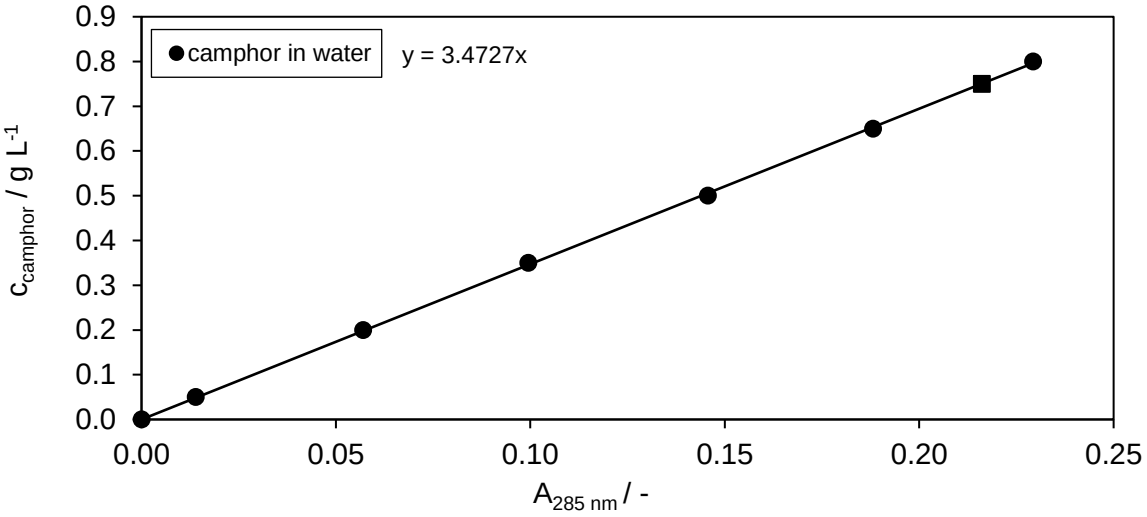

Figure A 4: Calibration curve of camphor in water.

Table A 1: Parameters for the calculation of $K_{W,theo}$ and K_W for the extraction of camphor from at a an aqueous feed flow rate of 151 mL min^{-1} from the feed (shell) into *n*-heptane (fibre).

k_f (*n*-heptane)	1.07E-05	m s^{-1}	$D_{i,feed}$	9.39E-06	cm^2 s^{-1}
$d_{f,i}$	0.003	m	x_{water}	2.6	-
$d_{f,a}$	0.0031	m	T	303.15	K
d_{log}	0.00305	m	M_{water}	18.01	g mol^{-1}
F_i	4.32E-06	m^3 s^{-1}	$M_{Camphor}$	152.23	g mol^{-1}
F_i	258.93	mL min^{-1}	$\rho_{Camphor}$	0.992	g cm^{-3}
$F_{f,i}$	6.16E-07	m^3 s^{-1}	v_n	153.5	cm^3 mol^{-1}
$F_{f,i}$	36.99	mL min^{-1}	η_{water}	0.7977	cP
$A_{f,i,total}$	4.95E-05	m^2	$D_{i,n\text{-heptane}}$	2.96E-05	cm^2 s^{-1}
$v_{f,i}$	0.0872	m s^{-1}	$x_{n\text{-heptane}}$	1	-
L	0.875	m	T	303.15	K
$D_{i,solvent}$	2.96E-09	m^2 s^{-1}	$M_{n\text{-heptane}}$	100.21	g mol^{-1}
N_f	7	-	$M_{Camphor}$	152.23	g mol^{-1}
$A_{f,o,total}$	5.28E-05	m^2	$\rho_{Camphor}$	0.992	g cm^{-3}
Re	477	-	v_n	153.5	cm^3 mol^{-1}
η	0.000370	Pas	$\eta_{n\text{-heptane}}$	0.370	cP
ρ	675	kg m^{-3}			
Gz	302.9				
k_s (feed)	1.14E-06	m s^{-1}			
F_s	2.51E-06	m^3 s^{-1}			
F_s	150.74	mL min^{-1}			
β	5.8	-			
d_s	0.0258	m			
A_s	0.00052	m^2			
d_h	0.028	m			
$D_{i,feed}$	9.39E-10	m^2 s^{-1}	F_s	9.0	L h^1
θ	0.101	-	F_f	15.5	L h^1
v_s	0.0048	m s^{-1}	V_{feed}	2.2	L
η	0.0007977	Pas	$V_{n\text{-heptane}}$	0.55	L
ρ	997.04	kg m^{-3}	$M_{camphor}$	152.23	g mol^{-1}
Re	165.63	-	$m_{camphor}$	1.65	g
Sc	851.98	-	$c_{feed,astaxanthin,start}$	0.75	g L^{-1}
k_m (*n*-heptane)	1.63E-05	m s^{-1}	P_i	77.1	-
ε	0.55	-	R	19.28	-
$D_{i,solvent}$	2.96E-09	m^2 s^{-1}	E	132.44	-
τ	2	-	slope	-0.000123	s^{-1}
$K_{W,theo}$	1.14E-06	m s^{-1}	K_W	4.55E-06	m s^{-1}

Table A 2: Parameters for the calculation of $K_{W,theo}$ and K_W for the extraction of camphor from at a an aqueous feed flow rate of 237 mL min^{-1} from the feed (shell) into *n*-heptane (fibre).

k_f (*n*-heptane)	1.14E-05	m s^{-1}	$D_{i,feed}$	9.39E-06	cm^2 s^{-1}
$d_{f,i}$	0.003	m	x_{water}	2.6	-
$d_{f,a}$	0.0031	m	T	303.15	K
d_{log}	0.00304	m	M_{water}	18.01	g mol^{-1}
F_i	5.22E-06	m^3 s^{-1}	$M_{Camphor}$	152.23	g mol^{-1}
F_i	313.15	mL min^{-1}	$\rho_{Camphor}$	0.992	g cm^{-3}
$F_{f,i}$	7.45E-07	m^3 s^{-1}	v_n	153.5	cm^3 mol^{-1}
$F_{f,i}$	44.73	mL min^{-1}	η_{water}	0.798	cP
$A_{f,i,total}$	4.94E-05	m^2	$D_{i,n\text{-heptane}}$	2.96E-05	cm^2 s^{-1}
$v_{f,i}$	0.1054	m s^{-1}	$x_{n\text{-heptane}}$	1	-
L	0.875	m	T	303.15	K
$D_{i,solvent}$	2.96E-09	m^2 s^{-1}	$M_{n\text{-heptane}}$	100.21	g mol^{-1}
N_f	7	-	$M_{Camphor}$	152.23	g mol^{-1}
$A_{f,o,total}$	5.28E-05	m^2	$\rho_{Camphor}$	0.992	g cm^{-3}
Re	268	-	v_n	153.46	cm^3 mol^{-1}
η	0.000370	Pas	$\eta_{n\text{-heptane}}$	0.370	cP
ρ	675.3	kg m^{-3}			
Gz	366.4				
k_s (feed)	1.45E-06	m s^{-1}			
F_s	3.95E-06	m^3 s^{-1}			
F_s	237.36	mL min^{-1}			
β	5.8	-			
d_s	0.0258	m			
A_s	0.000522	m^2			
d_h	0.0276	m			-
$D_{i,feed}$	9.39E-10	m^2 s^{-1}	F_s	14.2	L h^1
θ	0.101	-	F_f	18.8	L h^1
v_s	0.00756	m s^{-1}	V_{feed}	2.2	L
η	0.000891	Pas	$V_{n\text{-heptane}}$	0.55	L
ρ	997.04	kg m^{-3}	$M_{camphor}$	152.23	g mol^{-1}
Re	233.5	-	$m_{camphor}$	1.65	g
Sc	951.6	-	$c_{feed,astaxanthin,start}$	0.75	g L^{-1}
k_m (*n*-heptane)	1.63E-05	m s^{-1}	P_i	77.1	-
ε	0.55	-	R	8.8	-
$D_{i,solvent}$	2.96E-09	m^2 s^{-1}	E	46.44	-
τ	2	-	slope	-0.0001814	s^{-1}
$K_{W,theo}$	1.44E-05	m s^{-1}	K_W	6.30E-06	m s^{-1}

Table A 3: Parameters for the calculation of $K_{W,theo}$ and K_W for the extraction of camphor from at a an aqueous feed flow rate of 382 mL min^{-1} from the feed (shell) into *n*-heptane (fibre).

k_f (*n*-heptane)	1.09E-05	m s^{-1}	$D_{i,feed}$	9.39E-06	cm^2 s^{-1}
$d_{f,i}$	0.003	m	x_{water}	2.6	-
$d_{f,a}$	0.0031	m	T	303.15	K
d_{log}	0.00305	m	M_{water}	18.01	g mol^{-1}
F_i	4.54E-06	m^3 s^{-1}	$M_{Camphor}$	152.23	g mol^{-1}
F_i	272.11	mL min^{-1}	$\rho_{Camphor}$	0.992	g cm^{-3}
$F_{f,i}$	6.48E-07	m^3 s^{-1}	v_n	153.5	cm^3 mol^{-1}
$F_{f,i}$	38.87	mL min^{-1}	η_{water}	0.7977	cP
$A_{f,i,total}$	4.95E-05	m^2	$D_{i,n\text{-heptane}}$	2.96E-05	cm^2 s^{-1}
$v_{f,i}$	0.0917	m s^{-1}	$x_{n\text{-heptane}}$	1	-
L	0.875	m	T	303.15	K
$D_{i,solvent}$	2.96E-09	m^2 s^{-1}	$M_{n\text{-heptane}}$	100.21	g mol^{-1}
N_f	7	-	$M_{Camphor}$	152.23	g mol^{-1}
$A_{f,o,total}$	5.28E-05	m^2	$\rho_{Camphor}$	0.992	g cm^{-3}
Re	501.74	-	v_n	153.5	cm^3 mol^{-1}
η	0.000370	Pas	$\eta_{n\text{-heptane}}$	0.370	cP
ρ	675	kg m^{-3}			
Gz	318.4				
k_s (feed)	1.99E-06	m s^{-1}			
F_s	6.37E-06	m^3 s^{-1}			
F_s	382.17	mL min^{-1}			
β	5.8	-			
d_s	0.0258	m			
A_s	0.00052	m^2			
d_h	0.028	m			-
$D_{i,feed}$	9.39E-10	m^2 s^{-1}	F_s	22.9	L h^1
θ	0.101	-	F_f	16.3	L h^1
v_s	0.0122	m s^{-1}	V_{feed}	2.2	L
η	0.0007977	Pas	$V_{n\text{-heptane}}$	0.55	L
ρ	997.0	kg m^{-3}	$M_{camphor}$	152.23	g mol^{-1}
Re	419.9	-	$m_{camphor}$	1.65	g
Sc	851.9	-	$c_{feed,astaxanthin,start}$	0.75	g L^{-1}
k_m (*n*-heptane)	1.63E-05	m s^{-1}	P_i	77.1	-
ε	0.55	-	R	19.3	-
$D_{i,solvent}$	2.96E-09	m^2 s^{-1}	E	54.9	-
τ	2	-	slope	-0.000195	s^{-1}
$K_{W,theo}$	1.98E-06	m s^{-1}	K_W	7.06E-06	m s^{-1}

Table A 4: Parameters for the calculation of $K_{W,theo}$ and K_W for the extraction of camphor from at a an aqueous feed flow rate of 145 mL min^{-1} from the feed (fibre) into *n*-heptane (shell).

k_f (feed)	4.12E-06	m s^{-1}	$D_{i,feed}$	9.39E-06	cm^2 s^{-1}
$d_{f,i}$	0.003	m	x_{water}	2.6	-
$d_{f,a}$	0.0031	m	T	303.15	K
d_{log}	0.00305	m	M_{water}	18.01	g mol^{-1}
F_i	2.42E-06	m^3 s^{-1}	$M_{Camphor}$	152.23	g mol^{-1}
F_i	145.25	mL min^{-1}	$\rho_{Camphor}$	0.992	g cm^{-3}
$F_{f,i}$	3.46E-07	m^3 s^{-1}	v_n	153.5	cm^3 mol^{-1}
$F_{f,i}$	20.75	mL min^{-1}	η_{water}	0.7977	cP
$A_{f,i,total}$	4.95E-05	m^2	$D_{i,n\text{-heptane}}$	2.96E-05	cm^2 s^{-1}
$v_{f,i}$	0.0489	m s^{-1}	$x_{n\text{-heptane}}$	1	-
L	0.875	m	T	303.15	K
$D_{i,water}$	9.39E-10	m^2 s^{-1}	$M_{n\text{-heptane}}$	100.21	g mol^{-1}
N_f	7	-	$M_{Camphor}$	152.23	g mol^{-1}
$A_{f,o,total}$	5.28E-05	m^2	$\rho_{Camphor}$	0.992	g cm^{-3}
Re	394.90	-	v_n	153.5	cm^3 mol^{-1}
η	0.0007977	Pas	$\eta_{n\text{-heptane}}$	0.370	cP
ρ	996	kg m^{-3}			
Gz	535.9				
k_s (*n*-heptane)	3.92E-06	m s^{-1}			
F_s	4.65E-06	m^3 s^{-1}			
F_s	0.00	mL min^{-1}			
β	5.8	-			
d_s	0.0258	m			
A_s	0.00052	m^2			
d_h	0.028	m			-
$D_{i,n\text{-heptane}}$	2.96E-09	m^2 s^{-1}	F_s	15.75	L h^1
θ	0.101	-	F_f	8.7	L h^1
v_s	0.0089	m s^{-1}	V_{feed}	2.2	L
η	0.000370	Pas	$V_{n\text{-heptane}}$	0.55	L
ρ	675	kg m^{-3}	$M_{camphor}$	152.23	g mol^{-1}
Re	447.4	-	$m_{camphor}$	1.65	g
Sc	185.1	-	$c_{feed,astaxanthin,start}$	0.75	g L^{-1}
k_m (*n*-heptane)	1.63E-05	m s^{-1}	P_i	77.1	-
ε	0.55	-	R	19.3	-
$D_{i,solvent}$	2.96E-09	m^2 s^{-1}	E	139.3	-
τ	2	-	slope	-0.0000927	s^{-1}
$K_{W,theo}$	4.05E-06	m s^{-1}	K_W	3.50E-06	m s^{-1}

Table A 5: Parameters for the calculation of $K_{W,theo}$ and K_W for the extraction of camphor from at a an aqueous feed flow rate of 243 mL min^{-1} from the feed (fibre) into *n*-heptane (shell).

k_f (feed)	4.89E-06	m s^{-1}	$D_{i,feed}$	9.39E-06	cm^2 s^{-1}
$d_{f,i}$	0.003	m	x_{water}	2.6	-
$d_{f,a}$	0.0031	m	T	303.15	K
d_{log}	0.00305	m	M_{water}	18.01	g mol^{-1}
F_i	4.05E-06	m^3 s^{-1}	$M_{Camphor}$	152.23	g mol^{-1}
F_i	243.09	mL min^{-1}	$\rho_{Camphor}$	0.992	g cm^{-3}
$F_{f,i}$	5.79E-07	m^3 s^{-1}	v_n	153.5	cm^3 mol^{-1}
$F_{f,i}$	34.73	mL min^{-1}	η_{water}	0.7977	cP
$A_{f,i,total}$	4.95E-05	m^2	$D_{i,n\text{-heptane}}$	2.96E-05	cm^2 s^{-1}
$v_{f,i}$	0.0819	m s^{-1}	$x_{n\text{-heptane}}$	1	-
L	0.875	m	T	303.15	K
$D_{i,water}$	9.3907E-10	m^2 s^{-1}	$M_{n\text{-heptane}}$	100.21	g mol^{-1}
N_f	7	-	$M_{Camphor}$	152.23	g mol^{-1}
$A_{f,o,total}$	5.28E-05	m^2	$\rho_{Camphor}$	0.992	g cm^{-3}
Re	660.90	-	v_n	153.5	cm^3 mol^{-1}
η	0.0007977	Pas	$\eta_{n\text{-heptane}}$	0.370	cP
ρ	996	kg m^{-3}			
Gz	896.8				
k_s (*n*-heptane)	3.83E-06	m s^{-1}			
F_s	4.47E-06	m^3 s^{-1}			
F_s	268.47	mL min^{-1}			
β	5.8	-			
d_s	0.0258	m			
A_s	0.00052	m^2			
d_h	0.028	m			-
$D_{i,n\text{-heptane}}$	2.96E-09	m^2 s^{-1}	F_s	16.11	L h^1
θ	0.101	-	F_f	14.59	L h^1
v_s	0.0086	m s^{-1}	V_{feed}	2.2	L
η	0.000370	Pas	$V_{n\text{-heptane}}$	0.55	L
ρ	675	kg m^{-3}	$M_{camphor}$	152.23	g mol^{-1}
Re	430.65	-	$m_{camphor}$	1.65	g
Sc	185.06	-	$c_{feed,astaxanthin,start}$	0.75	g L^{-1}
k_m (*n*-heptane)	1.63E-05	m s^{-1}	P_i	77.1	-
ε	0.55	-	R	19.3	-
$D_{i,solvent}$	2.96E-09	m^2 s^{-1}	E	85.1	-
τ	2	-	slope	-0.000121	s^{-1}
$K_{W,theo}$	4.79E-06	m s^{-1}	K_W	4.51E-06	m s^{-1}

Table A 6: Parameters for the calculation of $K_{W,theo}$ and K_W for the extraction of camphor from at a an aqueous feed flow rate of 304 mL min^{-1} from the feed (fibre) into *n*-heptane (shell).

k_f (feed)	5.27E-06	m s^{-1}	$D_{i,feed}$	9.39E-06	cm^2 s^{-1}
$d_{f,i}$	0.003	m	x_{water}	2.6	-
$d_{f,a}$	0.0031	m	T	303.15	K
d_{log}	0.00305	m	M_{water}	18.01	g mol^{-1}
F_i	5.08E-06	m^3 s^{-1}	$M_{Camphor}$	152.23	g mol^{-1}
F_i	304.71	mL min^{-1}	$\rho_{Camphor}$	0.992	g cm^{-3}
$F_{f,i}$	7.25E-07	m^3 s^{-1}	v_n	153.5	cm^3 mol^{-1}
$F_{f,i}$	43.53	mL min^{-1}	η_{water}	0.7977	cP
$A_{f,i,total}$	4.95E-05	m^2	$D_{i,n\text{-heptane}}$	2.96E-05	cm^2 s^{-1}
$v_{f,i}$	0.1026	m s^{-1}	$x_{n\text{-heptane}}$	1	-
L	0.875	m	T	303.15	K
$D_{i,water}$	9.39E-10	m^2 s^{-1}	$M_{n\text{-heptane}}$	100.21	g mol^{-1}
N_f	7	-	$M_{Camphor}$	152.23	g mol^{-1}
$A_{f,o,total}$	5.28E-05	m^2	$\rho_{Camphor}$	0.992	g cm^{-3}
Re	828.4	-	v_n	153.5	cm^3 mol^{-1}
η		Pas	$\eta_{n\text{-heptane}}$	0.370	cP
ρ	996	kg m^{-3}			
Gz	1124.2				
k_s (*n*-heptane)	3.92E-06	m s^{-1}			
F_s	4.65E-06	m^3 s^{-1}			
F_s	278.93	mL min^{-1}			
β	5.8	-			
d_s	0.0258	m			
A_s	0.00052	m^2			
d_h	0.028	m			-
$D_{i,n\text{-heptane}}$	2.96E-09	m^2 s^{-1}	F_s	16.74	L h^1
θ	0.101	-	F_f	18.28	L h^1
v_s	0.0089	m s^{-1}	V_{feed}	2.2	L
η	0.000370	Pas	$V_{n\text{-heptane}}$	0.55	L
ρ	675	kg m^{-3}	$M_{camphor}$	152.23	g mol^{-1}
Re	447.43	-	$m_{camphor}$	1.65	g
Sc	185.06	-	$c_{feed,astaxanthin,start}$	0.75	g L^{-1}
k_m (*n*-heptane)	1.63E-05	m s^{-1}	P_i	77.1	-
ε	0.55	-	R	19.3	-
$D_{i,solvent}$	2.96E-09	m^2 s^{-1}	E	70.5	-
τ	2	-	slope	-0.000149	s^{-1}
$K_{W,theo}$	5.16E-06	m s^{-1}	K_W	5.56E-06	m s^{-1}

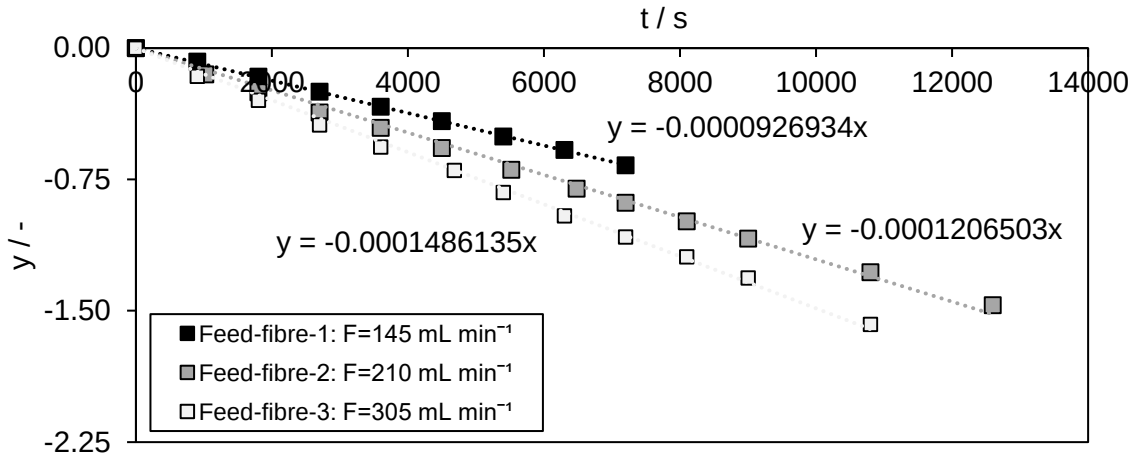

Figure A 5: Determination of the experimental K_W value for the extraction of camphor from the aqueous feed (fibre) into *n*-heptane (shell), plotting ln(y) from Equation 2.37 vs. the extraction time.

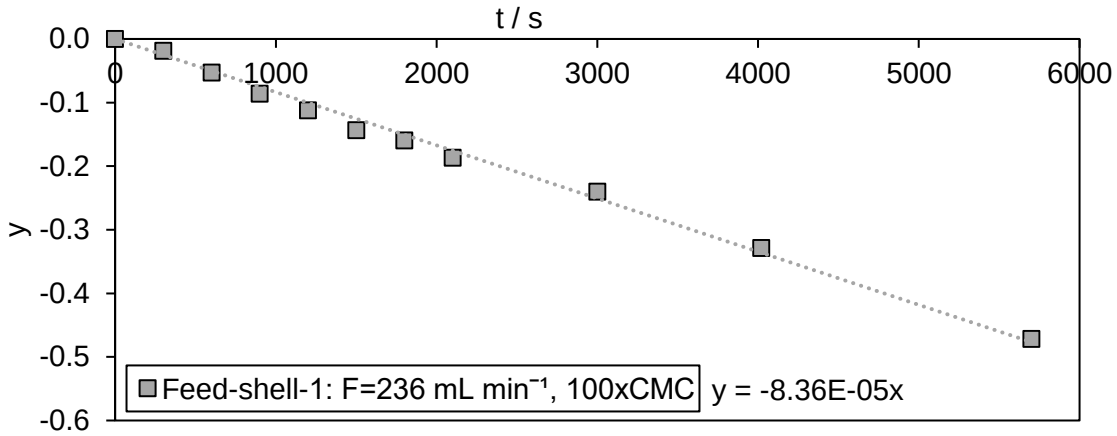

Figure A 6: Determination of the experimental K_W value for the extraction of oleoresin from the aqueous feed (shell) into *n*-heptane (fibre), plotting ln(y) from Equation 2.37 vs. the extraction time.

Table A 7: Data for calculating capacities, energy consumption, and mass balances of upstream processing.

Upstream processing		
Volume per photobioreactor	10	m^3
Operating time	330	d
Number of units	17	-
Total cultivation volume	150000	L
Reserve unit/cleaning	2	-
Energy Lighting	1188	MWh a^{-1}
Installed Watt per Litre	2.00	W L^{-1}
Temperature control	660	MWh a^{-1}
Control and sensors	65.9	MWh a^{-1}
Installed pumps for algae	68	-
Energy of pumps	592	MWh a^{-1}
Power pumps	74.8	kW
Theoretical required CO_2	17780	kg
Real required CO_2	23706	kg
Theoretical required Nitrogen	622.3	kg
Cost CO_2 per kg	0.39	€
Water used in 15 days	150,000	L
Water used in 330 days	3,300,000	L
Water used in 330 days	3,300	m^3
Costs medium per kg	0.76	€
Cultivation period	15	days
Total cultivation time per year	330	days
Final biomass concentration	2.7	g L^{-1}
Astaxanthin content in biomass	5	wt%
Volume harvested per day	10,000	L
Volume harvested per day	10	m^3
Biomass harvested per day	27	kg
Biomass harvested per year	8,910	kg
Volumetric biomass productivity	0.18	g $L^{-1}d^{-1}$
Astaxanthin harvested per day	1.35	kg
Astaxanthin harvested per year	445.5	kg
Lighting/biomass	266.7	MWh t^{-1}

Table A 8: Data for calculating capacities, energy consumption, and mass balances of the centrifugation, homogenisation and spray drying.

Centrifugation (Y=98%)					
$c_{DW,in}$	2.7	g L^{-1}	$c_{DW,out}$	250	g $L^{-1}{}_1$
$m_{DW,in}$	27.0	kg	$m_{DW,out}$	26.46	kg
$V_{water,in}$	10000	L	$V_{water,out}$	105.84	L
$V_{water,separated}$	9894.16	L			
Remaining water in biomass	105.84	L			
Centrifuge GEA SEE 10	2.5	m^3 h^{-1}			
$t_{harvest}$	4	h			
Power centrifuge	4	kW			
Energy requirements	5.28	MWh a^{-1}			

Homogenisation (Y=98%)					
$c_{DW,in}$	250	g L^{-1}	$c_{DW,out}$	250	g $L^{-1}{}_1$
$m_{DW,in}$	26.46	kg	$m_{DW,out}$	25.93	kg
$V_{water,in}$	105.84	L	$V_{water,out}$	103.72	L
remaining water in biomass	103.72	L			
Homogenizer GEA Ariete NS3006H (1500 bar)	25	L h^{-1}			
$t_{homogenisation}$	4.15	h			
Power Homogeniser	5.5	kW			
Energy requirements	7.53	MWh a^{-1}			

Spray drying (Y=98%)					
$c_{DW,in}$	250	g L^{-1}			
$m_{DW,in}$	25.93	kg	$m_{DW,out}$	25.41	kg
$V_{water,in}$	103.72	L	$V_{water,out}$	1.27	L
$V_{water,separated}$	102.45	L			
remaining water in biomass	1.27	L			
$t_{spray\ drying}$	6.4	h			
Evaporation enthalpy water (T=25°C)	2442.3	kJ kg^{-1}			
Energy evaporation	525462	kJ			
$t_{spray\ drying}$ in 330 days	2113.1	h			
Evaporation rate	16	L h^{-1}			
Energy requirement per Batch	146.0	kWh			
Energy requirement per 330 days	48.2	MWh a^{-1}			

Table A 9: Data for calculating capacities, energy consumption, and mass balances of the evaporation and supercritical CO_2 extraction.

Evaporation		
V_{liquid} per days	757.1	L
$V_{ethyl\ acetate}$ per day	738.3	L
V_{water} per day	18.88	L
Installed Watt 100L EcoChyll X7	13.3	kW
Evaporation rate	50	L h^{-1}
$t_{evaporation}$ per day	15.14	h
$t_{evaporation}$ in 330 days	4997	h
Energy requirement in 330 days	66.5	MWh a^{-1}

Supercritical extraction with CO_2		
m_{DW} per day	25.4	kg
time required for extraction per Batch	165	min
time required for extraction per day	16.5	h
time required for extraction per day real	24	h
Mass CO_2 per day	36.60	kg d^{-1}
Mass CO_2 per year	12000	kg a^{-1}
Installed Watt	29	kW
$t_{CO2\ extraction}$	24	h
Electric power consumption per year	229.68	MWh a^{-1}

Table A 10: Data for calculating capacities, energy consumption, and mass balances of the CPE extraction

V_{column}	0.244	5.0	L
scale up factor	20.49		
S_f	0.79	0.79	-
V_{SP}	0.19	3.96	L
Flow rate	40	820	mL min^{-1}
$V_{injection}$	240	4918	mL
$t_{filling}$	6.10	6.10	min
$t_{equilibration}$	6.10	6.10	min
t_{switch}	7.27	7.27	min
$t_{fractioning}$	6.10	6.10	min
$t_{cleaning}$	6.10	0.00	min
$t_{Process}$ je Batch	31.67	25.57	min
$m_{astaxanthin}$ je Batch	88.4	1812	mg
m_{DW} je Batch	7854	160943	mg
$m_{oleoresin}$ je Batch	3500	71721	mg
Operating time per day	24	24	h
Operating days per year	330	330	d
Operating hours per year	7920	7920	h
$V_{acetone}$ in 330 days		3300	L
$V_{water, SP}$ per Batch	0.006	0.117	L
$V_{ethyl\ acetate, SP}$ per Batch	0.187	3.84	L
$V_{water, SP}$ per day	0.257	6.56	L
$V_{ethyl\ acetate, SP}$ per day	8.44	215.1	L
$V_{water, SP}$ in 330 days	84.9	2165.2	L
$V_{ethyl\ acetate, SP}$ in 330 days	2813	71383	L
$V_{Injection\ and\ equilibration}$ per Batch	0.484	9.92	L
$V_{Injection\ and\ equilibration, water}$ per Batch	0.448	9.18	L
$V_{Injection\ and\ equilibration, ethyl\ acetate}$ per Batch	0.036	0.74	L
$V_{Injection\ and\ equilibration, water}$ per day	20.2	513.9	L
$V_{Injection\ and\ equilibration, ethyl\ acetate}$ per day	1.6	41.49	L
$V_{Injection\ and\ equilibration, water}$ in 330 days	6651	169594	L
$V_{Injection\ and\ equilibration, ethyl\ acetate}$ in 330 days	536.9	13691.4	L
Pure ethyl acetate required per batch	0.224	4.58	L
Water required per batch	0.454	9.29	L
Pure ethyl acetate required per day	10.1	256.6	L
Water required per day	20	520	L
Pure ethyl acetate required in 330 days	3349	85074	L
Water required in 330 days	6735	171759	L
Total replacement of ethyl acetate per year	33	33	-

Volume of total replacement of ethyl acetate per year	332	8468	L
volumetric solubility EtOAc in Water (30°C)	7.47		v/v
volumetric solubility Water in EtOAc (30°C)	2.96		v/v
Injections in 24 hours	45	56	-
Biomass extracted in 24 h	0.353	9.01	kg
Biomass extracted in 330 days	116.6	2974.2	kg
Oleoresin extracted in 24 h	0.158	4.02	kg
Astaxanthin extracted in 24 h (2.164 wt%)	0.0034	0.087	kg
Astaxanthin extracted in 24 h (10 wt%)	0.016	0.402	kg
Biomass processed in 24 h	25.93	25.93	kg
CPE units	73.4	2.88	-
Oleoresin in 24 hours	157.5	4016.4	g
Astaxanthin in 24 hours	15.8	401.6	g
Oleoresin in 330 days	52.0	1325.4	kg
Astaxanthin in 330 days	5.2	132.5	kg
Daily Batch injections		54	-
Daily process time per CPE		22.89	h
Installed Watt per CPE	0.4	2.5	kW
Electric power consumption per year and CPE unit		18.9	MW h^{-1}
Electric power in 330 days for three CPE		56.6	MW a^{-1}